

TABLE OF CONTENTS

	Page
Context.....	3
Goal of the thesis	4
1.1 Introduction.....	7
1.2 Gallium Nitride HEMT overview.....	8
1.2.1 GaN HEMT semiconductor properties	8
1.2.2 GaN HEMT growth	11
1.2.3 Principle of operation of GaN HEMT	13
1.2.4 GaN Structural Defects	17
1.3 Scattering functions	22
1.3.1 Small-signal S-parameters	22
1.3.2 Large-Signal S-Parameters	25
1.3.3 Large-Signal X-Parameters.....	28
1.4 Active device modeling	36
1.4.1 Physical modeling.....	36
1.4.2 Table-based model.....	37
1.4.3 Compact Models	38
1.5 A large-signal modeling example.....	40
1.5.1 Extrinsic parameter extraction using two step de-embedding structures..	41
1.5.2 Transistor small-signal modeling.....	47
1.5.3 Transistor large-signal modeling	50
1.6 Conclusion	51
2.1 Abstract.....	53
2.2 Introduction.....	53
2.3 Nonlinear Network parameters.....	56
2.3.1 Multi-harmonic wave, voltage and current quantities	56
2.3.2 X-parameters: a large-signal scattering function	57
2.3.3 Expression of nonlinear two-port network parameters.....	58
2.4 Conversion between nonlinear two-port network parameters	63
2.4.1 Conversion from X- to nonlinear Z-, Y-, ABCD-, T-, G-and H-parameters.....	63
2.4.2 Conversion from nonlinear Z- to X-, nonlinear Y-, ABCD-, T-, G-and H-parameters.....	71
2.4.3 Conversion from nonlinear Y- to X-, nonlinear Z-, ABCD-, T-, G-and H-parameters.....	73
2.4.4 Conversion from nonlinear ABCD- to X-, nonlinear Z-,Y-, T-, G-and H-parameters.....	76
2.4.5 Conversion from nonlinear T- to X-, nonlinear Z-,Y- ABCD-, G-and H-parameters.....	78
2.4.6 Conversion from nonlinear G- to X-, nonlinear Z-,Y- ABCD-, T- and H-parameters.....	82
2.4.7 Conversion from nonlinear H- to X-, nonlinear Z-,Y- ABCD-, T- and G-parameters.....	84

2.5	Linear operation mode validation of nonlinear two port network parameters.....	87
2.6	Non-Linear operation mode validation of nonlinear two-port network parameters....	88
2.6.1	Nonlinear operation mode validation of nonlinear Z-parameters.....	89
2.6.2	Nonlinear operation mode validation of nonlinear Y-parameters	92
2.6.3	Nonlinear operation mode validation of nonlinear ABCD-parameters	95
2.6.4	Nonlinear operation mode validation of nonlinear T-parameters.....	98
2.6.5	Nonlinear operation mode validation of nonlinear H-parameters	101
2.6.6	Nonlinear operation mode validation of nonlinear G-parameters	104
2.6.7	Nonlinear operation mode validation of nonlinear X-parameters	107
2.7	Conclusion	109
3.1	Abstract.....	111
3.2	Introduction.....	111
3.3	State of the Art.....	115
3.3.1	X-parameters: A large-signal scattering function.....	115
3.3.2	Nonlinear network parameters.....	117
3.4	Analytical Computation of Network Configuration	125
3.4.1	Series network configuration.....	125
3.4.2	Parallel network configuration.....	128
3.4.3	Cascaded network configuration.....	130
3.4.4	Series-to-parallel network configuration	135
3.4.5	Parallel-to-series network configuration.....	138
3.5	Validation of Nonlinear Two-Port Network Configurations	141
3.5.1	Cascaded network configuration.....	141
3.5.2	Series network configuration	150
3.5.3	Parallel network configuration.....	154
3.5.4	Series-to-parallel network configuration	158
3.5.5	Parallel-to-series network configuration.....	162
3.6	Conclusion	166
4.1	Abstract.....	167
4.2	Introduction.....	168
4.3	X-parameters and nonlinear characteristic parameters	171
4.3.1	X-parameter formalism.....	171
4.3.2	Nonlinear characteristic impedance.....	171
4.3.3	Nonlinear lumped element impedance and admittance	175
4.4	GaN HEMT extrinsic parameters extraction based on X-parameters	179
4.4.1	Model topology definition	179
4.4.2	Extrinsic parameter extraction using open structures and cold measurements.....	180
4.5	X-parameter based de-embedding technique.....	183
4.6	Intrinsic Parameters extraction	187
4.6.1	X-parameters based large-signal intrinsic model topology definition and extraction.....	187
4.6.2	Transistor intrinsic part modeling with frequency-domain defined devices.....	189
4.6.3	Trapping and self-heating effects in model embedding.....	190

4.7	Measurement results	196
4.7.1	Measurement setup	196
4.7.2	Extrinsic parameters extraction validation.....	197
4.7.3	X-parameter de-embedding technique validation.....	200
4.7.4	Nonlinear lumped element impedance and admittance validation	204
4.7.5	GaN HEMT nonlinear intrinsic part extraction technique validation.....	212
4.7.6	GaN HEMT equivalent circuit model validation.....	214
4.7.7	Small- and large-signal S-parameters simulation	229
4.8	DISCUSSION	232
4.9	Conclusion	234

LIST OF FIGURES

		Page
Figure 1.1	Gallium Nitride transistor performance	9
Figure 1.2	Schematic of the wurtzite GaN crystal structure	9
Figure 1.3	The bandgap energy of different semiconductor materials.....	10
Figure 1.4	Breakdown fields of different semiconductor materials	11
Figure 1.5	Schematic of NRF1 GaN HEMT material structure on Si substrate developed at Nitronex	11
Figure 1.6	Energy band diagram for wide and narrow band gap semiconductor prior (left) and after (right) the formation of a junction	13
Figure 1.7	Electric field and sheet charges due to spontaneous polarization in GaN and AlGaN crystals	14
Figure 1.8	Electric field and sheet charges due to piezoelectric polarization in the AlGaN layer	15
Figure 1.9	AlGaN/GaN HEMT structure, showing polarization induced charges, surface states, and 2DEG charges	16
Figure 1.10	Approximative distinction between extrinsic and intrinsic elements in a transistor	17
Figure 1.11	Two-dimensional CL images taken at ECL = 3.4eV for the samples. A three-dimensional schematic view of a GaN epilayer containing dislocations is shown. The dark spots in each two-dimensional CL image correspond to the dislocations whose locations should not produce any luminescence	18
Figure 1.12	Schematic representation of common point defects	19
Figure 1.13	Basal plane SFs along equation image direction (a) type I1 with stacking sequence of ...ABABCBCBC..., (b) type I2 with sequence ...ABABCACACA... and (c) type I3 with sequence ...ABABCABAB.....	19
Figure 1.14	Schematic view of the widely cited GaN inversion domain boundary structure on a sapphire substrate	20

Figure 1.15	Schematic view of the formation of a nanopipe (Left) Fresnel contrast images of a nanopipe in two beam condition (center) Atomic resolution TEM image of a nanopipe (right)	21
Figure 1.16	General Two-port network showing incident waves (a_1, a_2) and reflected waves (b_1, b_2) used in S-parameters definitions.....	23
Figure 1.17	Forward measurement of hot S-parameters	26
Figure 1.18	Reverse measurement of hot S-parameters.....	27
Figure 1.19	The concept of nonlinear describing functions.....	29
Figure 1.20	Agilent X-PNA's product	35
Figure 1.21	Simulation-X_Param' palette Agilent.....	35
Figure 1.22	A photograph of 200x10 μ m GaN HEMT on Si Substrate (Left) and its equivalent circuit model.....	42
Figure 1.23	On-wafer GaN Open de-embedding structure for a 2mm GaN HEMT (Left) and its equivalent circuit model (Right).....	42
Figure 1.24	On-wafer GaN short-through de-embedding structure for a 2mm GaN HEMT (Left) and its equivalent circuit model (Right).....	43
Figure 1.25	Extraction of extrinsic elements R_{gg} and R_{dd} for a 2mm GaN HEMT ...	44
Figure 1.26	Extraction of extrinsic elements C_{gg} and C_{dd} for a 2mm GaN HEMT ...	45
Figure 1.27	Extraction of extrinsic elements C_{pg} and C_{pd} for a 2mm GaN HEMT ...	45
Figure 1.28	Extraction of Source, gate and drain resistances (R_s, R_g and R_d) from short-thru structure of a 2mm GaN HEMT.....	47
Figure 1.29	Extraction of Source, gate and drain inductors (L_s, L_g and L_d) from short-thru structures of a 2mm GaN HEMT	47
Figure 1.30	Small-signal equivalent circuit model of the intrinsic transistor	48
Figure 1.31	Quasi-static large-signal equivalent circuit model of the intrinsic transistor.....	51
Figure 2.1	Comparison between the logarithmic amplitude (a) and phase (b) of harmonic voltages calculated through nonlinear impedance parameters and those simulated at the input and output ports.....	90

Figure 2.2	Logarithmic amplitude (a) and phase (b) of a random set of nonlinear impedance parameters converted from X-, nonlinear Y-, ABCD-, T-, H- and G-parameters.....	91
Figure 2.3	Comparison between the logarithmic amplitude (a) and the phase (b) of harmonic currents calculated through nonlinear admittance parameters and those simulated at the input and output ports.	93
Figure 2.4	Logarithmic amplitude (a) and phase (b) of a random set of nonlinear admittance parameters converted from X-, nonlinear Z-, ABCD-, T-, H- and G-parameters.....	94
Figure 2.5	Comparison between the logarithmic amplitude (a) and phase (b) of harmonic voltages and currents calculated through nonlinear cascade parameters and those simulated at device input.	96
Figure 2.6	Logarithmic amplitude (a) and phase (b) of a random set of nonlinear ABCD- parameters converted from X-, nonlinear Z-, Y-, T-, H- and G-parameters.....	97
Figure 2.7	Comparison between the logarithmic amplitude (a) and phase (b) of harmonic incident and scattered voltage wave calculated through nonlinear scattering transfer parameters and those simulated at device input port.....	99
Figure 2.8	Logarithmic amplitude (a) and phase (b) of a random set of nonlinear T-parameters determined from X-, nonlinear Z-, Y-, ABCD-, H- and G-parameters.....	100
Figure 2.9	Comparison between the logarithmic amplitude (a) and the phase (b) of harmonic voltage present at port1 and harmonic current present at port2 calculated through nonlinear H-parameters and of the simulated ones.....	102
Figure 2.10	Logarithmic amplitude (a) and phase (b) of a random set of nonlinear H-parameters determined from X, nonlinear Z-, Y-, ABCD-, T- and G-parameters.....	103
Figure 2.11	Comparison between the logarithmic amplitude (a) and phase (b) of harmonic current present at port1 and harmonic voltage present at port2 calculated through nonlinear G-parameters and of the simulated ones.....	105

Figure 2.12	Logarithmic amplitude (a) and phase (b) of a random set of nonlinear G-parameters determined from X, nonlinear Z-, Y-, ABCD-, T- and H-parameters.....	106
Figure 2.13	Logarithmic amplitude (a) and phase (b) of a random set of X-parameters determined from nonlinear Z-, Y-, ABCD-, T-, G- and H-parameters.....	108
Figure 3.1	Series connection of two nonlinear networks.....	126
Figure 3.2	Parallel connection of two nonlinear networks.....	128
Figure 3.3	Cascade connection of two nonlinear networks.....	130
Figure 3.4	Series-to-parallel connection of two nonlinear networks.....	135
Figure 3.5	Parallel-to-series connection of two nonlinear networks.....	138
Figure 3.6	Validation process of nonlinear cascaded network configuration.....	142
Figure 3.7	Comparison between the logarithmic amplitude (a) and the phase (b) of a random set of nonlinear ABCD-parameters calculated from the X-parameters of a cascaded system and those calculated through the cascaded nonlinear ABCD expressions in (3.61).	144
Figure 3.8	Comparison between the logarithmic amplitude (a) and the phase (b) of harmonic voltages and currents as mentioned in the graph presenting the validation process in Figure 3.6. v_{1j} -sim and i_{1j} -sim are the j th harmonic component of voltage and current, simulated with HB, at the input of cascaded system. v_{1j} -Calc and i_{1j} -Calc are the j th harmonic component of voltage and current at the input of cascaded system calculated through nonlinear ABCD matrix with (3.60). v_{a2j} -sim (v_{b1j} -sim) and i_{a2j} -sim (i_{b1j} -sim) are the j th harmonic component of voltage and current, simulated with HB, at the output (input) of circuit A (circuit B).....	146
Figure 3.9	Comparison between the logarithmic amplitude (a) and the phase (b) of a random set of nonlinear T-parameters calculated from the X-parameters of a cascaded system and those calculated through the cascaded nonlinear T expressions in (3.71).	148
Figure 3.10	Comparison between the logarithmic amplitude (a) and the phase (b) of harmonic A- and B-waves as mentioned in the graph presenting the validation process in Figure 3.6. b_{1j} -sim and a_{1j} -sim are the j th harmonic component of scattered and incident waves, simulated with HB, at the input of cascaded system. a_{1j} -Calc and b_{1j} -Calc are the j th harmonic component of incident and scattered waves at the input of	

cascaded system calculated through nonlinear T matrix with (3.68). a_{a2j} -sim (a_{b1j} -sim) and b_{a2j} -sim (b_{b1j} -sim) are the j^{th} harmonic component of incident and scattered waves, simulated with HB, at the output (input) of circuit A (circuit B).....149

Figure 3.11 Validation process of nonlinear series network configuration.151

Figure 3.12 Comparison between the logarithmic amplitude (a) and the phase (b) of a random set of nonlinear Z-parameters calculated from the X-parameters of a series system and those calculated through the series nonlinear Z expressions in (3.47).152

Figure 3.13 Comparison between the logarithmic amplitude (a) and the phase (b) of harmonic voltages and currents as mentioned in the graph presenting the validation process in Figure 3.11. v_{pj} -sim and i_{pj} -sim are the j^{th} harmonic component of voltage and current, simulated with HB, at the input ($p=1$) and output ($p=2$) of the series system. v_{pj} -Calc is the sum of the j^{th} harmonic component of voltages simulated with HB at the port p of circuit A (v_{apj}) and circuit B (v_{bpj}). v_{pj} -Model are calculated through nonlinear Z matrix with (3.53). i_{pj} -sim (i_{apj} -sim, i_{bpj} -sim, resp.) are the j^{th} harmonic component of current, simulated with HB, at the port p of the series circuit (circuit A, circuit B, resp.).....153

Figure 3.14 Validation process of nonlinear parallel network configuration.....155

Figure 3.15 Comparison between the logarithmic amplitude (a) and the phase (b) of a random set of nonlinear Y-parameters calculated from the X-parameters of a parallel system and those calculated through the parallel nonlinear Y expressions in (3.54).156

Figure 3.16 Comparison between the logarithmic amplitude (a) and the phase (b) of harmonic voltages and currents as mentioned in the graph presenting the validation process in Fig. 27. v_{pj} -sim and i_{pj} -sim are the j^{th} harmonic component of voltage and current, simulated with HB, at the input ($p=1$) and output ($p=2$) of the parallel system. i_{pj} -Calc is the sum of the j^{th} harmonic component of currents simulated with HB at the port p of circuit A (v_{apj}) and circuit B (v_{bpj}). i_{pj} -Model are calculated through nonlinear Y matrix with (3.53). v_{pj} -sim (v_{apj} -sim, v_{bpj} -sim, resp.) are the j^{th} harmonic component of voltage, simulated with HB, at the port p of the parallel circuit (circuit A, circuit B, resp.).....157

Figure 3.17 Validation process of nonlinear series-to-parallel network configuration.159

Figure 3.18	Comparison between the logarithmic amplitude (a) and the phase (b) of a random set of nonlinear H-parameters calculated from the X-parameters of a series-to-parallel system and those calculated through the series-to-parallel nonlinear H expressions in (3.81).160
Figure 3.19	Comparison between the logarithmic amplitude (a) and the phase (b) of harmonic voltages and currents as mentioned in the graph presenting the validation process in Fig. 30. v_{pj} -sim and i_{pj} -sim are the j th harmonic component of voltage and current, simulated with HB, at the input ($p=1$) and output ($p=2$) of the series -to-parallel system. v_{1j} -Calc (i_{2j} -Calc) are the sum of the j th harmonic component of voltages (currents) simulated with HB at the port 1 (port 2) of circuit A and circuit B. v_{1j} -Model and i_{2j} -Model are calculated through nonlinear H matrix with (3.80). v_{pj} -sim (v_{apj} -sim, v_{bpj} -sim, resp.) and i_{pj} -sim (i_{apj} -sim, i_{bpj} -sim, resp.) are the j th harmonic component of voltage and current, simulated with HB, at the port p of the series-to-parallel circuit (circuit A, circuit B, resp.).161
Figure 3.20	Validation process of nonlinear parallel-to-series network configuration.163
Figure 3.21	Comparison between the logarithmic amplitude (a) and the phase (b) of a random set of nonlinear G-parameters calculated from the X-parameters of a parallel-to-series system and those calculated through the parallel-to-series nonlinear G expressions in (3.90).164
Figure 3.22	Comparison between the logarithmic amplitude (a) and the phase (b) of harmonic voltages and currents as mentioned in the graph presenting the validation process in Figure 3.20. v_{pj} -sim and i_{pj} -sim are the j th harmonic component of voltage and current, simulated with HB, at the input ($p=1$) and output ($p=2$) of the parallel -to-series system. V_{2j} -Calc (i_{1j} -Calc) are the sum of the j th harmonic component of voltages (currents) simulated with HB at the output (input) of whole circuit. V_{2j} - Model and i_{1j} -Model are calculated through nonlinear G matrix with (3.90). v_{pj} - sim (v_{apj} -sim, v_{bpj} -sim, resp.) and i_{pj} -sim (i_{apj} -sim, i_{bpj} -sim, resp.) are the j th harmonic component of voltage and current, simulated with HB, at the port p of the parallel-to-series circuit (circuit A, circuit B, resp.).165
Figure 4.1	GaN HEMT equivalent circuit model.....176
Figure 4.2	A two-port network consisting of a series nonlinear impedance (left) and a parallel nonlinear admittance (right) between the input and output ports177
Figure 4.3	A nonlinear pi-network model179

Figure 4.4	A photograph of 200x10 μ m GaN HEMT on Si Substrate (Left) and its equivalent circuit model (Jarndal, Markos et al. 2011)	180
Figure 4.5	On-wafer GaN Open de-embedding structure for a 2mm GaN HEMT (Left) and its equivalent circuit model (Right)	181
Figure 4.6	GaN HEMT equivalent circuit model.....	184
Figure 4.7	Large-signal intrinsic model to be extracted from X-parameters	188
Figure 4.8	Transistor intrinsic part modeling with FDD components	190
Figure 4.9	Series (a) and parallel (b) nonlinear impedance FDD modeling	190
Figure 4.10	Equivalent circuit models for an intrinsic GaN HEMT model coupled with thermal and trapping effects.	193
Figure 4.11	X-parameters measurement setup	197
Figure 4.12	Extraction of extrinsic elements R_{gg} and R_{dd} for a 2mm GaN HEMT.....	198
Figure 4.13	Extraction of extrinsic elements C_{gg} and C_{dd} for a 2mm GaN HEMT.....	199
Figure 4.14	Extraction of extrinsic elements C_{pg} and C_{pd} for a 2mm GaN HEMT.....	199
Figure 4.15	A W200N10 GaN HEMT on Si substrate.....	202
Figure 4.16	Logarithmic amplitude of an arbitrary set of X-parameters. S_{pmqj}^{meas} and T_{pmqj}^{meas} are terms of measured X-parameters, and S_{pmqj}^{emb} and T_{pmqj}^{emb} are terms of embedded intrinsic part X-parameters. The transistor is a 2 mm GaN HEMT on Si substrate biased with $V_{ds}=25V$, $I_d=125mA$, $V_{gs}=-1V$ and $I_g=8mA$ and has an input power between 1 and 17 dBm. The measurement frequency is set to 6 GHz.	203
Figure 4.17	Phase of an arbitrary set of X-parameters. S_{pmqj}^{meas} and T_{pmqj}^{meas} are terms of measured X-parameters, and S_{pmqj}^{emb} and T_{pmqj}^{emb} are terms of embedded intrinsic part X-parameters. The transistor is a 2 mm GaN HEMT on Si substrate biased with $V_{ds}=25V$, $I_d=125mA$, $V_{gs}=-1V$ and $I_g=8mA$ and has an input power between 1 and 17 dBm. The measurement frequency is set to 6 GHz.	204
Figure 4.18	Simulation of a parallel nonlinear capacitor	205

Figure 4.19	Comparison between polynomial and FDD models through the logarithmic amplitude of a random set of nonlinear lumped element impedances of a parallel nonlinear capacitor.....	206
Figure 4.20	Comparison between polynomial and FDD models through the phase of a random set of nonlinear lumped element impedances of a parallel nonlinear capacitor.....	206
Figure 4.21	Simulation of a series nonlinear capacitor.....	207
Figure 4.22	Comparison between polynomial and FDD models through the logarithmic amplitude of a random set of nonlinear lumped element impedances of a series nonlinear capacitor.....	208
Figure 4.23	Comparison between polynomial and FDD models through the phase of a random set of nonlinear lumped element impedances of a series nonlinear capacitor.....	209
Figure 4.24	Simulation of a nonlinear pi network.....	210
Figure 4.25	Comparison between polynomial and FDD models through the logarithmic amplitude of a random set of nonlinear lumped element admittances of a nonlinear pi network.....	211
Figure 4.26	Comparison between polynomial and FDD models through the phase of a random set of nonlinear lumped element admittances of a nonlinear pi network.....	211
Figure 4.27	Comparison between deembedded X-parameters of a 2 mm GaN HEMT on Si substrate measured at 6 GHz for $V_{ds}=25V$, $I_{ds}=180$ mA, $V_{gs}=-1V$ and $I_{gs}=8mA$ and FDD models through the logarithmic amplitude of a random set of nonlinear lumped impedances of drain-to-source, gate-to-source, drain-to-gate and gate-to-drain junctions.....	213
Figure 4.28	Comparison between deembedded X-parameters of a 2 mm GaN HEMT on Si substrate measured at 6 GHz for $V_{ds}=25V$, $I_{ds}=180mA$, $V_{gs}=-1V$ and $I_{gs}=8mA$ and FDD models through the phase of a random set of nonlinear lumped element impedances of drain-to-source, gate-to-source, drain-to-gate and gate-to-drain junctions.....	214
Figure 4.29	Implementation of the equivalent circuit based model on ADS.....	216
Figure 4.30	Comparison between the logarithmic amplitude of measured and simulated X-parameters of a 2 mm GaN HEMT on Si substrate measured at 750 MHz for $V_{ds}=3V$, $I_d=113mA$, $V_{gs}=-1.28V$ and	

$I_g=11\text{mA}$ (a), at 1500 MHz for $V_{ds}=1\text{V}$, $I_d=30\text{mA}$, $V_{gs}=-1.48\text{V}$ and $I_g=13\text{mA}$ (b) and at 6 GHz for $V_{ds}=25\text{V}$, $I_d=125\text{mA}$, $V_{gs}=-1\text{V}$ and $I_g=8\text{mA}$ (c). S_{pmqj}^{Meas} and T_{pmqj}^{Meas} are terms of measured X-parameters, and S_{pmqj}^{Model} and T_{pmqj}^{Model} are terms of signal model X-parameters. The set of X-parameter terms are chosen randomly.....218

Figure 4.31 Comparison between the phase of measured and simulated X-parameters of a 2 mm GaN HEMT on Si substrate measured at 750 MHz for $V_{ds}=3\text{V}$, $I_d=113\text{mA}$, $V_{gs}=-1.28\text{V}$ and $I_g=11\text{mA}$ (a), at 1500 MHz for $V_{ds}=1\text{V}$, $I_d=30\text{mA}$, $V_{gs}=-1.48\text{V}$ and $I_g=13\text{mA}$ (b) and at 6 GHz for $V_{ds}=25\text{V}$, $I_d=125\text{mA}$, $V_{gs}=-1\text{V}$ and $I_g=8\text{mA}$ (c). S_{pmqj}^{Meas} and T_{pmqj}^{Meas} are terms of measured X-parameters, and S_{pmqj}^{Model} and T_{pmqj}^{Model} are terms of signal model X-parameters. The set of X-parameter terms are chosen randomly.220

Figure 4.32 Extrinsic input and output voltage and current waveforms simulation (lines) compared to measurements (symbols) of a 2 mm GaN HEMT on Si substrate at 750 MHz for $V_{ds}=3\text{V}$, $I_d=113\text{mA}$, $V_{gs}=-1.28\text{V}$ and $I_g=11\text{mA}$ and for an input power sweep between 1 and 15 dBm with a step of 2 dBm (a) and at 1500 MHz for $V_{ds}=1\text{V}$, $I_d=30\text{mA}$, $V_{gs}=-1\text{V}$ and $I_g=13\text{mA}$ and for an input power sweep between 1 and 15 dBm with a step of 2 dBm (b) and at 6 GHz for $V_{ds}=25\text{V}$, $I_d=125\text{mA}$, $V_{gs}=-1\text{V}$, $I_g=8\text{mA}$ and for an input power sweep between 1 and 17 dBm with a step of 2 dBm (c).....222

Figure 4.33 Intrinsic (de-embedded) input and output voltage and current waveforms simulation (lines) compared to measurements (symbols) of a 2 mm GaN HEMT on Si substrate at 750 MHz for $V_{ds}=3\text{V}$, $I_d=113\text{mA}$, $V_{gs}=-1.28\text{V}$ and $I_g=11\text{mA}$ and for an input power sweep between 1 and 15 dBm with a step of 2 dBm (a) and at 1500 MHz for $V_{ds}=1\text{V}$, $I_d=30\text{mA}$, $V_{gs}=-1\text{V}$ and $I_g=13\text{mA}$ and for an input power sweep between 1 and 15 dBm with a step of 2 dBm (b) and at 6 GHz for $V_{ds}=25\text{V}$, $I_d=125\text{mA}$, $V_{gs}=-1\text{V}$, $I_g=8\text{mA}$ and for an input power sweep between 1 and 17 dBm with a step of 2 dBm (c).....224

Figure 4.33 Extrinsic and Intrinsic (de-embedded) dynamic loadlines simulation (lines) compared to measurements (symbols) of a 2 mm GaN HEMT on Si substrate at 750 MHz for $V_{ds}=3\text{V}$, $V_{gs}=-1.28\text{V}$ and for an input power of 15 dBm (a) and at 1500 MHz for $V_{ds}=1\text{V}$, $V_{gs}=-1\text{V}$ and for an input power of 15 dBm (b) and at 6 GHz for $V_{ds}=25\text{V}$, $V_{gs}=-1\text{V}$ and for an input power of 17 dBm (c).....225

Figure 4.35 Output power simulations (lines) compared with measurements (symbols) of a 2 mm GaN HEMT on Si substrate at 750 MHz for $V_{ds}=3V$, $I_d=113mA$, $V_{gs}=-1.28V$ and $I_g=11mA$ (a), at 1500 MHz for $V_{ds}=1V$, $I_d=30mA$, $V_{gs}=-1.48V$ and $I_g=13mA$ (b) and at 6 GHz for $V_{ds}=25V$, $I_d=125mA$, $V_{gs}=-1V$ and $I_g=8mA$ (c).227

Figure 4.36 AM-AM and AM-PM simulations (lines) compared with measurements (symbols) of a 2 mm GaN HEMT on Si substrate at 750 MHz for $V_{ds}=3V$, $I_d=113mA$, $V_{gs}=-1.28V$ and $I_g=11mA$ (a), at 1500 MHz for $V_{ds}=1V$, $I_d=30mA$, $V_{gs}=-1.48V$ and $I_g=13mA$ (b) and at 6 GHz for $V_{ds}=25V$, $I_d=125mA$, $V_{gs}=-1V$ and $I_g=8mA$ (c).229

Figure 4.37 Measured S-parameters (S_{11} (a), S_{12} (b), S_{21} (c) and S_{22} (d)) compared to the simulated ones of the equivalent-circuit based model with ADS LSSP and to the simulated Xparameters (S_{1111} , S_{1121} , S_{2111} and S_{2121}) of the model with ADS X-parameters. The transistor is a 2 mm GaN HEMT on Si substrate biased with $V_{ds}=10V$, $I_{ds}=189mA$, $V_{gs}=-1V$ and $I_{gs}=14mA$ and has an input power of -20 dBm. The frequency range is between 500 MHz and 6 GHz.232

LIST OF ABBREVIATIONS AND ACRONYMS

2DEG:	Two-Dimensional Electron Gas
3G:	Third Generation
AAN:	Artificial Neural Network
ADS:	Advanced Design System
Al	Aluminium
AlGaN	Aluminium Gallium Nitride
DAC:	Data Access Component
dB:	Decibel
dBm:	Decibel(mW)
DC:	Direct Current
DS:	Drain Source
EER:	Envelope, Elimination and Restauration
FDD:	Frequency Defined Devices
FET:	Field Effect Transistor
Ga:	Gallium
GaN:	Gallium Nitride
GS:	Gate Source
HEMT:	High Electron Mobility Transistor
HPA:	High RF Power Amplifier
IMD:	Intermodulation Distortion
LINC:	Linear Amplification using nonlinear components
MESFET:	Metal-Semiconductor Field Effect Transistor
MILC:	Modified Implementation of LINC
MOCVD:	Metal Organic Chemical Vapor Deposition
N:	Nitride
RF:	Radio Frequency
S-parameters:	Scattering parameters
SF:	Stacking Fault
Si:	Silicon

SiC: Silicon Carbide
TEC: Thermal Expansion Coefficient
W: Watt

INTRODUCTION

Context

AlGaN/GaN HEMT technology is becoming an interesting candidate for the HPA design (Bae, Negra et al. 2007, Bensmida, Hammi et al. 2008, Aflaki, Negra et al. 2009, Jarndal, Markos et al. 2011). Since GaN is a wide band gap material, GaN-based device will have inherent high breakdown voltage (Tanaka, Ueda et al. 2010). Therefore, it can operate at higher bias voltage and higher RF power level (Nuttinck, Gebara et al. 2002, Milligan, Sheppard et al. 2007). Also due to its high saturation velocity, the device will have a high operating frequency (Oxley and Uren 2005). Another advantage of the device is the high operating temperature, which is attributed to the lower thermal resistance of GaN and the excellent thermal properties of the employed Si substrate (Khan, Simin et al. 2005, Killat, Montes et al. 2012). However, the main obstacle, which still limits the RF output power of the device, is the self-heating and trapping induced current dispersion (Islam and Anwar 2004).

The design of high efficient power amplifier based on AlGaN/GaN HEMT requires an accurate large-signal model for this device (Jarndal, Markos et al. 2011). This model should account for current dispersion and temperature dependent performance in addition to other high-power stimulated effects like gate forward and gate breakdown (Liu, Ng et al. 2011). Also the model should be able to predict intermodulation distortion (IMD), which is very important for power amplifier nonlinearity analysis (Wongtanarak and Chalermwisutkul 2011).

X-parameters were invented by Jan Verspecht in 2005 (Verspecht, Williams et al. 2005). The new nonlinear scattering parameters are applicable for linear and nonlinear circuits under large or small signal excitation (Verspecht 2005). They are a mathematical superset of S-parameters and hot S-parameters (Verspecht and Root Jun. 2006).

Goal of the thesis

The question is how to exploit X-parameters to more accurately and quickly build a nonlinear equivalent circuit based model that captures the device behavior at the fundamental and harmonic frequencies.

The main objective of this project is to develop a large and small signal model for AlGaIn/GaN HEMT, which can simulate the output power, the power added efficiency, and nonlinear behaviour of the device in an efficient manner. In our research works, X-parameter measurement is the basic point for the other tasks. Accurate X-parameter measurements are needed. However, in traditional transistor modeling, the conversion from S-parameters to impedance, admittance and ABCD matrices is essential for model parameters extraction (Dambrine, Cappy et al. 1988). Moreover, X-parameters are not directly suitable for the analytic analysis of different network configurations: series, parallel, cascaded, series to parallel and parallel to series. Similar to small-signal modeling, nonlinear network Z-, Y-, ABCD-, T-, G- and H-parameters are used to extract and validate large-signal model.

In the second chapter, a relation between nonlinear network Z-, Y-, ABCD-, T-, G-, H-parameters and X-parameters will be established. The conversion rules are needed to establish and extract a transistor signal model that can be implemented by a network of nonlinear components.

For linear circuits, Z-, Y-, ABCD-, T-, G- and H-parameters that are derived from S-parameters are successfully used to characterize series, parallel, cascaded, parallel-to-series and series-to-parallel configurations respectively. Unfortunately, these parameters cannot be used in nonlinear cases. The new analytic expressions presented in this paper circumvent this limitation. They are more general than those derived from S-parameters. Based on X-parameters, these parameters can describe a topology of pure linear or nonlinear or a mix of linear and nonlinear components. In the third chapter, after the validation of the new two-port nonlinear network, the possibility of using X-parameters to build a compact model by using X-parameters is proven. The utility of the new nonlinear parameters to describe series,

parallel, cascaded, series-to-parallel and parallel-to-series nonlinear network configuration is also developed.

Non-linear models for microwave and millimetre wave devices are commonly based on DC and S-parameter measurements (Schreurs, Verspecht et al. 1997, Jarndal, Bunz et al. 2006). These models are commonly described in terms of state functions (Schreurs, Verspecht et al. 2002). These quantities are classically determined via a small-signal detour based on multi-bias S-parameter measurements (Jarndal, Bunz et al. 2006). This technique is based on making a small-signal approximation of the non-linear state functions at different bias points (Jarndal, Bunz et al. 2006). This technique requires a large amount of S-parameter measurements. In the fourth chapter, a new large signal equivalent circuit modeling technique is proposed. This technique is very simple and reduces significantly the number of required measurements thanks to X-parameters measurements. All steps and analytic tools used to develop the new modeling technique are presented in this paper. The transistor model can be subdivided into extrinsic and intrinsic parts. Firstly, parasitic or extrinsic elements are extracted through a reliable technique based on GaN open on-wafer de-embedding structures and forward measurements. Secondly, X-parameters de-embedding technique is developed which allows determining X-parameter of the intrinsic part. After de-embedding the extrinsic elements, the intrinsic part, which is related to the physical operation of the transistor, is obtained by a direct extraction of the intrinsic elements from X-parameters measurements. The intrinsic part which consists of three nonlinear impedances describing gate-source, gate-drain and drain-source junctions is implemented by using frequency defined devices (FDD) components in ADS.

CHAPTER 1

LITERATURE REVIEW

1.1 Introduction

High power amplifiers have been receiving increasing attention as key components responsible for a sizable portion of base station cost in terms of power loss and cooling equipments in wireless communication systems (Jarndal, Aflaki et al. 2010). They are also responsible in large part for battery life and size of the mobile terminals. Thus, high power and high efficiency amplifiers with low power loss are critically needed (Oualid, Slim et al. 2006). To meet these requirements, higher attention should be given to the employed active devices and the circuit design. Today, GaN HEMT devices are the best choice in this regard since they can produce higher output power with lower self-heating and leakage currents, which accordingly results in good power efficiency (Nuttinck, Gebara et al. 2002, Oxley and Uren 2005, Bae, Negra et al. 2007, Milligan, Sheppard et al. 2007, Bensmida, Hammi et al. 2008, Aflaki, Negra et al. 2009, Tanaka, Ueda et al. 2010, Jarndal, Markos et al. 2011). The design of high efficient power amplifier based on AlGaIn/GaN HEMT requires an accurate large-signal model for this device (Jarndal, Markos et al. 2011).

In this chapter which is a summary of the literature related to the new work developed in this thesis. In the first part, an overview of Gallium Nitride high electron mobility transistor is presented. The principle of operation of GaN HEMT is detailed, demonstrating the potential performances of this kind of transistors. Moreover, continuous and pulsed DC IV characteristics of GaN HEMT give more information about its operation. In the second part, existing small-signal and large-signal scattering parameters are detailed. S-parameters are the most useful tool to describe a linear circuit. Unfortunately, they have one significant drawback: they are only valid under linear operating conditions (Verspecht 2005). X-parameters represent new nonlinear scattering parameters, applicable to passive and active circuits under small and large signal excitation (Verspecht 2005). They represent a mathematical superset of small-signal and large signal S-parameters (Verspecht and Root

Jun. 2006). In the third section, different transistor modeling techniques are classified into physics, table-based and compact models. The principle of each class is detailed. An example of the most used large signal modeling technique is explained. This model is based on DC and S-parameter measurements (Schreurs, Verspecht et al. 1997, Jarndal, Bunz et al. 2006). It is commonly described in terms of state functions (Schreurs, Verspecht et al. 2002). These quantities are classically determined via a small-signal detour based on multi-bias S-parameter measurements. This technique is based on making a small-signal approximation of the non-linear state functions at different bias points. It requires a large amount of S-parameter measurements.

1.2 Gallium Nitride HEMT overview

The choice of semiconductor materials is based on the physical properties of the materials which have to fulfill the requirements of the application like operating temperature, frequency and bandwidth (Von 2007). Since the power level and the operating frequency of high frequency circuits is steadily increasing, it is predictable that RF power devices based on GaAs will soon come to their performance limitations (Khan, Simin et al. 2005, Nitronex 2009). The most promising materials for high frequency, high power applications are silicon carbide (SiC) and Gallium Nitride (GaN) (Khan, Simin et al. 2005, Von 2007, Yong-Sub and Yoon-Ha 2007).

1.2.1 GaN HEMT semiconductor properties

Gallium Nitride is a wide-bandgap, compound semiconductor that will be a disruptive technology across a wide range of electronic applications (Tanaka, Ueda et al. 2010). As illustrated in Figure 1.1, Gallium Nitride (*GaN*) *HEMTs* (*High Electron Mobility Transistors*) are the next generation of RF power transistor technology that offers the unique combination of higher power, higher efficiency and wider bandwidth than competing GaAs and Si based technologies (Nitronex 2009).

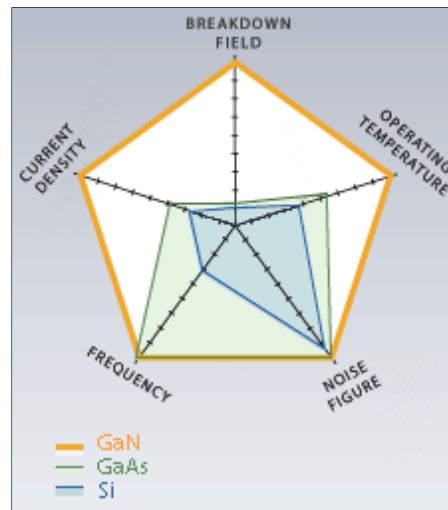


Figure 1.1 Gallium Nitride transistor performance
From Nitronex (2009)

An example of GaN crystal structures is shown in Figure 1.2. This wurtzite structure has hexagonal unit cell. An important property of this crystal cell is the lack of inversion symmetry, which leads to very strong polarization effects (Ambacher 1998).

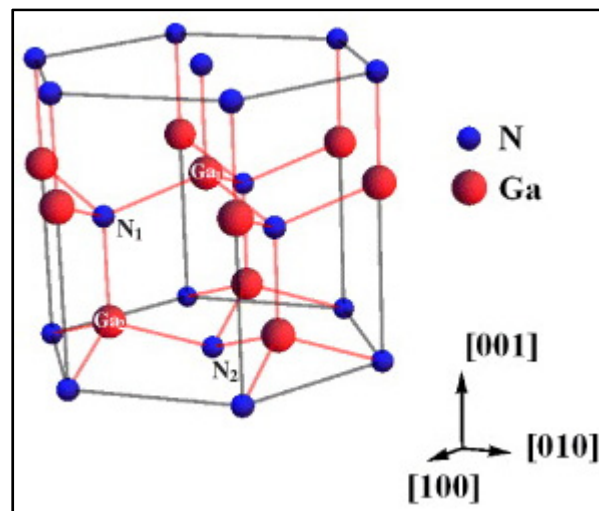


Figure 1.2 Schematic of the wurtzite GaN crystal structure
From Ambacher (1998)

The GaN structure consists of four atoms per unit cell and can be visualized as two interpenetrating hexagonal substructures, one of Ga and one of N atoms related by a spacing u along the c-axis (Komninou, Kioseoglou et al. 2005).

Super material properties for transistors that make them for high power, high energy efficiency and high temperature include wide bandgap energy, high electron mobility and saturation velocity, high sheet carrier concentration at heterojunction interfaces, high breakdown field, and low thermal impedance (Khan, Simin et al. 2005). The bandgap energy is the energy required to ionize atoms and create free electrons. A large bandgap is the key factor for high temperature operation, chemical inertness, and high breakdown voltage. The bandgap energy values for the most important semiconductor materials are shown in Figure 1.3.

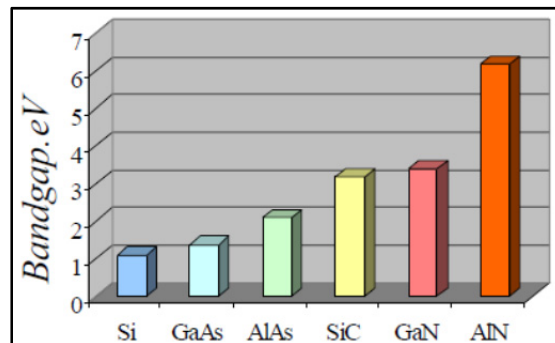


Figure 1.3 The bandgap energy of different semiconductor materials
From Khan, Simin et al. (2005)

The high breakdown voltages are of primary importance. Figure 1.4 compares the critical electric fields for the avalanche breakdown mechanism in the most important semiconductor materials.

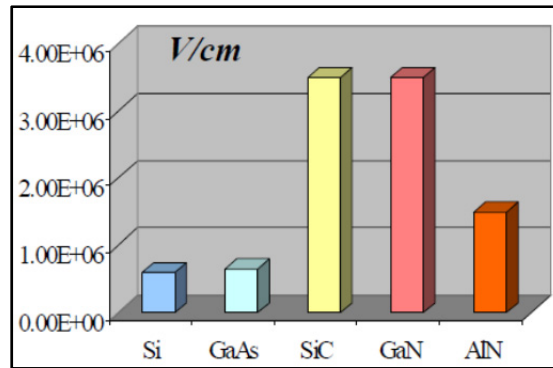


Figure 1.4 Breakdown fields of different semiconductor materials
From Khan, Simin et al. (2005)

1.2.2 GaN HEMT growth

An example of GaN HEMT material structure developed by Nitronex is illustrated in Figure 1.5. The GaN substrates are not a viable alternative for HEMT devices and circuits because of its weak thermal property. Thus, the deposition of GaN thin films on Si and SiC is the primary approach for the fabrication of GaN RF power devices and circuits. Si substrates have low crystal defect density, zero macro-defects, and offer a high quality surface as required for performing epitaxy (Corporation 2008).

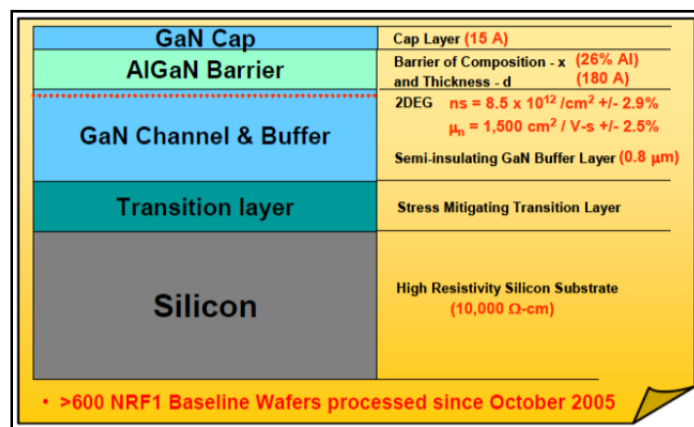


Figure 1.5 Schematic of NRF1 GaN HEMT material structure on Si substrate developed at Nitronex
From Nitronex (2009)

The deposition process is broadly termed as epitaxy and results in a crystalline thin film on the substrate. Metal Organic Chemical Vapor Deposition (MOCVD) is the preferred method of producing GaN-based thin films on Si or SiC for RF applications (Nitronex 2009). MOCVD systems are capable to operate in both conventional and atomic layer deposition regimes (Khan, Simin et al. 2005). Conventional deposition regime wherein precursors enter the growth chamber simultaneously is used to deposit GaN layers. Triethylgallium and ammonia are used as the precursor gases. $\text{Al}_x\text{Ga}_{1-x}\text{N}$ layers are deposited in atomic layer regime when precursors enter the chamber in a cyclic fashion. Triethylgallium, triethylaluminum and ammonia are used as precursors. The precursors are introduced into the chamber using hydrogen or nitrogen as a carrier gas. Epilayers are deposited on sapphire, Silicon or SiC substrates placed on graphite susceptor, which is heated to the growth temperature by RF-induction.

GaN HEMTs have been demonstrated on Si, SiC, sapphire and on native GaN substrates (Nitronex 2009). However, Si and SiC are the preferred choices for RF devices (Nitronex 2009). The maturity of the AlGaIn/GaN heterostructures in terms of reliability, cost and manufacturability has been demonstrated through the use of commercially available high resistivity 100-mm Si substrates. Si substrates have low crystal defect density, have zero micropipes or other macro-defects, and offer a high quality surface as required for performing epitaxy. High resistivity silicon (10^4Ohm-cm) substrates are available through the process of zone refining of Si ingots and have very low impurity concentrations (Nitronex 2009). Growth of high quality GaN on Si can be achieved by addressing the significant levels of lattice misfit ($\sim 17\%$) and thermal expansion coefficient (TEC) ($\sim 56\%$) mismatch (Nitronex 2009). To accommodate the strain associated in difference between crystal properties of Si and GaN and to manage this high level of lattice and thermal mismatch, Nitronex introduced a novel growth process, Sigantic that results in the growth of crack-free GaN. The transition layer addresses the two challenges necessary for the successful growth of GaN on Si: It manages both the lattice and thermal mismatch between the two materials. The AlN/Si interface absorbs most of the lattice mismatch while the (Al, Ga)N transition layer is successful in absorbing the stresses that arise due to the TEC mismatch.

1.2.3 Principle of operation of GaN HEMT

The HEMT is a heterostructure or heterojunction field effect transistor (Vassil Palankovski 2004). A heterostructure is an abrupt semiconductor/semiconductor transition in one direction. The abrupt change of the material leads to a number of desirable effects such as carrier confinement in a restricted volume and the spatial separation of electrons and holes (Vassil Palankovski 2004). A heterojunction is formed between two semiconductors with different energy bandgaps, permittivities, work functions and electron affinities.

The energy band diagram of such two semiconductors prior to the formation of a junction is shown in Figure 1.6 (Peter Javorka 2004). After putting the wide band gap semiconductor into contact with the narrow band gap semiconductor, a discontinuity in conduction band ΔE_c and valence band ΔE_v is present. The discontinuity in the conduction band creates a triangular quantum well, and near to the boundary at the bottom side, the two dimensional electron gas is formed (2DEG).

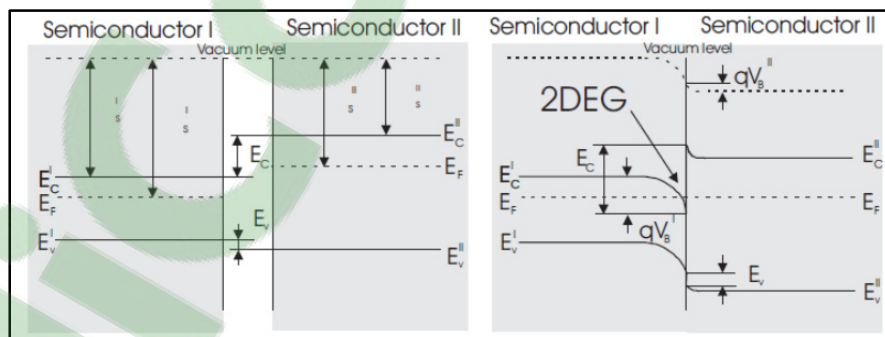


Figure 1.6 Energy band diagram for wide and narrow band gap semiconductor prior (left) and after (right) the formation of a junction
From Peter Javorka (2004)

In contrast to the conventional III-V semiconductors where a doped layer is necessary to create a 2DEG, AlGaIn/GaN HEMTs don't need doping to obtain a high electron density

(Mishra, Parikh et al. 2002). Polarisation effects lead to high carrier densities even in undoped structures (Ambacher, Foutz et al. 2000).

The distribution of free carriers and the magnitude of electric currents in a semiconductor are determined by electric fields. In a “classical” semiconductor or semiconductor structure, such as a Si-based junction, the field is of external origin (Wood and Jena 2008). The electric field inside the structure is determined by, e.g., the applied voltage, which is screened by electrons and nuclei of the solid. The situation is more complex in ferroelectrics, pyroelectrics, and piezoelectrics, where there may exist an internal field even in the absence of the external one, due to the presence of non-vanishing electric polarization.

Polarization effects in AlGaIn/GaN HEMT include spontaneous and piezoelectric polarization. The spontaneous polarization P_{SP} refers to the built-in polarization field present in an unstrained crystal (Jarndal 2006). Wurtzite group III-nitrides are tetrahedrally coordinated with a lack of symmetry along the c-direction. Because of this lack of symmetry and the large ionicity of the covalent bond in wurtzite GaN a large spontaneous polarization (P_{SP}) oriented along the hexagonal c-axis occurs (Peter Javorka 2004). This results in a displacement of the electron charge cloud towards one atom in the bond. In the direction along which the crystal lacks inversion symmetry, the asymmetric electron cloud results, as illustrated in Figure 1.7, in a net positive charge located at one face of the crystal and a net negative charge at the other face (Ambacher, Foutz et al. 2000, Jarndal 2006).

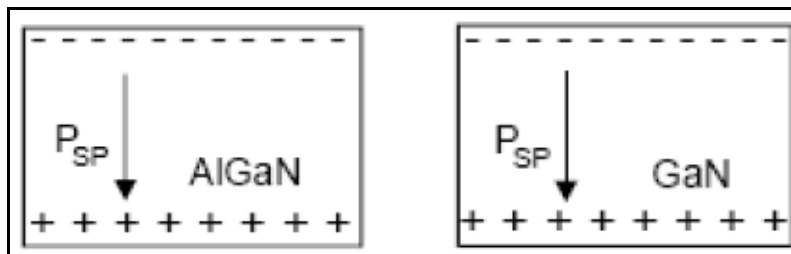


Figure 1.7 Electric field and sheet charges due to spontaneous polarization in GaN and AlGaIn crystals
From Ambacher, Foutz et al. (2000), Jarndal (2007)

Piezoelectric polarization is the presence of a polarization field resulting from the distortion of the crystal lattice (Peter Javorka 2004, Jarndal 2006). Due to large differences in lattice constant between AlGaIn and GaN materials, the AlGaIn layer which is grown on the GaN buffer layer is strained. Due to large value of piezoelectric coefficients of these materials, this strain results in a sheet charge at the two faces of AlGaIn layer as illustrated in Figure 1.8.

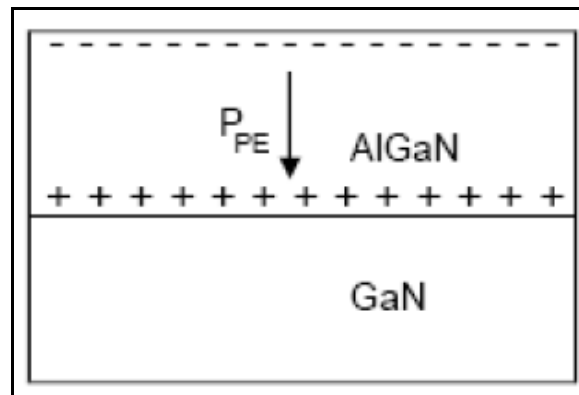


Figure 1.8 Electric field and sheet charges due to piezoelectric polarization in the AlGaIn layer
From Ambacher, Foutz et al. (2000), Jarndal (2007)

The total polarization field in the AlGaIn layer depends on the orientation of the GaN crystal. MOCVD produces GaN crystal orientation that makes the sheet charges caused by spontaneous and piezoelectric polarizations added constructively (Ambacher, Foutz et al. 2000, Jarndal 2006). Therefore, the polarization field in the AlGaIn layer will be higher than that in the buffer layer. Due to this discontinuity, a very high positive sheet charge will be present at the AlGaIn/GaN interface. As the thickness of the AlGaIn layer increases during the growth process, the crystal energy will also increase. Beyond a certain thickness the internal electric field becomes high enough to ionize donor states at the surface and cause electrons to drift toward the AlGaIn/GaN interface. As the electrons move from the surface to the interface, the magnitude of the electric field is reduced, thereby acting as a feedback mechanism to diminish the electron transfer process. Under equilibrium condition, a 2DEG charge at the interface will be generated due to the transferred electrons and a positive charge on the surface will be formed by the ionized donors as illustrated in Figure 1.9.

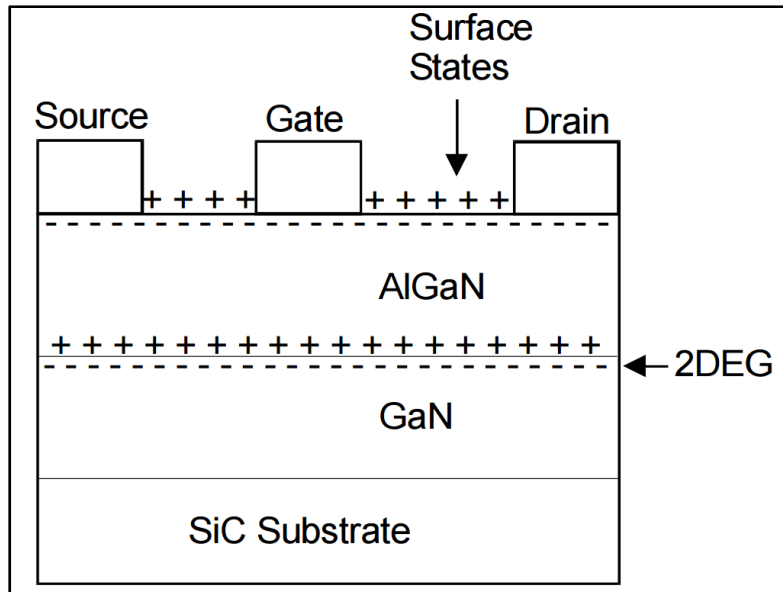


Figure 1.9 AlGaIn/GaN HEMT structure, showing polarization induced charges, surface states, and 2DEG charges
From Ambacher, Foutz et al. (2000), Jarndal (2006)

The transistor action occurs in the active channel that lies under the gate: This is where the current amplification happens (Jarndal 2006). This part of the transistor is called the intrinsic device. In the real device we need additional semiconductor and metal components to connect this active region to the outside world, to get the signal and the amplified signal out. These additional components are called extrinsic components, or, quite often, parasitics. The extrinsic components are unwanted and while they generally tend to degrade the fundamental electrical performance, they are essential to the structure of the device. Other considerations, such as thermal management, also play a role in the overall size of the transistor die.

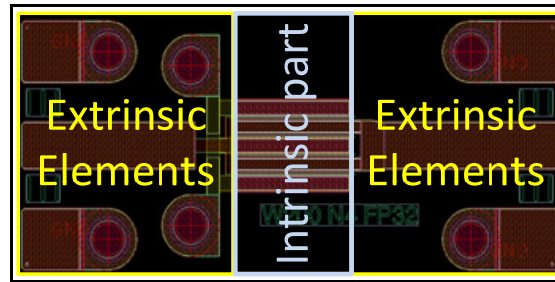


Figure 1.10 Approximative distinction between extrinsic and intrinsic elements in a transistor

1.2.4 GaN Structural Defects

Many research groups have made every effort to grow GaN on a Si substrate. Due to the lattice mismatch between GaN and Si, GaN films on Si substrates are well known to have many defects, particularly dislocations (Young S. Park 2010). The dislocations that form far below the surface can be detected and their distribution in the plane can be mapped with two-dimensional CL images techniques. Figure 1.11 shows the CL images for the samples. The bright background region originates from the GaN epitaxial layer, and the dark spots are related to the threading dislocations. They are due to lattice constant and thermal expansion coefficient mismatches between GaN and Si. Dislocations defects cause rapid recombination of holes with electrons without conversion of their available energy (Predeep 2011).

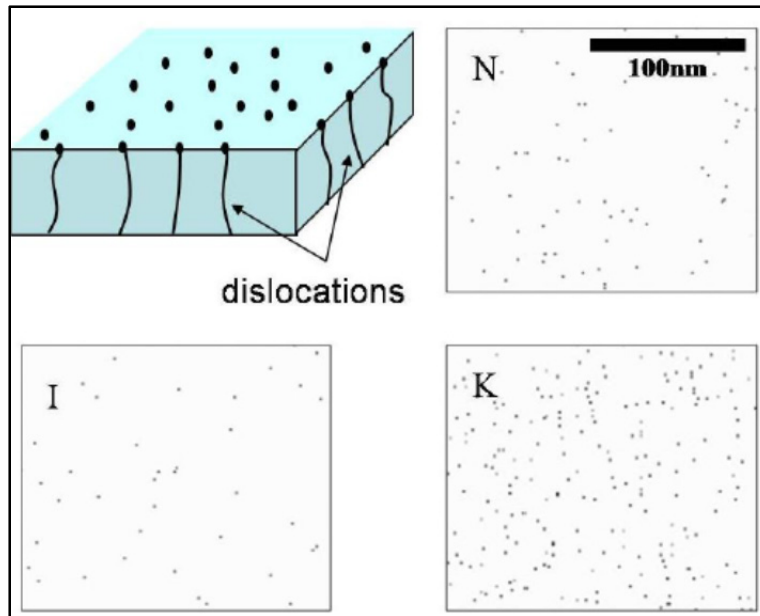


Figure 1.11 Two-dimensional CL images taken at ECL = 3.4eV for the samples. A three-dimensional schematic view of a GaN epilayer containing dislocations is shown. The dark spots in each two-dimensional CL image correspond to the dislocations whose locations should not produce any luminescence
From Young S. Park (2010)

Besides threading dislocations, there are many other structural defects, such as, inversion domain, stacking mismatch boundaries, micropipes/nanopipes or voids, and surface pits (Predeep 2011).

The formation of defects during growth is unavoidable. In general, there are three main types of point defects: a vacancy which is an unoccupied regular crystal, interstitial atom which is an atom that does not occupy a regular crystal site but a site between regular atoms and substitutional atoms when an impurity atom substitutes an atom of the host crystal (Predeep 2011).

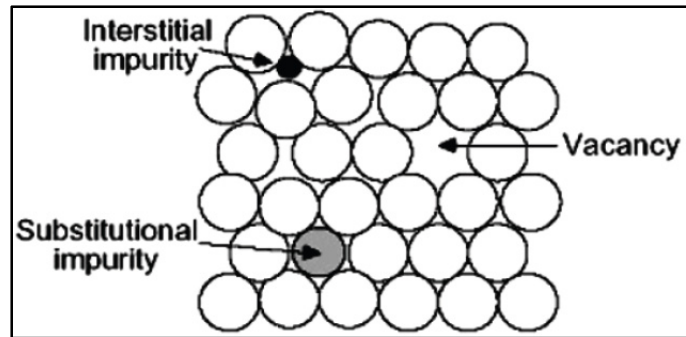


Figure 1.12 Schematic representation
of common point defects
From Predeep (2011)

Stacking faults are partial displacements which upset the regular sequence in the stacking of lattice planes (Batyrev, Sarney et al. 2011). Figure 1.13 illustrates different types of stacking faults.

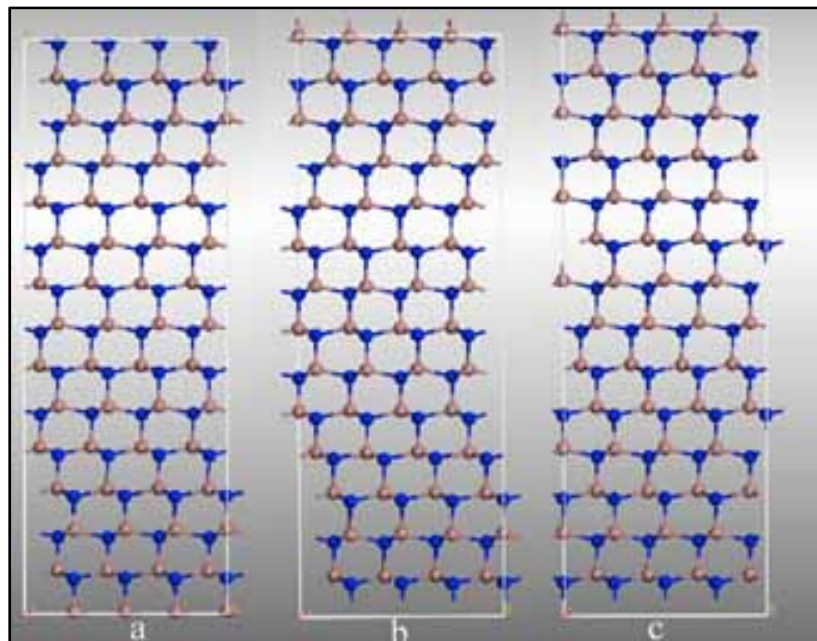


Figure 1.13 Basal plane SFs along equation image direction (a) type I1 with stacking sequence of ...ABABCBCBC..., (b) type I2 with sequence ...ABABCACACA... and (c) type I3 with sequence ...ABABCABAB...
From Batyrev, Sarney et al. (2011)

The stacking mismatch boundaries are created by surface steps on substrates. The defects originate at substrate/film interface (Predeep 2011). They can be identified as double-position boundaries, which originate at the substrate-buffer and buffer-film interfaces (Predeep 2011). The density of these defects seems to be related to the smoothness of the substrate. The formation of these domains is believed to account for the relaxation of the large lattice and thermal mismatches between nitrides and substrate.

GaN crystal grains formed during high temperature growth are not perfectly arranged, and misorientation of crystal grains occur in both a- and c- axes due to fast surface migration and clustering of atoms (Predeep 2011). The stacking faults, edge and mixed dislocations will be generated at grain boundaries to compensate the misorientation during coalescence of laterally growing crystal grains (Predeep 2011).

Inversion domains consist of region of GaN with the opposite polarity to the primary matrix as schematically depicted in Figure 1.14, where the section on the left is of Ga polarity and the section on the right is of N polarity (Predeep 2011). Boundaries between them are called inversion domain boundaries. When inversion domains happen, the alternating nature of anion-cation bonds can not be fully maintained.

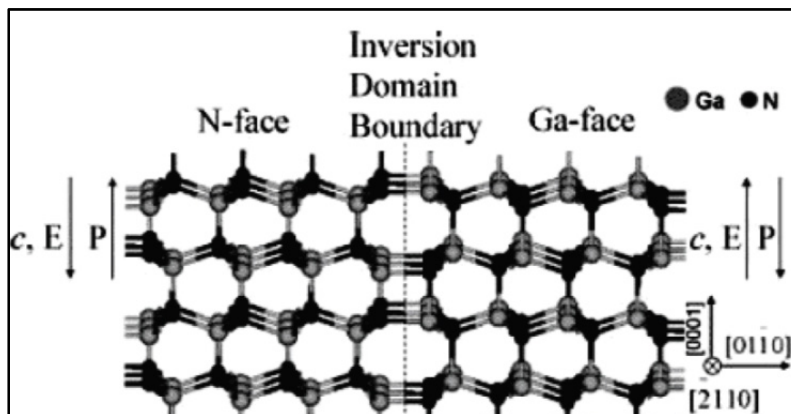


Figure 1.14 Schematic view of the widely cited GaN inversion domain boundary structure on a sapphire substrate
From Predeep (2011)

Another type of defect found in GaN films is nanopipes (Predeep 2011). This defect has the character of open core screw dislocation (Lazar, Weyher et al. 2004). The oxygen impurity is considered to be closely linked with the formation of this defect by poisoning the exposed facet walls thereby preventing complete layer coalescence (Lazar, Weyher et al. 2004).

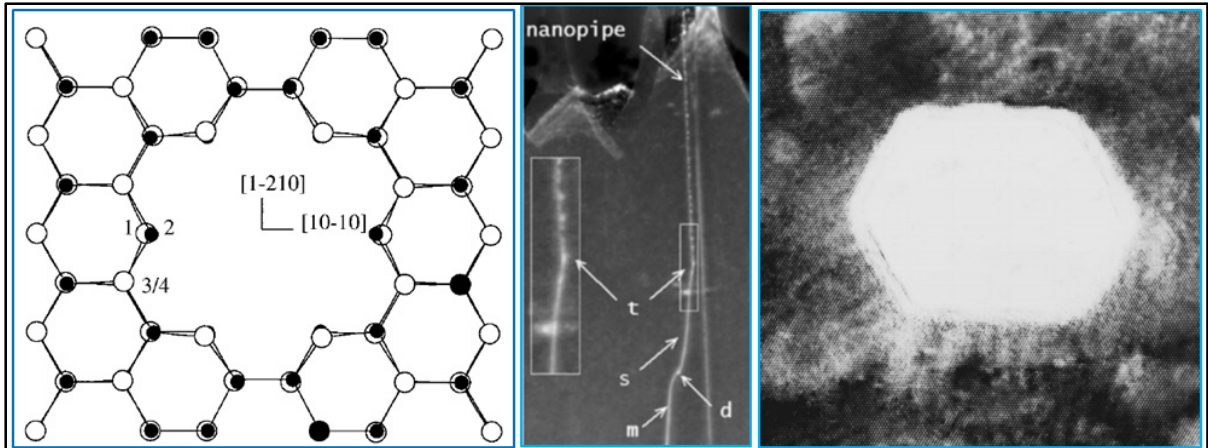


Figure 1.15 Schematic view of the formation of a nanopipe (Left) Fresnel contrast images of a nanopipe in two beam condition (center) Atomic resolution TEM image of a nanopipe (right)

From Lazar, Weyher et al. (2004), Qian, Rohrer et al. (1995)

When a film is grown on a substrate of different lattice constant, the film will expand (tensile strain) or contract (compressive strain) to accommodate the different lattice constant of the substrate (Predeep 2011). The type of strain which the film will be subjected to depends on whether the lattice constant is larger or smaller than that of the substrate. If the lattice constant of the film is larger than that of the substrate, the film will be subjected to compressive strain but if the lattice constant of the film is smaller than that of the substrate, the film will be under tensile strain.

The thermal expansion coefficient describes the change in length (linear thermal expansion coefficient) or volume (volume thermal expansion coefficient) of a material (Predeep 2011). When a sample is cooled down after growth, a difference in the thermal expansion coefficient between substrate and film may cause strain to develop, to a degree dependent on the cool down procedure and if any defect formed during the cool-down is not sufficient to

cause complete relaxation. Buffer traps refers to the deep levels located in the interface between the buffer layer and the substrate. Under high electric field condition, due to high drain-source voltage, electrons moving in the 2DEG channel could get injected into the buffer traps. Due to the longer trapping time constant, the trapped electrons cannot follow the high frequency signal and hence, they are not available for conduction. The trapped electrons produce a negative charge, which depletes the 2DEG, and therefore reduce the channel current. This reduction in the current under RF operation is called current dispersion, or more precisely, buffer traps induced current dispersion. These traps are primarily related to the existing large number of threading dislocation in the GaN layer due to the large lattice mismatch between the GaN and the substrate (Anouar 2006).

Another source of traps is the buffer compensation process to obtain high insulating material. Availability of background electron concentration in the buffer material due to native shallow donors cannot be avoided. These donors are mostly compensated by adding deep acceptors. This leakage current deteriorates the pinch-off characteristic of the device (Anouar 2006).

The kink effect in the DC characteristic can be assumed as a signature of buffer trapping effect. This effect is attributed to hot electrons injected into the buffer traps under the influence of high drain voltage. These trapped electrons deplete the 2DEG and result in a reduction of the drain current for subsequent V_{ds} traces (Anouar 2006).

1.3 Scattering functions

Scattering parameters are called this way because they relate incident and scattered travelling voltage waves at the signal ports, thereby completely describing the behavior of a microwave device (Guoquan 2008).

1.3.1 Small-signal S-parameters

Since the early 70's S-parameters have revolutionized the microwave industry (Belevitch 1962, Van Valkenburg 1974, Pozar 1990). One of the main reasons is that they are efficient.

That is because S-parameters completely and accurately describe the four main small-signal characteristics of any two-port device: transmission (S_{21}), output match (S_{22}), isolation (S_{12}) and input match (S_{11}) (Jan Verspecht 2005).

The measurement of small-signal S-parameter is perhaps the most common and useful way to provide a linear description of a circuit and its frequency response (Peter H.Aaen 2007). S-parameter measurements are fundamental to the development of linear models and they are often divided into two broad categories by the type of component measured: active or passive. The basic distinction is that active components require the injection of a DC component in addition to the RF signal that is used to determine the frequency-dependent S-parameters.

Although a network may have any number of ports, network parameters can be explained most easily by considering a network with only two ports, an input port and an output port, like the network shown in Figure 1.16.

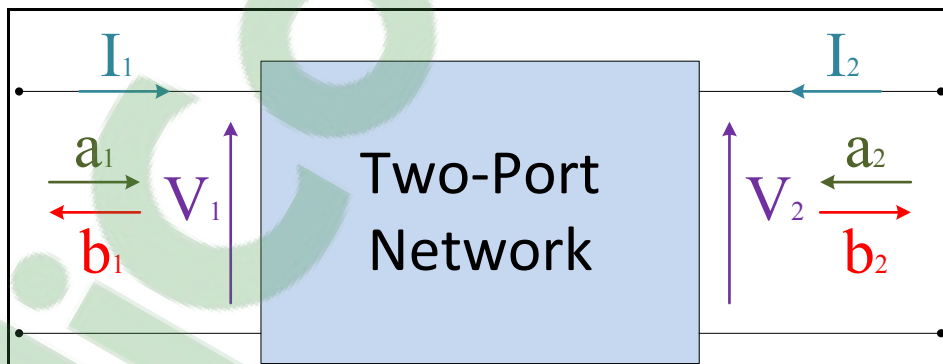


Figure 1.16 General Two-port network showing incident waves (a_1, a_2) and reflected waves (b_1, b_2) used in S-parameters definitions

The ease with which scattering parameters can be measured makes them well suited for describing systems (Packard 1995). Measuring most impedance and admittance parameters calls for the input and output of the device to be successively opened and short circuited.

This can be hard to do, especially at RF frequencies where lead inductance and capacitance make short and open circuits difficult to obtain (Packard 1995).

S-parameters, on the other hand, are usually measured with the device embedded between a 50 Ω load and source, and there is very little chance for oscillations to occur. Another important advantage of S-parameters stems from the fact that traveling waves do not vary in magnitude at points along a lossless transmission line (Packard 1995).

S-parameters describe the interrelationships of a new set of variables (a_i , b_i) (Packard 1995). The variables a_i and b_i are normalized complex voltage waves incident on and reflected from the i^{th} port of the network. They are defined, respectively in (1.1) and (1.2), in terms of the terminal voltage V_i , the terminal current I_i , and an arbitrary reference impedance Z_i , where the asterisk denotes the complex conjugate:

$$a_i = \frac{V_i + Z_i I_i}{2\sqrt{|\text{real}(Z_i)|}} \quad (1.1)$$

$$b_i = \frac{V_i - Z_i^* I_i}{2\sqrt{|\text{real}(Z_i)|}} \quad (1.2)$$

The two-Port network is then described by the matrix form in (1.3) (Gonzalez 1997). The term $S_{11}a_1$ represents the contribution to the reflected waves b_1 due to the incident wave a_1 at port 1. Similarly, $S_{12}a_2$ represents the contribution to the reflected wave b_1 due to the incident wave a_2 at port 2 and so on (Gonzalez 1997).

$$\begin{bmatrix} b_1 \\ b_2 \end{bmatrix} = \begin{bmatrix} S_{11} & S_{12} \\ S_{21} & S_{22} \end{bmatrix} \begin{bmatrix} a_1 \\ a_2 \end{bmatrix} \quad (1.3)$$

S-parameters enable the general response of a linear network to an arbitrary input signal to be computed by superposition of the responses to unit stimuli (Root, Verspecht et al. 2013). Superposition enables great simplifications in analysis and measurement. Superposition is the

reason S-parameters can be measured by independent experiments with one sinusoidal stimulus at a time, one stimulus per port per frequency. The general response to any set of input signals can be obtained by superposition (Root, Verspecht et al. 2013).

Time invariance is a property of common linear and nonlinear components (Root, Verspecht et al. 2013). A DUT description in terms of S-parameters naturally embodies time invariance principle. Time invariance states that if $y(t)$ is the DUT response to an excitation $x(t)$, the DUT response to the time-shifted excitation $x(t-T)$, must be $y(t-T)$ (Root, Verspecht et al. 2013).

S-parameters are still commonly used for nonlinear devices (Root, Verspecht et al. 2013). The problem is that S-parameters only describe properly the behavior of a nonlinear component in response to small-signal stimuli. That is, only when the nonlinear device is assumed to depend linearly on all RF components of the incident signals is the S-parameter paradigm valid. S-parameters contain no information about how a nonlinear component generates distortion (Root, Verspecht et al. 2013).

1.3.2 Large-Signal S-Parameters

S-parameters have one significant drawback: they are only valid under linear operating conditions (Verspecht 2005). They cannot be used to describe nonlinear distortions that are challenging today's amplifier designers like compression, AM-PM conversion and spectral regrowth.

The idea of hot S-parameters or large signal S-parameters is to put the DUT under realistic operating conditions by applying the appropriate large-signal stimulus signal. The applied signal is a one-tone signal or a modulated carrier (Jan Verspecht 2005). While this signal is being applied one injects a small one-tone signal first into the DUT signal port 1, this is called the forward measurement, and next in signal port 2, this is called the reverse measurement.

Each time one measures the injected signal, which are called the a-waves, and the corresponding reflected waves, which are called the b-waves. Just as it is done with small signal S-parameters, the hot S-parameters are defined as the ratios between the incident a-waves and the reflected b-waves. This process is illustrated in Figure 1.17 and Figure 1.18. Figure 1.17 illustrates the spectrum of the incident a-waves and the scattered b-waves during the forward hot S-parameter measurements and Figure 1.18 illustrates the spectra of the incident a-waves and the scattered b-waves during a reverse hot S-parameters measurement. The large signal carrier is applied at a frequency f_c , and f_s denotes the frequency at which the hot S-parameters are being measured. The large signal carrier at frequency f_c is always present in the a-wave that is incident to the input port of the DUT (a_1), the small signal, the so called probe tone, is present in the a_1 wave during the forward measurement and is present in the a_2 -wave during the reverse measurement.

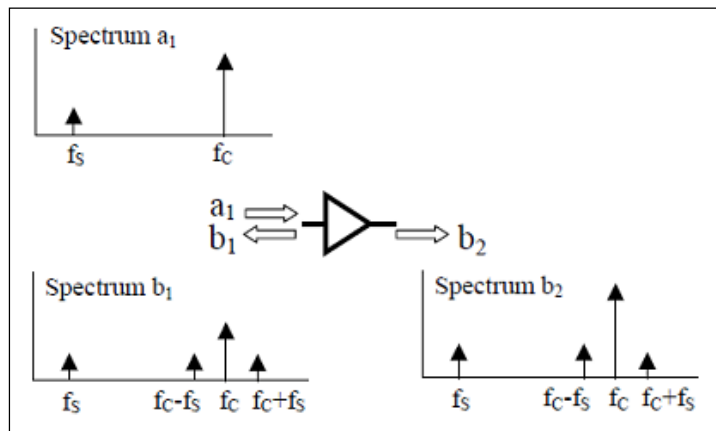


Figure 1.17 Forward measurement of hot S-parameters
From Jan Verspecht (2005)

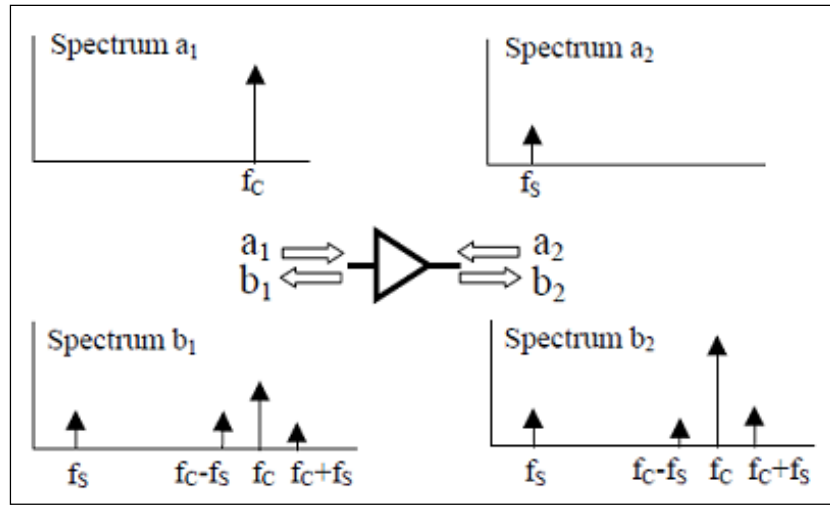


Figure 1.18 Reverse measurement
of hot S-parameters
From Jan Verspecht (2005)

The hot S-parameters are defined by taking the ratio's between the b-waves and the a-waves at the frequency f_s in a way identical to classic small signal S-parameters. The definition of hot S-parameters is given by (1.4), (1.5), (1.6) and (1.7).

$$hotS_{11} = \left. \frac{b_1(f_s)}{a_1(f_s)} \right|_{forward} \quad (1.4)$$

$$hotS_{21} = \left. \frac{b_2(f_s)}{a_1(f_s)} \right|_{forward} \quad (1.5)$$

$$hotS_{12} = \left. \frac{b_1(f_s)}{a_2(f_s)} \right|_{reverse} \quad (1.6)$$

$$hotS_{22} = \left. \frac{b_2(f_s)}{a_2(f_s)} \right|_{reverse} \quad (1.7)$$

Large-signal S-parameters is an attempt to generalize S-parameters to the nonlinear domain. The measurement of hot S-parameters appears non-repeatable and unable to make predictable design interferences from such measurements or simulations. Hot S-parameters measurements are incomplete, insufficient, and ultimately inaccurate measurement approach (Root, Verspecht et al. 2013).

1.3.3 Large-Signal X-Parameters

X-parameters are mathematically rigorous supersets of S-parameters, applicable to nonlinear and linear components under both large-signal and small-signal conditions (Verspecht 2005). X-parameters include the magnitude and phase characteristics of device-generated spectral components corresponding to distortion, which can include harmonics and intermodulation products, in addition to those spectral components present in the incident signal. X-parameters represent both the nonlinear characteristics of the DUT due to a large-signal stimulus, and also the spectrally linearized response around the large-signal state of the system to additional injected signals, that now depends nonlinearly on the DUT operating conditions that are determined by the large-signal excitation. X-parameters can be used to calculate the effects of mismatch at fundamental and harmonic frequencies, and correctly predict effects of source harmonics on DUT response.

For a given DUT, determine the set of multivariate complex functions $F_{pm}(\cdot)$ that correlate all of the relevant input spectral components a_{qn} with the output spectral components B_{pm} , whereby q and p range from one to the number of signal ports, and whereby m and n range from zero to the highest harmonic index. This is mathematically expressed as in (1.8).

$$b_{pm} = F_{pm}(a_{11}, a_{12}, \dots, a_{21}, a_{22}, \dots) \quad (1.8)$$

The functions $F_{pm}(\cdot)$ are called the describing functions. The concept is illustrated in Figure 1.19.

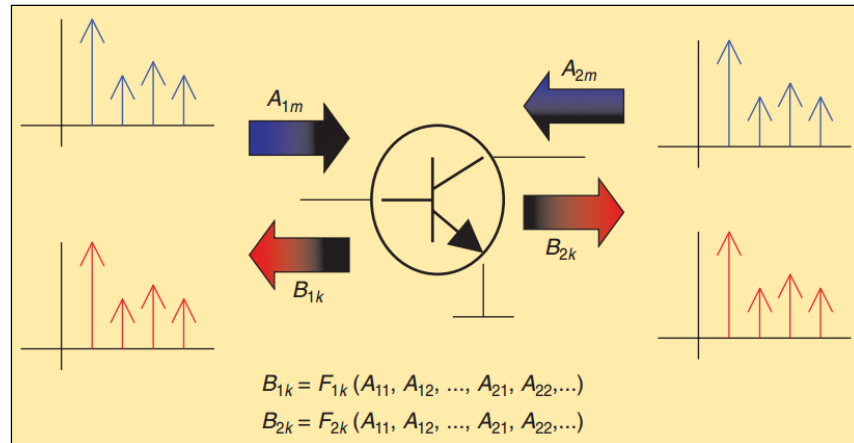


Figure 1.19 The concept of nonlinear
describing functions
From Jan Verspecht (1996)

Under large-signal and nonlinear operating conditions, the superposition principle is not valid. In power amplifier case, there is only one dominant large-signal input component present (A_{11}) whereas all other input harmonic frequency components are relatively small. In that case, we will be able to use the harmonic superposition principle.

The function $F_{pm}(\cdot)$ is linearized around a stable single-valued and continuous operating point by writing the travelling voltage wave vectors A and B as $A = A_0 + a$ and $B = B_0 + b$ where B_0 is the large-signal steady-state response to the large steady-state excitation A_0 , and b is the response to a small excitation signal a superimposed on A_0 (Verspecht, Williams et al. 2005).

The scattering function F describing the electrical behavior of a weakly nonlinear device is generally not analytic, so, even in the weakly nonlinear case, we cannot relate A and B , or even a and b , with linear scattering-parameter matrices.

The derivation of X-parameters is based on the Taylor series. For a single variable Taylor series, let f be an infinitely differentiable function in some open interval around $x = a$:

$$f(x) = \sum_{k=0}^{\infty} \frac{f^{(k)}(a)}{k!} (x-a)^k = f(a) + f'(a)(x-a) + \frac{f''(a)}{2!} (x-a)^2 + \dots \quad (1.9)$$

The linear approximation in one variable case takes the constant and linear terms from the Taylor series. In an open interval around $x = a$.

$$f(x) = \sum_{k=0}^{\infty} \frac{f^{(k)}(a)}{k!} (x-a)^k = f(a) + f'(a)(x-a) \quad (1.10)$$

For a multi-variable Taylor series, let f be an infinitely differentiable function in some open neighborhood around $(x, y) = (a, b)$:

$$f(x, y) = f(a, b) + f_x(a, b)(x-a) + f_y(a, b)(y-b) + \frac{1}{2!} \left[f_{xx}(a, b)(x-a)^2 + 2f_{xy}(a, b)(x-a)(y-b) + f_{yy}(a, b)(y-b)^2 \right] \quad (1.11)$$

where $f_x = \frac{\partial f}{\partial x}$, $f_y = \frac{\partial f}{\partial y}$, $f_{xy} = \frac{\partial^2 f}{\partial x \partial y}$, $f_{xx} = \frac{\partial^2 f}{\partial x \partial x}$, $f_{yy} = \frac{\partial^2 f}{\partial y \partial y}$. A more compact form, let's define $[X] = [x, y]^T$ and let's $[A] = [a, b]^T$. Therefore, the Taylor series can be written as

$$[f([X])] = [f([A])] + \nabla[f]([A])[X - A] + [X - A]^T [H]([A])[X - A] + \dots \quad (1.12)$$

Where $\nabla[f]$ and H are the gradient or the jacobian of the multi-variable function and the hessian matrix respectively. The linear approximation is:

$$[f([X])] \approx [f([A])] + \nabla[f]([A])[X - A] \quad (1.13)$$

The Taylor series can be applied to nonlinear circuit characterization and modeling. Let's set the vector $[A]$ composed by the incident waves and the vector $[B]$ composed by the reflected waves. The vector $[A]$ can be written as a sum of large steady state excitation $[A_0]$ with a small excitation signal $[a] = [\text{Re}(a), \text{Im}(a)]^T$ composed by the real and imaginary parts of small excitation incident waves. Therefore the vector $[B]$ can be approximated by:

$$[B] = [F([A])] = [F([A_0])] + \nabla[F]([A_0])[a] \quad (1.14)$$

The gradient or the jacobian can be written as:

$$\nabla[F]([A_0]) = \begin{bmatrix} [J_{RR}([A_0])] & [J_{RI}([A_0])] \\ [J_{IR}([A_0])] & [J_{II}([A_0])] \end{bmatrix} \quad (1.15)$$

Equation (1.14) can be rewritten as:

$$[B] = [F([A])] = [F([A_0])] + \begin{bmatrix} [J_{RR}([A_0])] & [J_{RI}([A_0])] \\ [J_{IR}([A_0])] & [J_{II}([A_0])] \end{bmatrix} \begin{bmatrix} [\text{Re}(a)] \\ [\text{Im}(a)] \end{bmatrix} \quad (1.16)$$

If we set $[S] = \frac{1}{2}([J_{RR}] + [J_{II}] + j([J_{IR}] - [J_{RI}]))$ and $[T] = \frac{1}{2}([J_{RR}] - [J_{II}] + j([J_{IR}] + [J_{RI}]))$

, equation (1.16) is equivalent to :

$$[B] = [F([A_0])] + [S([A_0])[a] + [T([A_0])][a^*]] \quad (1.17)$$

As a device enters its nonlinear regime of operation, the elements of the scattering matrix relating different frequencies to each other will become nonzero. In addition, even weakly nonlinear devices usually create mixing products at both sum and difference frequencies of the input signals. Mixing products that include a difference frequency are particularly problematic, as increasing the phase or frequency of an input signal can result in a decrease in the phase or frequency of an output signal. This behaviour will be described by the matrix $[T]$. This extra degree of freedom is required to complete the linearization, and it allows the linearization to apply to all first-order mixing products generated by a weakly nonlinear device.

In the case where large steady state excitation $[A_0] = [a_{11}]$, thus the small excitation vector is $[a] = [a_{12}, a_{13}, \dots, a_{21}, a_{22}, a_{23}, \dots]^T$. The vector of the scattered voltage waves $[B] = [b_{11}, b_{12}, b_{13}, \dots, b_{21}, b_{22}, b_{23}, \dots]^T$ is:

$$[B] = [F(a_{11})] + [S(a_{11})][a] + [T(a_{11})][a^*] \quad (1.18)$$

The vector $[F(a_{11})]$ can be set as $[X_{11}^F(|a_{11}|), X_{12}^F(|a_{11}|), \dots, X_{21}^F(|a_{11}|), X_{22}^F(|a_{11}|), \dots]^T$. The matrices $[S(a_{11})]$ and $[T(a_{11})]$ can be set as :

$$[S(a_{11})] = \begin{bmatrix} X_{11,12}^S(a_{11}) & \cdots & X_{11,23}^S(a_{11}) \\ \vdots & \ddots & \vdots \\ X_{23,12}^S(a_{11}) & \cdots & X_{23,23}^S(a_{11}) \end{bmatrix} \quad (1.19)$$

$$[T(a_{11})] = \begin{bmatrix} X_{11,12}^T(a_{11}) & \cdots & X_{11,23}^T(a_{11}) \\ \vdots & \ddots & \vdots \\ X_{23,12}^T(a_{11}) & \cdots & X_{23,23}^T(a_{11}) \end{bmatrix} \quad (1.20)$$

Therefore, the expression of the scattered voltage wave at port p and at mth harmonic index is:

$$b_{pm} = X_{pm}^F(|a_{11}|) + \sum_{(j,l) \neq (1,1)} X_{pm,jl}^S(|a_{11}|) a_{jl} + \sum_{(j,l) \neq (1,1)} X_{pm,jl}^T(|a_{11}|) a_{jl}^* \quad (1.21)$$

Time invariance is a property of common linear and nonlinear components such as inductors capacitors, resistors, diodes and transistors (Root, Verspecht et al. 2013). Time invariance states that if $y(t)$ is the DUT response to an excitation $x(t)$, the DUT response to the time-shifted excitation, $x(t-\tau)$, must be $y(t-\tau)$. In the frequency domain, the delayed version of the response can be expressed as:

$$b_{pm} e^{-j\omega_m \tau} = F_{pm}(a_{11} e^{-j\omega_1 \tau}, a_{12} e^{-j\omega_2 \tau}, \dots, a_{21} e^{-j\omega_1 \tau}, a_{22} e^{-j\omega_2 \tau}, \dots) \quad (1.22)$$

By applying the time invariance principle, equation (1.22) is equivalent to:

$$F_{pm}(a_{11} e^{-j\omega_1 \tau}, a_{12} (e^{-j\omega_1 \tau})^2, \dots, a_{21} e^{-j\omega_1 \tau}, a_{22} (e^{-j\omega_1 \tau})^2, \dots) = F_{pm}(a_{11}, a_{12}, \dots, a_{21}, a_{22}, \dots) e^{-j\omega_m \tau} \quad (1.23)$$

This property can now be used to separate the dependence on the magnitude and phase of the fundamental frequency:

$$F_{pm}(a_{11}, a_{12}, \dots, a_{21}, a_{22}, \dots) = F_{pm}(|a_{11}|, a_{12} P^{-2}, \dots, a_{21} P^{-1}, a_{22} P^{-2}, \dots) P^m \quad (1.24)$$

where $P = e^{j \text{phase}(a_{11})}$,

Therefore, equation (1.24) can be rewritten as:

$$b_{pm} = X_{pm}^F(|a_{11}|)P^{+m} + \sum_{(j,l) \neq (1,1)} X_{pm,jl}^S(|a_{11}|)P^{m-l} a_{jl} + \sum_{(j,l) \neq (1,1)} X_{pm,jl}^T(|a_{11}|)P^{m+l} a_{jl}^* \quad (1.25)$$

For expression uniformity purposes, the expression of the scattered voltage wave at port p and at mth harmonic index can also be written as:

$$b_{pm} = F_{pm}(|a_{11}|)P^{+m} + \sum_{(j,l) \neq (1,1)} S_{pm,jl}(|a_{11}|)P^{m-l} a_{jl} + T_{pm,jl}(|a_{11}|)P^{m+l} a_{jl}^* \quad (1.26)$$

where $X_{pm}^F = F_{pm}$, $X_{pm,jl}^S = S_{pm,jl}$ and $X_{pm,jl}^T = T_{pm,jl}$.

The X-Power network analyzer which is developed by Agilent is illustrated in Figure 1.20. It measures X-parameters about a single-tone LSOP (technologies 2008). This is achieved by stimulating the DUT with a single large tone at port 1 and, while continuing to apply the large tone, injecting additional small tones at both ports 1 and 2 at all harmonics of interest. At least two phase-offset small tones must be injected at each port/frequency of interest in order to extract the corresponding X-parameters. All resulting waves are measured for each stimulus, and the X-parameters are solved for directly (if only two phases are used) or using regression (in the case of 3 or more phases).

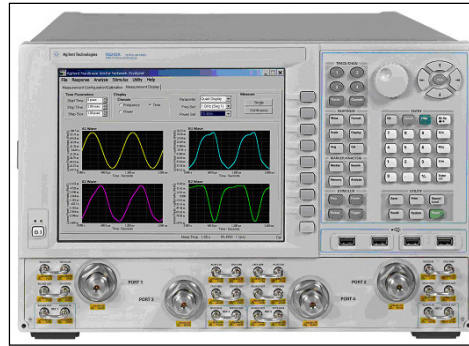


Figure 1.20 Agilent X-PNA's product
From Agilent (2008)

The software Advanced Design System which is developed by Agilent provides access to X-Parameter Generator parameters enabling to define aspects of the simulation. Using the X-Parameter Generator from the 'Simulation-X_Param' palette enables to obtain the X-parameters of a component, circuit, or subnetwork (technologies 2009). The extracted X-parameter data can be used as a behavioral model in simulation by using the XnP component. In the Simulation-X_Param palette, we can find XP term components such as XP_Bias applied to DC ports, XP_Source to large signal input ports, and XP_Load to outputs. A snapshot taken from ADS showing the 'Simulation-X_Param' palette is illustrated in Figure 1.21.



Figure 1.21 Simulation-X_Param' palette Agilent
From Agilent (2009)

1.4 Active device modeling

Active device models are classified to physic-based, empirical analytic and table-based models (Von 2007).

1.4.1 Physical modeling

The physics of operation of a given transistor are best described using a physical model simulation, in which the geometry, topography, and the material properties of the semiconductors, metals, and insulators that form the transistor are captured in the model description in the simulator. The physical model simulation describing the semiconductor equations and device geometry can be coupled with a thermal model describing the heat transfer in the transistor, and an electromagnetic simulation of the device geometry, metallization and substrate (Peter H.Aaen 2007).

In physical modeling, the nonlinear partial differential equations that describe charge distribution, charge transport, current continuity in the transistor structure are solved in the simulator (Peter H.Aaen 2007). As the transistor geometries become smaller, quantum-mechanical effects also need to be incorporated into the solution. In the simulation, the transistor geometry is discretized in two or three dimensions. This requires complex solution techniques to be used, such as finite-difference and finite-elements methods.

The solution of these equations takes a long time, and the accuracy of the solution depends on how well the physical properties and dimensions of the device are estimated, on the approximations used in the fundamental semiconductor equations and on the numerical techniques applied in the solution of the system of equations (Peter H.Aaen 2007).

These modeling techniques have been applied successfully to the technology development cycle for new generations of transistors. Physical model simulations can be used to generate DC I-V characteristics and bias-dependant S-parameter data directly from the simulation.

These data can then be used to assess how the physical and geometrical design of the transistor needs to be adjusted to improve the device RF performance (Peter H.Aaen 2007).

The advantage of this modeling method is the accurate device description for any operating range using extrapolation based on the physical behavior of the device. Since physical models are very complex and require a long simulation time, this modeling approach is not appropriate for the circuit design purpose. The other problem of this model type is the availability of the physical material parameters, since the acquisition of such data requires sophisticated device measurement systems. Mostly, this kind of model is used to model devices of a small size in order to investigate the quality of a device process for the development and improvement of device performance (Von 2007).

1.4.2 Table-based model

Table-based models describe the response of a network upon the incoming signal in form of current and voltage based on measured data (Von 2007). The continuity of the description can be derived using spline interpolation between the measurement points. On the one hand, this modeling approach presented by Root (Root and Fan 1992) offers the flexibility to describe the device behavior in regions where physical or empirical models fail to fit the measurement data due to fixed, predefined equations. On the other hand, understanding of the device is limited with this kind of model at the boundaries of the I-V characteristic unlike the case with physical or empirical models (Von 2007).

Measurement based models use characterization techniques such as S parameters and pulsed I-V data (Von 2007). These techniques are the most common and provide improved large-signal simulation accuracy because the model nonlinearities are constructed from measurements that emulate actual device application.

In general, the first step is the definition of the equivalent circuit topology of the device. This is necessary as the circuit simulators solve equations based on Kirchhoff's current and

voltage laws (Von 2007). The equivalent circuit models are derived with careful consideration of the physical layout of the device for the small-signal equivalent circuit. The measurement data must be processed to extract the linear and nonlinear model elements of the equivalent circuit. There are basically two ways to make use of the processed data in a nonlinear simulator. The intrinsic large-signal model elements may be approximated by standard analytical functions or can be implemented in table form, which can then be interpolated and/or extrapolated.

1.4.3 Compact Models

Generally, compact models are equivalent circuit representations of the transistor. The electrical measurements that are performed during the characterization of the transistor can be mapped directly onto a network of circuit components. The values of the equivalent circuit parameters are extracted directly from the DC I-V and S-parameters measurements. After de-embedding the extrinsic components, this yields an equivalent circuit containing conductance and susceptance components that can be readily incorporated into the circuit simulator (Peter H.Aaen 2007).

The extraction of the equivalent circuit parameter values can be carried out over a range of bias voltage (V_{gs}, V_{ds}), and the values can be stored in a table indexed by the bias, using interpolation to find the required component values for the given bias voltage, to produce a bias-dependent linear transistor model. The equivalent circuit parameter values can be fitted with parameterized functions of the bias voltages, and the model extraction consists of finding these function parameters for each of the circuit elements in the model (Peter H.Aaen 2007).

The intrinsic large-signal model is quasi-static. In other words, the model can describe the transistor's RF frequency dependence through the various reactive components in the model, such as the intrinsic capacitances at the gate and drain of the device, and the extrinsic

inductance and capacitance associated with the manifold and extrinsic parts of the transistor (Peter H.Aaen 2007).

The effects of the self heating and traps can be seen in the DC $I_d - V_{ds}$ characteristics, so we need to add parameters or components to describe these frequency dispersive effects, to complete the model of the active transistor. A sub-circuit describing the thermal environment can be added to the quasi-static electrical model so that the effects of both the static or ambient temperature as well as the dynamic electro-thermal behaviour are accounted for in a consistent manner. We use a similar approach to accommodate trapping effects into the model (Peter H.Aaen 2007).

The separation of extrinsic and intrinsic parts of the transistor in electrical terms is perhaps not so clear cut (Peter H.Aaen 2007). A very common way to partition the overall model is to define the extrinsic shell to be only the linear components and the intrinsic region to be the nonlinear part of the model.

The manifolds at the gate and the drain are physically large structures and they have both frequency and spatial dependence of their transmission characteristics (Peter H.Aaen 2007). The frequency-dispersive property can be used as the basis of the partition between the manifold structure and the extrinsic shell. The lumped components that comprise the extrinsic equivalent circuit-capacitors, inductors, and resistors should be independent of frequency. After parameter extraction, if any of these components does show significant frequency dependence, then the partition between the extrinsic and manifold shells may be incorrectly located. A frequency-dependent component may also be an indicator that our extrinsic circuit is incorrect, and perhaps a different topology is required to represent the extrinsic shell of the transistor over the desired bandwidth.

The metal manifold can be represented in the model in different ways, depending on its size and the frequency of interest (Peter H.Aaen 2007). If the frequency of operation is low enough, or the manifold is small enough, it can be represented simply by a capacitance to

ground. At higher frequencies, or for very large structures, the metal manifold is represented by a transmission line model.

After de-embedding the manifold and bond-pad structures, we now need to determine and extract the extrinsic circuit components, to get access to the intrinsic transistor reference plane (Peter H.Aaen 2007). Once we have de-embedded the extrinsic circuit components, the small-signal equivalent circuit parameters can be obtained by direct manipulation of the intrinsic plane S-parameter data.

When we build our model in the simulator, we will use the terminal voltages as the control inputs to the model (Peter H.Aaen 2007). By this statement, we mean that the electrical effects of the extrinsic components, manifolds, and so on, have been removed, and the measurement reference planes now lie at the intrinsic device plane. When we construct the complete model, we can, if necessary, re-reference the voltages and currents to the transistor's external terminals. Isothermal conditions can be achieved by taking carefully controlled pulse measurements or by using some means of thermal de-embedding.

Once we have constructed our large-signal, nonlinear, isothermal model for the intrinsic transistor, we will add the dispersive effects to create a non-quasi-static model (Peter H.Aaen 2007). These dispersive effects include electron trapping effects and thermal effects. The thermal effects include the static thermal influence due to ambient temperature, and the dynamic effects of the electrical power that is dissipated as heat.

1.5 A large-signal modeling example

The separation of a circuit-level transistor model into intrinsic and extrinsic parts is an idealization that simplifies the treatment of an otherwise very complicated device (Dominique schreurs , Aflaki, Negra et al. 2009, Jarndal, Markos et al. 2011, Root, Verspecht et al. 2013). Conceptually, the intrinsic model describes the dominant nonlinearities of the transistor that occur in the active region, inside the feed networks, manifolds, and other

parasitic particularities of the layout. Parasitic elements are usually modeled with simple circuit elements whose parameter values do not change with bias. The parasitic elements that make up the extrinsic model are usually associated with capacitive coupling between the electrodes, and inductance and resistance of feed structures and manifold metallization, dependent on the device layout (Vandamme, Schreurs et al. 2001, Rudolph, Fager et al. 2012). The model is constructed by first determining the parasitic elements (Jarndal, Bunz et al. 2006) and then de-embedding the extrinsic network to isolate the intrinsic part. Thus, careful attention to the extrinsic model elements is required for accurate transistor modelling (Rudolph, Fager et al. 2012). There are several techniques for determining the extrinsic parameters (Laredj, Degachi et al. 2011). A three-step de-embedding technique, which is the most recent, was proposed by (Cho and Burk 1991, Vandamme, Schreurs et al. 2001, Siti, Mohd et al. 2009). This technique requires four on-wafer de-embedding structures, namely, open, short1, short2 and thru. In this section, we present a new simpler technique based on only two de-embedding GaN structures: open and short-thru structures (Essaadali, Kouki et al. 2015).

1.5.1 Extrinsic parameter extraction using two step de-embedding structures

The small-signal equivalent circuit model, shown in Figure 1.22 has been used to simulate the small signal characteristics of on-wafer GaN HEMT on silicon (Si) substrate (Jarndal, Markos et al. 2011). In the extrinsic part of this model, C_{pg} and C_{pd} account for parasitic capacitances due to the pad connections, inter-electrode and crossover capacitances between gate, source and drain which is due to air-bridge source connections. R_g , R_d , and R_s represent contact and semiconductor bulk resistances; while L_g , L_d , and L_s model the effects of metallization inductances. To take into account the significant substrate/buffer loading effect of this device (Jarndal, Essaadali et al. 2016), shunt RC circuits are added to represent this extra parasitic effect. These are R_{gg} and C_{gg} (respectively R_{dd} and C_{dd}) which describe the parasitic conduction and fringing capacitance between gate and source (respectively drain and source) electrodes via the buffer layer or the substrate (Jarndal, Essaadali et al. 2016).

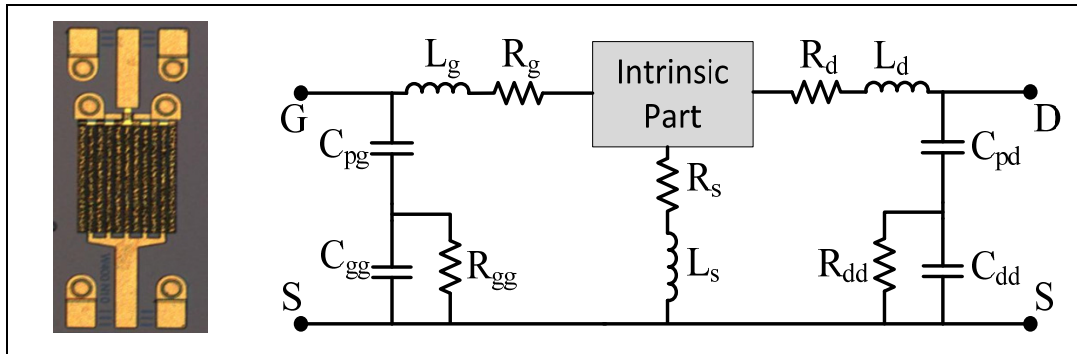


Figure 1.22 A photograph of 200x10 μ m GaN HEMT on Si Substrate (Left) and its equivalent circuit model (Right)
From Essaadali (2015)

This new extraction technique requires only open and short-thru structures. The layout of the GaN open de-embedding structure corresponding to a 2mm GaN transistor being and its equivalent circuit model are shown in Figure 1.23. The Open structure which makes no connection between the gate and the source is used to de-embed the extrinsic shunt impedance. The short-thru structure connects the two RF test ports of gate and drain together to the source through a common via. This structure is used to extract source, drain and gate series impedance. Its layout and its equivalent circuit model are shown in Figure 1.24.

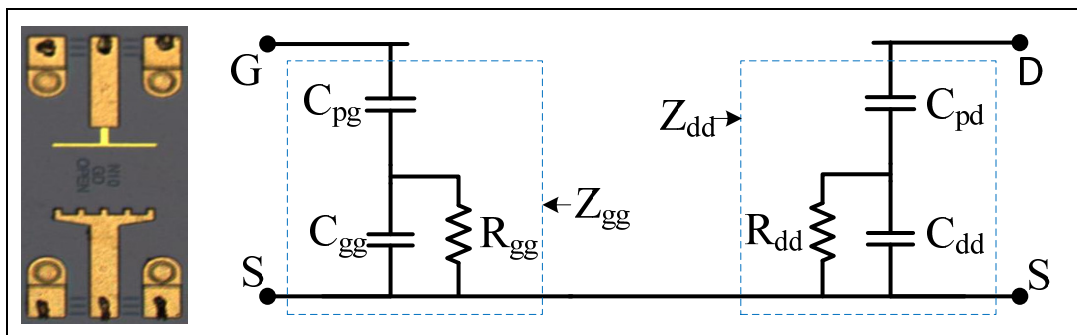


Figure 1.23 On-wafer GaN Open de-embedding structure for a 2mm GaN HEMT (Left) and its equivalent circuit model (Right)
From Essaadali (2015)

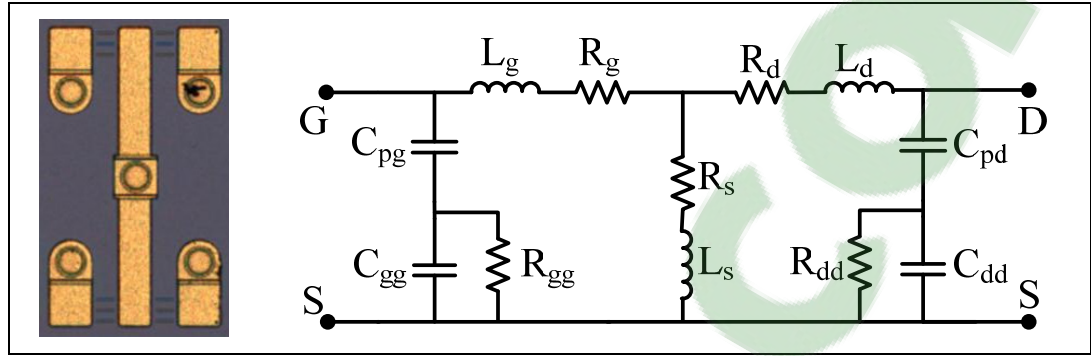


Figure 1.24 On-wafer GaN short-through de-embedding structure for a 2mm GaN HEMT (Left) and its equivalent circuit model (Right)
From Essaadali (2015)

The gate-source and drain-source impedance expressions of the circuit of Figure 1.23 are given by:

$$Z_{gg} = 1/j\omega C_{gp} + R_{gg} / (1 + j\omega C_{gg} R_{gg}). \quad (1.27)$$

$$Z_{dd} = 1/j\omega C_{dp} + R_{dd} / (1 + j\omega C_{dd} R_{dd}). \quad (1.28)$$

The extrinsic elements R_{gg} and R_{dd} can be extracted from the above impedances expressions. Their values can be determined by the extrapolation of real part of Z_{gg} , $\text{Real}(Z_{gg})$ and real part of Z_{dd} , $\text{Real}(Z_{dd})$, at $\omega=0$, as shown in Figure 1.25, the accuracy of the method depends on the extrapolation technique used. Another approach more accurate is to extract R_{gg} and R_{dd} from the slope of the curve of $1/(\omega^2 \text{real}(Z_{gg}))$ ($1/(\omega^2 \text{real}(Z_{dd}))$) versus $1/\omega^2$. The expressions of these curves are given by:

$$1/(\omega^2 \text{real}[Z_{gg}]) = 1/R_{gg} (1/\omega^2) + R_{gg} C_{gg}^2. \quad (1.29)$$

$$1/(\omega^2 \text{real}[Z_{dd}]) = 1/R_{dd} (1/\omega^2) + R_{dd} C_{dd}^2. \quad (1.30)$$

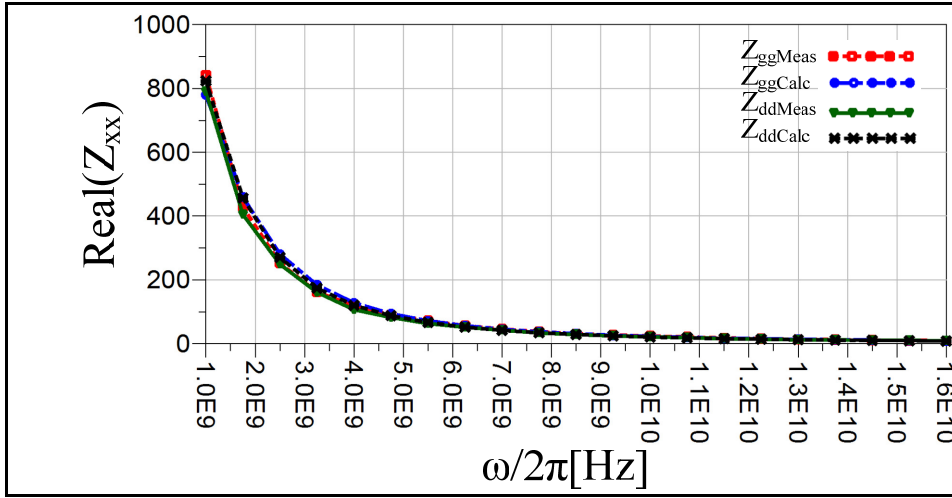


Figure 1.25 Extraction of extrinsic elements R_{gg} and R_{dd} for a 2mm GaN HEMT
From Essaadali (2015)

The inverse of the slopes are the values of parasitic resistances $R_{dd}=1350 \Omega$ and $R_{gg}=1180 \Omega$. As shown in Figure 1.26. The parasitic capacitances C_{gg} and C_{dd} can then be easily resolved using:

$$1/\text{real}[Z_{gg}] = 1/R_{gg} + R_{gg} C_{gg}^2 \omega^2. \quad (1.31)$$

$$1/\text{real}[Z_{dd}] = 1/R_{dd} + R_{dd} C_{dd}^2 \omega^2. \quad (1.32)$$

The extracted values are $C_{dd}= 0.0943 \text{ pF}$ and $C_{gg}= 0.0966 \text{ pF}$. Next, using the structure of Figure 1.23, the parasitic capacitances C_{pg} and C_{pd} can be extracted by extrapolating the equation $\text{imag}(Z_{gg})\omega$ and $\text{imag}(Z_{dd})\omega$, at $\omega = 0$, respectively. However the accuracy of the approach will depend on the extrapolation approach used. For this reason it would be better to extract their values as follows.

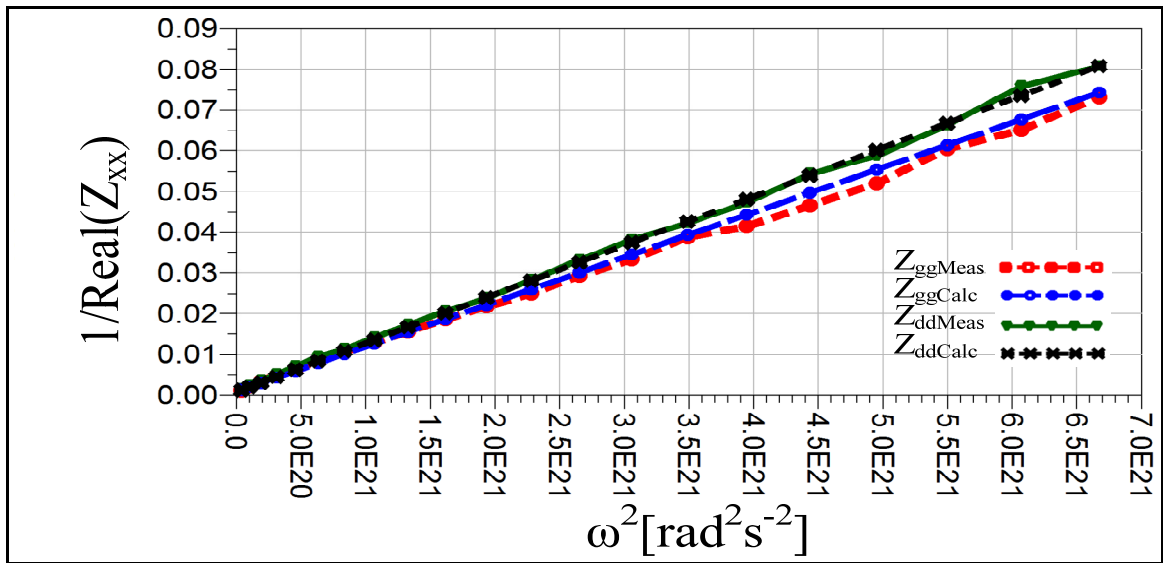


Figure 1.26 Extraction of extrinsic elements C_{gg} and C_{dd} for a 2mm GaN HEMT
From Essaadali (2015)

At higher frequency, $\text{imag}(Z_{gg})\omega$ and $\text{imag}(Z_{dd})\omega$ tend to a constant, as shown in Figure 1.27. Their limits are given by (1.33) and (1.34), respectively. Using this approach, the extracted values are found to be $C_{pg} = 0.388$ pF and $C_{pd} = 0.88$ pF.

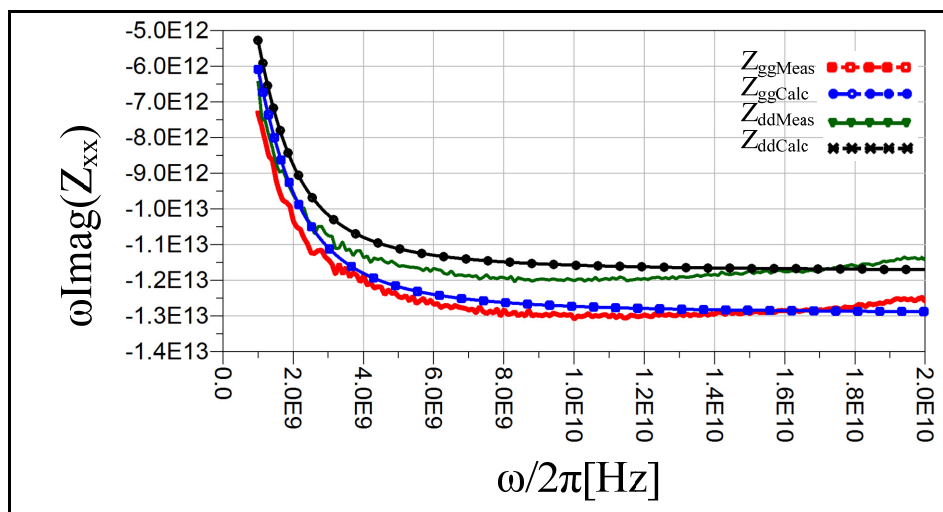


Figure 1.27 Extraction of extrinsic elements C_{pg} and C_{pd} for a 2mm GaN HEMT
From Essaadali (2015)

$$\lim_{\omega \rightarrow \infty} \text{imag}(Z_{gg})\omega = \lim_{\omega \rightarrow \infty} \frac{1}{C_{pg}} - \frac{C_{gg}R_{gg}^2\omega^2}{1 + R_{gg}^2C_{gg}^2\omega^2} = -\frac{1}{C_{pg}} - \frac{1}{C_{gg}}. \quad (1.33)$$

$$\lim_{\omega \rightarrow \infty} \text{imag}(Z_{dd})\omega = \lim_{\omega \rightarrow \infty} \frac{1}{C_{pd}} - \frac{C_{dd}R_{dd}^2\omega^2}{1 + R_{dd}^2C_{dd}^2\omega^2} = -\frac{1}{C_{pd}} - \frac{1}{C_{dd}}. \quad (1.34)$$

Next, the quantities R_s , R_d , R_g , L_s , L_d and L_g can be extracted from the short-thru structure shown in Figure 1.24. To extract the parameters in the inner T-network, de-embedding of gate and drain parasitic impedances is required. The inner Y-parameters of the T-network are given in (1.35) where the parameters $Y_{21\text{open}}$ and $Y_{12\text{open}}$ of the open structure have been neglected based on practical considerations. Thus,

$$\begin{bmatrix} Y_{11\text{inner}} & Y_{12\text{inner}} \\ Y_{21\text{inner}} & Y_{22\text{inner}} \end{bmatrix} = [Y_{\text{thru-short}}] - \begin{bmatrix} Y_{11\text{open}} & 0 \\ 0 & Y_{22\text{open}} \end{bmatrix}. \quad (1.35)$$

The resistors and inductors of the source, gate and drain are determined respectively from:

$$R_s + jL_s\omega = Z_{21\text{inner}}. \quad (1.36)$$

$$R_g + jL_g\omega = Z_{11\text{inner}} - Z_{21\text{inner}}. \quad (1.37)$$

$$R_d + jL_d\omega = Z_{22\text{inner}} - Z_{21\text{inner}}. \quad (1.38)$$

The curves of source, gate and drain resistances and inductances are shown in Figure 1.28 and Figure 1.29. The extracted values are found to be $R_s=0.01\Omega$, $R_d=0.65\Omega$, $R_g=0.7\Omega$, $L_s=20\text{pH}$, $L_d=130\text{pH}$ and $L_g=134\text{pH}$.

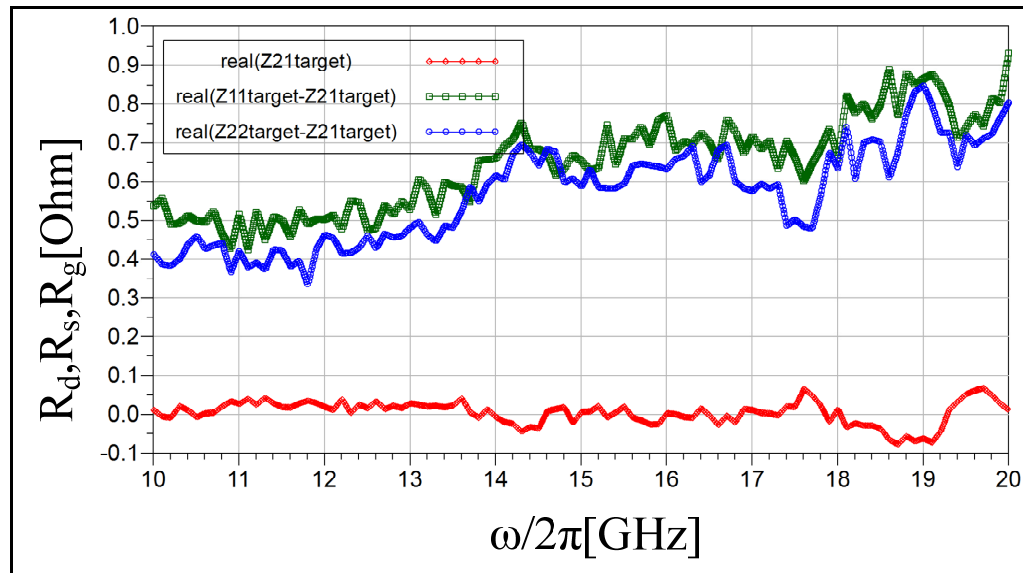


Figure 1.28 Extraction of Source, gate and drain resistances (R_s , R_g and R_d) from short-thru structure of a 2mm GaN HEMT
From Essaadali (2015)

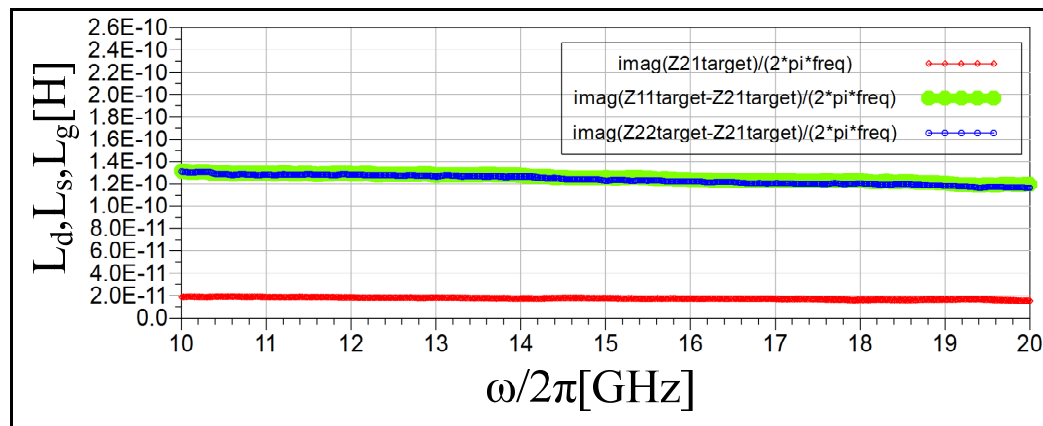


Figure 1.29 Extraction of Source, gate and drain inductors (L_s , L_g and L_d) from short-thru structures of a 2mm GaN HEMT
From Essaadali (2015)

1.5.2 Transistor small-signal modeling

After deembedding, the electrical effects of the extrinsic components, manifolds, and so on, have been removed. And the measurement reference planes lie at the intrinsic device plane. The S-parameters represent the linearized or small-signal response of the transistor at a specified bias V_{gs} , V_{ds} and frequency, ω (Essaadali, Kouki et al. 2015). This is simply the

measured and de-embedded data, which could be stored in a three dimensional table, indexed by the bias voltages and frequency. During simulation, the required S-parameters would be read by indexing, or interpolating to the off-grid or non-measured values. Ambient temperature could be built in by adding another dimension to the table. Index look-up models can be quite slow, especially if interpolating over several dimensions as the simulator drives to convergence. The S-parameters represent the linearized or small-signal response of the transistor at a specified bias V_{gs} , V_{ds} and frequency, ω .

Commonly, for FET models operating in the active regime, that is, above threshold and positive drain-to-source voltage, the controlled current source representing y_{21} are added to the passive network representation, as a transadmittance. An example of a small-signal equivalent circuit model of the intrinsic transistor is shown in Figure 1.30. Following the direct extraction method of Dambrine (Dambrine, Cappy et al. 1988), the values for the equivalent circuit parameters can be obtained (Dambrine, Cappy et al. 1988).

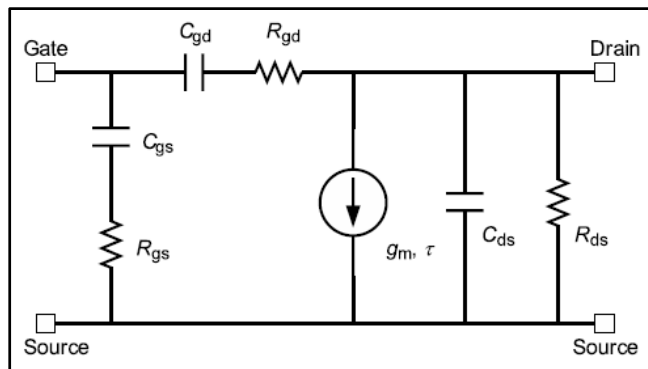


Figure 1.30 Small-signal equivalent circuit model of the intrinsic transistor
From Aaen, Plá et al. (2007)

The equivalent circuit component values for the gate-drain voltage are obtained through:

$$C_{gd} = \frac{1}{\omega} \text{imag}(Y_{gd}) = -\frac{1}{\omega} \text{imag}(y_{12}). \quad (1.39)$$

$$R_{gd} = \frac{1}{\omega^2 C_{gd}^2} \text{real}(Y_{gd}) = -\frac{1}{\omega^2 C_{gd}^2} \text{real}(y_{12}). \quad (1.40)$$

The gate-source admittance is also represented by a series R-C network in the equivalent circuit and their values are obtained by:

$$C_{gs} = \frac{1}{\omega} \text{imag}(y_{11} + y_{12}). \quad (1.41)$$

$$R_{gs} = \frac{1}{\omega^2 C_{gs}^2} \text{real}(y_{11} + y_{12}). \quad (1.42)$$

The drain-source admittance is a parallel R-C network and is obtained directly from:

$$C_{ds} = \frac{1}{\omega} \text{imag}(y_{22} + y_{12}). \quad (1.43)$$

$$R_{ds} = \frac{1}{\text{real}(y_{22} + y_{12})}. \quad (1.44)$$

The transadmittance, G_m , is written as a transconductance term g_m with a delay term τ That accounts for the distributed effect of the charge moving along the channel of the transistor during operation.

$$G_m = y_{21} - y_{12} = g_m e^{-j\omega\tau}. \quad (1.45)$$

In this way, from the measured and isothermal S-parameters, the elements of the intrinsic part are extracted at every DC bias point. The values of these intrinsic model elements can be stored at each bias point in a table.

1.5.3 Transistor large-signal modeling

The S-parameters represent the linearized or small-signal response of the transistor at a specified bias V_{gs} , V_{ds} and frequency, ω . This is simply the measured (and de-embedded) data, which could be stored in a three dimensional table, indexed by the bias voltages and frequency. During simulation, the required S-parameters would be read by indexing, or interpolating to the off-grid or non-measured values. Index look-up models can be quite slow, especially if interpolating over several dimensions as the simulator drives to convergence (Peter H.Aaen 2007). The Y-parameters of the transistor intrinsic part shown in Figure 1.30 are: (Jarndal 2006)

$$Y = \begin{bmatrix} G_{gs} + G_{gd} + j\omega(C_{gs} + C_{gd}) & -G_{gd} - j\omega C_{gd} \\ G_m - G_{gd} - j\omega C_{gd} & G_{ds} + G_{gd} + j\omega(C_{ds} + C_{gd}) \end{bmatrix}. \quad (1.46)$$

Where $G_{gs} = 1/R_{gs}$, $G_{gd} = 1/R_{gd}$ and $G_{ds} = 1/R_{ds}$ are the conductances.

The real part of the Y-parameter corresponds to incremental values of a current large-signal function, while the imaginary part corresponds to incremental values of a charge large-signal function (Kompa 1995, Jarndal 2006). Therefore, the large-signal characteristics of the device can be obtained by path independent integrals of the voltage-dependent Y-parameters as follow:

$$I_g(V_{gs}, V_{ds}) = I_g(V_{gs0}, V_{ds0}) + \int_{V_{gs0}}^{V_{gs}} G_{gs}(v_{gs}, V_{ds0}) + G_{gd}(v_{gs}, V_{ds0}) dv_{gs} - \int_{V_{ds0}}^{V_{ds}} G_{gd}(V_{gs}, v_{ds}) dv_{ds} \quad (1.47)$$

$$Q_g(V_{gs}, V_{ds}) = Q_g(V_{gs0}, V_{ds0}) + \int_{V_{gs0}}^{V_{gs}} C_{gs}(v_{gs}, V_{ds0}) + C_{gd}(v_{gs}, V_{ds0}) dv_{gs} - \int_{V_{ds0}}^{V_{ds}} C_{gd}(V_{gs}, v_{ds}) dv_{ds} \quad (1.48)$$

$$I_d(V_{gs}, V_{ds}) = I_d(V_{gs0}, V_{ds0}) + \int_{V_{gs0}}^{V_{gs}} G_m(v_{gs}, V_{ds0}) - G_{gd}(v_{gs}, V_{ds0}) dv_{gs} \quad (1.49)$$

$$+ \int_{V_{ds0}}^{V_{ds}} G_{ds}(V_{gs}, v_{ds}) + G_{gd}(V_{gs}, v_{ds}) dv_{ds}$$

$$Q_d(V_{gs}, V_{ds}) = Q_d(V_{gs0}, V_{ds0}) - \int_{V_{gs0}}^{V_{gs}} C_{gd}(v_{gs}, V_{ds0}) dv_{gs} + \int_{V_{ds0}}^{V_{ds}} C_{ds}(V_{gs}, v_{ds}) + C_{gd}(V_{gs}, v_{ds}) dv_{ds} \quad (1.50)$$

The quasi-static large-signal model of the device consists at least of two sources (current and charge) at the gate and the drain as shown in Figure 1.31.

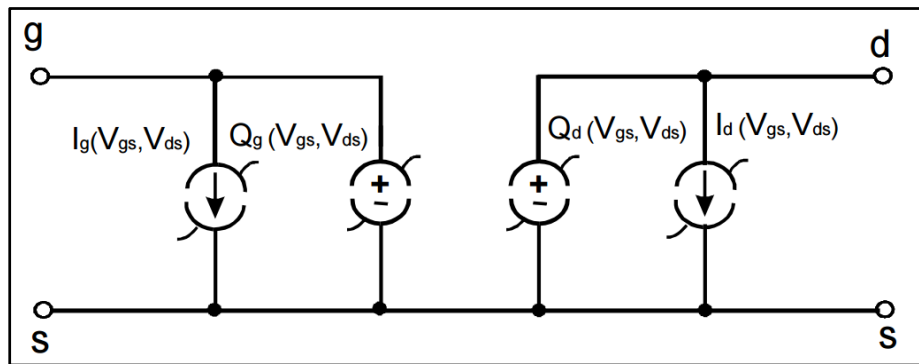


Figure 1.31 Quasi-static large-signal equivalent circuit model of the intrinsic transistor
From Jarndal (2007)

1.6 Conclusion

Gallium Nitride (GaN) HEMTs (High Electron Mobility Transistors) are the next generation of RF power transistor technology that offers the unique combination of higher power, higher efficiency and wider bandwidth. Besides, the design of an RF power amplifier requires an accurate large signal model of this device. There are many types of modeling techniques. Equivalent circuit models are the most used. The traditional techniques are relied on DC, multi-bias s-parameters and Pin-Pout-type measurements at the fundamental frequency. However s-parameters are only valid under linear operating conditions. The availability of X-

parameters measurements and their benefits compared to S-parameters are an opportunity for incorporating non-linear data directly in the modeling process. The main goal of the thesis is to develop a new modeling technique that exploit X-parameters for a quick build of an accurate nonlinear equivalent circuit based model that captures the device behavior at the fundamental and harmonic frequencies.

CHAPTER 2

NEW NONLINEAR TWO-PORT NETWORK PARAMETERS AND THEIR CONVERSION RULES

Riadh Essaadali¹, Anwar Jarndal², Ammar Kouki¹ and Fadhel Ghannouchi³

¹Department of Electrical Engineering, École de Technologie Supérieure,
1100 Notre-Dame West, Montreal, Quebec, (H3C 1K3) Canada

²Electrical and Computer Engineering Department of University of Sharjah, Sharjah, UAE

³Intelligent RF Radio Laboratory (iRadio Lab), Department of Electrical and Computer
Engineering, University of Calgary, Calgary, Alberta, (T2N 1N4) Canada

This paper has been submitted for publication in
IEEE Microwave Theory and Techniques Society.

2.1 Abstract

New nonlinear two-port network parameters consisting of nonlinear impedance parameters (Z-parameters), nonlinear admittance parameters (Y-parameters), nonlinear cascade parameters (ABCD-parameters), nonlinear scattering transfer parameters (T-parameters), nonlinear hybrid parameters (G-parameters) and nonlinear inverse hybrid parameters (H-parameters) are presented and are determined from X-parameters. Conversion rules between them are also presented. Validation results using measured X-parameters and non-linear circuit simulation are presented.

Keywords: X-parameters, nonlinear impedance, nonlinear admittance, nonlinear cascade parameters, nonlinear scattering transfer parameters, nonlinear hybrid parameters, nonlinear inverse hybrid parameters and conversion rules.

2.2 Introduction

Up until the mid-1940's, when S-parameters were first introduced (Belevitch 1962, Van Valkenburg 1974), circuit design and analysis were carried out using classical circuit

parameters, namely impedance and admittance matrices. The advent of S-parameters revolutionized the microwave engineering field since they could be used at very high frequencies, relied on matched loads instead of open or short terminations and provided explicit information about directionality (Pozar 1990). However, while S-parameters provide complete information for passive (linear) networks as well as nonlinear circuits operating in the linear regime, they cannot capture the all-important nonlinear behavior intrinsic to a wide range of modern RF front-ends and in particular their power amplifiers (Root, Verspecht et al. 2013, Verspecht and Root Jun. 2006). In fact, the use of nonlinear amplifiers for linear amplification dates back to the mid-1930's when Doherty (Doherty 1936) and Chireix (Chireix 1935) proposed amplifier architectures that have been recently revived for use in modern wireless communication systems (El-Asmar, Birafane et al. 2012, Hammi, Sharawi et al. 2013). These, and other amplification techniques, such as Envelope Elimination and Restoration (EER), MILC, Linear Amplification using Nonlinear Components (LINC) ... rely on nonlinear devices to achieve power-efficient amplification of modulated signals with increasingly high peak to average power ratios (Hamdane, Birafane et al. 2007, Helaoui, Boumaiza et al. 2007, Birafane, El-Asmar et al. 2010). This challenge has led to many important innovations on the various circuit design and signal processing fronts (Fadhel M. Ghannouchi 2001, Ammar B. Kouki 2008, Fadhel M Ghannouchi 2012) and has generated a significant push for advanced nonlinear measurement and modeling tools.

While significant progress has been made over the years in large-signal (nonlinear) modeling of active devices (Jarndal, Bunz et al. 2006, Aflaki, Negra et al. 2009, Hui, Yuehang et al. 2012, Liu, Wang et al. 2012), this has been accomplished while using, for the most part, classical techniques that relied on DC, multi-bias s-parameters and Pin-Pout-type measurements at the fundamental frequency, all accessible through common measurement equipment. Other efforts included the use of specialized equipment for time-domain current and voltage waveform measurement based on applying an arbitrary waveform and sampling scope (Tektronix , Benedikt and Tasker 2002, Lecklider 2009) and active load pull characterization (Fadhel M Ghannouchi , microwave 1996, Marchetti, Pelk et al. 2008) to improve model accuracy. Still, none of these techniques used a standardized, single set of

measurements for modeling and model parameter extraction. This is due to the fact that commercial nonlinear vector network analyzers were not available until 2008 (Lecklider 2009).

The first large signal network analyzer (LSNA) was developed by Hewlett-Packard (HP) and the Network Measurement and Description Group (NMDG) during the 1990's (Lecklider 2009). The LSNA is based on harmonic sampling down-conversion, measuring simultaneously all frequency components (Lott 1989, Corporation 2003). During the 2004 to 2007 period, nonlinear measurement industry name moved from LSNA to NVNA (Lecklider 2009). In 2008, Agilent introduced the PNA-X, a mixer-based NVNA (Root, Verspecht et al. 2013). The PNA-X is a combination of NVNA with X-parameters (Horn, Gunyan et al. 2008). X-parameters are invented by Jan Verpecht in 2003's (Verspecht 2008) and they represent new nonlinear scattering parameters, applicable to passive and active circuits under small and large signal excitation (Verspecht 2005, Horn, Gunyan et al. 2008). They represent a mathematical superset of small-signal and large signal S-parameters (Horn, Gunyan et al. 2008, Verspecht and Root Jun. 2006). In addition to measurement equipment, Agilent upgraded ADS to include X-parameters simulator (technologies). To ensure the interoperability between measurement hardware and circuit simulators, the .xnp standard file format was introduced (Environment , technologies , Horn, Gunyan et al. 2008).

The question is how to exploit X-parameters to more accurately and quickly build a nonlinear equivalent circuit based model that captures the device behavior at the fundamental and harmonic frequencies. In traditional transistor modeling, the conversion from S-parameters to impedance, admittance and ABCD matrices is essential for model parameters extraction (Jarndal and Kompa 2005, Laredj, Degachi et al. 2011, Jarndal 2014). Moreover, X-parameters are not directly suitable for the analytic analysis of different network configuration: series, parallel, cascaded, series to parallel and parallel to series. Thus, there is a need to define other nonlinear parameters -in addition to X-parameters- that describe the behavior of a nonlinear system and compute analytically the performance of different circuit topologies. These new nonlinear parameters cannot be limited to device modeling

applications, but, can be used in a high variety of circuit characterization, simulation, design and measurement.

The goal of this paper is to define new nonlinear two-port network parameters that can model different network topologies: Nonlinear impedance parameters (Z -parameters), nonlinear admittance parameters (Y -parameters), nonlinear cascade parameters (ABCD-parameters), nonlinear scattering transfer parameters (T-parameters), nonlinear hybrid parameters (G-parameters) and nonlinear inverse hybrid parameters (H-parameters). These parameters are mainly defined from X-parameters. The conversion rules between X-parameters and the new nonlinear two-port network parameters are developed in this paper. To the best knowledge of the authors, the concept of these nonlinear network parameters has not been mentioned in the literature.

This paper is organized as follows: section II outlines the concept of X-parameter and defines the expressions of nonlinear two-port network parameters. Section III presents all conversion rules between the new nonlinear two-port network parameters. In section IV and V, the validation of the expression of nonlinear parameters and the conversion rules are validated in linear and nonlinear operation modes respectively.

2.3 Nonlinear Network parameters

X-parameters use travelling voltage waves whereas other nonlinear network parameters use multi-harmonic voltage and current quantities. The conversion between travelling waves and voltage/current quantities is essential to define the expression of nonlinear network parameters function starting from X-parameters.

2.3.1 Multi-harmonic wave, voltage and current quantities

The basic quantities used for X-parameters are traveling voltage waves (Root, Verspecht et al. 2013). The waves are defined as linear combinations of the signal port voltage v , and the signal port current, i (Verspecht, Williams et al. 2005). The incident waves are called the a-

waves and the scattered waves are called the b-waves. They are defined in (2.1) and (2.2), as in (Verspecht and Root Jun. 2006). Each spectral component has an associated harmonic index, which denotes the ratio between the associated frequency and the fundamental tone. The harmonic index is indicated by the last subscript k. A harmonic index equal to zero corresponds to DC. The first subscript i indicates the respective DUT signal port. Port 1 typically corresponds to the input and port 2 to the output of the DUT. The incident waves a_{ik} and scattered waves b_{ik} are defined as functions of the spectral components of voltage v_{ik} , current i_{ik} and the reference impedance Z_c that is assumed to be a real constant in this work.

$$a_{ik} = \frac{v_{ik} + Z_c i_{ik}}{2} \quad (2.1)$$

$$b_{ik} = \frac{v_{ik} - Z_c i_{ik}}{2} \quad (2.2)$$

Harmonic voltages and currents can be expressed respectively in (2.3) and (2.4) as a function of spectral components of incident and scattered waves.

$$v_{ik} = a_{ik} + b_{ik} \quad (2.3)$$

$$i_{ik} = \frac{a_{ik} - b_{ik}}{Z_c}. \quad (2.4)$$

2.3.2 X-parameters: a large-signal scattering function

For a given DUT, the linearization of the multivariate complex functions that correlate all of the relevant input spectral components with the output spectral components leads to the X-parameters expression (Root, Verspecht et al. 2013, Verspecht and Root Jun. 2006):

$$b_{ik} = F_{ik}(|a_{11}|)P^k + \sum_{(j,l) \neq (1,1)} S_{ik,jl}(|a_{11}|)P^{k-l} a_{jl} + T_{ik,jl}(|a_{11}|)P^{k+l} a_{jl}^*. \quad (2.5)$$

Where b_{ik} and a_{jl} are respectively the scattered and incident travelling voltage waves. The indices i and j range from one to the number of signal ports. The indices k and l range from one to the highest harmonic index. The terms F_{ik} , $S_{ik,jl}$ and $T_{ik,jl}$ are complex functions of $|a_{11}|$.

2.3.3 Expression of nonlinear two-port network parameters

When extracting X-parameters, the phase of the input signal at the fundamental frequency a_{11} is always set to zero. The term $F_{ik}(|a_{11}|)$ is complex. For simplification purposes, we can rewrite it as $S_{ik,11}(|a_{11}|) a_{11}$, since the input drive a_{11} is always different than 0. We can rewrite also $S_{ik,jl}(|a_{11}|)$ and $T_{ik,jl}(|a_{11}|)$ simply as $S_{ik,jl}$ and $T_{ik,jl}$ respectively. Substituting a_{jl} and b_{ik} by their expression in (2.1) and (2.2), we obtain $2n$ equations relating voltage and current harmonic components. Note that n is the total number of scattered voltage waves. Thus, (2.5) becomes as in (2.6). The development of nonlinear Z-parameters will be limited to only two ports. Equation (2.6) is arranged to get the voltage terms in the left-hand side and the current terms in the right-hand side. For $i=1,2; j=1,2; k=1:n$ and $l=1:n$;

$$v_{ik} - S_{ik,11}v_{11} - \sum_{(j,l) \neq (1,1)} S_{ik,jl}v_{jl} - \sum_{(j,l) \neq (1,1)} T_{ik,jl}v_{jl}^* = Z_c S_{ik,11}i_{11} + Z_c i_{ik} + \sum_{(j,l) \neq (1,1)} S_{ik,jl}Z_c i_{jl} + T_{ik,jl}Z_c i_{jl}^* \quad (2.6)$$

Each variable involved in (2.6) is rewritten in the complex Cartesian form ($x_{ik} = x_{ik}^r + jx_{ik}^i$).

Thus, Equation (2.6) leads to two orthogonal equations (2.7) and (2.8): The real and imaginary parts of the whole equation. Thus, for $i=1,2; j=1,2; k=1:n; l=1:n$, we have:

$$v_{ik}^r - (S_{ik,11}^r v_{11}^r - S_{ik,11}^i v_{11}^i) - \sum_{(j,l) \neq (1,1)} (S_{ik,jl}^r v_{jl}^r - S_{ik,jl}^i v_{jl}^i) - \sum_{(j,l) \neq (1,1)} (T_{ik,jl}^r v_{jl}^r + T_{ik,jl}^i v_{jl}^i) = Z_c \left\{ S_{ik,11}^r i_{11}^r - S_{ik,11}^i i_{11}^i + i_{ik}^r + \sum_{(j,l) \neq (1,1)} (S_{ik,jl}^r i_{jl}^r - S_{ik,jl}^i i_{jl}^i) + \sum_{(j,l) \neq (1,1)} (T_{ik,jl}^r i_{jl}^r + T_{ik,jl}^i i_{jl}^i) \right\} \quad (2.7)$$

$$\begin{aligned}
v_{ik}^i - (S_{ik,11}^i v_{11}^r + S_{ik,11}^r v_{11}^i) - \sum_{(j,l) \neq (1,1)} (S_{ik,jl}^i v_{jl}^r + S_{ik,jl}^r v_{jl}^i) + \sum_{(j,l) \neq (1,1)} (T_{ik,jl}^r v_{jl}^i - T_{ik,jl}^i v_{jl}^r) = \\
Z_c \left\{ S_{ik,11}^r i_{11}^i + S_{ik,11}^i i_{11}^r + i_{ik}^i + \sum_{(j,l) \neq (1,1)} (S_{ik,jl}^r i_{jl}^i + S_{ik,jl}^i i_{jl}^r) - \sum_{(j,l) \neq (1,1)} (T_{ik,jl}^r i_{jl}^i - T_{ik,jl}^i i_{jl}^r) \right\}. \quad (2.8)
\end{aligned}$$

Simplification and reformulation of (2.7) and (2.8) into matrix forms leads to:

$$[M][V] = Z_c [N][I]. \quad (2.9)$$

where $[V] = [v_{11}^r \ v_{11}^i \ \dots \ v_{1n}^r \ v_{1n}^i \ \dots \ v_{2n}^r \ v_{2n}^i]^T$ is the voltage vector and $[I] = [i_{11}^r \ i_{11}^i \ \dots \ i_{1n}^r \ i_{1n}^i \ \dots \ i_{2n}^r \ i_{2n}^i]^T$ current vector. Note that the symbol $[\]^T$ is the matrix transpose operator. $[M]$ and $[N]$ are $4n$ -by- $4n$ matrices expressed in (2.10) and (2.11) respectively.

$$[M] = \begin{bmatrix} 1 - S_{11,11}^r & S_{11,11}^i & \cdots & -(S_{112n}^r + T_{112n}^r) & (S_{112n}^i - T_{112n}^i) \\ -S_{11,11}^i & 1 - S_{11,11}^r & \cdots & -(S_{112n}^i + T_{112n}^i) & -(S_{112n}^r - T_{112n}^r) \\ \vdots & \vdots & \ddots & \vdots & \vdots \\ -S_{2n,11}^r & S_{2n,11}^i & \cdots & 1 - (S_{2n2n}^r + T_{2n2n}^r) & (S_{2n2n}^i - T_{2n2n}^i) \\ -S_{2n,11}^i & -S_{2n,11}^r & \cdots & -(S_{2n2n}^i + T_{2n2n}^i) & 1 - (S_{2n2n}^r - T_{2n2n}^r) \end{bmatrix} \quad (2.10)$$

$$[N] = \begin{bmatrix} 1 + S_{11,11}^r & -S_{11,11}^i & \cdots & (S_{112n}^r + T_{112n}^r) & -(S_{112n}^i - T_{112n}^i) \\ S_{11,11}^i & 1 + S_{11,11}^r & \cdots & (S_{112n}^i + T_{112n}^i) & (S_{112n}^r - T_{112n}^r) \\ \vdots & \vdots & \ddots & \vdots & \vdots \\ S_{2n,11}^r & -S_{2n,11}^i & \cdots & 1 + (S_{2n2n}^r + T_{2n2n}^r) & -(S_{2n2n}^i - T_{2n2n}^i) \\ S_{2n,11}^i & S_{2n,11}^r & \cdots & (S_{2n2n}^i + T_{2n2n}^i) & 1 + (S_{2n2n}^r - T_{2n2n}^r) \end{bmatrix} \quad (2.11)$$

The matrix $Z_c[M]^{-1}[N]$ can be defined simply by $[R]$ and (2.9) is equivalent to:

$$[V] = [R][I]. \quad (2.12)$$

For each harmonic voltage component, the real part is in (2.13), the imaginary part is in (2.14). Note that p is the port index

$$v_{pm}^r = \sum_{k=0}^{n-1} R_{(2(p-1)n+2m)(2k+1)} i_{1(k+1)}^r + R_{(2(p-1)n+2m)(2k+2)} i_{1(k+1)}^i + \sum_{k=n}^{2n-1} R_{(2(p-1)n+2m)(2k+1)} i_{2(k+1-n)}^r + R_{(2(p-1)n+2m)(2k+2)} i_{2(k+1-n)}^i \quad (2.13)$$

$$v_{pm}^i = \sum_{k=0}^{n-1} R_{(2(p-1)n+2m+1)(2k+1)} i_{1(k+1)}^r + R_{(2(p-1)n+2m+1)(2k+2)} i_{1(k+1)}^i + \sum_{k=n}^{2n-1} R_{(2(p-1)n+2m+1)(2k+1)} i_{2(k+1-n)}^r + R_{(2(p-1)n+2m+1)(2k+2)} i_{2(k+1-n)}^i \quad (2.14)$$

The term $R_{(2m)(2k+1)} + jR_{(2m+1)(2k+1)}$ in (2.13) and (2.14) is different to $R_{(2m)(2k+2)} + jR_{(2m+1)(2k+2)}$, thus, the harmonic voltage component is expressed in:

$$v_{pm} = \frac{1}{2} \left[\sum_{k=0}^{n-1} \left\{ R_{(2m+2(p-1)n)(2k+1)} + R_{(2m+2(p-1)n)(2k+2)} + jR_{(2m+1+2(p-1)n)(2k+1)} + jR_{(2m+1+2(p-1)n)(2k+2)} \right\} i_{1(k+1)} + \left\{ R_{(2m+2(p-1)n)(2k+1)} - R_{(2m+2(p-1)n)(2k+2)} + jR_{(2m+1+2(p-1)n)(2k+1)} - jR_{(2m+1+2(p-1)n)(2k+2)} \right\} i_{1(k+1)}^* + \sum_{k=n}^{2n-1} \left\{ R_{(2m+2(p-1)n)(2k+1)} + R_{(2m+2(p-1)n)(2k+2)} + R_{(2m+1+2(p-1)n)(2k+1)} + R_{(2m+1+2(p-1)n)(2k+2)} \right\} i_{2(k+1-n)} + \left\{ R_{(2m+2(p-1)n)(2k+1)} - R_{(2m+2(p-1)n)(2k+2)} + jR_{(2m+1+2(p-1)n)(2k+1)} - jR_{(2m+1+2(p-1)n)(2k+2)} \right\} i_{2(k+1-n)}^* \right] \quad (2.15)$$

Equation (2.15) is the expression of each harmonic component voltage as a function of nonlinear impedance, harmonic component currents and their conjugate. The expression of each nonlinear impedance parameter can be found from (2.15). An elegant expression harmonic component voltage is:

$$v_{pm} = \sum_{\substack{j=1..n \\ q=1,2}} Z_{pmqj}^{\alpha} i_{qj} + \sum_{\substack{j=1..n \\ q=1,2}} Z_{pmqj}^{\beta} i_{qj}^* . \quad (2.16)$$

In this section, we demonstrated that nonlinear Z-parameters include two-term categories Z_{pmqj}^{α} and Z_{pmqj}^{β} , where p and q are the port indexes, m and j are the harmonic indexes. The term Z_{pmqj}^{α} are associated to i_{qj} and Z_{pmqj}^{β} are associated to i_{qj}^* . By using the same demonstration philosophy, we demonstrated also that nonlinear Y-parameters include two-term categories Y_{pmqj}^{α} and Y_{pmqj}^{β} . The terms Y_{pmqj}^{α} are associated to v_{qj} and Y_{pmqj}^{β} are associated to v_{qj}^* . The expression of each harmonic component current as a function of nonlinear admittance, harmonic current component and its conjugate is:

$$i_{pm} = \sum_{\substack{j=1..n \\ q=1,2}} Y_{pmqj}^{\alpha} v_{qj} + \sum_{\substack{j=1..n \\ q=1,2}} Y_{pmqj}^{\beta} v_{qj}^* . \quad (2.17)$$

By using the same procedure, we demonstrate also that nonlinear T-parameters include two-term categories T_{pmqj}^{α} and T_{pmqj}^{β} associated respectively to a harmonic component and its conjugate of a-waves and b-waves present at output port. The formulation of the nonlinear model based on nonlinear T-parameters is:

$$b_{1m} = \sum_{j=1..n} T_{1m1j}^{\alpha} a_{2j} + T_{1m1j}^{\beta} a_{2j}^* + T_{1m2j}^{\alpha} b_{2j} + T_{1m2j}^{\beta} b_{2j}^* \quad (2.18)$$

$$a_{1m} = \sum_{j=1..n} T_{2m1j}^{\alpha} b_{2j} + T_{2m1j}^{\beta} b_{2j}^* + T_{2m2j}^{\alpha} a_{2j} + T_{2m2j}^{\beta} a_{2j}^* \quad (2.19)$$

Like in linear case, nonlinear ABCD-matrix includes 4 parameter categories: A-, B-, C- and D-terms. A-parameters relate input harmonic voltages to output harmonic voltages. B-parameters relate input harmonic voltages to output harmonic currents. C-parameters relate input harmonic currents to output harmonic voltages. D-parameters relate input harmonic currents to output harmonic currents. Like nonlinear parameters defined in sections below and by using the same demonstration philosophy, each ABCD parameters include two-term

categories associated respectively to a harmonic component and its conjugate of voltage and current present at second port. The formulation of the nonlinear model based on nonlinear ABCD-parameters is:

$$v_{1m} = \sum_{j=1..n} A_{1m2j}^{\alpha} v_{2j} + A_{1m2j}^{\beta} v_{2j}^* + B_{1m2j}^{\alpha} i_{2j} + B_{1m2j}^{\beta} i_{2j}^* \quad (2.20)$$

$$i_{1m} = \sum_{j=1..n} C_{1m2j}^{\alpha} v_{2j} + C_{1m2j}^{\beta} v_{2j}^* + D_{1m2j}^{\alpha} i_{2j} + D_{1m2j}^{\beta} i_{2j}^* \quad (2.21)$$

Nonlinear hybrid parameters use the input harmonic current components at port 1 and the output harmonic voltage components at port 2 as independent variables. By using the same procedure, nonlinear H-parameters include two-term categories H_{pmqj}^{α} and H_{pmqj}^{β} associated to a harmonic component and its conjugate of voltage and current. The formulation of the nonlinear model based on nonlinear H-parameters is:

$$v_{1m} = \sum_{j=1..n} H_{1m1j}^{\alpha} i_{1j} + H_{1m1j}^{\beta} i_{1j}^* + H_{1m2j}^{\alpha} v_{2j} + H_{1m2j}^{\beta} v_{2j}^* \quad (2.22)$$

$$i_{2m} = \sum_{j=1..n} H_{2m1j}^{\alpha} i_{1j} + H_{2m1j}^{\beta} i_{1j}^* + H_{2m2j}^{\alpha} v_{2j} + H_{2m2j}^{\beta} v_{2j}^* \quad (2.23)$$

Nonlinear G-parameters use the input harmonic voltage components and the output harmonic current components as independent variables. Using the same demonstration technique leads to the formulation of the nonlinear model based on nonlinear G-parameters in:

$$i_{1m} = \sum_{j=1..n} G_{1m1j}^{\alpha} v_{1j} + G_{1m1j}^{\beta} v_{1j}^* + G_{1m2j}^{\alpha} i_{2j} + G_{1m2j}^{\beta} i_{2j}^* \quad (2.24)$$

$$v_{2m} = \sum_{j=1..n} G_{2m1j}^{\alpha} v_{1j} + G_{2m1j}^{\beta} v_{1j}^* + G_{2m2j}^{\alpha} i_{2j} + G_{2m2j}^{\beta} i_{2j}^* \quad (2.25)$$

2.4 Conversion between nonlinear two-port network parameters

In this section, we present a transparent matricial transformation between nonlinear parameters.

2.4.1 Conversion from X- to nonlinear Z-, Y-, ABCD-, T-, G- and H-parameters

Since nonlinear parameters including X-parameters include many terms, the best way is to represent them with a matricial relation. For example, the relation between A-waves and B-waves through X-parameters can be represented by:

$$[B] = [X][A] \quad (2.26)$$

where the matrix $[X]$ is defined in (2.27). The A-waves and B-waves vectors are defined as:

$$[B] = \left[[B_1]^T, [B_2]^T \right]^T \quad \text{and} \quad [A] = \left[[A_1]^T, [A_2]^T \right]^T, \quad [B_i] = \left[b_{i1} \quad b_{i1}^* \quad \dots \quad b_{in} \quad b_{in}^* \right]^T \quad \text{and}$$

$$[A_i] = \left[a_{i1} \quad a_{i1}^* \quad \dots \quad a_{in} \quad a_{in}^* \right]^T.$$

$$[X] = \begin{bmatrix} [X_{11}] & [X_{12}] \\ [X_{21}] & [X_{22}] \end{bmatrix} \quad (2.27)$$

where

$$[X_{ij}]_{\substack{i=1,2 \\ j=1,2}} = \begin{bmatrix} S_{i1j1} & T_{i1j1} & \dots & S_{i1jn} & T_{i1jn} \\ T_{i1j1}^* & S_{i1j1}^* & \dots & T_{i1jn}^* & S_{i1jn}^* \\ \vdots & \vdots & \ddots & \vdots & \vdots \\ S_{inj1} & T_{inj1} & \dots & S_{injn} & T_{injn} \\ T_{inj1}^* & S_{inj1}^* & \dots & T_{injn}^* & S_{injn}^* \end{bmatrix}$$

The terms S and T in X-matrix are expressed in terms of X-parameters: $S_{pmqj} = X_{pmqj}^S P^{m-j}$

and $T_{pmqj} = X_{pmqj}^T P^{m+j}$. We can set $T_{pm11} = 0$, thus $S_{ik,11} = F_{ik} / |a_{11}|$ because

$F_{ik}P^k = S_{ik,11}P^{k-1}a_{11}$. Thus $F_{ik} = S_{ik,11}|a_{11}|$. If we use the definition expression of A- and B-travelling waves in terms of voltages and currents (2.1) and (2.2), we get the expression of voltage vector in:

$$[V] = Z_c \{[Id] - [X]\}^{-1} \{[Id] + [X]\} [I]. \quad (2.28)$$

where $[Id]$, $[V] = \left[[V_1]^T, [V_2]^T \right]^T$ and $[I] = \left[[I_1]^T, [I_2]^T \right]^T$ are respectively the identity matrix, voltage and current vectors. The sub-vector $[V_i] = \left[v_{i1} \quad v_{i1}^* \quad \cdots \quad v_{in} \quad v_{in}^* \right]^T$ is expressed in terms of n harmonic voltage components. The current sub-vector is $[I_i] = \left[i_{i1} \quad i_{i1}^* \quad \cdots \quad i_{in} \quad i_{in}^* \right]^T$. Finally, the expression of nonlinear Z in terms of X-parameters is derived in:

$$[Z_{nonlin}] = Z_c \{[Id] - [X]\}^{-1} \{[Id] + [X]\}. \quad (2.29)$$

where the nonlinear impedance matrix $[Z_{nonlin}]$ can be rewritten as in:

$$[Z_{nonlin}] = \begin{bmatrix} [Z_{11}] & [Z_{12}] \\ [Z_{21}] & [Z_{22}] \end{bmatrix} \quad (2.30)$$

where

$$[Z_{ij}]_{\substack{i=1,2 \\ j=1,2}} = \begin{bmatrix} Z_{i1j1}^\alpha & Z_{i1j1}^\beta & \cdots & Z_{i1jn}^\alpha & Z_{i1jn}^\beta \\ Z_{i1j1}^{\beta^*} & Z_{i1j1}^{\alpha^*} & \cdots & Z_{i1jn}^{\beta^*} & Z_{i1jn}^{\alpha^*} \\ \vdots & \vdots & \ddots & \vdots & \vdots \\ Z_{inj1}^\alpha & Z_{inj1}^\beta & \cdots & Z_{injn}^\alpha & Z_{injn}^\beta \\ Z_{inj1}^{\beta^*} & Z_{inj1}^{\alpha^*} & \cdots & Z_{injn}^{\beta^*} & Z_{injn}^{\alpha^*} \end{bmatrix}$$

The expression of current vector in terms of voltage vector and X-parameters is:

$$[I] = \frac{1}{Z_c} \{[Id] + [X]\}^{-1} \{[Id] - [X]\} [V]. \quad (2.31)$$

Thus, we can define the nonlinear admittance matrix to describe the relationship between harmonic currents and harmonic voltages in:

$$[Y_{nonlin}] = \frac{1}{Z_c} \{[Id] + [X]\}^{-1} \{[Id] - [X]\}. \quad (2.32)$$

where the expression of the nonlinear admittance is in:

$$[Y_{nonlin}] = \begin{bmatrix} [Y_{11}] & [Y_{12}] \\ [Y_{21}] & [Y_{22}] \end{bmatrix} \quad (2.33)$$

where

$$[Y_{ij}]_{\substack{i=1,2 \\ j=1,2}} = \begin{bmatrix} Y_{i1j1}^\alpha & Y_{i1j1}^\beta & \dots & Y_{i1jn}^\alpha & Y_{i1jn}^\beta \\ Y_{i1j1}^{\beta^*} & Y_{i1j1}^{\alpha^*} & \dots & Y_{i1jn}^{\beta^*} & Y_{i1jn}^{\alpha^*} \\ \vdots & \vdots & \ddots & \vdots & \vdots \\ Y_{inj1}^\alpha & Y_{inj1}^\beta & \dots & Y_{injn}^\alpha & Y_{injn}^\beta \\ Y_{inj1}^{\beta^*} & Y_{inj1}^{\alpha^*} & \dots & Y_{injn}^{\beta^*} & Y_{injn}^{\alpha^*} \end{bmatrix}$$

The reformulation of (2.20) and (2.21) in a matrix form makes easier the manipulation of nonlinear ABCD-parameters:

$$\begin{bmatrix} [V_1] \\ [I_1] \end{bmatrix} = [ABCD_{nonlin}] \begin{bmatrix} [V_2] \\ [I_2] \end{bmatrix} = \begin{bmatrix} [A_{nonlin}] & [B_{nonlin}] \\ [C_{nonlin}] & [D_{nonlin}] \end{bmatrix} \begin{bmatrix} [V_2] \\ [I_2] \end{bmatrix}. \quad (2.34)$$

The expressions of $[ABCD_{nonlin}]$ sub-matrices: $[A_{nonlin}]$, $[B_{nonlin}]$, $[C_{nonlin}]$ and $[D_{nonlin}]$ in terms of A_{pmqj}^α , B_{pmqj}^α , C_{pmqj}^α , D_{pmqj}^α , A_{pmqj}^β , B_{pmqj}^β , C_{pmqj}^β and D_{pmqj}^β in (2.35). For simplification purpose, the letter R symbolizes A, B, C and D symbols.

$$[R_{nonlin}] = \begin{bmatrix} R_{1121}^\alpha & R_{1121}^\beta & \dots & R_{112n}^\alpha & R_{112n}^\beta \\ R_{1121}^{\beta^*} & R_{1121}^{\alpha^*} & \dots & R_{112n}^{\beta^*} & R_{112n}^{\alpha^*} \\ \vdots & \vdots & \ddots & \vdots & \vdots \\ R_{1n21}^\alpha & R_{1n21}^\beta & \dots & R_{1n2n}^\alpha & R_{1n2n}^\beta \\ R_{1n21}^{\beta^*} & R_{1n21}^{\alpha^*} & \dots & R_{1n2n}^{\beta^*} & R_{1n2n}^{\alpha^*} \end{bmatrix}. \quad (2.35)$$

To determine nonlinear $[A]$ and $[C]$ sub-matrices in terms of X-parameters, we should assume that $[I_2] = 0$. In this case, equation (2.26) is equivalent to:

$$\begin{bmatrix} [V_1] - Z_c [I_1] \\ [V_2] \end{bmatrix} = \begin{bmatrix} [X_{11}] & [X_{12}] \\ [X_{21}] & [X_{22}] \end{bmatrix} \begin{bmatrix} [V_1] + Z_c [I_1] \\ [V_2] \end{bmatrix} \quad (2.36)$$

The manipulation of (2.36) leads to the expression of $[A]$ and $[C]$ in:

$$[A] = \left[I_d + [I_d - X_{11}]^{-1} [I_d + X_{11}] \right]^{-1} \left\{ [I_d - X_{11}]^{-1} [I_d + X_{11}] [X_{21}]^{-1} [I_d - X_{22}] + [I_d - X_{11}]^{-1} [X_{12}] \right\} \quad (2.37)$$

$$[C] = \frac{1}{Z_c} [X_{22}]^{-1} [I_d - X_{22}] - \frac{1}{Z_c} \left[I_d + [I_d - X_{11}]^{-1} [I_d + X_{11}] \right]^{-1} \left\{ [I_d - X_{11}]^{-1} [I_d + X_{11}] [X_{21}]^{-1} [I_d - X_{22}] + [I_d - X_{11}]^{-1} [X_{12}] \right\} \quad (2.38)$$

To determine nonlinear $[B]$ and $[D]$ sub-matrices in terms of X-parameters, we should assume that $[V_2] = 0$. In this case, (2.26) is equivalent to:

$$\begin{bmatrix} [V_1] - Z_c [I_1] \\ -Z_c [I_2] \end{bmatrix} = \begin{bmatrix} [X_{11}] & [X_{12}] \\ [X_{21}] & [X_{22}] \end{bmatrix} \begin{bmatrix} [V_1] + Z_c [I_1] \\ Z_c [I_2] \end{bmatrix} \quad (2.39)$$

The manipulation of (2.39) leads to the expression of $[B]$ and $[D]$ in:

$$[B] = \frac{Z_c}{2} \left([X_{12}] - [I_d + X_{11}][X_{21}]^{-1}[I_d + X_{22}] \right) \quad (2.40)$$

$$[D] = \frac{1}{2} \left(([X_{11}] - [I_d])[X_{21}]^{-1}([I_d] + [X_{22}]) - [X_{12}] \right) \quad (2.41)$$

The most common application of the G-parameters is in the device modeling of a transistor. They use the input voltage at port 1 and the output current at port 2 as the independent variables. Thus the harmonic voltage and current related through nonlinear G-parameters are expressed in:

$$\begin{bmatrix} [I_1] \\ [V_2] \end{bmatrix} = [G_{nonlin}] \begin{bmatrix} [V_1] \\ [I_2] \end{bmatrix}. \quad (2.42)$$

Like other nonlinear parameters defined previously, nonlinear hybrid parameters include two-term categories G_{pmqj}^α and G_{pmqj}^β . The matrix $[G_{nonlin}]$ is square, so it can be redefined as:

$$[G_{nonlin}] = \begin{bmatrix} [G_{11}] & [G_{12}] \\ [G_{21}] & [G_{22}] \end{bmatrix} \quad (2.43)$$

where the nonlinear G sub-matrices can be defined as:

$$[G_{ij}]_{\substack{i=1,2 \\ j=1,2}} = \begin{bmatrix} G_{i1j1}^\alpha & G_{i1j1}^\beta & \dots & G_{i1jn}^\alpha & G_{i1jn}^\beta \\ G_{i1j1}^{\beta^*} & G_{i1j1}^{\alpha^*} & \dots & G_{i1jn}^{\beta^*} & G_{i1jn}^{\alpha^*} \\ \vdots & \vdots & \ddots & \vdots & \vdots \\ G_{inj1}^\alpha & G_{inj1}^\beta & \dots & G_{injn}^\alpha & G_{injn}^\beta \\ G_{inj1}^{\beta^*} & G_{inj1}^{\alpha^*} & \dots & G_{injn}^{\beta^*} & G_{injn}^{\alpha^*} \end{bmatrix}$$

To derive the expression of nonlinear G-parameters in terms of nonlinear X-parameters, the definition expression of voltage waves in terms of harmonic voltages can be used. Then, the expression of $[G_{11}]$, $[G_{12}]$, $[G_{21}]$ and $[G_{22}]$ are respectively in (2.44), (2.45), (2.46) and (2.47).

$$[G_{11}] = \frac{-1}{Z_c} \left[[I_d] + [X_{11}] + [X_{12}] \left[[I_d] - [X_{22}] \right]^{-1} [X_{21}] \right]^{-1} \cdot \left[[X_{11}] - [I_d] + [X_{12}] \left[[I_d] - [X_{22}] \right]^{-1} [X_{21}] \right] \quad (2.44)$$

$$[G_{21}] = 2 \left[[X_{12}] + \left[[X_{11}] + [I_d] \right] [X_{21}]^{-1} \left[[I_d] - [X_{22}] \right] \right]^{-1} \quad (2.45)$$

$$[G_{12}] = 2 \left[\left[[X_{22}] - [I_d] \right] [X_{12}]^{-1} \left[[X_{11}] + [I_d] \right] - [X_{21}] \right]^{-1} \quad (2.46)$$

$$[G_{22}] = Z_c \left[[X_{21}] - \left[[X_{22}] + [I_d] \right] [X_{12}]^{-1} \left[[X_{11}] + [I_d] \right] \right] \cdot \left[\left[[X_{22}] - [I_d] \right] [X_{12}]^{-1} \left[[X_{11}] + [I_d] \right] - [X_{21}] \right]^{-1} \quad (2.47)$$

Nonlinear H-parameters use the input current at port 1 and the output voltage at port 2 as independent variables. Thus, the harmonic voltage and current related through nonlinear H-parameters are expressed in:

$$\begin{bmatrix} [V_1] \\ [I_2] \end{bmatrix} = [H_{nonlin}] \begin{bmatrix} [I_1] \\ [V_2] \end{bmatrix}. \quad (2.48)$$

Like other nonlinear parameters defined previously, nonlinear hybrid parameters include two-term categories H_{pmqj}^α and H_{pmqj}^β . The matrix $[H_{nonlin}]$ can be redefined as:

$$[H_{nonlin}] = \begin{bmatrix} [H_{11}] & [H_{12}] \\ [H_{21}] & [H_{22}] \end{bmatrix} \quad (2.49)$$

where

$$[H_{ij}]_{\substack{i=1,2 \\ j=1,2}} = \begin{bmatrix} H_{i1j1}^\alpha & H_{i1j1}^\beta & \dots & H_{i1jn}^\alpha & H_{i1jn}^\beta \\ H_{i1j1}^{\beta^*} & H_{i1j1}^{\alpha^*} & \dots & H_{i1jn}^{\beta^*} & H_{i1jn}^{\alpha^*} \\ \vdots & \vdots & \ddots & \vdots & \vdots \\ H_{inj1}^\alpha & H_{inj1}^\beta & \dots & H_{injn}^\alpha & H_{injn}^\beta \\ H_{inj1}^{\beta^*} & H_{inj1}^{\alpha^*} & \dots & H_{injn}^{\beta^*} & H_{injn}^{\alpha^*} \end{bmatrix}$$

Let's start by calculating $[H_{11}]$ and $[H_{21}]$ in terms of X-parameters. To determine them we assume that $[V_2]=0$, X-matrix is equivalent to (2.39). The manipulation of (2.39) leads to the expressions of nonlinear H sub-matrices in terms of X-parameters in (2.50), (2.51), (2.52) and (2.53)

$$[H_{11}] = Z_c \left[[I_d] - [X_{11}] + [X_{12}][I_d + X_{22}]^{-1} [X_{21}] \right]^{-1} \cdot \left[[I_d] + [X_{11}] - [X_{12}][I_d + X_{22}]^{-1} [X_{21}] \right] \quad (2.50)$$

$$[H_{21}] = -[I_d + X_{22}]^{-1} [X_{21}] \cdot \left\{ [I_d] + \left[[I_d] - [X_{11}] + [X_{12}][I_d + X_{22}]^{-1} [X_{21}] \right]^{-1} \cdot \left[[I_d] + [X_{11}] - [X_{12}][I_d + X_{22}]^{-1} [X_{21}] \right] \right\} \quad (2.51)$$

$$[H_{12}] = \left[[I_d] - [X_{11}] + [X_{12}][I_d + X_{22}]^{-1} [X_{21}] \right]^{-1} \cdot \left[[X_{12}] - [X_{12}][I_d + X_{22}]^{-1} [X_{22} - I_d] \right] \quad (2.52)$$

$$[H_{22}] = \frac{1}{Z_c} \left[[I_d] + [X_{22}] + [X_{21}][I_d - X_{11}]^{-1}[X_{12}] \right]^{-1} \cdot \left[[I_d] - [X_{22}] - [X_{21}][I_d - X_{11}]^{-1}[X_{12}] \right] \quad (2.53)$$

In practice, many microwave networks consist of a cascade connection of two or more nonlinear two-port networks or a connection of nonlinear with a linear circuit. In this case, it is convenient to define a nonlinear T-matrix or nonlinear ABCD-matrix. Like nonlinear Z- and Y-parameters, nonlinear T-parameters include two-term categories T_{pmqj}^α and T_{pmqj}^β . The relation between A-waves and B-waves through nonlinear T-parameters is given by matricial expression:

$$\begin{bmatrix} [B_1] \\ [A_1] \end{bmatrix} = [T_{nonlin}] \begin{bmatrix} [A_2] \\ [B_2] \end{bmatrix}. \quad (2.54)$$

The matrix $[T_{nonlin}]$ is square, so it can be redefined as:

$$[T_{nonlin}] = \begin{bmatrix} [T_{11}] & [T_{12}] \\ [T_{21}] & [T_{22}] \end{bmatrix} \quad (2.55)$$

where nonlinear T sub-matrices can be defined as:

$$[T_{ij}]_{\substack{i=1,2 \\ j=1,2}} = \begin{bmatrix} T_{i1j1}^\alpha & T_{i1j1}^\beta & \dots & T_{i1jn}^\alpha & T_{i1jn}^\beta \\ T_{i1j1}^{\beta^*} & T_{i1j1}^{\alpha^*} & \dots & T_{i1jn}^{\beta^*} & T_{i1jn}^{\alpha^*} \\ \vdots & \vdots & \ddots & \vdots & \vdots \\ T_{inj1}^\alpha & T_{inj1}^\beta & \dots & T_{injn}^\alpha & T_{injn}^\beta \\ T_{inj1}^{\beta^*} & T_{inj1}^{\alpha^*} & \dots & T_{injn}^{\beta^*} & T_{injn}^{\alpha^*} \end{bmatrix}$$

The expression of $[T_{11}]$ and $[T_{21}]$ in terms of X-parameters are determined in (2.56) and (2.57) by assuming that $[B_2]=[0]$. The expression of $[T_{12}]$ and $[T_{22}]$ in terms of X-parameters are determined in (2.58) and (2.59) by assuming that $[A_2]=[0]$.

$$[T_{11}] = [X_{12}] - [X_{11}][X_{21}]^{-1}[X_{22}] \quad (2.56)$$

$$[T_{21}] = -[X_{21}]^{-1}[X_{22}] \quad (2.57)$$

$$[T_{12}] = [X_{11}][X_{21}]^{-1} \quad (2.58)$$

$$[T_{22}] = [X_{21}]^{-1} \quad (2.59)$$

2.4.2 Conversion from nonlinear Z- to X-, nonlinear Y-, ABCD-, T-, G-and H-parameters

Nonlinear Z-parameters use voltages and currents whereas X- and nonlinear T-parameters use travelling waves. To derive the expression of X- and nonlinear T-parameters in terms of nonlinear Z-parameters, (2.3) and (2.4) are used. The expression of X- in terms of nonlinear Z-parameters is derived in (2.60).

$$[X] = \left[[I_d] + \frac{1}{Z_c} [Z_{nonlin}] \right]^{-1} \left[\frac{1}{Z_c} [Z_{nonlin}] - [I_d] \right] \quad (2.60)$$

The expressions of nonlinear T- sub-matrices $[T_{11}]$, $[T_{21}]$, $[T_{12}]$ and $[T_{22}]$ are respectively derived in (2.61), (2.62), (2.63) and (2.64).

$$[T_{11}] = \frac{[Z_{12}]}{2Z_c} + \frac{1}{2} \left(\frac{[Z_{11}]}{Z_c} - [I_d] \right) \left(Z_c [Z_{21}]^{-1} - [Z_{21}]^{-1} [Z_{22}] \right) \quad (2.61)$$

$$[T_{21}] = \frac{[Z_{12}]}{2Z_c} + \frac{1}{2} \left(\frac{[Z_{11}]}{Z_c} + [I_d] \right) \left(Z_c [Z_{21}]^{-1} - [Z_{21}]^{-1} [Z_{22}] \right) \quad (2.62)$$

$$[T_{12}] = \frac{1}{2} \left([Z_{11}] - Z_c [I_d] \right) [Z_{21}]^{-1} \left(\frac{[Z_{22}]}{Z_c} + [I_d] \right) - \frac{[Z_{12}]}{2Z_c} \quad (2.63)$$

$$[T_{12}] = \frac{1}{2} \left([Z_{11}] - Z_c [I_d] \right) [Z_{21}]^{-1} \left(\frac{[Z_{22}]}{Z_c} + [I_d] \right) - \frac{[Z_{12}]}{2Z_c} \quad (2.64)$$

The expressions of nonlinear H- sub-matrices $[H_{11}]$, $[H_{21}]$, $[H_{12}]$ and $[H_{22}]$ in terms of nonlinear Z-parameters are respectively derived in (2.65), (2.66), (2.67) and (2.68).

$$[H_{11}] = [Z_{11}] - [Z_{12}][Z_{22}]^{-1}[Z_{21}] \quad (2.65)$$

$$[H_{21}] = -[Z_{22}]^{-1}[Z_{21}] \quad (2.66)$$

$$[H_{12}] = [Z_{12}][Z_{22}]^{-1} \quad (2.67)$$

$$[H_{22}] = [Z_{22}]^{-1} \quad (2.68)$$

The expressions of nonlinear G- sub-matrices $[G_{11}]$, $[G_{21}]$, $[G_{12}]$ and $[G_{22}]$ in terms of nonlinear Z-parameters are respectively derived in (2.69), (2.70), (2.71) and (2.72).

$$[G_{11}] = [Z_{11}]^{-1} \quad (2.69)$$

$$[G_{21}] = [Z_{21}][Z_{11}]^{-1} \quad (2.70)$$

$$[G_{12}] = -[Z_{11}]^{-1}[Z_{12}] \quad (2.71)$$

$$[G_{22}] = [Z_{22}] - [Z_{21}][Z_{11}]^{-1}[Z_{12}] \quad (2.72)$$

The expressions of nonlinear ABCD sub-matrices $[A]$, $[B]$, $[C]$ and $[D]$ in terms of nonlinear Z-parameters are respectively derived in (2.73), (2.74), (2.75) and (2.76).

$$[A] = [Z_{11}][Z_{21}]^{-1} \quad (2.73)$$

$$[C] = [Z_{21}]^{-1} \quad (2.74)$$

$$[B] = [Z_{12}] - [Z_{11}][Z_{21}]^{-1}[Z_{22}] \quad (2.75)$$

$$[D] = -[Z_{21}]^{-1}[Z_{22}] \quad (2.76)$$

For nonlinear Y-parameters, it is obvious that nonlinear impedance matrix $[Z_{nonlin}]$ is the inverse of $[Y_{nonlin}]$:

$$[Y_{nonlin}] = [Z_{nonlin}]^{-1} \quad (2.77)$$

2.4.3 Conversion from nonlinear Y- to X-, nonlinear Z-, ABCD-, T-, G-and H-parameters

Nonlinear Y-parameters use voltages and currents whereas X- and nonlinear T-parameters use travelling waves. To derive the expression of X- and nonlinear T-parameters in terms of nonlinear Z-parameters, (2.3) and (2.4) are used. The expression of X- in terms of nonlinear Y-parameters is derived in:

$$[X] = [[Id] - Z_c [Y_{nonlin}]] [Z_c [Y_{nonlin}] + [Id]]^{-1} \quad (2.78)$$

The expressions of nonlinear T- sub matrices $[T_{11}]$, $[T_{21}]$, $[T_{12}]$ and $[T_{22}]$ are respectively derived from nonlinear Y-parameters in (2.79), (2.80), (2.81) and (2.82).

$$[T_{11}] = \frac{1}{2}([I_d] - Z_c [Y_{11}])[Y_{21}]^{-1} \left(\frac{[I_d]}{Z_c} - [Y_{22}] \right) - \frac{1}{2} Z_c [Y_{12}]. \quad (2.79)$$

$$[T_{21}] = \frac{1}{2}(Z_c [Y_{11}] + [I_d])[Y_{21}]^{-1} \left(\frac{[I_d]}{Z_c} - [Y_{22}] \right) + \frac{1}{2} Z_c [Y_{12}]. \quad (2.80)$$

$$[T_{12}] = \frac{1}{2} \left\{ (Z_c [Y_{11}] - [I_d])[Y_{21}]^{-1} \left(\frac{[I_d]}{Z_c} + [Y_{22}] \right) - Z_c [Y_{12}] \right\} \quad (2.81)$$

$$[T_{22}] = \frac{1}{2} \left\{ Z_c [Y_{12}] - (Z_c [Y_{11}] + [I_d])[Y_{21}]^{-1} \left(\frac{[I_d]}{Z_c} + [Y_{22}] \right) \right\} \quad (2.82)$$

The expressions of nonlinear H- sub-matrices $[H_{11}]$, $[H_{21}]$, $[H_{12}]$ and $[H_{22}]$ in terms of nonlinear Y-parameters are respectively derived in (2.83), (2.84), (2.85) and (2.86).

$$[H_{11}] = [Y_{11}]^{-1} \quad (2.83)$$

$$[H_{21}] = [Y_{21}][Y_{11}]^{-1} \quad (2.84)$$

$$[H_{12}] = -[Y_{11}]^{-1} [Y_{12}] \quad (2.85)$$

$$[H_{22}] = [Y_{22}] - [Y_{21}][Y_{11}]^{-1} [Y_{12}] \quad (2.86)$$

The expressions of nonlinear G- sub-matrices $[G_{11}]$, $[G_{21}]$, $[G_{12}]$ and $[G_{22}]$ in terms of nonlinear Y-parameters are respectively derived in (2.87), (2.88), (2.89) and (2.90).

$$[G_{11}] = [Y_{11}] - [Y_{12}][Y_{22}]^{-1}[Y_{21}] \quad (2.87)$$

$$[G_{21}] = -[Y_{22}]^{-1}[Y_{21}] \quad (2.88)$$

$$[G_{12}] = [Y_{12}][Y_{22}]^{-1} \quad (2.89)$$

$$[G_{22}] = [Y_{22}]^{-1} \quad (2.90)$$

The expressions of nonlinear ABCD- sub-matrices $[A]$, $[B]$, $[C]$ and $[D]$ in terms of nonlinear Y-parameters are respectively derived in (2.91), (2.92), (2.93) and (2.94).

$$[A] = -[Y_{21}]^{-1}[Y_{22}] \quad (2.91)$$

$$[C] = [Y_{12}] - [Y_{11}][Y_{21}]^{-1}[Y_{22}] \quad (2.92)$$

$$[B] = [Y_{21}]^{-1} \quad (2.93)$$

$$[D] = [Y_{11}][Y_{21}]^{-1} \quad (2.94)$$

Nonlinear impedance matrix $[Z_{nonlin}]$ is the inverse of $[Y_{nonlin}]$.

$$[Z_{nonlin}] = [Y_{nonlin}]^{-1} \quad (2.95)$$

2.4.4 Conversion from nonlinear ABCD- to X-, nonlinear Z-, Y-, T-, G- and H- parameters

Nonlinear ABCD-parameters use voltages and currents whereas X- and nonlinear T-parameters use travelling waves. To derive the expression of X- and nonlinear T-parameters in terms of nonlinear ABCD-parameters, (2.3) and (2.4) are used. The expressions of X sub-matrices $[X_{11}]$, $[X_{21}]$, $[X_{12}]$ and $[X_{22}]$ in terms of nonlinear ABCD-parameters are respectively derived in (2.96), (2.97), (2.98) and (2.99).

$$[X_{11}] = 2 \left[[A] - \frac{[B]}{Z_c} \right] \left[\left[[A] - \frac{[B]}{Z_c} + Z_c [C] - [D] \right]^{-1} - [I_d] \right] \quad (2.96)$$

$$[X_{21}] = 2 \left[[A] - \frac{[B]}{Z_c} + Z_c [C] - [D] \right]^{-1} \quad (2.97)$$

$$[X_{12}] = \left[[A] + \frac{[B]}{Z_c} \right] + \left[[A] - \frac{[B]}{Z_c} \right] [X_{22}] \quad (2.98)$$

$$[X_{22}] = - \left[[A] - \frac{[B]}{Z_c} + Z_c [C] - [D] \right]^{-1} \left[[A] + \frac{[B]}{Z_c} + Z_c [C] + [D] \right] \quad (2.99)$$

The expressions of nonlinear T- sub matrices $[T_{11}]$, $[T_{21}]$, $[T_{12}]$ and $[T_{22}]$ are respectively derived from nonlinear ABCD-parameters in (2.100), (2.101), (2.102) and (2.103).

$$[T_{11}] = \frac{1}{2} \left([A] + 1/Z_c [B] - Z_c [C] - [D] \right) \quad (2.100)$$

$$[T_{21}] = \frac{1}{2} \left([A] + 1/Z_c [B] + Z_c [C] + [D] \right) \quad (2.101)$$

$$[T_{12}] = \frac{1}{2}([A] - 1/Z_c [B] - Z_c [C] + [D]) \quad (2.102)$$

$$[T_{22}] = \frac{1}{2}([A] - 1/Z_c [B] + Z_c [C] - [D]) \quad (2.103)$$

The expressions of nonlinear Z - sub-matrices in terms of nonlinear ABCD-parameters are respectively derived in (2.104), (2.105), (2.106) and (2.107).

$$[Z_{11}] = [A][C]^{-1} \quad (2.104)$$

$$[Z_{21}] = [C]^{-1} \quad (2.105)$$

$$[Z_{12}] = [B] - [A][C]^{-1}[D] \quad (2.106)$$

$$[Z_{22}] = -[C]^{-1}[D] \quad (2.107)$$

The expressions of nonlinear Y - sub-matrices in terms of nonlinear ABCD-parameters are respectively derived in (2.108), (2.109), (2.110) and (2.111).

$$[Y_{11}] = [D][B]^{-1} \quad (2.108)$$

$$[Y_{21}] = [B]^{-1} \quad (2.109)$$

$$[Y_{12}] = [C] - [D][B]^{-1}[A] \quad (2.110)$$

$$[Y_{22}] = -[B]^{-1}[A] \quad (2.111)$$

The expressions of nonlinear H- sub-matrices in terms of nonlinear ABCD-parameters are respectively derived in (2.112), (2.113), (2.114) and (2.115).

$$[H_{11}] = [B][D]^{-1} \quad (2.112)$$

$$[H_{21}] = [D]^{-1} \quad (2.113)$$

$$[H_{12}] = [A] - [B][D]^{-1}[C] \quad (2.114)$$

$$[H_{22}] = -[D]^{-1}[C] \quad (2.115)$$

The expressions of nonlinear G- sub-matrices in terms of nonlinear ABCD-parameters are respectively derived in (2.116), (2.117), (2.118) and (2.119).

$$[G_{11}] = [C][A]^{-1} \quad (2.116)$$

$$[G_{21}] = [A]^{-1} \quad (2.117)$$

$$[G_{12}] = [D] - [C][A]^{-1}[B] \quad (2.118)$$

$$[G_{22}] = -[A]^{-1}[B] \quad (2.119)$$

2.4.5 Conversion from nonlinear T- to X-, nonlinear Z-,Y- ABCD-, G-and H-parameters

The expressions of X sub-matrices in terms of nonlinear T sub-matrices are given by (2.120), (2.121), (2.122) and (2.123).

$$[X_{11}] = [T_{12}][T_{22}]^{-1} \quad (2.120)$$

$$[X_{12}] = [T_{11}] - [T_{12}][T_{22}]^{-1}[T_{21}] \quad (2.121)$$

$$[X_{21}] = [T_{22}]^{-1} \quad (2.122)$$

$$[X_{22}] = -[T_{22}]^{-1}[T_{21}] \quad (2.123)$$

The expressions of nonlinear ABCD- sub-matrices $[A]$, $[B]$, $[C]$ and $[D]$ in terms of nonlinear T-parameters are respectively derived in (2.124), (2.125), (2.126) and (2.127).

$$[A] = \frac{1}{2}([T_{11}] + [T_{12}] + [T_{21}] + [T_{22}]) \quad (2.124)$$

$$[C] = \frac{1}{2Z_c}([T_{21}] + [T_{22}] - [T_{11}] - [T_{12}]) \quad (2.125)$$

$$[B] = \frac{Z_c}{2}([T_{11}] - [T_{12}] + [T_{21}] - [T_{22}]) \quad (2.126)$$

$$[D] = \frac{1}{2}([T_{21}] - [T_{22}] - [T_{11}] + [T_{12}]) \quad (2.127)$$

The expressions of nonlinear Z- sub-matrices in terms of nonlinear T-parameters are respectively derived in (2.128), (2.129), (2.130) and (2.131).

$$[Z_{11}] = Z_c \left([I_d] + 2[[T_{11}] + [T_{12}]] [[T_{21}] + [T_{22}] - [T_{11}] - [T_{12}]]^{-1} \right) \quad (2.128)$$

$$[Z_{21}] = 2Z_c \left[[T_{21}] + [T_{22}] - [T_{11}] - [T_{12}] \right]^{-1} \quad (2.129)$$

$$[Z_{12}] = Z_c \left[[T_{21}] - [T_{22}] \right] + Z_c \left[[T_{21}] + [T_{22}] \right] \cdot \left[[T_{11}] + [T_{12}] - [T_{21}] - [T_{22}] \right]^{-1} \left[[T_{21}] - [T_{22}] - [T_{11}] + [T_{12}] \right] \quad (2.130)$$

$$[Z_{22}] = Z_c \left[[T_{11}] + [T_{12}] - [T_{21}] - [T_{22}] \right]^{-1} \cdot \left[[T_{21}] - [T_{22}] - [T_{11}] + [T_{12}] \right] \quad (2.131)$$

The expressions of nonlinear Y- sub-matrices in terms of nonlinear T-parameters are respectively derived in (2.132), (2.133), (2.134) and (2.135).

$$[Y_{11}] = \frac{1}{Z_c} \left[[T_{21}] - [T_{22}] - [T_{11}] + [T_{12}] \right] \cdot \left[[T_{11}] - [T_{12}] + [T_{21}] - [T_{22}] \right]^{-1} \quad (2.132)$$

$$[Y_{21}] = \frac{2}{Z_c} \left[[T_{11}] - [T_{12}] + [T_{21}] - [T_{22}] \right]^{-1} \quad (2.133)$$

$$[Y_{12}] = \frac{1}{Z_c} \left(\left[[T_{21}] + [T_{22}] - \left[[T_{21}] - [T_{22}] \right] \left[[T_{11}] - [T_{12}] + [T_{21}] - [T_{22}] \right]^{-1} \cdot \left[[T_{11}] + [T_{12}] + [T_{21}] + [T_{22}] \right] \right) \quad (2.134)$$

$$[Y_{22}] = -\frac{1}{Z_c} \left[[T_{11}] - [T_{12}] + [T_{21}] - [T_{22}] \right]^{-1} \left[[T_{11}] + [T_{12}] + [T_{21}] + [T_{22}] \right] \quad (2.135)$$

The expressions of nonlinear H- sub-matrices in terms of nonlinear T-parameters are respectively derived in (2.136), (2.137), (2.138) and (2.139).

$$[H_{11}] = Z_c \left[[T_{11}] + [T_{21}] - [T_{12}] - [T_{22}] \right] \left[[T_{21}] - [T_{22}] - [T_{11}] + [T_{12}] \right]^{-1} \quad (2.136)$$

$$[H_{21}] = 2 \left[[T_{21}] - [T_{22}] - [T_{11}] + [T_{12}] \right]^{-1} \quad (2.137)$$

$$\begin{aligned} [H_{12}] = & [T_{11}] + [T_{12}] + \left[[T_{11}] - [T_{12}] \right] \\ & \cdot \left[[T_{11}] - [T_{12}] - [T_{21}] + [T_{22}] \right]^{-1} \\ & \cdot \left[[T_{21}] + [T_{22}] - [T_{11}] - [T_{12}] \right] \end{aligned} \quad (2.138)$$

$$[H_{22}] = \frac{1}{Z_c} \left[[T_{11}] - [T_{12}] - [T_{21}] + [T_{22}] \right]^{-1} \left[[T_{21}] + [T_{22}] - [T_{11}] - [T_{12}] \right] \quad (2.139)$$

The expressions of nonlinear G- sub-matrices in terms of nonlinear T-parameters are respectively derived in (2.140), (2.141), (2.142) and (2.143).

$$[G_{11}] = \frac{1}{Z_c} \left[[T_{21}] + [T_{22}] - [T_{11}] - [T_{12}] \right] \left[[T_{11}] + [T_{12}] + [T_{21}] + [T_{22}] \right]^{-1} \quad (2.140)$$

$$[G_{21}] = 2 \left[[T_{11}] + [T_{12}] + [T_{21}] + [T_{22}] \right]^{-1} \quad (2.141)$$

$$\begin{aligned} [G_{12}] = & [T_{21}] - [T_{22}] - \left[[T_{21}] + [T_{22}] \right] \\ & \cdot \left[[T_{11}] + [T_{12}] + [T_{21}] + [T_{22}] \right]^{-1} \\ & \cdot \left[[T_{11}] + [T_{21}] - [T_{12}] - [T_{22}] \right] \end{aligned} \quad (2.142)$$

$$\begin{aligned} [G_{22}] = & -Z_c \left[[T_{11}] + [T_{12}] + [T_{21}] + [T_{22}] \right]^{-1} \\ & \cdot \left[[T_{11}] + [T_{21}] - [T_{12}] - [T_{22}] \right] \end{aligned} \quad (2.143)$$

2.4.6 Conversion from nonlinear G- to X-, nonlinear Z-,Y- ABCD-, T- and H-parameters

The expressions of X sub-matrices in terms of nonlinear G sub-matrices are given by (2.144), (2.145), (2.146) and (2.147).

$$\begin{aligned}
 [X_{11}] = & \left[[G_{11}] + \frac{[I_d]}{Z_c} - \frac{[G_{12}]}{Z_c} \left[[I_d] + \frac{[G_{22}]}{Z_c} \right]^{-1} [G_{21}] \right]^{-1} \\
 & \cdot \left[\frac{[I_d]}{Z_c} - [G_{11}] + \frac{[G_{12}]}{Z_c} \left[[I_d] + \frac{[G_{22}]}{Z_c} \right]^{-1} [G_{21}] \right]
 \end{aligned} \tag{2.144}$$

$$\begin{aligned}
 [X_{21}] = & \left[[I_d] + \frac{[G_{22}]}{Z_c} \right]^{-1} [G_{21}] \left\{ [I_d] + \right. \\
 & \cdot \left[[G_{11}] + \frac{[I_d]}{Z_c} - \frac{[G_{12}]}{Z_c} \left[[I_d] + \frac{[G_{22}]}{Z_c} \right]^{-1} [G_{21}] \right]^{-1} \\
 & \left. \cdot \left[\frac{[I_d]}{Z_c} - [G_{11}] + \frac{[G_{12}]}{Z_c} \left[[I_d] + \frac{[G_{22}]}{Z_c} \right]^{-1} [G_{21}] \right] \right\}
 \end{aligned} \tag{2.145}$$

$$\begin{aligned}
 [X_{12}] = & \left[[G_{11}] + \frac{[I_d]}{Z_c} - \frac{[G_{12}]}{Z_c} \left[[I_d] + \frac{[G_{22}]}{Z_c} \right]^{-1} [G_{21}] \right]^{-1} \\
 & \cdot \frac{[G_{12}]}{Z_c} \left[\left[[I_d] + \frac{[G_{22}]}{Z_c} \right]^{-1} \left[\frac{[G_{22}]}{Z_c} - [I_d] \right] - [I_d] \right]
 \end{aligned} \tag{2.146}$$

$$\begin{aligned}
 [X_{22}] = & \left[[I_d] + \frac{[G_{22}]}{Z_c} \right]^{-1} \left\{ [G_{21}] \right. \\
 & \cdot \left[[G_{11}] + \frac{[I_d]}{Z_c} - \frac{[G_{12}]}{Z_c} \left[[I_d] + \frac{[G_{22}]}{Z_c} \right]^{-1} [G_{21}] \right]^{-1} \\
 & \left. \cdot \frac{[G_{12}]}{Z_c} \left[\left[[I_d] + \frac{[G_{22}]}{Z_c} \right]^{-1} \left[\frac{[G_{22}]}{Z_c} - [I_d] \right] - [I_d] \right] + \left[\frac{[G_{22}]}{Z_c} - [I_d] \right] \right\}
 \end{aligned} \tag{2.147}$$

The expressions of nonlinear T sub-matrices in terms of nonlinear G sub-matrices are given by (2.148), (2.149), (2.150) and (2.151).

$$[T_{11}] = \frac{1}{2} \left\{ [[I_d] - Z_c [G_{11}]] [G_{21}]^{-1} \left[[I_d] - \frac{[G_{22}]}{Z_c} \right] - [G_{12}] \right\} \quad (2.148)$$

$$[T_{21}] = \frac{1}{2} \left\{ [[I_d] + Z_c [G_{11}]] [G_{21}]^{-1} \left[[I_d] - \frac{[G_{22}]}{Z_c} \right] + [G_{12}] \right\} \quad (2.149)$$

$$[T_{12}] = \frac{1}{2} \left\{ [[I_d] - Z_c [G_{11}]] [G_{21}]^{-1} \left[[I_d] + \frac{[G_{22}]}{Z_c} \right] + [G_{12}] \right\} \quad (2.150)$$

$$[T_{22}] = \frac{1}{2} \left\{ [[I_d] + Z_c [G_{11}]] [G_{21}]^{-1} \left[[I_d] + \frac{[G_{22}]}{Z_c} \right] - [G_{12}] \right\} \quad (2.151)$$

The expressions of nonlinear Z sub-matrices in terms of nonlinear G sub-matrices are given by (2.152), (2.153), (2.154) and (2.155).

$$[Z_{11}] = [G_{11}]^{-1} \quad (2.152)$$

$$[Z_{21}] = [G_{21}] [G_{11}]^{-1} \quad (2.153)$$

$$[Z_{12}] = -[G_{11}]^{-1} [G_{12}] \quad (2.154)$$

$$[Z_{22}] = [G_{22}] - [G_{21}] [G_{11}]^{-1} [G_{12}] \quad (2.155)$$

The expressions of nonlinear Y sub-matrices in terms of nonlinear G sub-matrices are given by (2.156), (2.157), (2.158) and (2.159).

$$[Y_{11}] = [G_{11}] - [G_{12}][G_{22}]^{-1}[G_{21}] \quad (2.156)$$

$$[Y_{21}] = -[G_{22}]^{-1}[G_{21}] \quad (2.157)$$

$$[Y_{12}] = [G_{12}][G_{22}]^{-1} \quad (2.158)$$

$$[Y_{22}] = [G_{22}]^{-1} \quad (2.159)$$

The expressions of nonlinear ABCD sub-matrices in terms of nonlinear G sub-matrices are given by (2.160), (2.161), (2.162) and (2.163).

$$[A] = [G_{21}]^{-1} \quad (2.160)$$

$$[C] = [G_{11}][G_{21}]^{-1} \quad (2.161)$$

$$[B] = -[G_{21}]^{-1}[G_{22}] \quad (2.162)$$

$$[D] = [G_{12}] - [G_{11}][G_{21}]^{-1}[G_{22}] \quad (2.163)$$

Nonlinear H- matrix $[H_{nonlin}]$ is the inverse of nonlinear G- matrix $[G_{nonlin}]$:

$$[H_{nonlin}] = [G_{nonlin}]^{-1} \quad (2.164)$$

2.4.7 Conversion from nonlinear H- to X-, nonlinear Z-, Y- ABCD-, T- and G- parameters

The expressions of nonlinear X- sub-matrices in terms of nonlinear H sub-matrices are given by (2.165), (2.166), (2.167) and (2.168).

$$\begin{aligned}
[X_{11}] = & \left[[I_d] + \frac{[H_{11}]}{Z_c} - [H_{12}] \left[\frac{[I_d]}{Z_c} + [H_{22}] \right]^{-1} \frac{[H_{21}]}{Z_c} \right]^{-1} \\
& \cdot \left[\frac{[H_{11}]}{Z_c} - [I_d] - [H_{12}] \left[\frac{[I_d]}{Z_c} + [H_{22}] \right]^{-1} \frac{[H_{21}]}{Z_c} \right]
\end{aligned} \tag{2.165}$$

$$\begin{aligned}
[X_{21}] = & \left[\left[\frac{[I_d]}{Z_c} \right] + [H_{22}] \right]^{-1} \frac{[H_{21}]}{Z_c} \\
& \cdot \left\{ \left[[I_d] + \frac{[H_{11}]}{Z_c} - [H_{12}] \left[\frac{[I_d]}{Z_c} + [H_{22}] \right]^{-1} \frac{[H_{21}]}{Z_c} \right]^{-1} \right. \\
& \left. \cdot \left[\frac{[H_{11}]}{Z_c} - [I_d] - [H_{12}] \left[\frac{[I_d]}{Z_c} + [H_{22}] \right]^{-1} \frac{[H_{21}]}{Z_c} \right] - [I_d] \right\}
\end{aligned} \tag{2.166}$$

$$[X_{12}] = -\frac{2}{Z_c} \left[\frac{[H_{21}]}{Z_c} - \left[\frac{[I_d]}{Z_c} + [H_{22}] \right] [H_{12}]^{-1} \left[[I_d] + \frac{[H_{11}]}{Z_c} \right] \right]^{-1} \tag{2.167}$$

$$\begin{aligned}
[X_{22}] = & -\frac{2}{Z_c} [H_{12}]^{-1} \left[[I_d] + \frac{[H_{11}]}{Z_c} \right] \\
& \cdot \left[\frac{[H_{21}]}{Z_c} - \left[\frac{[I_d]}{Z_c} + [H_{22}] \right] [H_{12}]^{-1} \left[[I_d] + \frac{[H_{11}]}{Z_c} \right] \right]^{-1} - [I_d]
\end{aligned} \tag{2.168}$$

The expressions of nonlinear Z sub-matrices in terms of nonlinear H are given by (2.169), (2.170), (2.171) and (2.172).

$$[Z_{11}] = [H_{11}] - [H_{12}] [H_{22}]^{-1} [H_{21}] \tag{2.169}$$

$$[Z_{21}] = -[H_{22}]^{-1} [H_{21}] \tag{2.170}$$

$$[Z_{12}] = [H_{12}][H_{22}]^{-1} \quad (2.171)$$

$$[Z_{22}] = [H_{22}]^{-1} \quad (2.172)$$

The expressions of nonlinear Y sub-matrices in terms of nonlinear H are given by (2.173), (2.174), (2.175) and (2.176).

$$[Y_{11}] = [H_{11}]^{-1} \quad (2.173)$$

$$[Y_{21}] = [H_{21}][H_{11}]^{-1} \quad (2.174)$$

$$[Y_{12}] = -[H_{11}]^{-1}[H_{12}] \quad (2.175)$$

$$[Y_{22}] = [H_{22}] - [H_{21}][H_{11}]^{-1}[H_{12}] \quad (2.176)$$

The expressions of nonlinear ABCD sub-matrices in terms of nonlinear H are given by (2.177), (2.178), (2.179) and (2.180).

$$[A] = [H_{12}] - [H_{11}][H_{21}]^{-1}[H_{22}] \quad (2.177)$$

$$[B] = [H_{11}][H_{21}]^{-1} \quad (2.178)$$

$$[C] = -[H_{21}]^{-1}[H_{22}] \quad (2.179)$$

$$[D] = [H_{21}]^{-1} \quad (2.180)$$

The expressions of nonlinear T sub-matrices in terms of nonlinear H are given by (2.181), (2.182), (2.183) and (2.184).

$$[T_{11}] = \frac{1}{2} \left[[H_{12}] + Z_c \left[\frac{[H_{11}]}{Z_c} - [I_d] \right] [H_{21}]^{-1} \left[\frac{[I_d]}{Z_c} - [H_{22}] \right] \right] \quad (2.181)$$

$$[T_{21}] = \frac{1}{2} \left[[H_{12}] + \left[\frac{[H_{11}]}{Z_c} - [I_d] \right] [H_{21}]^{-1} \left[[I_d] - Z_c [H_{22}] \right] \right] \quad (2.182)$$

$$[T_{12}] = \frac{1}{2} \left[[H_{12}] - \left[\frac{[H_{11}]}{Z_c} - [I_d] \right] [H_{21}]^{-1} \left[[I_d] + Z_c [H_{22}] \right] \right] \quad (2.183)$$

$$[T_{22}] = \frac{1}{2} \left[[H_{12}] - \left[\frac{[H_{11}]}{Z_c} + [I_d] \right] [H_{21}]^{-1} \left[[I_d] + Z_c [H_{22}] \right] \right] \quad (2.184)$$

Nonlinear G- matrix $[G_{nonlin}]$ is the inverse of nonlinear H- matrix $[H_{nonlin}]$.

$$[G_{nonlin}] = [H_{nonlin}]^{-1} \quad (2.185)$$

2.5 Linear operation mode validation of nonlinear two port network parameters

X-parameters reduce to S-parameters when the device is operated in linear mode. For small $|a_{11}|$ (linear operation), all F_{ik} terms for $k > 1$ vanish as well as all cross frequency S_{ikjl} terms and all T_{ikjl} terms. To determine the expression of nonlinear Z in linear operation mode, we just calculate the analytical expression (2.29). The result concludes that all nonlinear Z^β terms vanish as well as all cross frequency $Z_{m \neq j}^{\alpha pmqj}$ terms. The expressions of nonlinear Z_{pmqm}^α terms vanish to linear impedance in linear operation mode and they are equal to Z_{pq} . With the same manner, the expression of nonlinear admittances in linear operation

mode is determined by calculating (2.32). The result concludes that all nonlinear Y^β terms vanish as well as all cross frequency Y_{pmqj}^α terms. The expressions of nonlinear Y_{pmqm}^α terms vanish to linear impedance in linear operation mode and they are equal to Y_{pq} . Like nonlinear impedance and admittance, nonlinear ABCD-parameters are reduced to linear counterparts. Based on the analytic calculation, we conclude that in linear mode, all nonlinear terms A^β , B^β , C^β and D^β vanish as well as all cross frequency terms A_{pmqj}^α , B_{pmqj}^α , C_{pmqj}^α and D_{pmqj}^α . The expressions of nonlinear A_{pmqm}^α , B_{pmqm}^α , C_{pmqm}^α and D_{pmqm}^α terms vanish to linear impedance in linear operation mode and they are equal respectively to A , B , C and D . Nonlinear T-parameters are also reduced to linear counterparts. In linear operation mode, the analytic calculation of T-parameters proves that all nonlinear T^β terms vanish as well as all cross frequency T_{pmqj}^α terms and nonlinear T_{pmqm}^α terms vanish to linear T_{pq} . Nonlinear H-parameters are also reduced to linear counterparts. In linear operation mode, the analytic calculation of H-parameters proves that all nonlinear H^β terms vanish as well as all cross frequency H_{pmqj}^α terms and nonlinear H_{pmqm}^α terms vanish to linear H_{pq} . Nonlinear G-parameters are also reduced to linear counterparts. In linear operation mode, the analytic calculation of G-parameters proves that all nonlinear G^β terms vanish as well as all cross frequency G_{pmqj}^α terms and nonlinear G_{pmqm}^α terms vanish to linear G_{pq} . Besides, in linear operation mode, conversion rules between nonlinear parameters are also reduced to linear counterparts.

2.6 Non-Linear operation mode validation of nonlinear two-port network parameters

The process of large-signal validation consists of performing both harmonic balance and X-parameters simulations of the same xnp measurement file under the same conditions, i.e, the same input power, dc bias and terminations. X-parameters data are used to calculate other

nonlinear parameters. Harmonic Balance simulation is used to measure the different harmonic components of voltage and currents. The process of the validation is applied to a measurement file ‘ZX602522M_X2P.xnp’ provided by ADS with a 50 ohm termination and a power range between -10 dBm to 4 dBm.

2.6.1 Nonlinear operation mode validation of nonlinear Z-parameters

To validate the expression of nonlinear Z-parameters, harmonic component voltages are compared. The amplitude and phase parts of measured and calculated voltages by (2.16) at the fundamental, second harmonic and third harmonic are illustrated in Figure 2.1. The figure shows a good agreement between calculated and measured harmonic component voltages at the input and output of the amplifier. Both kinds of harmonic voltages coincide in small-signal as well as in large-signal operation mode. This result validates the expression of nonlinear voltage in terms of nonlinear impedance parameters and nonlinear current. To verify the conversion rules from the other nonlinear parameters to nonlinear impedance parameters, Figure 2.2 illustrate the amplitude and phase of nonlinear impedance parameters determined from X-, nonlinear Y-, nonlinear ABCD-, nonlinear T-, nonlinear G- and nonlinear H- parameters. For a 2 port-circuit and 3 harmonic orders, 72 nonlinear impedance terms could be obtained. In order to keep the figures legible, only 6 arbitrary terms are used: Z_{2322}^{β} , Z_{2222}^{β} , Z_{1212}^{α} , Z_{1123}^{α} , Z_{2121}^{β} and Z_{1322}^{α} . Figure 2.2 illustrates a good agreement between nonlinear impedance parameters calculated from X-, nonlinear Y-, ABCD-, T-, G- and H- parameters.

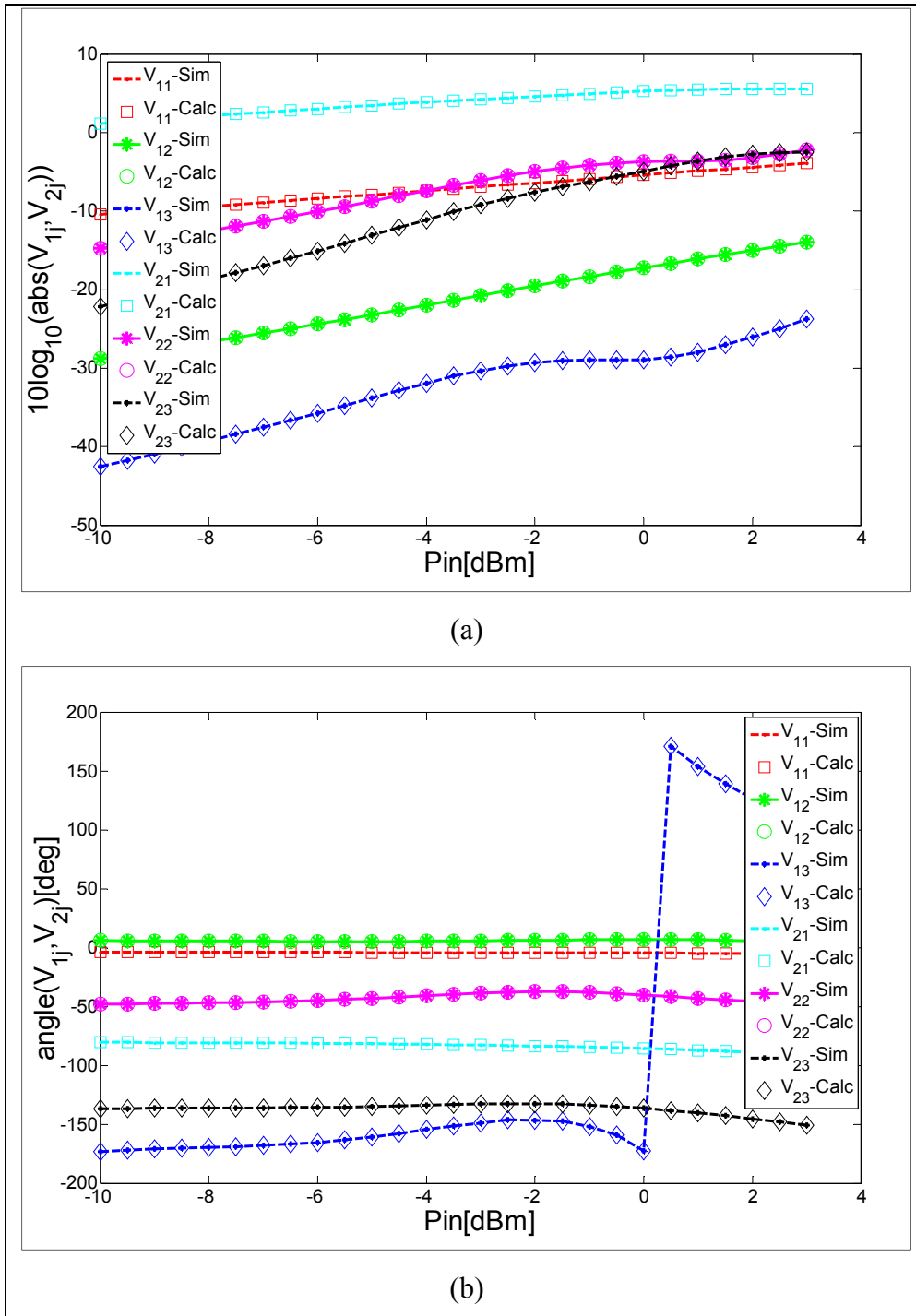


Figure 2.1 Comparison between the logarithmic amplitude (a) and phase (b) of harmonic voltages calculated through nonlinear impedance parameters and those simulated at the input and output ports.

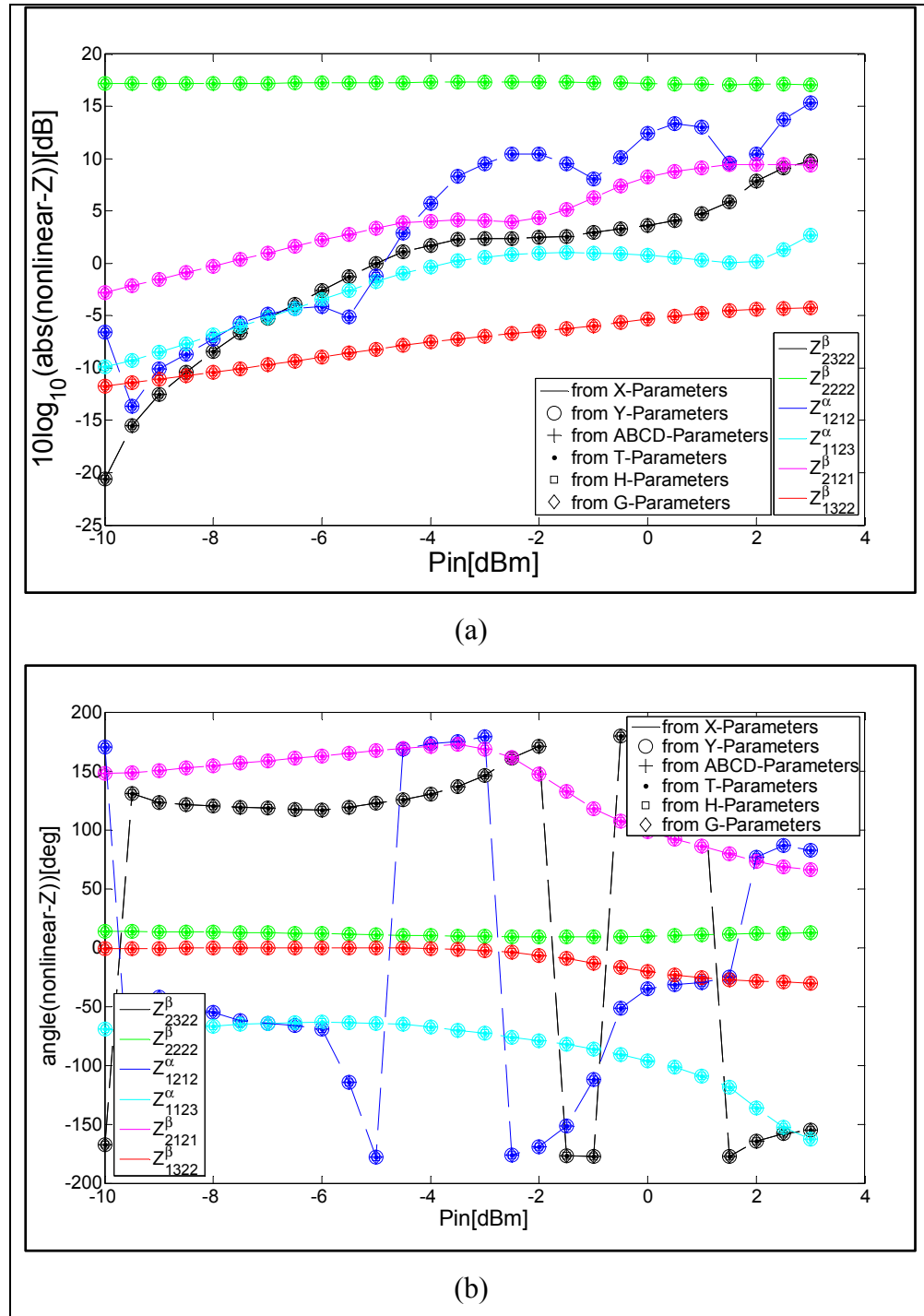


Figure 2.2 Logarithmic amplitude (a) and phase (b) of a random set of nonlinear impedance parameters converted from X-, nonlinear Y-, ABCD-, T-, H- and G-parameters.

2.6.2 Nonlinear operation mode validation of nonlinear Y-parameters

To validate the expression of nonlinear Y-parameters, harmonic component currents are compared. The amplitude and phase parts of measured and calculated currents by (2.17) at input and output device ports, corresponding to the fundamental, second and third harmonic are illustrated in Figure 2.3, respectively. The figure shows a good agreement between calculated and measured harmonic component currents. Both kinds of harmonic currents coincide in small-signal as well as in large-signal operation mode. This result confirms the expression of nonlinear currents in terms of nonlinear admittance parameters and nonlinear voltages.

To confirm the conversion rules between nonlinear admittance and the other nonlinear parameters, Figure 2.4 illustrates the amplitude and phase of nonlinear admittance parameters determined from X-, nonlinear Z-, ABCD-, T-, G- and H- parameters. For a 2 port-circuit and 3 harmonic orders, 72 nonlinear impedance terms could be obtained. In order to keep the figure legible, only 6 arbitrary terms are used: Y_{2323}^{β} , Y_{1213}^{α} , Y_{2221}^{β} , Y_{2112}^{α} , Y_{1122}^{β} and Y_{1321}^{α} . Figure 2.4 illustrates a good agreement between nonlinear admittance parameters calculated from X-, nonlinear Z-, ABCD-, T-, G- and H- parameters.

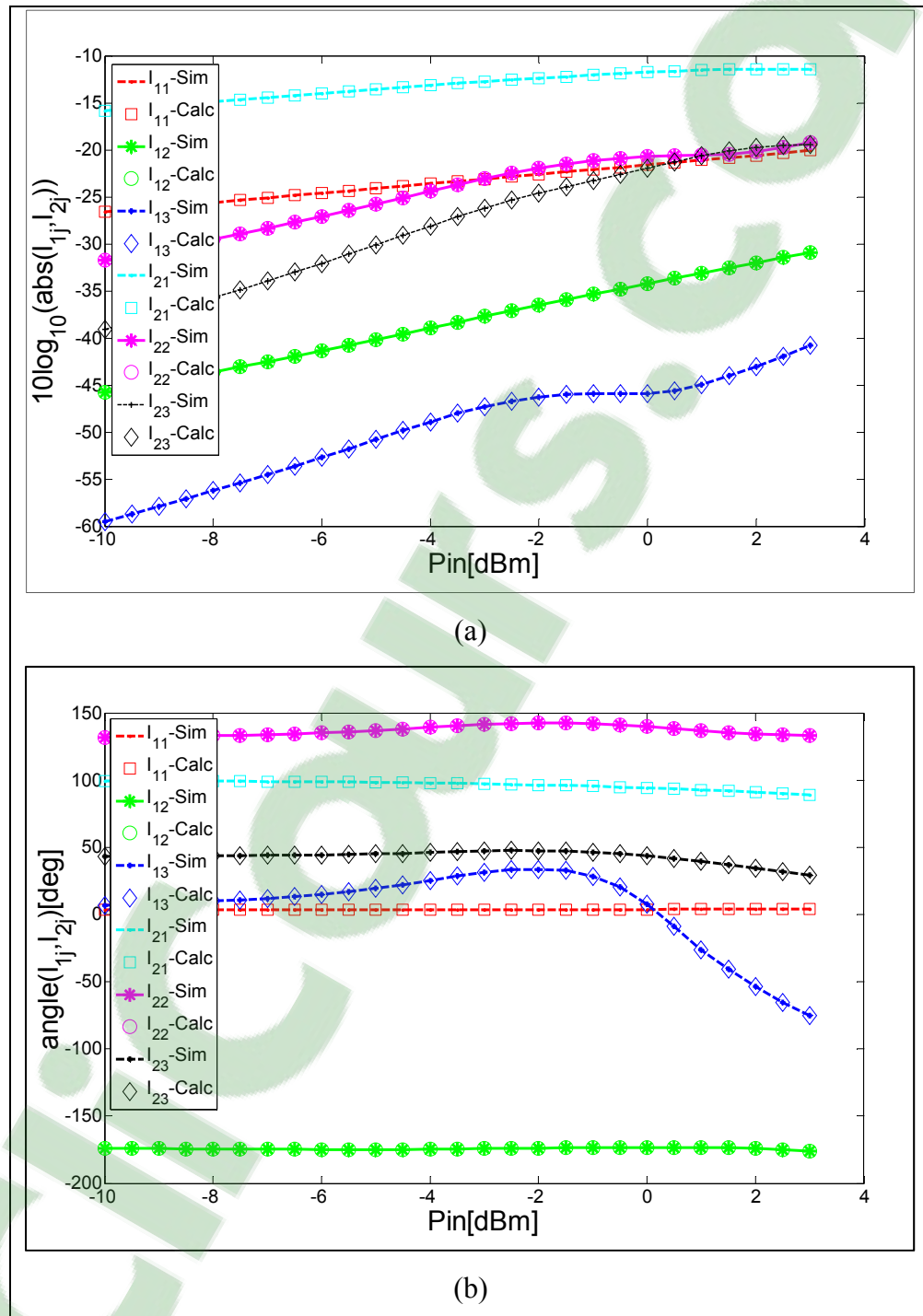


Figure 2.3 Comparison between the logarithmic amplitude (a) and the phase (b) of harmonic currents calculated through nonlinear admittance parameters and those simulated at the input and output ports.

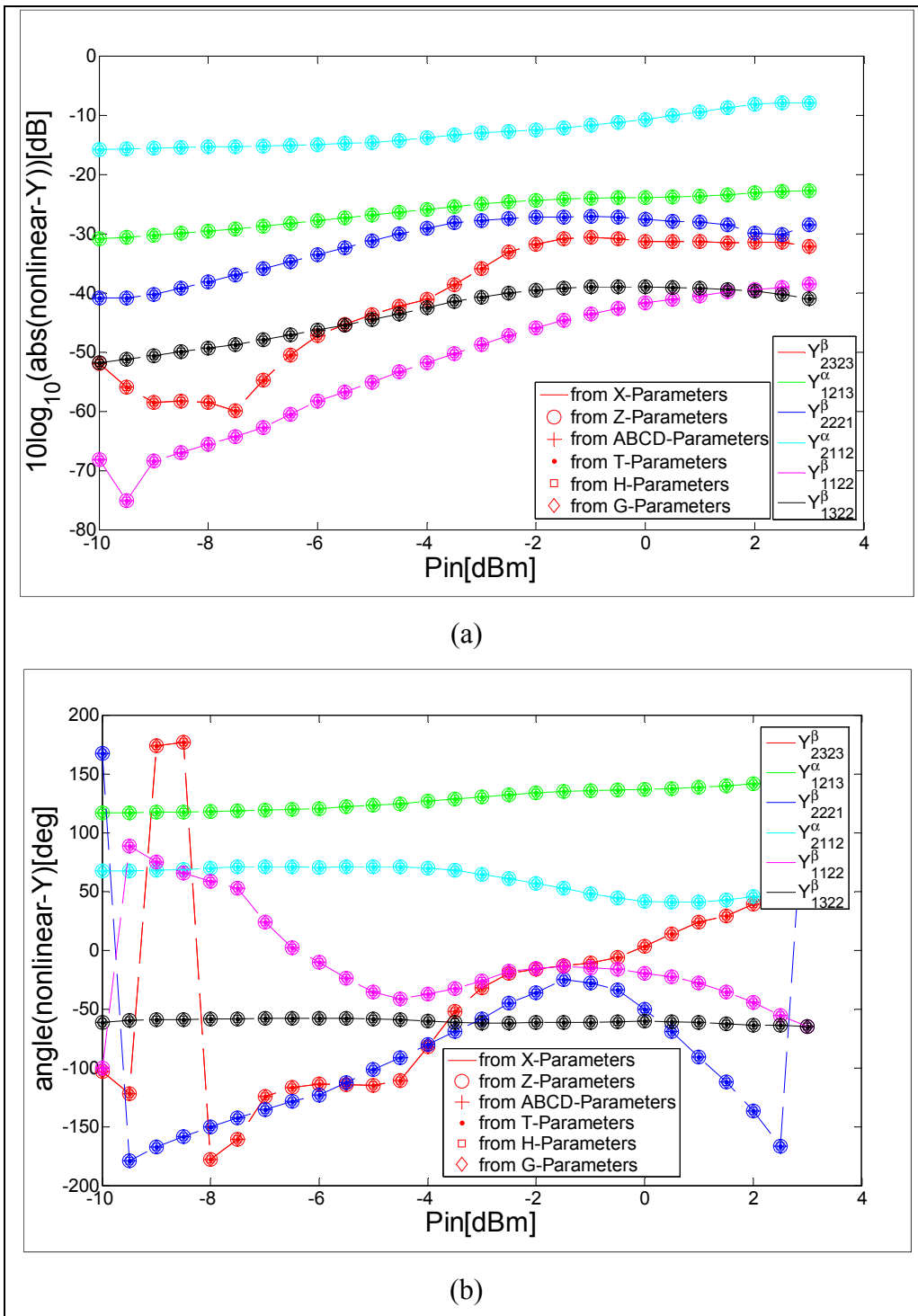


Figure 2.4 Logarithmic amplitude (a) and phase (b) of a random set of nonlinear admittance parameters converted from X-, nonlinear Z-, ABCD-, T-, H- and G-parameters.

2.6.3 Nonlinear operation mode validation of nonlinear ABCD-parameters

To validate the expression of nonlinear ABCD-parameters, harmonic voltages and currents present at the first port of the device are compared. The amplitude and phase parts of measured and calculated voltages and currents, present at the input, corresponding to the fundamental, second and third harmonics are illustrated in Figure 2.5, respectively. The figure shows a good agreement between calculated and measured input harmonic component voltages and currents. They coincide in small-signal as well as in large-signal operation mode. This result confirms the expression of ABCD matrix. To confirm the conversion rules from the other nonlinear parameters to nonlinear ABCD-parameters, Figure 2.6 illustrates the amplitude and phase of nonlinear ABCD parameters determined from X-, nonlinear Z-, Y-, T-, G- and H-parameters. The figures are limited to 6 arbitrary terms: A_{1122}^{β} , A_{1321}^{α} , B_{1123}^{β} , B_{1223}^{α} , C_{1123}^{β} and D_{1121}^{α} for legibility purposes. The figure illustrates a good agreement.

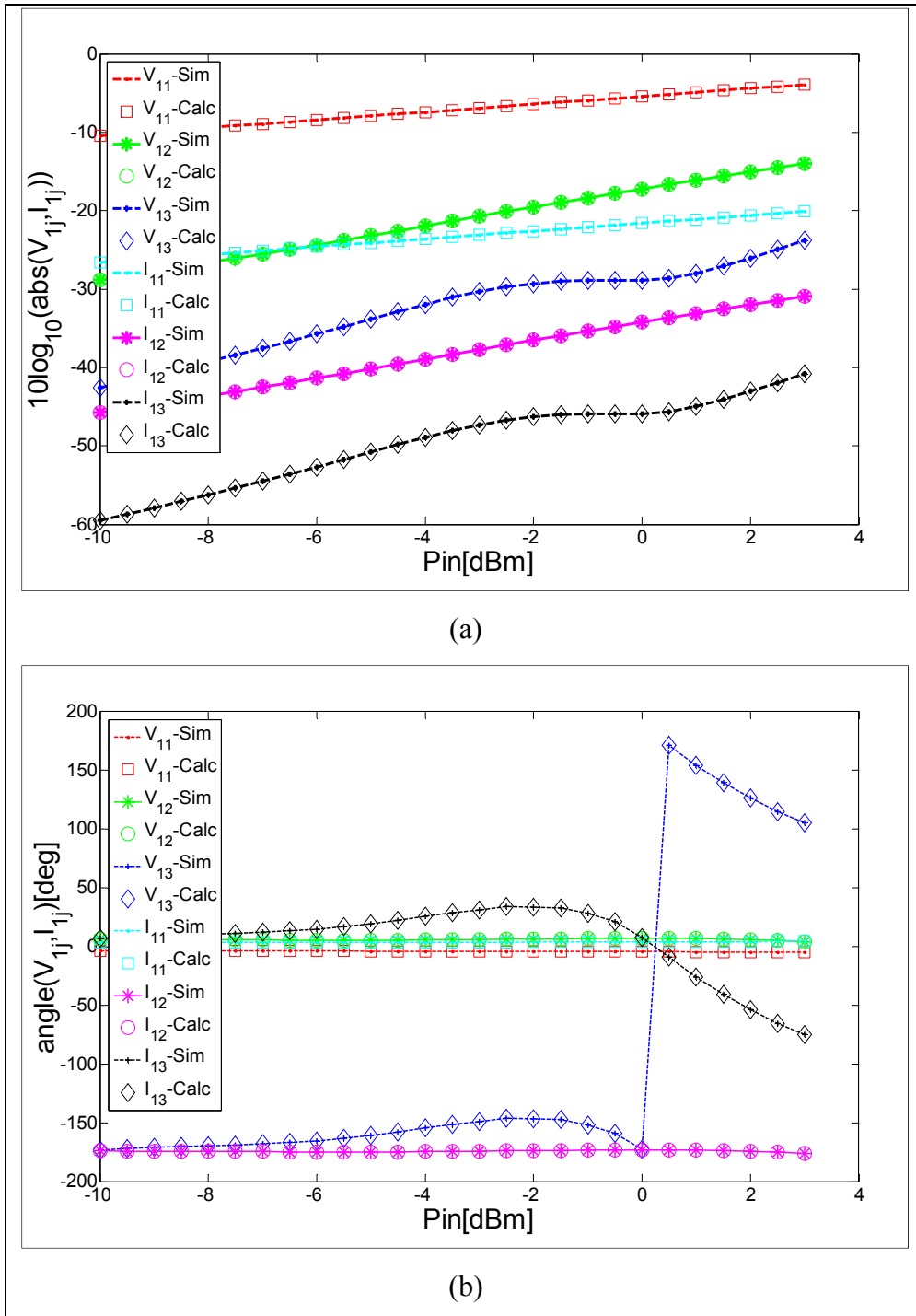


Figure 2.5 Comparison between the logarithmic amplitude (a) and phase (b) of harmonic voltages and currents calculated through nonlinear cascade parameters and those simulated at device input.

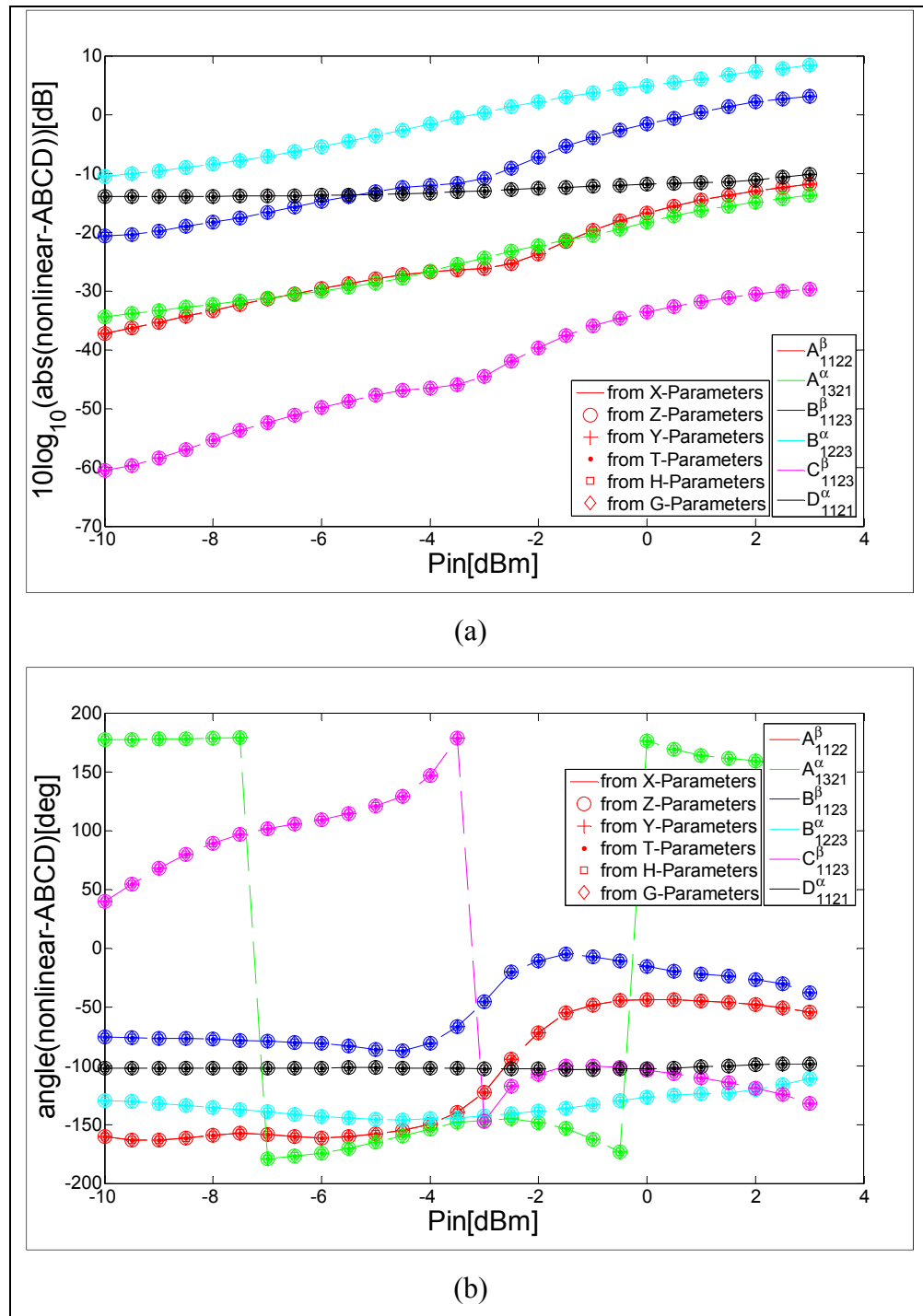


Figure 2.6 Logarithmic amplitude (a) and phase (b) of a random set of nonlinear ABCD-parameters converted from X-, nonlinear Z-, Y-, T-, H- and G-parameters

2.6.4 Nonlinear operation mode validation of nonlinear T-parameters

To validate the expression of nonlinear T-parameters, calculated travelling voltage waves present at the first port are compared the measured ones. The amplitude and phase parts of measured and calculated travelling voltage waves, present at the input, corresponding to the fundamental, second and third harmonics are illustrated in Figure 2.7.

To validate the conversion rules giving the expressions of nonlinear T-parameters in terms of the other nonlinear parameters, Figure 2.8 illustrates the amplitude and phase of nonlinear T-parameters determined from nonlinear Z-, Y-, ABCD-, T-, G- and H-parameters. In order to not burden the figures with different parameters and since the aim is to show validation results, we will limit ourselves to the following terms that are chosen randomly: T_{1123}^{β} , T_{2311}^{α} ,

$$T_{2211}^{\alpha}, T_{1312}^{\alpha}, T_{2113}^{\beta}, T_{1221}^{\beta}.$$

Figure 2.8 shows a good agreement between the curves of nonlinear T-parameters calculated from nonlinear Z, Y-, ABCD-, G- and H-parameters. This agreement proves the exactness of the conversion rules demonstrated in this paper.

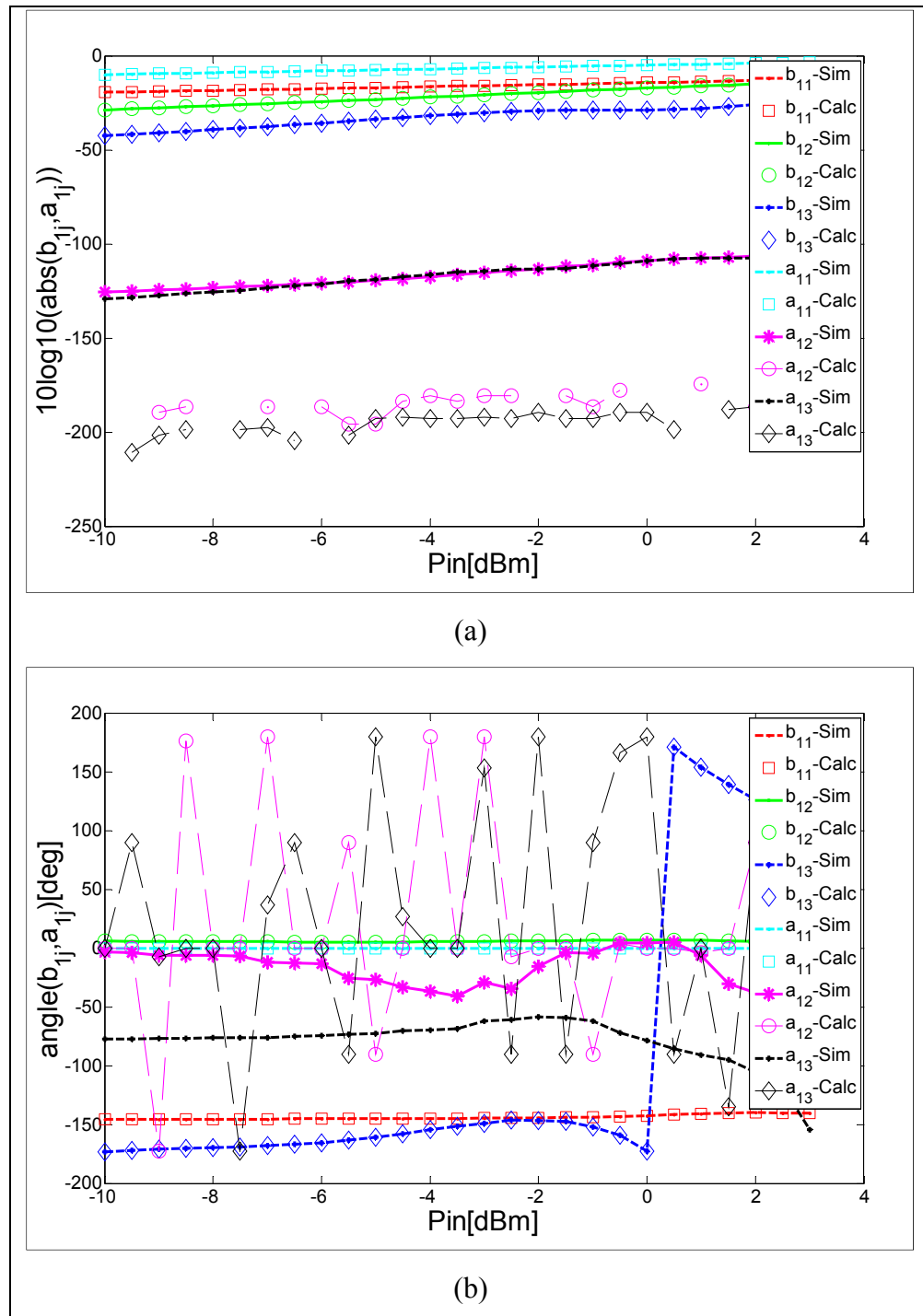


Figure 2.7 Comparison between the logarithmic amplitude (a) and phase (b) of harmonic incident and scattered voltage wave calculated through nonlinear scattering transfer parameters and those simulated at device input port.

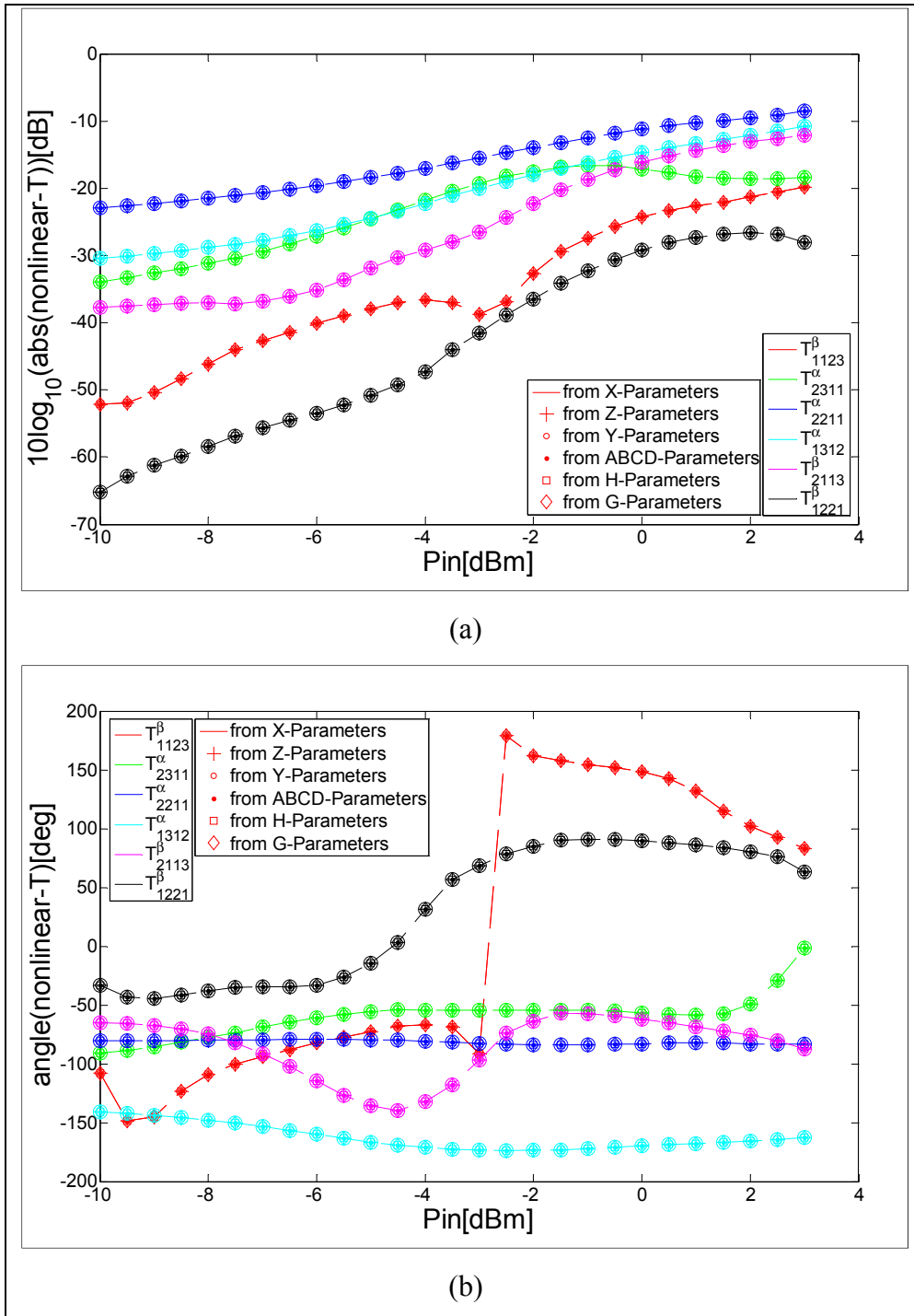


Figure 2.8 Logarithmic amplitude (a) and phase (b) of a random set of nonlinear T-parameters determined from X-, nonlinear Z-, Y-, ABCD-, H- and G-parameters.

2.6.5 Nonlinear operation mode validation of nonlinear H-parameters

To validate the expression of nonlinear H-parameters in (2.22) and (2.23), calculated harmonic voltages at the first port and harmonic currents present at the second port are compared to the measured ones. The amplitude and phase parts of measured and calculated voltages and currents, present at the input and the output respectively, corresponding to the fundamental, second harmonic and third harmonic are illustrated in Figure 2.9.

To validate the conversion rules giving the expressions of nonlinear H-parameters in terms of the other nonlinear parameters, Figure 2.10 illustrates the amplitude and phase of nonlinear H-parameters determined from X-, nonlinear Z-, Y-, ABCD-, T- and G-parameters.

The figure is limited to 7 arbitrary terms: H_{2311}^{α} , H_{1312}^{α} , H_{2223}^{β} , H_{2113}^{β} , H_{1122}^{α} and H_{1111}^{α} . Figure 2.10 shows a good agreement between the curves of nonlinear H-parameters calculated from nonlinear Z-, Y-, ABCD-, G- and T-parameters. This agreement proves the exactness of the conversion rules demonstrated in this paper.

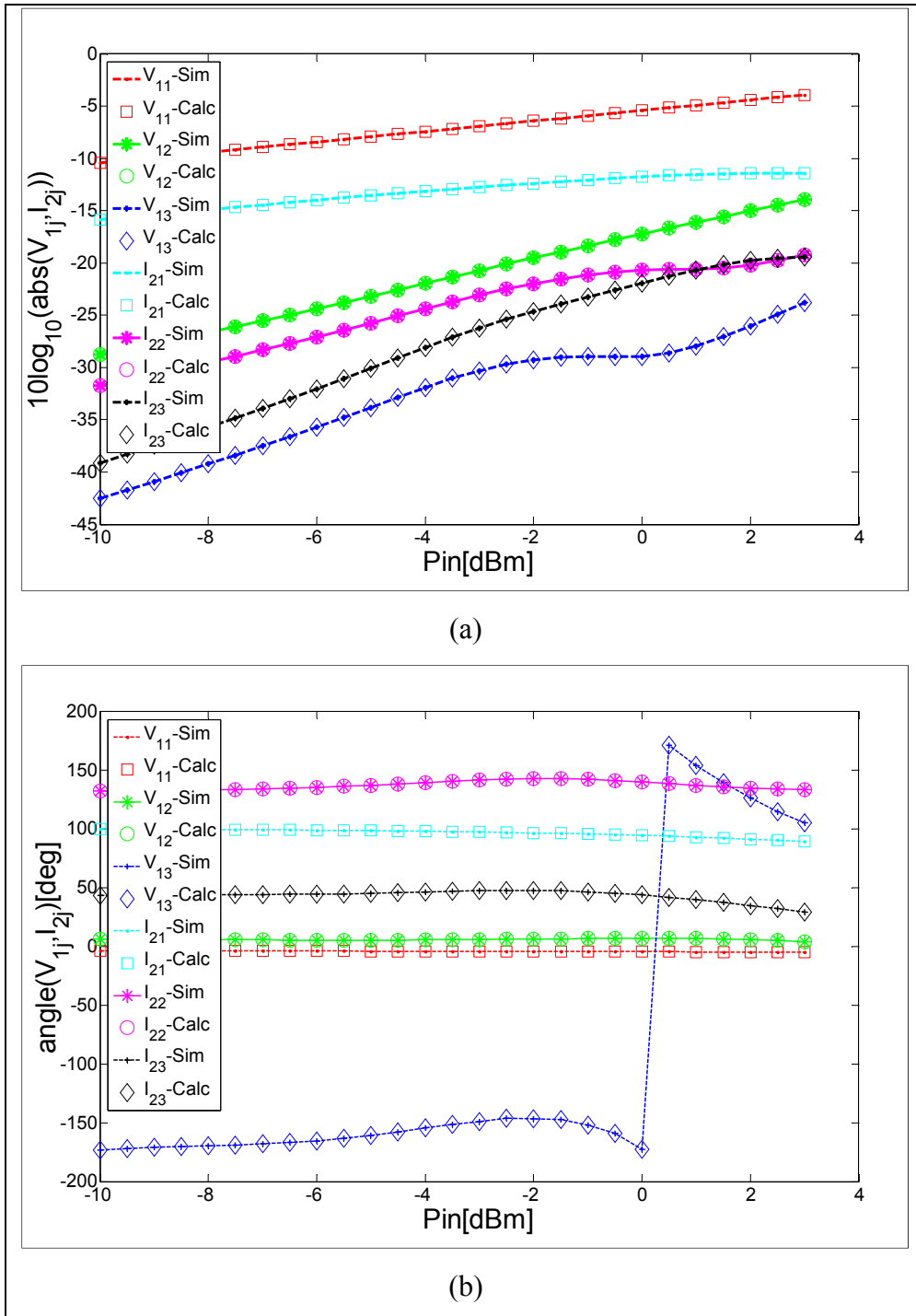


Figure 2.9 Comparison between the logarithmic amplitude (a) and the phase (b) of harmonic voltage present at port1 and harmonic current present at port2 calculated through nonlinear H-parameters and of the simulated ones.

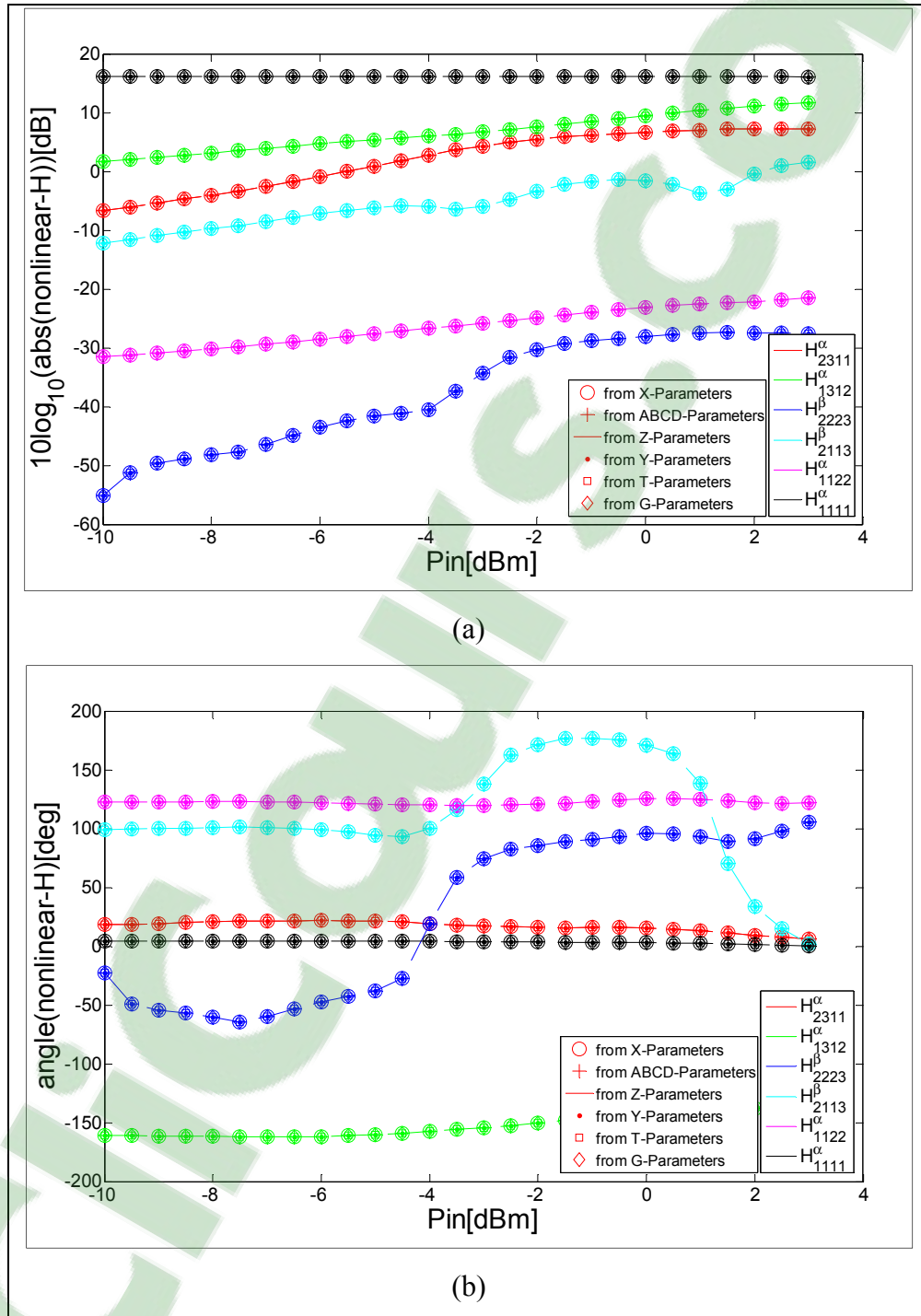


Figure 2.10 Logarithmic amplitude (a) and phase (b) of a random set of nonlinear H-parameters determined from X, nonlinear Z-, Y-, ABCD-, T- and G-parameters

2.6.6 Nonlinear operation mode validation of nonlinear G-parameters

To validate the expression of nonlinear G-parameters in (2.42), calculated harmonic currents at the first port and harmonic voltages present at the second port are compared to the measurement in Figure 2.11. The good agreement proves the exactness of the expression. To validate the conversion rules giving the expressions of nonlinear G-parameters in terms of the other nonlinear parameters, Figure 2.12 illustrates the amplitude and phase of nonlinear G-parameters determined from X-, nonlinear Z-, Y-, ABCD-, T- and H-parameters. In order to not overload figures or the paper and since we just like to illustrate the agreement of curves, we will limit to the following terms that are chosen randomly: G_{1322}^{β} , G_{1111}^{β} , G_{1213}^{α} , G_{2222}^{α} , G_{1113}^{α} and G_{2113}^{β} . The figure shows a good agreement between the curves of calculated nonlinear G-parameters. This agreement proves the exactness of the conversion rules demonstrated in this paper.

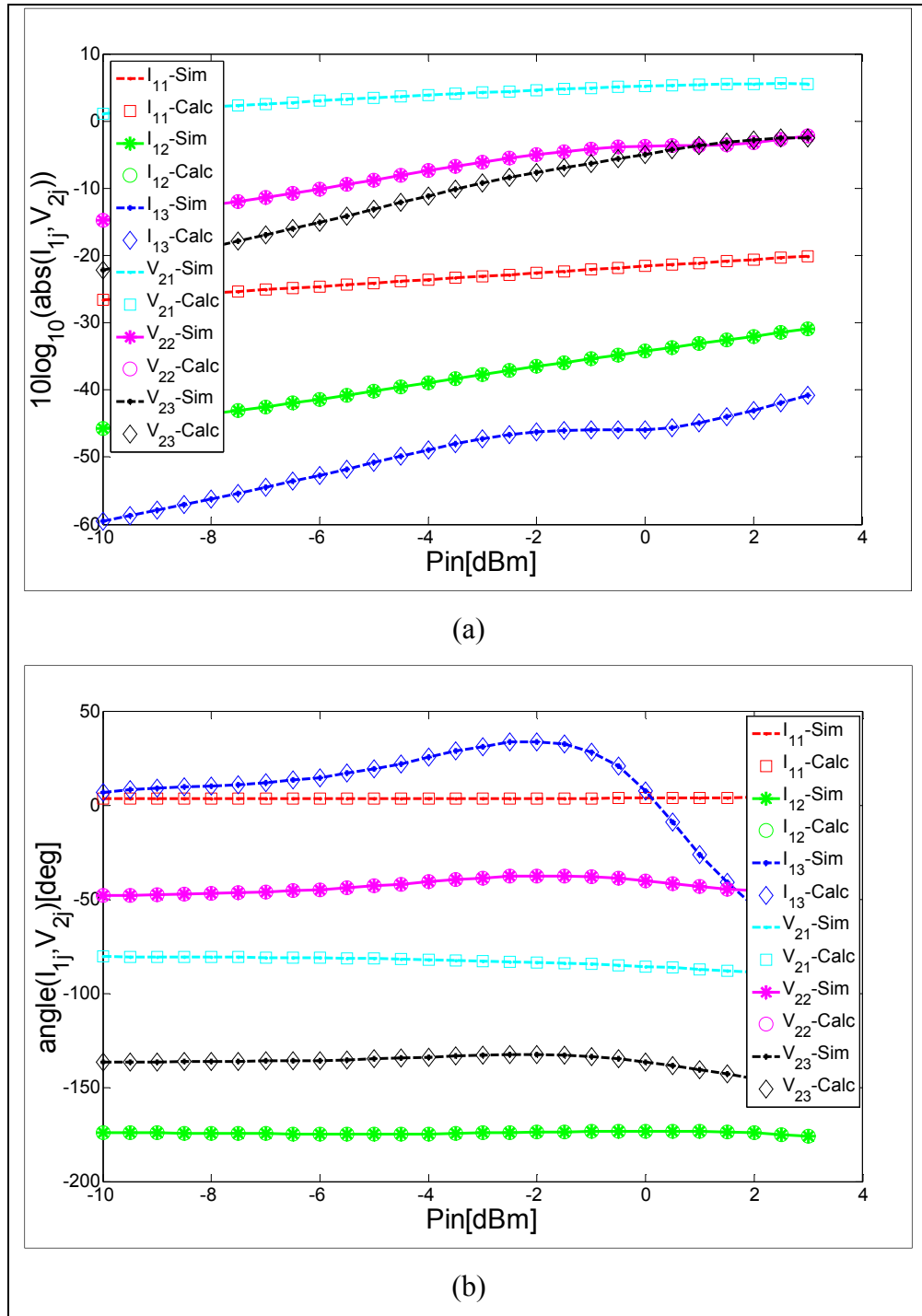


Figure 2.11 Comparison between the logarithmic amplitude (a) and phase (b) of harmonic current present at port1 and harmonic voltage present at port2 calculated through nonlinear G-parameters and of the simulated ones.

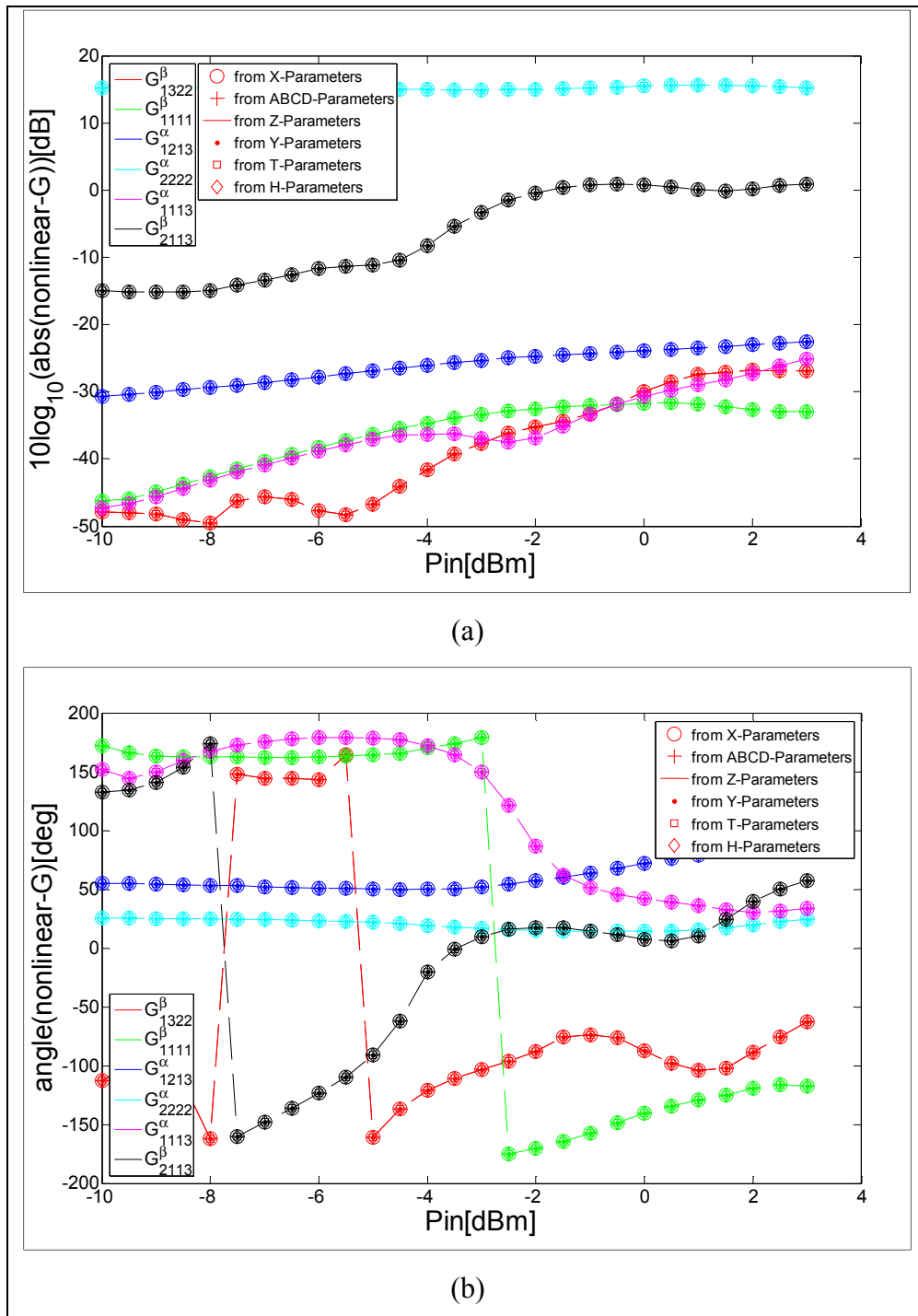


Figure 2.12 Logarithmic amplitude (a) and phase (b) of a random set of nonlinear G-parameters determined from X, nonlinear Z-, Y-, ABCD-, T- and H-parameters.

2.6.7 Nonlinear operation mode validation of nonlinear X-parameters

To validate the conversion rules giving the expressions of X-parameters in terms of other nonlinear parameters, Figure 2.13 illustrates the amplitude and phase of nonlinear X-parameters determined from nonlinear Z-, Y-, ABCD-, T-, G- and H-parameters. In order to not burden the figures with all X-parameters and since the aim is to show validation results, we will limit ourselves to the following terms that are chosen randomly: S_{1111} , S_{1223} , S_{2112} , S_{2312} , T_{1212} , and T_{2322} . Figure 2.13 shows a good agreement between the curves of X-parameters calculated from different nonlinear parameters. This agreement proves the exactness of the conversion rules demonstrated in this paper.

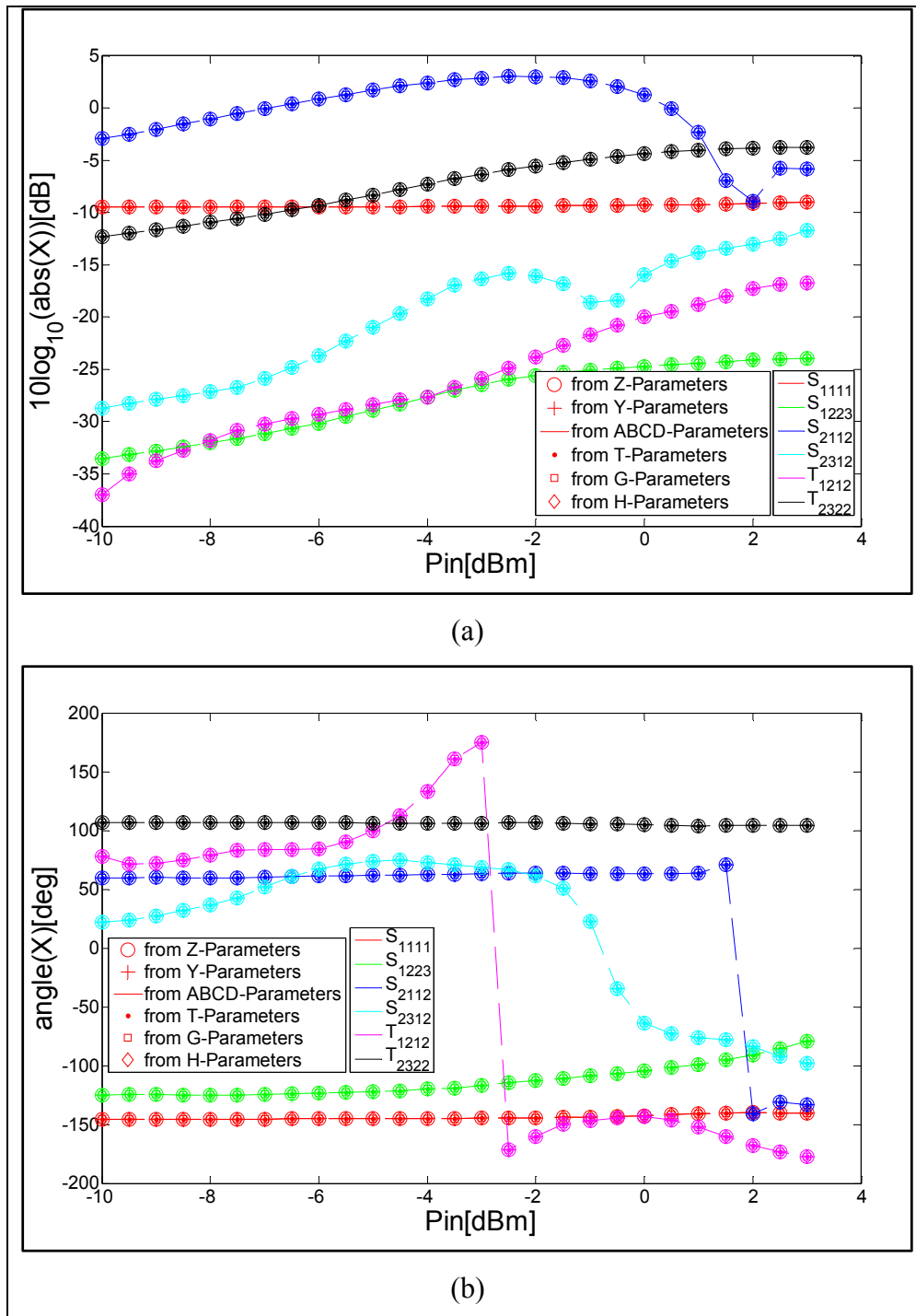


Figure 2.13 Logarithmic amplitude (a) and phase (b) of a random set of X- parameters determined from nonlinear Z-, Y-, ABCD-, T-, G- and H-parameters.

2.7 Conclusion

New nonlinear network Z-, Y-, ABCD-, T-, G- and H-parameters have been presented. These parameters can be used to characterize and analyze different nonlinear circuits with arbitrary topologies. Like X-parameters, each of these new nonlinear network parameters includes components associated with the independent current/voltage variables as well as their complex conjugate. The conversion rules between these new parameters and the measurable X-parameters have been developed and presented. The validation process showed that, just as X-parameters represent a superset of the linear S-parameters; these new nonlinear parameters are also supersets of their corresponding linear versions. These nonlinear parameters can be used in a variety of circuit simulation and nonlinear device modeling applications.

CHAPTER 3

NONLINEAR CIRCUIT ANALYSIS USING NONLINEAR TWO-PORTS NETWORK PARAMETERS

Riadh Essaadali¹, Anwar Jarndal², Ammar Kouki¹ and Fadhel Ghannouchi³

¹Department of Electrical Engineering, École de Technologie Supérieure,
1100 Notre-Dame West, Montreal, Quebec, (H3C 1K3) Canada

²Electrical and Computer Engineering Department of University of Sharjah, Sharjah, UAE

³Intelligent RF Radio Laboratory (iRadio Lab), Department of Electrical and Computer
Engineering, University of Calgary, Calgary, Alberta, (T2N 1N4) Canada

This paper has been submitted for publication in
IEEE Microwave Theory and Techniques Society.

3.1 Abstract

X-parameters that are mathematically rigorous supersets of S-parameters are applicable to linear and nonlinear components under both small- and large-signal conditions. X-parameters can be converted to other nonlinear network parameters, such as nonlinear Z-, Y-, ABCD-, T-, H- and G-parameters. These parameters are used to model different network topologies. This work presents how these nonlinear parameters can be used to describe series, parallel, cascaded, series-to-parallel and parallel-to-series connections of pure nonlinear, pure linear or a mixed topology of nonlinear and linear components. The goal of this work is the provision of evidence that it is possible to build a compact model using X-parameters.

Keywords: X-parameters, nonlinear network parameters, series, parallel, cascaded, series-to-parallel, parallel-to-series.

3.2 Introduction

High power amplifiers have been receiving increasing attention, since they are key components responsible for a sizable portion of base station costs in wireless communication

systems (Jarndal, Aflaki et al. 2010). The design of these power amplifiers (PAs) requires an accurate small- and large-signal model. There are many published linear or nonlinear models for different kinds of devices (Angelov, Desmaris et al. 2005, Jarndal and Kompa 2007, Negra, Chu et al. 2007, Jarndal, Aflaki et al. 2010). In general, most of these models are accurate only in linear mode. Classically, compact models are defined by nonlinear equivalent circuits or by a system of nonlinear ordinary differential equations describing current-voltage and charge-voltage relations for nonlinear lumped elements (Jarndal 2006, Root 2012). Nonlinear models for microwave and millimetre wave devices are commonly based on DC and S-parameter measurements (Schreurs, Verspecht et al. 1997, Jarndal, Bunz et al. 2006) and their non-linear elements are described in terms of state functions (Schreurs, Verspecht et al. 2002). The values of the state functions are generally determined via a small-signal detour based on multi-bias S-parameter measurements (Root 2012, Root, Xu et al. 2012).

This technique is based on small-signal approximations of the nonlinear state functions at different bias points and requires a large data of S-parameter measurements (Schreurs, Verspecht et al. 1997, Jarndal, Bunz et al. 2006, Root 2012, Root, Xu et al. 2012). While model topology is independent of measurement techniques, model accuracy and parameter extraction depend on the set of available measured data. Traditional modeling techniques relied on DC and multi-bias S-parameter measurements for parameters extraction. Neither static (i.e., continuous wave signals) nor dynamic (i.e., modulated signals) nonlinear measurements are used in the model parameter extraction process, but such measurements are used for model validation and possibly for model parameter tuning.

The most successful method for the characterization of such devices is to use a lumped circuit model that includes a mix of linear and nonlinear components (Maas 2003, Jarndal 2006). A compact model that consists of lumped linear and nonlinear elements is usually the most practical for the design of a nonlinear system (Jarndal 2006, Jarndal and Kompa 2007, Jarndal, Markos et al. 2011).

In traditional transistor modeling, the conversion from S-parameters to other linear network parameters like Z-parameters, Y-parameters and ABCD-parameters is essential for the model topology definition and parameter extraction process (Dambrine, Cappy et al. 1988, Degachi and Ghannouchi 2006, Laredj, Degachi et al. 2011). However, this type of parameter cannot describe a nonlinear circuit (Horn, Root et al. 2010, Verspecht and Root Jun. 2006). Accordingly, the most popular means for characterizing transistors' S-parameters, admittance parameters (Y-parameters) or other multiport parameters cannot be used to model nonlinear devices (Maas 2003, Horn, Root et al. 2010).

The intended outcome of the approach using vectorial large-signal measurements in nonlinear modeling is to efficiently extract the device's state functions directly from these measurements (Schreurs, Verspecht et al. 1997, Root 2012, Root, Xu et al. 2012). In 2008, Agilent introduced the PNA-X, a mixer-based NVNA (Root, Verspecht et al. 2013). The PNA-X is combination of NVNA with X-parameters (Horn, Gunyan et al. 2008). X-parameters are introduced in (Verspecht 2008) and they represent new nonlinear scattering parameters, applicable to passive and active circuits under small and large signal excitation (Verspecht 2005, Horn, Gunyan et al. 2008). They represent a mathematical superset of small-signal and large signal S-parameters (Horn, Gunyan et al. 2008, Verspecht and Root Jun. 2006). X-parameters have begun to be explored for transistor modeling applications (Chia-Sung, Kun-Ming et al. 2009, Horn, Root et al. 2010, Root, Xu et al. 2010, Root 2012, Root, Marcu et al. 2012, Root, Verspecht et al. 2013).

In addition to X-parameters, the behavior of a nonlinear circuit, component, or system can be described by nonlinear impedance parameters (Z-parameters), nonlinear Y-parameters, nonlinear cascade parameters (ABCD-parameters), nonlinear scattering transfer parameters (T-parameters), nonlinear hybrid parameters (H-parameters) or nonlinear inverse hybrid parameters (G-parameters). The availability of X-parameter measurements and the conversion rules between X-parameters and nonlinear two-port parameters present an opportunity to describe and compute, with simple matrix calculation, the performance of

different circuit topologies: series, parallel, cascaded, series-to-parallel and parallel-to-series configurations (Riadh Essaadali, Anwar Jarndal et al. 2011).

A first attempt to use X-parameters to analyze a series connection of two-port networks was in (Pelaez-Perez, Alonso et al. 2011, Fernandez-Barciela, Pelaez-Perez et al. 2014). This work was limited to the analysis of a mixed series connection topology of nonlinear and linear component, i.e, a transistor operating in large signal mode with a feedback capacitor. Cascadability of two DUT's is evoked in (Root, Verspecht et al. 2013) and it was demonstrated that X-parameters have the full capability to describe accurately a cascade configuration. Kirchhoff's Current Law (KCL) and Kirchhoff's Voltage Law (KVL) were used to find the steady-state behavior of a cascade of nonlinear systems. However, there is no analytical solution presented in (Root, Verspecht et al. 2013). The solution of a- and b-waves, harmonic voltage and current harmonic components is still numeric.

In this paper, a general analysis of all possible network configurations is presented. It is proven that the judicious matrix representation of different nonlinear parameters in (Riadh Essaadali, Anwar Jarndal et al. 2011) improves the manipulation of different circuit topologies. It is also proven that nonlinear Z-parameters, nonlinear Y-parameters, nonlinear ABCD- or T- parameters, nonlinear G-parameters and nonlinear H-parameters can predict series, parallel, cascade, parallel-to-series and series-to-parallel connections, respectively, of two nonlinear networks, two linear networks or a mixed topology of nonlinear and linear components. It is not limited just to two components but also generalized to N elements. An advantage of the work presented in this paper is that X-parameters of a cascade system or for other configuration can be calculated starting from X-parameters of each component. Another advantage is that this analysis allows a fast direct computation of the performance of any circuit topology.

This work can be used in a circuit design or to analyze complex systems in CAD software which may be helpful in resources optimization and circuit performance prediction. A good example of the application of the concept developed in this paper is the incorporation of the

nonlinear data directly into model parameter construction and extraction processes (Riadh Essaadali, Anwar Jarndal et al. 2011). Generally, compact models are equivalent circuit representations of the transistor (Peter H.Aaen 2007). The electrical measurements that are performed during the characterization of a transistor can be mapped directly onto a network of circuit components to mimic this electrical behavior. The values of the equivalent circuit parameters can be extracted from X-parameter measurements that can be converted into other nonlinear parameters (Riadh Essaadali, Anwar Jarndal et al. 2011, Riadh Essaadali, Anwar Jarndal et al. 2014).

This paper is organized as follows: the first section outlines the concept of X-parameter and nonlinear two-port network parameters: nonlinear impedance Z -, nonlinear admittance Y -, nonlinear ABCD-parameters, nonlinear T-parameters, nonlinear G-parameters and nonlinear H-parameters. And, for the first time, the analytical computation of all possible different network configurations is presented. As mentioned earlier, a circuit topology can be series, parallel, cascaded, series-to-parallel and parallel-to-series configurations of two nonlinear networks, two linear networks or a mixed series topology of nonlinear and linear components. The validity of the proposed analytical computation is discussed in the final section.

3.3 State of the Art

3.3.1 X-parameters: A large-signal scattering function

The use of S-parameters revolutionized the microwave industry in the early 1970s, because S-parameters completely and accurately describe the four main characteristics of linear two-port devices: transmission (S_{21}), output match (S_{22}), isolation (S_{12}) and input match (S_{11}) (Jan Verspecht 2005). The measurement of small-signal S-parameters is currently perhaps the most common and effective method to provide a linear description of a circuit and its frequency response (Peter H.Aaen 2007).

S-parameters have one significant drawback: they are only valid under linear operating conditions (Verspecht 2005); therefore, they cannot be used to describe the nonlinear features that are challenging PA designers, such as compression, AMAM, AMPM and spectral regrowth.

The idea of hot or large-signal S-parameters consists of operating a device under test (DUT) under realistic conditions by applying an appropriate large-signal stimulus signal (Jan Verspecht 2005). While this signal is being applied, one injects a small one-tone signal first into port 1 of the DUT: this is called a forward measurement. A small one-tone signal is then injected into port 2, which is called a reverse measurement. Each time, the incident waves (a-waves) and corresponding scattered waves (b-waves) are measured. Just as is done with small-signal S-parameters, hot S-parameters are defined as the ratios between the a- and b-waves.

As a DUT enters its nonlinear regime of operation, the elements of the scattering matrix relating different frequency components to each other become nonzero (Verspecht, Williams et al. 2005). Even weakly nonlinear devices usually create mixing products at both sum and difference frequencies of the input signals. Mixing products that include different frequencies are particularly problematic, as increasing the phase or frequency of an input signal can result in a decrease in the phase or frequency of an output signal. The scattering function describing the electrical behavior of a weakly nonlinear device is generally not analytical; therefore, even in the weakly nonlinear case, a- and b-waves cannot be related with linear scattering-parameter matrices, even in a weakly nonlinear case (Verspecht and Root Jun. 2006).

For a given DUT, the linearization of the multivariate complex functions that correlate all of the relevant input spectral components with the output spectral components leads to the X-parameter expression (Verspecht and Root Jun. 2006):

$$b_{ik} = X_{ik}^F(|a_{11}|)P^k + \sum_{(j,l) \neq (1,1)} X_{ik,jl}^S(|a_{11}|)P^{k-l}a_{jl} + \sum_{(j,l) \neq (1,1)} X_{ik,jl}^T(|a_{11}|)P^{k+l}a_{jl}^* \quad (3.1)$$

where b_{ik} and a_{jl} are the scattered and incident traveling voltage waves, respectively. Indices i and j range from one to the number of signal ports, and indices k and l range from one to the highest harmonic index. The F_{ik} , $S_{ik,jl}$ and $T_{ik,jl}$ terms are complex functions of $|a_{11}|$.

There are some significant differences with S-parameters: the contribution associated with a-waves and the conjugates of the a-waves. The conjugate part is not present at all in S-parameters' formulations. With S-parameters, any phase shift in the a-wave just results in the same phase shift in the corresponding b-wave.

3.3.2 Nonlinear network parameters

In addition to X-parameters that relate harmonic components of a- and b-waves, other nonlinear parameters have been introduced in (Riadh Essaadali, Anwar Jarndal et al. 2011). Nonlinear impedance parameters (Z-parameters) relate the harmonic current to harmonic voltage components at both ports of a dual-port device. Nonlinear Z-parameters include two-term categories, Z_{pmqj}^{α} and Z_{pmqj}^{β} , which are associated with harmonic component current i_{qj} and its conjugate i_{qj}^* , respectively. Indices p and q range from one to the number of signal ports, and indices m and j range from one to the highest harmonic index. A nonlinear device model based on nonlinear Z-parameters can be represented as:(Riadh Essaadali, Anwar Jarndal et al. 2011)

$$v_{pm} = \sum_{(q,j)} Z_{pmqj}^{\alpha} (|a_{11}|) i_{qj} + Z_{pmqj}^{\beta} (|a_{11}|) i_{qj}^* \quad (3.2)$$

The reformulation of (3.2) into a matrix form improves the manipulation of nonlinear Z-parameters. For a two-port network, (3.2) can be reformulated into a matrix as:

$$\begin{bmatrix} [V_1] \\ [V_2] \end{bmatrix} = [Z_{nonlin}] \begin{bmatrix} [I_1] \\ [I_2] \end{bmatrix} = \begin{bmatrix} [Z_{nonlin11}] & [Z_{nonlin12}] \\ [Z_{nonlin21}] & [Z_{nonlin22}] \end{bmatrix} \begin{bmatrix} [I_1] \\ [I_2] \end{bmatrix} \quad (3.3)$$

Where the voltage vector at the input ($i=1$) and at the output ($i=2$) is $[V_i] = [v_{i1} \ v_{i1}^* \ \dots \ v_{in} \ v_{in}^*]^T$ and the current vector at the input and the output $[I_i] = [i_{i1} \ i_{i1}^* \ \dots \ i_{in} \ i_{in}^*]^T$. The expressions of $[Z_{nonlinij}]$ sub-matrices in terms of Z_{pmaj}^α and Z_{pmaj}^β is:

$$[Z_{nonlinij}]_{\substack{i=1,2 \\ j=1,2}} = \begin{bmatrix} Z_{i1j1}^\alpha & Z_{i1j1}^\beta & \dots & Z_{i1jn}^\alpha & Z_{i1jn}^\beta \\ Z_{i1j1}^{\beta*} & Z_{i1j1}^{\alpha*} & \dots & Z_{i1jn}^{\beta*} & Z_{i1jn}^{\alpha*} \\ \vdots & \vdots & \ddots & \vdots & \vdots \\ Z_{inj1}^\alpha & Z_{inj1}^\beta & \dots & Z_{injn}^\alpha & Z_{injn}^\beta \\ Z_{inj1}^{\beta*} & Z_{inj1}^{\alpha*} & \dots & Z_{injn}^{\beta*} & Z_{injn}^{\alpha*} \end{bmatrix}. \quad (3.4)$$

Nonlinear Z-parameters are determined from X-parameters through (Riadh Essaadali, Anwar Jarndal et al. 2011):

$$[Z_{nonlin}] = Z_c [[Id] - [X]]^{-1} [[Id] + [X]]. \quad (3.5)$$

where Z_c is the characteristic impedance, $[Id]$ is the identity matrix and $[X]$ is the X-parameters matrix defined as:

$$[X] = \begin{bmatrix} [X_{11}] & [X_{12}] \\ [X_{21}] & [X_{22}] \end{bmatrix}. \quad (3.6)$$

where

$$[X_{ij}]_{\substack{i=1,2 \\ j=1,2}} = \begin{bmatrix} S_{i1j1} & T_{i1j1} & \dots & S_{i1jn} & T_{i1jn} \\ T_{i1j1}^* & S_{i1j1}^* & \dots & T_{i1jn}^* & S_{i1jn}^* \\ \vdots & \vdots & \ddots & \vdots & \vdots \\ S_{inj1} & T_{inj1} & \dots & S_{injn} & T_{injn} \\ T_{inj1}^* & S_{inj1}^* & \dots & T_{injn}^* & S_{injn}^* \end{bmatrix}. \quad (3.7)$$

The terms S and T in X-matrix are expressed in terms of X-parameters that are defined in

$$(3.1): S_{pmqj} = X_{pmqj}^S P^{m-j}, T_{pmqj} = X_{pmqj}^T P^{m+j}, T_{pm11} = 0 \text{ and } S_{ik,11} = X_{ik}^F / |a_{11}|.$$

Nonlinear admittance parameters (Y-parameters) relate harmonic voltage components to harmonic current components at both ports. Nonlinear Y-parameters include two-term categories, Y_{pmqj}^α and Y_{pmqj}^β , which are associated with harmonic component voltage v_{qj} and its conjugate v_{qj}^* , respectively. A nonlinear device model based on nonlinear Y-parameters can be characterized as:(Riadh Essaadali, Anwar Jarndal et al. 2011)

$$i_{pm} = \sum_{(q,j)} Y_{pmqj}^\alpha (|a_{11}|) v_{qj} + Y_{pmqj}^\beta (|a_{11}|) v_{qj}^*. \quad (3.8)$$

The reformulation of (3.8) into the form of a matrix improves the manipulation of nonlinear Y-parameters. For a two-port network, (3.8) can be reformulated into a matrix as:

$$\begin{bmatrix} [I_1] \\ [I_2] \end{bmatrix} = [Y_{nonlin}] \begin{bmatrix} [V_1] \\ [V_2] \end{bmatrix} = \begin{bmatrix} [Y_{nonlin11}] & [Y_{nonlin12}] \\ [Y_{nonlin21}] & [Y_{nonlin22}] \end{bmatrix} \begin{bmatrix} [V_1] \\ [V_2] \end{bmatrix}. \quad (3.9)$$

The expressions of $[Y_{nonlinij}]$ sub-matrices in terms of Y_{pmqj}^α and Y_{pmqj}^β are:

$$[Y_{nonlinij}]_{\substack{i=1,2 \\ j=1,2}} = \begin{bmatrix} Y_{i1j1}^\alpha & Y_{i1j1}^\beta & \dots & Y_{i1jn}^\alpha & Y_{i1jn}^\beta \\ Y_{i1j1}^{\beta^*} & Y_{i1j1}^{\alpha^*} & \dots & Y_{i1jn}^{\beta^*} & Y_{i1jn}^{\alpha^*} \\ \vdots & \vdots & \ddots & \vdots & \vdots \\ Y_{inj1}^\alpha & Y_{inj1}^\beta & \dots & Y_{injn}^\alpha & Y_{injn}^\beta \\ Y_{inj1}^{\beta^*} & Y_{inj1}^{\alpha^*} & \dots & Y_{injn}^{\beta^*} & Y_{injn}^{\alpha^*} \end{bmatrix}. \quad (3.10)$$

Nonlinear Y-parameters are determined from X-parameters through:(Riadh Essaadali, Anwar Jarndal et al. 2011)

$$[Y_{nonlin}] = \frac{1}{Z_c} [[Id] + [X]]^{-1} [[Id] - [X]]. \quad (3.11)$$

Nonlinear T-parameters include two-term categories T_{pmqj}^α and T_{pmqj}^β , which are respectively associated with a harmonic component and its conjugate of a- and b-waves present at input port. The formulations of a nonlinear model based on nonlinear T-parameters are:(Riadh Essaadali, Anwar Jarndal et al. 2011)

$$b_{1m} = \sum_{(q,j)} T_{1m1j}^\alpha (|a_{11}|) a_{2j} + T_{1m1j}^\beta (|a_{11}|) a_{2j}^* + \sum_{(q,j)} T_{1m2j}^\alpha (|a_{11}|) b_{2j} + T_{1m2j}^\beta (|a_{11}|) b_{2j}^*. \quad (3.12)$$

$$a_{1m} = \sum_{(q,j)} T_{2m1j}^\alpha (|a_{11}|) b_{2j} + T_{2m1j}^\beta (|a_{11}|) b_{2j}^* + \sum_{(q,j)} T_{2m2j}^\alpha (|a_{11}|) a_{2j} + T_{2m2j}^\beta (|a_{11}|) a_{2j}^*. \quad (3.13)$$

The reformulation of (3.12) and (3.13) into matrices improves the manipulation of nonlinear T-parameters. Equations (3.12) and (3.13) can be reformulated into a matrix as:

$$\begin{bmatrix} [B_1] \\ [A_1] \end{bmatrix} = [T_{nonlin}] \begin{bmatrix} [A_2] \\ [B_2] \end{bmatrix} = \begin{bmatrix} [T_{nonlin11}] & [T_{nonlin12}] \\ [T_{nonlin21}] & [T_{nonlin22}] \end{bmatrix} \begin{bmatrix} [A_2] \\ [B_2] \end{bmatrix}. \quad (3.14)$$

where the scattered wave vector at the input (i=1) and at the output (i=2) is $[B_i] = [b_{i1} \ b_{i1}^* \ \dots \ b_{in} \ b_{in}^*]^T$ and the incident wave vector at the input and the output is $[A_i] = [a_{i1} \ a_{i1}^* \ \dots \ a_{in} \ a_{in}^*]^T$. The expressions of $[T_{nonlinij}]$ sub-matrices in terms of T_{pmqj}^α and T_{pmqj}^β are:

$$[T_{nonlinij}]_{\substack{i=1,2 \\ j=1,2}} = \begin{bmatrix} T_{i1j1}^\alpha & T_{i1j1}^\beta & \dots & T_{i1jn}^\alpha & T_{i1jn}^\beta \\ T_{i1j1}^{\beta^*} & T_{i1j1}^{\alpha^*} & \dots & T_{i1jn}^{\beta^*} & T_{i1jn}^{\alpha^*} \\ \vdots & \vdots & \ddots & \vdots & \vdots \\ T_{inj1}^\alpha & T_{inj1}^\beta & \dots & T_{injn}^\alpha & T_{injn}^\beta \\ T_{inj1}^{\beta^*} & T_{inj1}^{\alpha^*} & \dots & T_{injn}^{\beta^*} & T_{injn}^{\alpha^*} \end{bmatrix}. \quad (3.15)$$

Nonlinear T-parameters are determined from X-parameters through:(Riadh Essaadali, Anwar Jarndal et al. 2011)

$$[T_{nonlin11}] = [X_{12}] - [X_{11}][X_{21}]^{-1}[X_{22}]. \quad (3.16)$$

$$[T_{nonlin21}] = -[X_{21}]^{-1}[X_{22}]. \quad (3.17)$$

$$[T_{nonlin12}] = [X_{11}][X_{21}]^{-1}. \quad (3.18)$$

$$[T_{nonlin22}] = [X_{21}]^{-1}. \quad (3.19)$$

A nonlinear ABCD matrix includes 4 parameter categories: A-, B-, C- and D-terms. A-parameters relate input harmonic voltages to output harmonic voltages, and B-parameters relate input harmonic voltages to output harmonic currents. C-parameters relate input harmonic currents to output harmonic voltages, and D-parameters relate input harmonic currents to output harmonic currents. Each ABCD parameter includes two-term categories associated respectively with a harmonic component and its conjugate of voltage and current present at the second port. The formulations of a nonlinear model based on nonlinear ABCD-parameters are: (Riadh Essaadali, Anwar Jarndal et al. 2011)

$$v_{1m} = \sum_{(q,j)} A_{1m2j}^{\alpha}(|a_{11}|)v_{2j} + A_{1m2j}^{\beta}(|a_{11}|)v_{2j}^* + \sum_{(q,j)} B_{1m2j}^{\alpha}(|a_{11}|)i_{2j} + B_{1m2j}^{\beta}(|a_{11}|)i_{2j}^*. \quad (3.20)$$

$$i_{1m} = \sum_{(q,j)} C_{1m2j}^{\alpha}(|a_{11}|)v_{2j} + C_{1m2j}^{\beta}(|a_{11}|)v_{2j}^* + \sum_{(q,j)} D_{1m2j}^{\alpha}(|a_{11}|)i_{2j} + D_{1m2j}^{\beta}(|a_{11}|)i_{2j}^*. \quad (3.21)$$

The reformulation of (3.20) and (3.21) into a matrix form improves the manipulation of nonlinear ABCD-parameters. Equations (3.20) and (3.21) can be reformulated into a matrix as:

$$\begin{bmatrix} [V_1] \\ [I_1] \end{bmatrix} = [ABCD_{nonlin}] \begin{bmatrix} [V_2] \\ [I_2] \end{bmatrix} = \begin{bmatrix} [A_{nonlin}] & [B_{nonlin}] \\ [C_{nonlin}] & [D_{nonlin}] \end{bmatrix} \begin{bmatrix} [V_2] \\ [I_2] \end{bmatrix}. \quad (3.22)$$

The expressions of $[ABCD_{nonlin}]$ sub-matrices $[A_{nonlin}]$, $[B_{nonlin}]$, $[C_{nonlin}]$ and $[D_{nonlin}]$, in terms of A_{pmqj}^α , B_{pmqj}^α , C_{pmqj}^α , D_{pmqj}^α , A_{pmqj}^β , B_{pmqj}^β , C_{pmqj}^β and D_{pmqj}^β , are presented in (3.23). For simplification purposes, the letter R symbolizes the A, B, C and D symbols.

$$[R_{nonlin}] = \begin{bmatrix} R_{1121}^\alpha & R_{1121}^\beta & \dots & R_{112n}^\alpha & R_{112n}^\beta \\ R_{1121}^{\beta^*} & R_{1121}^{\alpha^*} & \dots & R_{112n}^{\beta^*} & R_{112n}^{\alpha^*} \\ \vdots & \vdots & \ddots & \vdots & \vdots \\ R_{1n21}^\alpha & R_{1n21}^\beta & \dots & R_{1n2n}^\alpha & R_{1n2n}^\beta \\ R_{1n21}^{\beta^*} & R_{1n21}^{\alpha^*} & \dots & R_{1n2n}^{\beta^*} & R_{1n2n}^{\alpha^*} \end{bmatrix}. \quad (3.23)$$

Nonlinear ABCD-parameters are determined from X-parameters through:(Riadh Essaadali, Anwar Jarndal et al. 2011)

$$[A_{nonlin}] = \left[I_d + [I_d - X_{11}]^{-1} [I_d + X_{11}] \right]^{-1} \left\{ [I_d - X_{11}]^{-1} \cdot [I_d + X_{11}] [X_{21}]^{-1} [I_d - X_{22}] + [I_d - X_{11}]^{-1} [X_{12}] \right\}. \quad (3.24)$$

$$[B_{nonlin}] = \frac{Z_c}{2} \left([X_{12}] - [I_d + X_{11}] [X_{21}]^{-1} [I_d + X_{22}] \right). \quad (3.25)$$

$$[C_{nonlin}] = \frac{[X_{22}]^{-1} [I_d - X_{22}]}{Z_c} - \frac{[I_d + [I_d - X_{11}]^{-1} [I_d + X_{11}]]^{-1}}{Z_c} \cdot [I_d - X_{11}]^{-1} \left\{ [I_d + X_{11}] [X_{21}]^{-1} [I_d - X_{22}] + [X_{12}] \right\}. \quad (3.26)$$

$$[D_{nonlin}] = \frac{1}{2} \left(([X_{11}] - [I_d]) [X_{21}]^{-1} ([I_d] + [X_{22}]) - [X_{12}] \right). \quad (3.27)$$

Nonlinear hybrid parameters (H-parameters) use the input harmonic current components at port 1 and the output harmonic voltage components at port 2 as independent variables. Nonlinear H-parameters include two-term categories, H_{pmqj}^α and H_{pmqj}^β , which are associated with a harmonic component and its conjugate of voltage and current. The formulations of a

nonlinear model based on nonlinear H-parameters are:(Riadh Essaadali, Anwar Jarndal et al. 2011)

$$v_{1m} = \sum_{(q,j)} H_{1m1j}^{\alpha}(|a_{11}|)i_{1j} + H_{1m1j}^{\beta}(|a_{11}|)i_{1j}^* + \sum_{(q,j)} H_{1m2j}^{\alpha}(|a_{11}|)v_{2j} + H_{1m2j}^{\beta}(|a_{11}|)v_{2j}^*. \quad (3.28)$$

$$i_{2m} = \sum_{(q,j)} H_{2m1j}^{\alpha}(|a_{11}|)i_{1j} + H_{2m1j}^{\beta}(|a_{11}|)i_{1j}^* + \sum_{(q,j)} H_{2m2j}^{\alpha}(|a_{11}|)v_{2j} + H_{2m2j}^{\beta}(|a_{11}|)v_{2j}^*. \quad (3.29)$$

The reformulation of (3.28) and (3.29) into the form of matrix improves the manipulation of nonlinear H-parameters:

$$\begin{bmatrix} [V_1] \\ [I_2] \end{bmatrix} = [H_{nonlin}] \begin{bmatrix} [I_1] \\ [V_2] \end{bmatrix} = \begin{bmatrix} [H_{nonlin11}] & [H_{nonlin12}] \\ [H_{nonlin21}] & [H_{nonlin22}] \end{bmatrix} \begin{bmatrix} [I_1] \\ [V_2] \end{bmatrix}. \quad (3.30)$$

The expressions of $[H_{nonlin}]$ sub-matrices in terms of H_{pmqj}^{α} and H_{pmqj}^{β} are:

$$[H_{nonlinij}]_{\substack{i=1,2 \\ j=1,2}} = \begin{bmatrix} H_{i1j1}^{\alpha} & H_{i1j1}^{\beta} & \dots & H_{i1jn}^{\alpha} & H_{i1jn}^{\beta} \\ H_{i1j1}^{\beta^*} & H_{i1j1}^{\alpha^*} & \dots & H_{i1jn}^{\beta^*} & H_{i1jn}^{\alpha^*} \\ \vdots & \vdots & \ddots & \vdots & \vdots \\ H_{inj1}^{\alpha} & H_{inj1}^{\beta} & \dots & H_{injn}^{\alpha} & H_{injn}^{\beta} \\ H_{inj1}^{\beta^*} & H_{inj1}^{\alpha^*} & \dots & H_{injn}^{\beta^*} & H_{injn}^{\alpha^*} \end{bmatrix}. \quad (3.31)$$

Nonlinear H-parameters are determined from X-parameters through:(Riadh Essaadali, Anwar Jarndal et al. 2011)

$$[H_{nonlin11}] = Z_c \left[[I_d] - [X_{11}] + [X_{12}][I_d + X_{22}]^{-1} [X_{21}] \right]^{-1} \cdot \left[[I_d] + [X_{11}] - [X_{12}][I_d + X_{22}]^{-1} [X_{21}] \right] \quad (3.32)$$

$$[H_{nonlin21}] = -[I_d + X_{22}]^{-1} [X_{21}] \cdot \left\{ [I_d] + \left[[I_d] - [X_{11}] + [X_{12}][I_d + X_{22}]^{-1} [X_{21}] \right]^{-1} \cdot \left[[I_d] + [X_{11}] - [X_{12}][I_d + X_{22}]^{-1} [X_{21}] \right] \right\}. \quad (3.33)$$

$$[H_{nonlin12}] = \left[[I_d] - [X_{11}] + [X_{12}][I_d + X_{22}]^{-1}[X_{21}] \right]^{-1} \cdot \left[[X_{12}] - [X_{12}][I_d + X_{22}]^{-1}[X_{22} - I_d] \right]. \quad (3.34)$$

$$[H_{nonlin22}] = \frac{1}{Z_c} \left[[I_d] + [X_{22}] + [X_{21}][I_d - X_{11}]^{-1}[X_{12}] \right]^{-1} \cdot \left[[I_d] - [X_{22}] - [X_{21}][I_d - X_{11}]^{-1}[X_{12}] \right]. \quad (3.35)$$

Nonlinear inverse hybrid parameters (G-parameters) use the input harmonic voltage components and the output harmonic current components as independent variables. The formulations of a nonlinear model based on nonlinear G-parameters are:(Riadh Essaadali, Anwar Jarndal et al. 2011)

$$i_{1m} = \sum_{(q,j)} G_{1m1j}^{\alpha}(|a_{11}|)v_{1j} + G_{1m1j}^{\beta}(|a_{11}|)v_{1j}^* + \sum_{(q,j)} G_{1m2j}^{\alpha}(|a_{11}|)i_{2j} + G_{1m2j}^{\beta}(|a_{11}|)i_{2j}^*. \quad (3.36)$$

$$v_{2m} = \sum_{(q,j)} G_{2m1j}^{\alpha}(|a_{11}|)v_{1j} + G_{2m1j}^{\beta}(|a_{11}|)v_{1j}^* + \sum_{(q,j)} G_{2m2j}^{\alpha}(|a_{11}|)i_{2j} + G_{2m2j}^{\beta}(|a_{11}|)i_{2j}^*. \quad (3.37)$$

The reformulation of (3.36) and (3.37) into a matrix improves the manipulation of nonlinear G-parameters.

$$\begin{bmatrix} [I_1] \\ [V_2] \end{bmatrix} = [G_{nonlin}] \begin{bmatrix} [V_1] \\ [I_2] \end{bmatrix} = \begin{bmatrix} [G_{nonlin11}] & [G_{nonlin12}] \\ [G_{nonlin21}] & [G_{nonlin22}] \end{bmatrix} \begin{bmatrix} [V_1] \\ [I_2] \end{bmatrix}. \quad (3.38)$$

The expressions of $[G_{nonlinij}]$ sub-matrices in terms of G_{pmkj}^{α} and G_{pmkj}^{β} are:(Riadh Essaadali, Anwar Jarndal et al. 2011).

$$[G_{nonlinij}]_{\substack{i=1,2 \\ j=1,2}} = \begin{bmatrix} G_{i1j1}^{\alpha} & G_{i1j1}^{\beta} & \dots & G_{i1jn}^{\alpha} & G_{i1jn}^{\beta} \\ G_{i1j1}^{\beta^*} & G_{i1j1}^{\alpha^*} & \dots & G_{i1jn}^{\beta^*} & G_{i1jn}^{\alpha^*} \\ \vdots & \vdots & \ddots & \vdots & \vdots \\ G_{inj1}^{\alpha} & G_{inj1}^{\beta} & \dots & G_{injn}^{\alpha} & G_{injn}^{\beta} \\ G_{inj1}^{\beta^*} & G_{inj1}^{\alpha^*} & \dots & G_{injn}^{\beta^*} & G_{injn}^{\alpha^*} \end{bmatrix}. \quad (3.39)$$

Nonlinear G-parameters are determined from X-parameters through:(Riadh Essaadali, Anwar Jarndal et al. 2011)

$$[G_{nonlin11}] = \frac{-1}{Z_c} \left[[I_d] + [X_{11}] + [X_{12}] \left[[I_d] - [X_{22}] \right]^{-1} [X_{21}] \right]^{-1} \cdot \left[[X_{11}] - [I_d] + [X_{12}] \left[[I_d] - [X_{22}] \right]^{-1} [X_{21}] \right]. \quad (3.40)$$

$$[G_{nonlin21}] = 2 \left[[X_{12}] + \left[[X_{11}] + [I_d] \right] [X_{21}]^{-1} \left[[I_d] - [X_{22}] \right] \right]^{-1}. \quad (3.41)$$

$$[G_{nonlin12}] = 2 \left[\left[[X_{22}] - [I_d] \right] [X_{12}]^{-1} \left[[X_{11}] + [I_d] \right] - [X_{21}] \right]^{-1}. \quad (3.42)$$

$$[G_{nonlin22}] = Z_c \left[[X_{21}] - \left[[X_{22}] + [I_d] \right] [X_{12}]^{-1} \left[[X_{11}] + [I_d] \right] \right] \left[\left[[X_{22}] - [I_d] \right] [X_{12}]^{-1} \left[[X_{11}] + [I_d] \right] - [X_{21}] \right]^{-1}. \quad (3.43)$$

3.4 Analytical Computation of Network Configuration

3.4.1 Series network configuration

Three series topologies are possible: two nonlinear networks, two linear networks or a mixed series topology of nonlinear and linear components. The series configuration of two nonlinear components is illustrated in Figure 3.1.

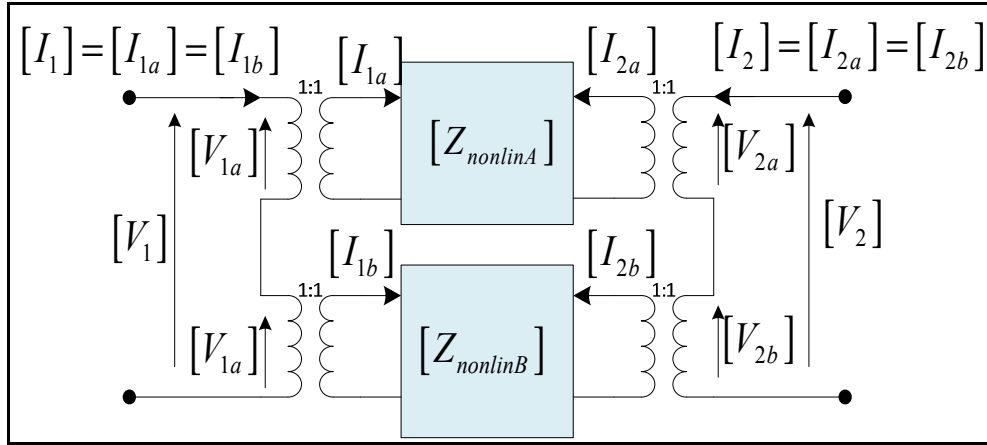


Figure 3.1 Series connection of two nonlinear networks

Nonlinear impedances can be used to model a series configuration of two nonlinear components or two active components operating in large-signal operation. The analytical voltage-current relationships for the first and second nonlinear components are:

$$\begin{bmatrix} [V_{1a}] \\ [V_{2a}] \end{bmatrix} = [Z_{nonlinA}] \begin{bmatrix} [I_{1a}] \\ [I_{2a}] \end{bmatrix}. \quad (3.44)$$

$$\begin{bmatrix} [V_{1b}] \\ [V_{2b}] \end{bmatrix} = [Z_{nonlinB}] \begin{bmatrix} [I_{1b}] \\ [I_{2b}] \end{bmatrix}. \quad (3.45)$$

The summation of $[V_{1a}]$ and $[V_{1b}]$ is equal to $[V_1]$, and the sum of $[V_{2a}]$ and $[V_{2b}]$ is equal to $[V_2]$. The current through both components is the same, i.e., $[I_1] = [I_{1a}] = [I_{1b}]$ and $[I_2] = [I_{2a}] = [I_{2b}]$. Thus, voltage-current relationship can be rewritten as:

$$\begin{bmatrix} [V_1] \\ [V_2] \end{bmatrix} = \begin{bmatrix} [V_{1a}] \\ [V_{2a}] \end{bmatrix} + \begin{bmatrix} [V_{1b}] \\ [V_{2b}] \end{bmatrix} = \{[Z_{nonlinA}] + [Z_{nonlinB}]\} \begin{bmatrix} [I_1] \\ [I_2] \end{bmatrix}. \quad (3.46)$$

Therefore, the equivalent nonlinear impedance is the sum of nonlinear impedances of both nonlinear components:

$$[Z_{nonlinEq}] = [Z_{nonlinA}] + [Z_{nonlinB}]. \quad (3.47)$$

Equation (3.47) is still valid when a mixed series topology of nonlinear and linear components or a series topology of two linear networks is used. For a mixed series topology of nonlinear and linear components, the expressions of nonlinear Z_{pmqm}^α terms vanish to linear impedance in linear operation mode and are equal to $Z_{pq}(m\omega)$ (Riadh Essaadali, Anwar Jarndal et al. 2011), where ω is the fundamental frequency and m is the frequency index.

When a series topology of two linear networks is used, $Z_{pmqm}^\alpha = 0$ for $m > 1$, since only the fundamental frequency is present in the circuit. The expression of nonlinear Z in the linear operation mode is:

$$[Z_{LinearMode}] = \begin{bmatrix} Z_{1111}^\alpha & 0 & \dots & 0 & 0 & Z_{1121}^\alpha & 0 & \dots & 0 & 0 \\ 0 & Z_{1111}^{\alpha'} & \dots & 0 & 0 & 0 & Z_{1121}^{\alpha'} & \dots & 0 & 0 \\ \vdots & \vdots & \ddots & \vdots & \vdots & \vdots & \vdots & \ddots & \vdots & \vdots \\ 0 & 0 & \dots & Z_{1n1n}^\alpha & 0 & 0 & 0 & \dots & Z_{1n2n}^\alpha & 0 \\ 0 & 0 & \dots & 0 & Z_{1n1n}^{\alpha'} & 0 & 0 & \dots & 0 & Z_{1n2n}^{\alpha'} \\ Z_{2111}^\alpha & 0 & \dots & 0 & 0 & Z_{2121}^\alpha & 0 & \dots & 0 & 0 \\ 0 & Z_{2111}^{\alpha'} & \dots & 0 & 0 & 0 & Z_{2121}^{\alpha'} & \dots & 0 & 0 \\ \vdots & \vdots & \ddots & \vdots & \vdots & \vdots & \vdots & \ddots & \vdots & \vdots \\ 0 & 0 & \dots & Z_{2n1n}^\alpha & 0 & 0 & 0 & \dots & Z_{2n2n}^\alpha & 0 \\ 0 & 0 & \dots & 0 & Z_{2n1n}^{\alpha'} & 0 & 0 & \dots & 0 & Z_{2n2n}^{\alpha'} \end{bmatrix}. \quad (3.48)$$

The analytical impedance of a series topology can be generalized to model a series configuration of N nonlinear components:

$$[Z_{nonlinEq}] = \sum_{i=1}^N [Z_{nonlin_i}]. \quad (3.49)$$

X-parameters of a series topology are calculated through the conversion rule from nonlinear Z-parameters to X-parameters: (Riadh Essaadali, Anwar Jarndal et al. 2011)

$$[X_{Eq}] = \left[[I_d] + \frac{1}{Z_c} [Z_{nonlinEq}] \right]^{-1} \left[\frac{1}{Z_c} [Z_{nonlinEq}] - [I_d] \right]. \quad (3.50)$$

3.4.2 Parallel network configuration

As with series configurations, there are three possible parallel topologies. The parallel configuration of two nonlinear components is illustrated in Figure 3.2.

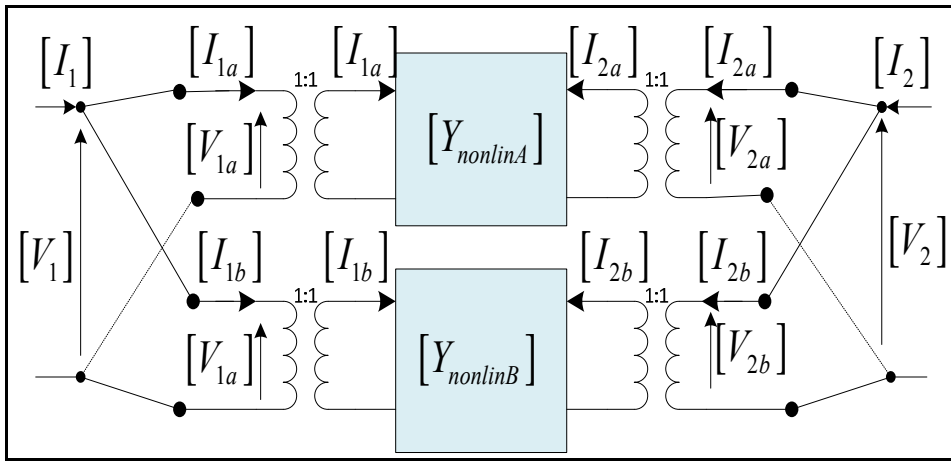


Figure 3.2 Parallel connection of two nonlinear networks

The analytical current-voltage relationships for the first and second nonlinear components are:

$$\begin{bmatrix} [I_{1a}] \\ [I_{2a}] \end{bmatrix} = [Y_{nonlinA}] \begin{bmatrix} [V_{1a}] \\ [V_{2a}] \end{bmatrix}. \quad (3.51)$$

$$\begin{bmatrix} [I_{1b}] \\ [I_{2b}] \end{bmatrix} = [Y_{nonlinB}] \begin{bmatrix} [V_{1b}] \\ [V_{2b}] \end{bmatrix}. \quad (3.52)$$

The summation of $[I_{1a}]$ and $[I_{1b}]$ is equal to $[I_1]$, and the sum of $[I_{2a}]$ and $[I_{2b}]$ is equal to $[I_2]$. The voltages at the same port of both nonlinear components are equal, i.e.,

$[V_1]=[V_{1a}]=[V_{1b}]$ and $[V_2]=[V_{2a}]=[V_{2b}]$. Thus, the current- voltage relationship can be rewritten as:

$$\begin{bmatrix} [I_1] \\ [I_2] \end{bmatrix} = \begin{bmatrix} [I_{1a}] \\ [I_{2a}] \end{bmatrix} + \begin{bmatrix} [I_{1b}] \\ [I_{2b}] \end{bmatrix} = \{[Y_{nonlinA}] + [Y_{nonlinB}]\} \begin{bmatrix} [V_1] \\ [V_2] \end{bmatrix}. \quad (3.53)$$

The equivalent nonlinear admittance is, therefore, equal to the sum of nonlinear admittances of both nonlinear components:

$$[Y_{nonlinEq}] = [Y_{nonlinA}] + [Y_{nonlinB}]. \quad (3.54)$$

Equation (3.54) is still valid when a mixed parallel topology of nonlinear and linear components or a parallel topology of two linear networks is used. For a mixed parallel topology of nonlinear and linear components, the expressions of nonlinear Y_{pmqm}^α terms vanish to linear admittance in the linear operation mode and are equal to $Y_{pq}(m\omega)$, where ω is the fundamental frequency and m is the frequency index. When parallel topology of two linear networks is used, $Y_{pmqm}^\alpha = 0$ for $m > 1$, since only the fundamental frequency is present in the circuit. The expression of nonlinear Z in the linear operation mode is:

$$[Y_{LinearMode}] = \begin{bmatrix} Y_{1111}^\alpha & 0 & \dots & 0 & 0 & Y_{1121}^\alpha & 0 & \dots & 0 & 0 \\ 0 & Y_{1111}^{\alpha'} & \dots & 0 & 0 & 0 & Y_{1121}^{\alpha'} & \dots & 0 & 0 \\ \vdots & \vdots & \ddots & \vdots & \vdots & \vdots & \vdots & \ddots & \vdots & \vdots \\ 0 & 0 & \dots & Y_{1n1n}^\alpha & 0 & 0 & 0 & \dots & Y_{1n2n}^\alpha & 0 \\ 0 & 0 & \dots & 0 & Y_{1n1n}^{\alpha'} & 0 & 0 & \dots & 0 & Y_{1n2n}^{\alpha'} \\ Y_{2111}^\alpha & 0 & \dots & 0 & 0 & Y_{2121}^\alpha & 0 & \dots & 0 & 0 \\ 0 & Y_{2111}^{\alpha'} & \dots & 0 & 0 & 0 & Y_{2121}^{\alpha'} & \dots & 0 & 0 \\ \vdots & \vdots & \ddots & \vdots & \vdots & \vdots & \vdots & \ddots & \vdots & \vdots \\ 0 & 0 & \dots & Y_{2n1n}^\alpha & 0 & 0 & 0 & \dots & Y_{2n2n}^\alpha & 0 \\ 0 & 0 & \dots & 0 & Y_{2n1n}^{\alpha'} & 0 & 0 & \dots & 0 & Y_{2n2n}^{\alpha'} \end{bmatrix}. \quad (3.55)$$

The analytical admittance of parallel topology can be generalized to model a parallel configuration of N nonlinear components:

$$[Y_{nonlinEq}] = \sum_{i=1}^N [Y_{nonlin_i}]. \quad (3.56)$$

X-parameters of a parallel topology are calculated through the conversion rule from nonlinear Y-parameters to X-parameters:(Riadh Essaadali, Anwar Jarndal et al. 2011)

$$[X_{Eq}] = \left[[Id] - Z_c [Y_{nonlinEq}] \right] \left[Z_c [Y_{nonlinEq}] + [Id] \right]^{-1}. \quad (3.57)$$

3.4.3 Cascaded network configuration

To model a cascaded configuration of nonlinear systems, nonlinear ABCD- or T-parameters can be used. The cascaded configuration of two nonlinear components is illustrated in Figure 3.3.

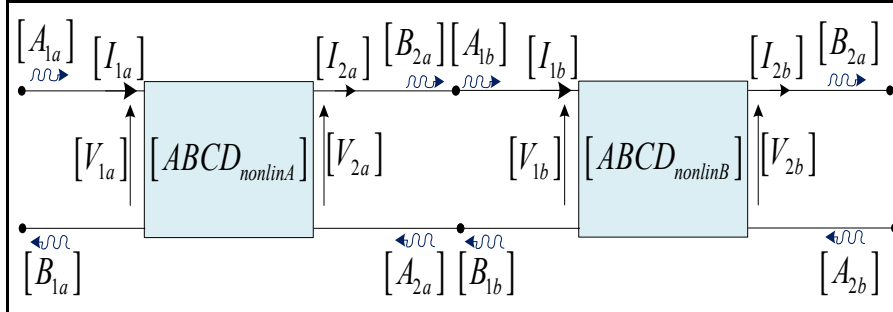


Figure 3.3 Cascade connection of two nonlinear networks

The expressions of the harmonic voltage and current of the input port of the first and second nonlinear components are:

$$\begin{bmatrix} [V_{1a}] \\ [I_{1a}] \end{bmatrix} = [ABCD_{nonlinA}] \begin{bmatrix} [V_{2a}] \\ [I_{2a}] \end{bmatrix}. \quad (3.58)$$

$$\begin{bmatrix} [V_{1b}] \\ [I_{1b}] \end{bmatrix} = [ABCD_{nonlinB}] \begin{bmatrix} [V_{2b}] \\ [I_{2b}] \end{bmatrix}. \quad (3.59)$$

The voltage vector $[V_{2a}]$ and current vector $[I_{2a}]$ at the output of the first nonlinear component are equal to the voltage $[V_{1b}]$ and current $[I_{1b}]$, respectively, at the input of the second nonlinear component. Thus, the expression of $\begin{bmatrix} [V_{1a}] \\ [I_{1a}] \end{bmatrix}^T$, in terms of the vector $\begin{bmatrix} [V_{2b}] \\ [I_{2b}] \end{bmatrix}^T$, is:

$$\begin{bmatrix} [V_{1a}] \\ [I_{1a}] \end{bmatrix} = [ABCD_{nonlinA}] [ABCD_{nonlinB}] \begin{bmatrix} [V_{2b}] \\ [I_{2b}] \end{bmatrix}. \quad (3.60)$$

The equivalent nonlinear ABCD-parameters is, therefore, the product of nonlinear ABCD of both nonlinear components:

$$[ABCD_{nonlinEq}] = [ABCD_{nonlinA}] [ABCD_{nonlinB}]. \quad (3.61)$$

X-parameters of a cascade topology are calculated through the conversion rule from nonlinear ABCD-parameters to X-parameters:(Riadh Essaadali, Anwar Jarndal et al. 2011)

$$[X_{11Eq}] = 2 \left[\begin{bmatrix} [A_{Eq}] - \frac{[B_{Eq}]}{Z_c} \end{bmatrix} \right] \left[\begin{bmatrix} [A_{Eq}] - \frac{[B_{Eq}]}{Z_c} + Z_c [C_{Eq}] - [D_{Eq}] \end{bmatrix} \right]^{-1} - [I_d]. \quad (3.62)$$

$$[X_{21Eq}] = 2 \left[\begin{bmatrix} [A_{Eq}] - \frac{[B_{Eq}]}{Z_c} + Z_c [C_{Eq}] - [D_{Eq}] \end{bmatrix} \right]^{-1}. \quad (3.63)$$

$$[X_{12Eq}] = \left[\begin{bmatrix} [A_{Eq}] + \frac{[B_{Eq}]}{Z_c} \end{bmatrix} \right] + \left[\begin{bmatrix} [A_{Eq}] - \frac{[B_{Eq}]}{Z_c} \end{bmatrix} \right] [X_{22Eq}]. \quad (3.64)$$

$$[X_{22Eq}] = - \left[[A_{Eq}] - \frac{[B_{Eq}]}{Z_c} + Z_c [C_{Eq}] - [D_{Eq}] \right]^{-1} \left[[A_{Eq}] + \frac{[B_{Eq}]}{Z_c} + Z_c [C_{Eq}] + [D_{Eq}] \right]. \quad (3.65)$$

Equation (3.61) is still valid when a mixed cascaded topology of nonlinear and linear components or a cascaded topology of two linear networks is used. For a mixed cascade topology of nonlinear and linear components, the expressions of nonlinear A_{pmqm}^α , B_{pmqm}^α , C_{pmqm}^α and D_{pmqm}^α terms vanish to linear ABCD in the linear operation mode and are equal to $A_{pq}(m\omega)$, $B_{pq}(m\omega)$, $C_{pq}(m\omega)$ and $D_{pq}(m\omega)$, respectively (Riadh Essaadali, Anwar Jarndal et al. 2011). When a parallel topology of two linear networks is used, $A_{pmqm}^\alpha = B_{pmqm}^\alpha = C_{pmqm}^\alpha = D_{pmqm}^\alpha = 0$ for $m > 1$, since only the fundamental frequency is present in the circuit. The expression of nonlinear ABCD in the linear operation mode is

$$[ABCD_{Linear}] = \begin{bmatrix} A_{1111}^\alpha & 0 & \dots & 0 & 0 & B_{1121}^\alpha & 0 & \dots & 0 & 0 \\ 0 & A_{1111}^{\alpha^*} & \dots & 0 & 0 & 0 & B_{1121}^{\alpha^*} & \dots & 0 & 0 \\ \vdots & \vdots & \ddots & \vdots & \vdots & \vdots & \vdots & \ddots & \vdots & \vdots \\ 0 & 0 & \dots & A_{1n1n}^\alpha & 0 & 0 & 0 & \dots & B_{1n2n}^\alpha & 0 \\ 0 & 0 & \dots & 0 & A_{1n1n}^{\alpha^*} & 0 & 0 & \dots & 0 & B_{1n2n}^{\alpha^*} \\ C_{2111}^\alpha & 0 & \dots & 0 & 0 & D_{2121}^\alpha & 0 & \dots & 0 & 0 \\ 0 & C_{2111}^{\alpha^*} & \dots & 0 & 0 & 0 & D_{2121}^{\alpha^*} & \dots & 0 & 0 \\ \vdots & \vdots & \ddots & \vdots & \vdots & \vdots & \vdots & \ddots & \vdots & \vdots \\ 0 & 0 & \dots & C_{2n1n}^\alpha & 0 & 0 & 0 & \dots & D_{2n2n}^\alpha & 0 \\ 0 & 0 & \dots & 0 & C_{2n1n}^{\alpha^*} & 0 & 0 & \dots & 0 & D_{2n2n}^{\alpha^*} \end{bmatrix}. \quad (3.66)$$

The analytical nonlinear ABCD can be generalized to model a cascaded configuration of N nonlinear components:

$$[ABCD_{nonlinEq}] = \prod_{i=1}^N [ABCD_{nonlin_i}]. \quad (3.67)$$

Nonlinear T-parameters can also be used to model a cascaded configuration of nonlinear systems. The relations between a- and b-waves through nonlinear T-parameters of the first and second nonlinear components are expressed as:

$$\begin{bmatrix} [B_{1a}] \\ [A_{1a}] \end{bmatrix} = [T_{nonlinA}] \begin{bmatrix} [A_{2a}] \\ [B_{2a}] \end{bmatrix}. \quad (3.68)$$

$$\begin{bmatrix} [B_{1b}] \\ [A_{1b}] \end{bmatrix} = [T_{nonlinB}] \begin{bmatrix} [A_{2b}] \\ [B_{2b}] \end{bmatrix}. \quad (3.69)$$

Multi-harmonic wave vector $[B_{2a}]$ scattered at the output of the first nonlinear component is equal to multi-harmonic wave vector $[A_b]$ incident to the second nonlinear components. Moreover, multi-harmonic wave vector $[B_{1b}]$ scattered at the input of the second nonlinear component is equal to multi-harmonic wave vector $[A_{2a}]$ incident to the second nonlinear components at its output. Thus, $[[A_{2a}], [B_{2a}]]^T$ is equal to $[[B_{1b}], [A_{1b}]]^T$, and the relation between a- and b-waves of the whole system is given by:

$$\begin{bmatrix} [B_{1b}] \\ [A_{1b}] \end{bmatrix} = [T_{nonlinB}] \begin{bmatrix} [A_{2b}] \\ [B_{2b}] \end{bmatrix}. \quad (3.70)$$

The equivalent nonlinear T-parameters are the products of nonlinear T-parameters of both nonlinear parameters.

$$[T_{nonlin_Eq}] = [T_{nonlinA}][T_{nonlinB}]. \quad (3.71)$$

Equation (3.71) is still valid when a mixed cascaded topology of nonlinear and linear components or a cascaded topology of two linear networks is used. For a mixed cascaded topology of nonlinear and linear components, the expressions of nonlinear T_{pqm}^α terms vanish

to linear impedance in the linear operation mode and are equal to $T_{pq}(m\omega)$ (Riadh Essaadali, Anwar Jarndal et al. 2011), where ω is the fundamental frequency and m is the frequency index. In a series topology of two linear networks, $T_{pmqm}^\alpha = 0$ for $m > 1$, since only the fundamental frequency is present in the circuit. The expression of nonlinear T in the linear operation mode is:

$$[T_{LinearMode}] = \begin{bmatrix} T_{1111}^\alpha & 0 & \dots & 0 & 0 & T_{1121}^\alpha & 0 & \dots & 0 & 0 \\ 0 & T_{1111}^{\alpha^*} & \dots & 0 & 0 & 0 & T_{1121}^{\alpha^*} & \dots & 0 & 0 \\ \vdots & \vdots & \ddots & \vdots & \vdots & \vdots & \vdots & \ddots & \vdots & \vdots \\ 0 & 0 & \dots & T_{1n1n}^\alpha & 0 & 0 & 0 & \dots & T_{1n2n}^\alpha & 0 \\ 0 & 0 & \dots & 0 & T_{1n1n}^{\alpha^*} & 0 & 0 & \dots & 0 & T_{1n2n}^{\alpha^*} \\ T_{2111}^\alpha & 0 & \dots & 0 & 0 & T_{2121}^\alpha & 0 & \dots & 0 & 0 \\ 0 & T_{2111}^{\alpha^*} & \dots & 0 & 0 & 0 & T_{2121}^{\alpha^*} & \dots & 0 & 0 \\ \vdots & \vdots & \ddots & \vdots & \vdots & \vdots & \vdots & \ddots & \vdots & \vdots \\ 0 & 0 & \dots & T_{2n1n}^\alpha & 0 & 0 & 0 & \dots & T_{2n2n}^\alpha & 0 \\ 0 & 0 & \dots & 0 & T_{2n1n}^{\alpha^*} & 0 & 0 & \dots & 0 & T_{2n2n}^{\alpha^*} \end{bmatrix} \quad (3.72)$$

The analytical nonlinear T-parameters can be generalized to model a cascaded configuration of N nonlinear components:

$$[T_{nonlinEq}] = \prod_{i=1}^N [T_{nonlin_i}]. \quad (3.73)$$

X-parameters of a cascade topology are calculated through the conversion rule from nonlinear T-parameters to X-parameters:(Riadh Essaadali, Anwar Jarndal et al. 2011)

$$[X_{11Eq}] = [T_{11Eq}] [T_{22Eq}]^{-1}. \quad (3.74)$$

$$[X_{12Eq}] = [T_{11Eq}] - [T_{12Eq}] [T_{22Eq}]^{-1} [T_{21Eq}]. \quad (3.75)$$

$$[X_{21Eq}] = [T_{22Eq}]^{-1}. \quad (3.76)$$

$$[X_{22Eq}] = -[T_{22Eq}]^{-1}[T_{21Eq}]. \quad (3.77)$$

3.4.4 Series-to-parallel network configuration

To model a series-to-parallel configuration of nonlinear systems, nonlinear H-parameters can be used. The series-to-parallel configuration of two nonlinear components is illustrated in Figure 3.4.

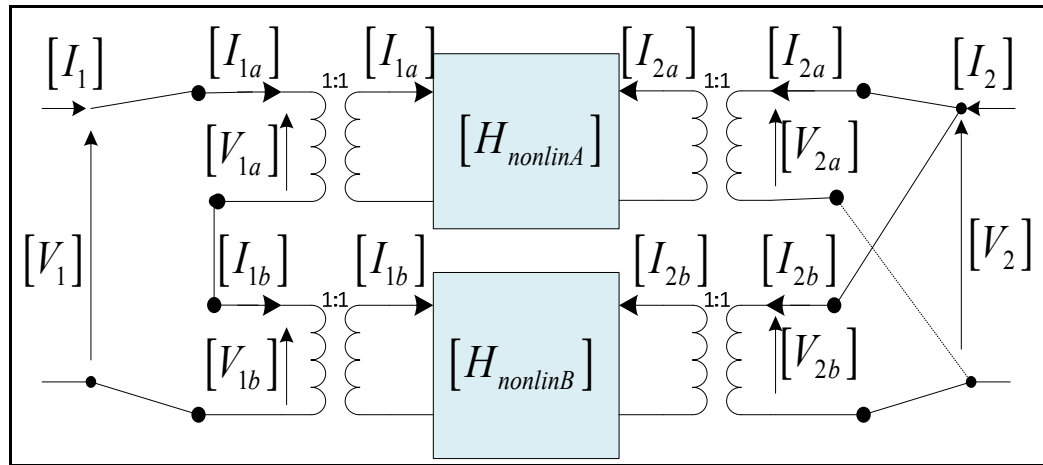


Figure 3.4 Series-to-parallel connection of two nonlinear networks

The expressions of the harmonic voltage vector at the first port and the harmonic current vector of the second port of the first and second nonlinear components are expressed, respectively, as:

$$\begin{bmatrix} [V_{1a}] \\ [I_{2a}] \end{bmatrix} = [H_{nonlinA}] \begin{bmatrix} [I_{1a}] \\ [V_{2a}] \end{bmatrix}. \quad (3.78)$$

$$\begin{bmatrix} [V_{1b}] \\ [I_{2b}] \end{bmatrix} = [H_{nonlinB}] \begin{bmatrix} [I_{1b}] \\ [V_{2b}] \end{bmatrix}. \quad (3.79)$$

The summation of $[V_{1a}]$ and $[V_{1b}]$ is equal to $[V_1]$, and the sum of $[I_{2a}]$ and $[I_{2b}]$ is equal to $[I_2]$. The voltages at the output port of both nonlinear components are equal, i.e., $[V_2]=[V_{2a}]=[V_{2b}]$; and, the currents at the input port of both nonlinear components are equal, i.e., $[I_1]=[I_{1a}]=[I_{1b}]$. Thus, the current-voltage relationship can be rewritten as:

$$\begin{bmatrix} [V_1] \\ [I_2] \end{bmatrix} = \begin{bmatrix} [V_{1a}] + [V_{1b}] \\ [I_{2a}] + [I_{2b}] \end{bmatrix} = \{ [H_{nonlinA}] + [H_{nonlinB}] \} \begin{bmatrix} [I_1] \\ [V_2] \end{bmatrix}. \quad (3.80)$$

The equivalent nonlinear H-parameters is the sum of nonlinear H-parameters of both nonlinear components:

$$[H_{nonlinEq}] = [H_{nonlinA}] + [H_{nonlinB}]. \quad (3.81)$$

Equation (3.81) is still valid when a mixed series-to-parallel topology of nonlinear and linear components or a series-to-parallel topology of two linear networks is used. For a mixed series-parallel topology of nonlinear and linear components, the expressions of nonlinear H_{pmqm}^α terms vanish to the linear H-parameter in the linear operation mode and are equal to $H_{pq}(m\omega)$, where ω is the fundamental frequency and m is the frequency index. In a series-to-parallel topology of two linear networks, $H_{pmqm}^\alpha = 0$ for $m > 1$, since only the fundamental frequency is present in the circuit. The expression of nonlinear H in the linear operation mode is:

$$[H_{LinearMode}] = \begin{bmatrix} H_{1111}^\alpha & 0 & \dots & 0 & 0 & H_{1121}^\alpha & 0 & \dots & 0 & 0 \\ 0 & H_{1111}^{\alpha^*} & \dots & 0 & 0 & 0 & H_{1121}^{\alpha^*} & \dots & 0 & 0 \\ \vdots & \vdots & \ddots & \vdots & \vdots & \vdots & \vdots & \ddots & \vdots & \vdots \\ 0 & 0 & \dots & H_{1n1n}^\alpha & 0 & 0 & 0 & \dots & H_{1n2n}^\alpha & 0 \\ 0 & 0 & \dots & 0 & H_{1n1n}^{\alpha^*} & 0 & 0 & \dots & 0 & H_{1n2n}^{\alpha^*} \\ H_{2111}^\alpha & 0 & \dots & 0 & 0 & H_{2121}^\alpha & 0 & \dots & 0 & 0 \\ 0 & H_{2111}^{\alpha^*} & \dots & 0 & 0 & 0 & H_{2121}^{\alpha^*} & \dots & 0 & 0 \\ \vdots & \vdots & \ddots & \vdots & \vdots & \vdots & \vdots & \ddots & \vdots & \vdots \\ 0 & 0 & \dots & H_{2n1n}^\alpha & 0 & 0 & 0 & \dots & H_{2n2n}^\alpha & 0 \\ 0 & 0 & \dots & 0 & H_{2n1n}^{\alpha^*} & 0 & 0 & \dots & 0 & H_{2n2n}^{\alpha^*} \end{bmatrix}. \quad (3.82)$$

The analytical nonlinear H-parameters can be generalized to model a series-parallel configuration of N nonlinear components as:

$$[H_{nonlinEq}] = \sum_{i=1}^N [H_{nonlin_i}]. \quad (3.83)$$

X-parameters of a series-to-parallel topology are calculated through the conversion rule from nonlinear H-parameters to X-parameters:(Riadh Essaadali, Anwar Jarndal et al. 2011)

$$[X_{11Eq}] = \left[[I_d] + \frac{[H_{11Eq}]}{Z_c} - [H_{12Eq}] \left[\frac{[I_d]}{Z_c} + [H_{22Eq}] \right]^{-1} \frac{[H_{21Eq}]}{Z_c} \right]^{-1} \left[\frac{[H_{11Eq}]}{Z_c} - [I_d] - [H_{12Eq}] \left[\frac{[I_d]}{Z_c} + [H_{22Eq}] \right]^{-1} \frac{[H_{21Eq}]}{Z_c} \right]. \quad (3.84)$$

$$[X_{12Eq}] = -\frac{2}{Z_c} \cdot \left[\frac{[H_{21Eq}]}{Z_c} - \left[\frac{[I_d]}{Z_c} + [H_{22Eq}] \right] [H_{12Eq}]^{-1} \left[[I_d] + \frac{[H_{11Eq}]}{Z_c} \right] \right]^{-1} \quad (3.85)$$

$$\begin{aligned}
[X_{21Eq}] &= \left[\left[\frac{I_d}{Z_c} \right] + [H_{22Eq}] \right]^{-1} \left[\frac{H_{21Eq}}{Z_c} \right] \\
&\cdot \left\{ \left[[I_d] + \frac{H_{11Eq}}{Z_c} \right] - [H_{12Eq}] \left[\left[\frac{I_d}{Z_c} \right] + [H_{22Eq}] \right]^{-1} \left[\frac{H_{21Eq}}{Z_c} \right] \right\}^{-1} \\
&\cdot \left\{ \left[\frac{H_{11Eq}}{Z_c} \right] - [I_d] - [H_{12Eq}] \left[\left[\frac{I_d}{Z_c} \right] + [H_{22Eq}] \right]^{-1} \left[\frac{H_{21Eq}}{Z_c} \right] - [I_d] \right\}.
\end{aligned} \tag{3.86}$$

$$\begin{aligned}
[X_{22Eq}] &= -\frac{2}{Z_c} [H_{12Eq}]^{-1} \left[[I_d] + \frac{H_{11Eq}}{Z_c} \right] \\
&\left[\frac{H_{21Eq}}{Z_c} \right] - \left[\left[\frac{I_d}{Z_c} \right] + [H_{22Eq}] \right] [H_{12Eq}]^{-1} \left[[I_d] + \frac{H_{11Eq}}{Z_c} \right] \right]^{-1} - [I_d].
\end{aligned} \tag{3.87}$$

3.4.5 Parallel-to-series network configuration

To model a parallel-to-series configuration of nonlinear systems, nonlinear G-parameters can be used. The parallel-to-series configuration of two nonlinear components is illustrated in Figure 3.5.

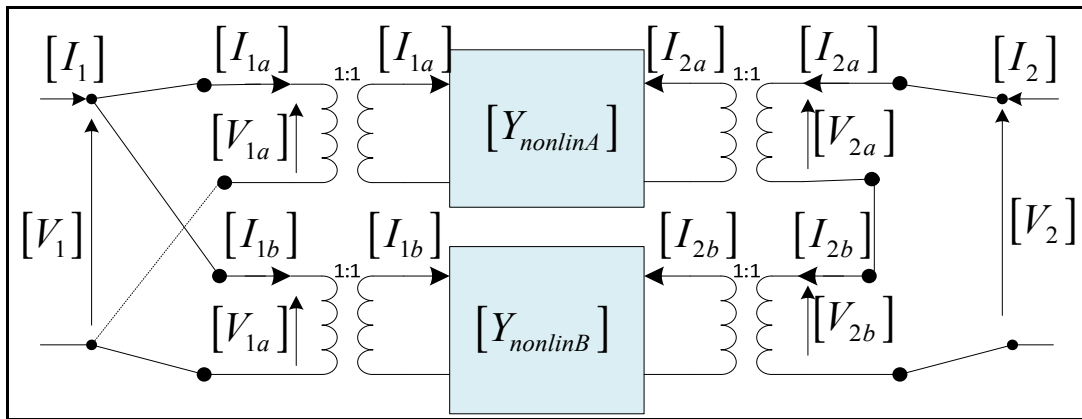


Figure 3.5 Parallel-to-series connection of two nonlinear networks

The expressions of the harmonic voltage at the first port and the harmonic current of the second port of the first and the second nonlinear component are expressed as:

$$\begin{bmatrix} [I_{1a}] \\ [V_{2a}] \end{bmatrix} = [G_{nonlinA}] \begin{bmatrix} [V_{1a}] \\ [I_{2a}] \end{bmatrix}. \quad (3.88)$$

$$\begin{bmatrix} [I_{1b}] \\ [V_{2b}] \end{bmatrix} = [G_{nonlinB}] \begin{bmatrix} [V_{1b}] \\ [I_{2b}] \end{bmatrix}. \quad (3.89)$$

The summation of $[I_{1a}]$ and $[I_{1b}]$ is equal to $[I_1]$, and the sum of $[V_{2a}]$ and $[V_{2b}]$ is equal to $[V_2]$. The currents at the output port of both nonlinear components are equal, i.e., $[I_2] = [I_{2a}] = [I_{2b}]$; and, the voltages at the input port of both nonlinear components are equal, i.e., $[V_1] = [V_{1a}] = [V_{1b}]$. Thus, the current-voltage relationship can be rewritten as:

$$\begin{bmatrix} [I_1] \\ [V_2] \end{bmatrix} = \begin{bmatrix} [I_{1a}] + [I_{1b}] \\ [V_{2a}] + [V_{2b}] \end{bmatrix} = \{[G_{nonlinA}] + [G_{nonlinB}]\} \begin{bmatrix} [V_1] \\ [I_2] \end{bmatrix}. \quad (3.90)$$

The equivalent nonlinear G-parameter is the sum of the nonlinear G-parameters of both nonlinear components:

$$[G_{nonlin\acute{e}q}] = [G_{nonlinA}] + [G_{nonlinB}]. \quad (3.91)$$

Equation (3.91) is still valid for a mixed parallel-series topology of nonlinear and linear components or a parallel-series topology of two linear networks. For a mixed parallel-series topology of nonlinear and linear components, the expressions of nonlinear G_{pmqm}^α terms vanish to linear G-parameters in the linear operation mode and are equal to $G_{pq}(m\omega)$, where ω is the fundamental frequency and m is the frequency index (Riadh Essaadali, Anwar Jarndal et al. 2011). In a parallel-to-series topology of two linear networks, $G_{pmqm}^\alpha = 0$ for $m > 1$, since only the fundamental frequency is present in the circuit. The expression of nonlinear G-parameter in the linear operation mode is:

$$[G_{Linear}] = \begin{bmatrix} G_{1111}^{\alpha} & 0 & \dots & 0 & 0 & G_{1121}^{\alpha} & 0 & \dots & 0 & 0 \\ 0 & G_{1111}^{\alpha^*} & \dots & 0 & 0 & 0 & G_{1121}^{\alpha^*} & \dots & 0 & 0 \\ \vdots & \vdots & \ddots & \vdots & \vdots & \vdots & \vdots & \ddots & \vdots & \vdots \\ 0 & 0 & \dots & G_{1n1n}^{\alpha} & 0 & 0 & 0 & \dots & G_{1n2n}^{\alpha} & 0 \\ 0 & 0 & \dots & 0 & G_{1n1n}^{\alpha^*} & 0 & 0 & \dots & 0 & G_{1n2n}^{\alpha^*} \\ G_{2111}^{\alpha} & 0 & \dots & 0 & 0 & G_{2121}^{\alpha} & 0 & \dots & 0 & 0 \\ 0 & G_{2111}^{\alpha^*} & \dots & 0 & 0 & 0 & G_{2121}^{\alpha^*} & \dots & 0 & 0 \\ \vdots & \vdots & \ddots & \vdots & \vdots & \vdots & \vdots & \ddots & \vdots & \vdots \\ 0 & 0 & \dots & G_{2n1n}^{\alpha} & 0 & 0 & 0 & \dots & G_{2n2n}^{\alpha} & 0 \\ 0 & 0 & \dots & 0 & G_{2n1n}^{\alpha^*} & 0 & 0 & \dots & 0 & G_{2n2n}^{\alpha^*} \end{bmatrix}. \quad (3.92)$$

The analytical nonlinear G-parameters can be generalized to model a parallel-series configuration of N nonlinear components:

$$[G_{nonlinEq}] = \sum_{i=1}^N [G_{nonlin_i}]. \quad (3.93)$$

X-parameters of a parallel-to-series topology are calculated through the conversion rule from nonlinear G-parameters to X-parameters:(Riadh Essaadali, Anwar Jarndal et al. 2011)

$$[X_{11Eq}] = \left[\left[G_{11Eq} \right] + \frac{[I_d]}{Z_c} - \frac{[G_{12Eq}]}{Z_c} \left[[I_d] + \frac{[G_{22Eq}]}{Z_c} \right]^{-1} \left[G_{21Eq} \right] \right]^{-1} \cdot \left[\frac{[I_d]}{Z_c} - \left[G_{11Eq} \right] + \frac{[G_{12Eq}]}{Z_c} \left[[I_d] + \frac{[G_{22Eq}]}{Z_c} \right]^{-1} \left[G_{21Eq} \right] \right]. \quad (3.94)$$

$$[X_{21Eq}] = \left[[I_d] + \frac{[G_{22Eq}]}{Z_c} \right]^{-1} \left[G_{21Eq} \right] \left\{ [I_d] + \left[\left[G_{11Eq} \right] + \frac{[I_d]}{Z_c} - \frac{[G_{12Eq}]}{Z_c} \left[[I_d] + \frac{[G_{22Eq}]}{Z_c} \right]^{-1} \left[G_{21Eq} \right] \right]^{-1} \cdot \left[\frac{[I_d]}{Z_c} - \left[G_{11Eq} \right] + \frac{[G_{12Eq}]}{Z_c} \left[[I_d] + \frac{[G_{22Eq}]}{Z_c} \right]^{-1} \left[G_{21Eq} \right] \right] \right\}. \quad (3.95)$$

$$\begin{aligned}
[X_{12}] = & \left[\left[G_{11Eq} \right] + \frac{[I_d]}{Z_c} - \frac{[G_{12Eq}]}{Z_c} \left[\left[I_d \right] + \frac{[G_{22Eq}]}{Z_c} \right]^{-1} \left[G_{21Eq} \right] \right]^{-1} \\
& \cdot \frac{[G_{12Eq}]}{Z_c} \left[\left[I_d \right] + \frac{[G_{22Eq}]}{Z_c} \right]^{-1} \left[\frac{[G_{22Eq}]}{Z_c} - [I_d] \right] - [I_d] \right]. \tag{3.96}
\end{aligned}$$

$$\begin{aligned}
[X_{22}] = & \left[\left[I_d \right] + \frac{[G_{22Eq}]}{Z_c} \right]^{-1} \left\{ \left[G_{21Eq} \right] \cdot \left[\left[G_{11Eq} \right] + \frac{[I_d]}{Z_c} - \frac{[G_{12Eq}]}{Z_c} \left[\left[I_d \right] + \frac{[G_{22Eq}]}{Z_c} \right]^{-1} \left[G_{21Eq} \right] \right]^{-1} \right. \\
& \left. \cdot \frac{[G_{12Eq}]}{Z_c} \left[\left[I_d \right] + \frac{[G_{22Eq}]}{Z_c} \right]^{-1} \left[\frac{[G_{22Eq}]}{Z_c} - [I_d] \right] - [I_d] \right\} + \left[\frac{[G_{22Eq}]}{Z_c} - [I_d] \right] \right\}. \tag{3.97}
\end{aligned}$$

3.5 Validation of Nonlinear Two-Port Network Configurations

The different nonlinear network configurations have been validated. For each configuration, topologies of two nonlinear components, two linear networks and a mix of nonlinear and linear components have been validated. For each validation case, two components with different small- and large-signal operation regions were used. In each case, the simulating signals used in the validation are able to excite the PAs highly above the 1 dB compression.

3.5.1 Cascaded network configuration

The validity of analytical cascaded nonlinear ABCD-parameters was evaluated by computing the X-parameters of a nonlinear cascaded system of two mini-circuits PAs, ZFL11AD and ZX602522M. Two types of simulation are used. X-parameters and harmonic balance (HB) simulations of xnp measurement files in ADS (Advanced Design System) simulator software could be sufficient to validate the cascade behavior. The process of the validation is summarized in Figure 3.6. X-parameters simulations are used to generate X-parameters data of the whole cascaded system and of each component simulated alone under the same conditions as when it is in the cascaded network.

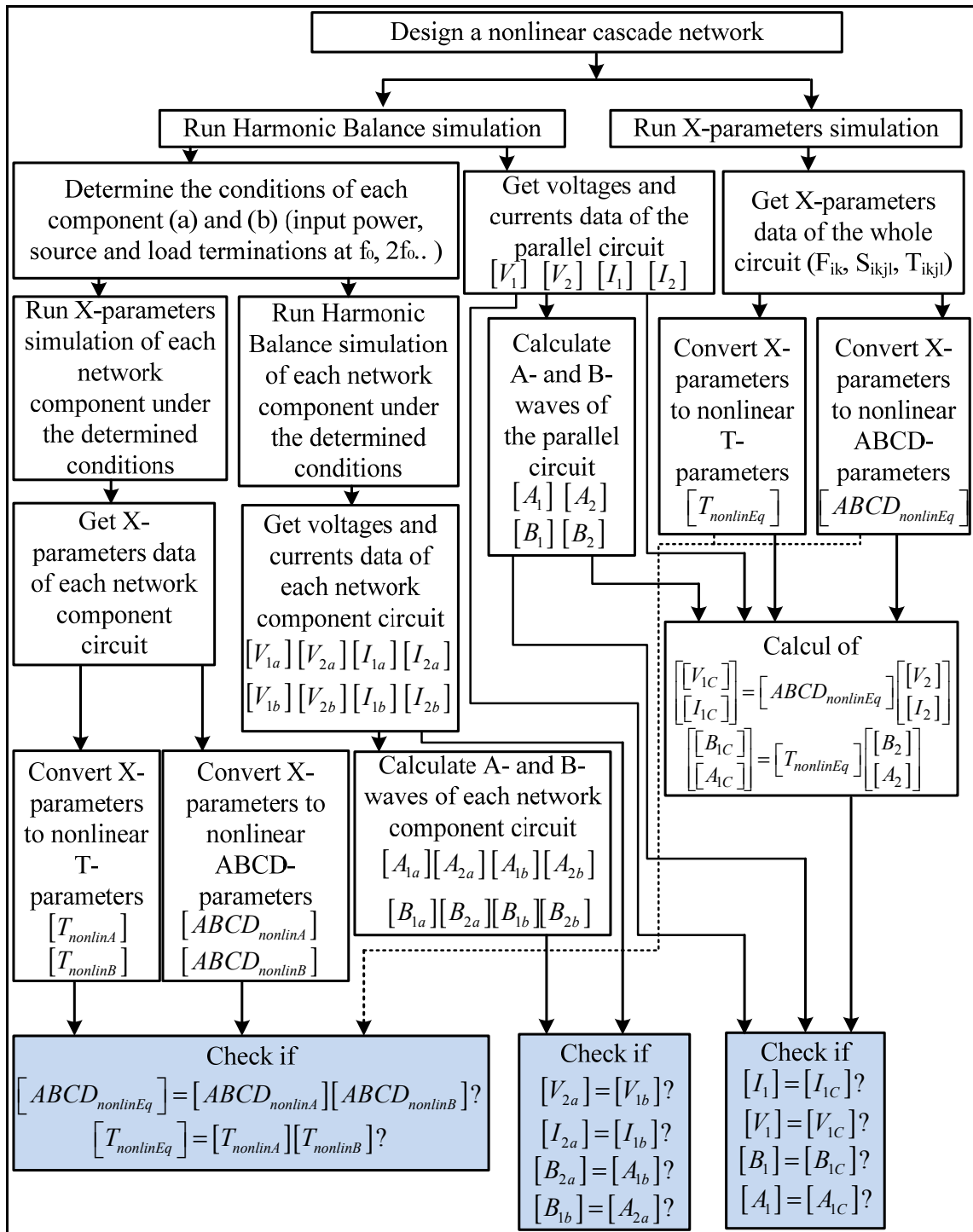


Figure 3.6 Validation process of nonlinear cascaded network configuration.

The conditions of input power, source and load terminations are determined through the HB simulation. X-parameters of the whole circuit (circuit A, circuit B, resp.) are then converted to nonlinear ABCD-parameters $[ABCD_{nonlinEq}]$ ($[ABCD_{nonlinA}], [ABCD_{nonlinB}]$). HB simulation yields harmonic voltage and current harmonic components at the input and the output of the whole circuit ($[V_1], [V_2], [I_1], [I_2]$), circuit A ($[V_{1a}], [V_{2a}], [I_{1a}], [I_{2a}]$) and circuit B ($[V_{1b}], [V_{2b}], [I_{1b}], [I_{2b}]$). To validate the usefulness of nonlinear ABCD-parameters to describe a cascade nonlinear network, the matrix $[ABCD_{nonlinEq}]$ is compared to the multiplication of nonlinear ABCD matrices calculated from the X-parameters of each component in Figure 3.7 that demonstrates a good agreement. For a 2-port circuit and 3 harmonic orders, 72 nonlinear ABCD terms could be obtained. In order to keep the figures legible, only 7 arbitrary terms are presented: $A_{1111}^\alpha, A_{1112}^\beta, C_{2311}^\alpha, C_{2112}^\beta, C_{2311}^\beta, D_{2223}^\alpha, B_{1121}^\beta$.

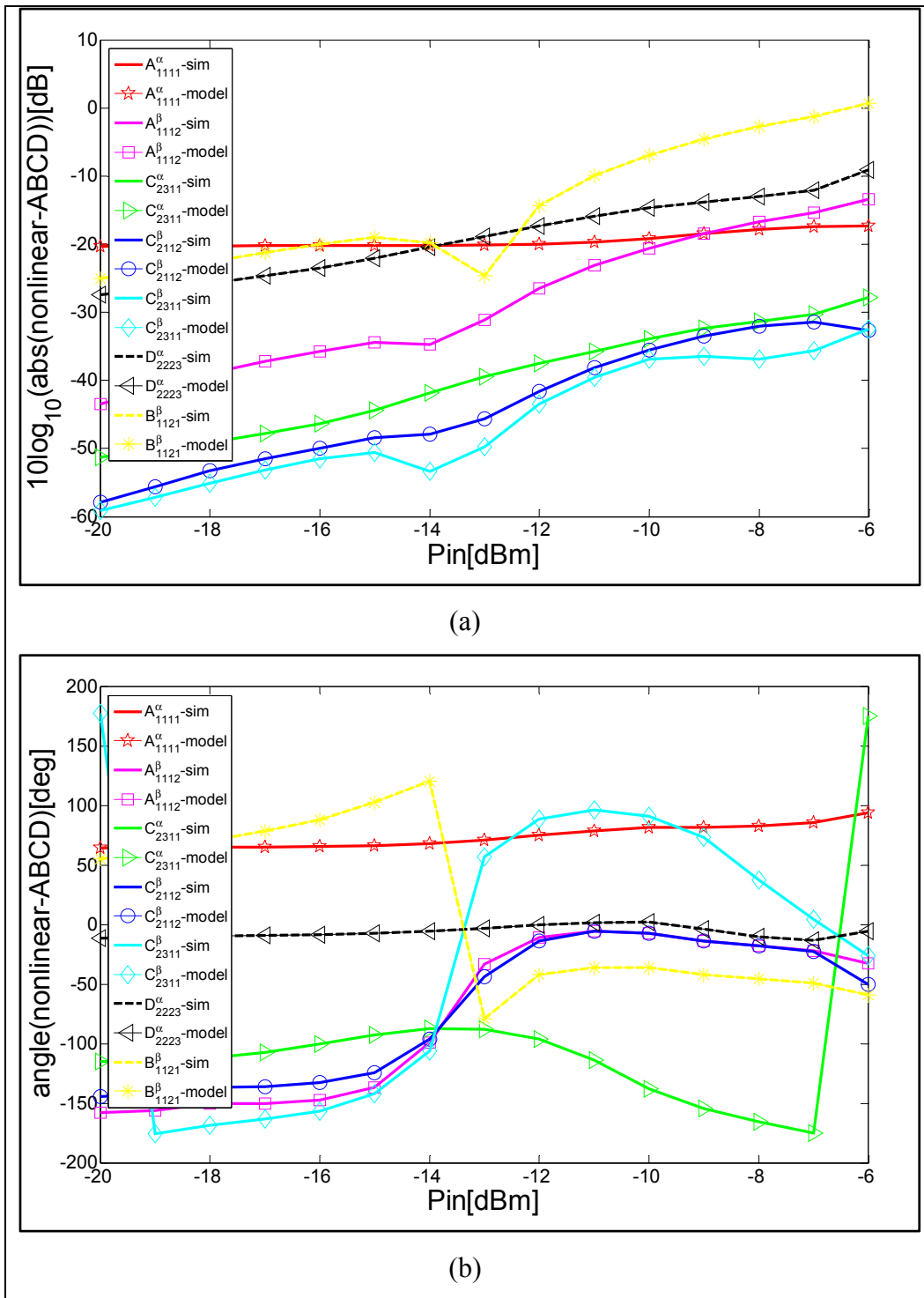


Figure 3.7 Comparison between the logarithmic amplitude (a) and the phase (b) of a random set of nonlinear ABCD-parameters calculated from the X-parameters of a cascaded system and those calculated through the cascaded nonlinear ABCD expressions in (3.61).

In the analytical development, it was assumed that the voltage vector $[V_{2a}]$ and current vector $[I_{2a}]$ at the output of the first nonlinear component are equal to the voltage $[V_{1b}]$ and current $[I_{1b}]$, respectively, at the input of the second nonlinear component. In Figure 3.8, the assumption is checked ($[V_{2a}] = [V_{1b}]$ and $[I_{2a}] = [I_{1b}]$). Moreover, in Figure 3.8, the harmonic components of voltage and current at the input of the cascaded circuit calculated through nonlinear ABCD matrix with (3.60) are compared to those obtained with HB simulation. The agreement between the curves proves more the concept of analytical cascaded nonlinear ABCD-parameters.

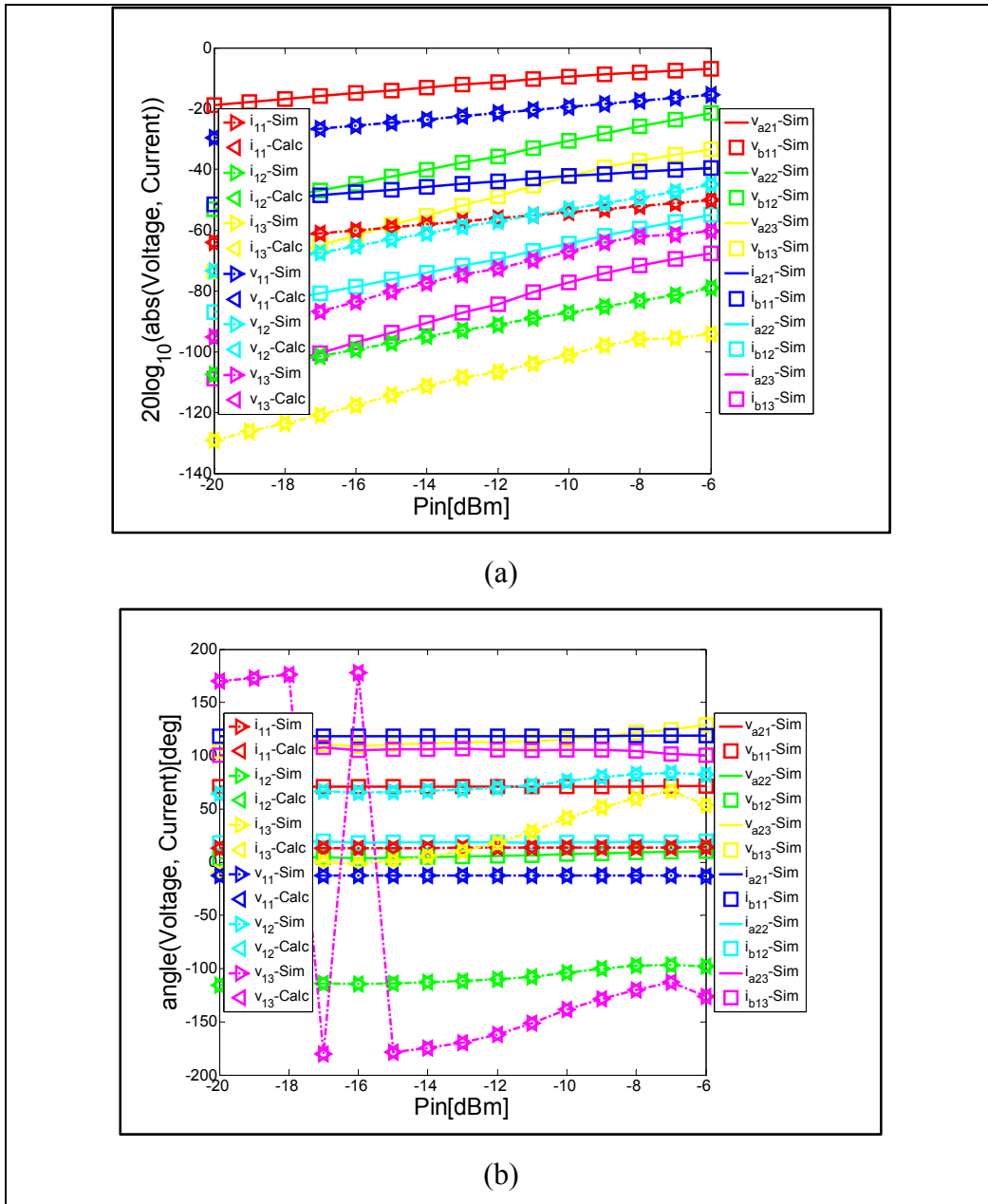


Figure 3.8 Comparison between the logarithmic amplitude (a) and the phase (b) of harmonic voltages and currents as mentioned in the graph presenting the validation process in Figure 3.6. v_{1j} -sim and i_{1j} -sim are the j th harmonic component of voltage and current, simulated with HB, at the input of cascaded system. v_{1j} -Calc and i_{1j} -Calc are the j th harmonic component of voltage and current at the input of cascaded system calculated through nonlinear ABCD matrix with (3.60). v_{a2j} -sim (v_{b1j} -sim) and i_{a2j} -sim (i_{b1j} -sim) are the j th harmonic component of voltage and current, simulated with HB, at the output (input) of circuit A (circuit B).

Nonlinear T-parameters are also used to model a nonlinear cascaded system. The same data used to validate the cascaded nonlinear ABCD-parameters are also used to evaluate the cascaded nonlinear T-parameters. The comparison between the amplitudes and phases in Figure 3.9 demonstrates a good agreement between the nonlinear T-parameters calculated from the X-parameters of the cascaded system and the results of the multiplication of nonlinear T matrices calculated from the X-parameters of each component. In the figure, only 7 arbitrary terms are considered: T_{1311}^{β} , T_{1211}^{α} , T_{1221}^{α} , T_{1321}^{β} , T_{2112}^{β} , T_{2221}^{β} , T_{2221}^{α} , T_{2321}^{α} . In the analytical development, it was assumed that A- and B-waves at the output of the first component are equals to B- and A-waves of the second component. This assumption ($[A_{2a}] = [B_{1b}]$ and $[B_{2a}] = [A_{1b}]$) is validated in Figure 3.10. Moreover, in Figure 3.10, the harmonic components of A- and B-waves at the input of the cascaded circuit calculated through nonlinear T matrix with (3.71) are compared to those obtained with HB simulation. The agreement between the curves proves more the concept of analytical cascaded nonlinear T-parameters.

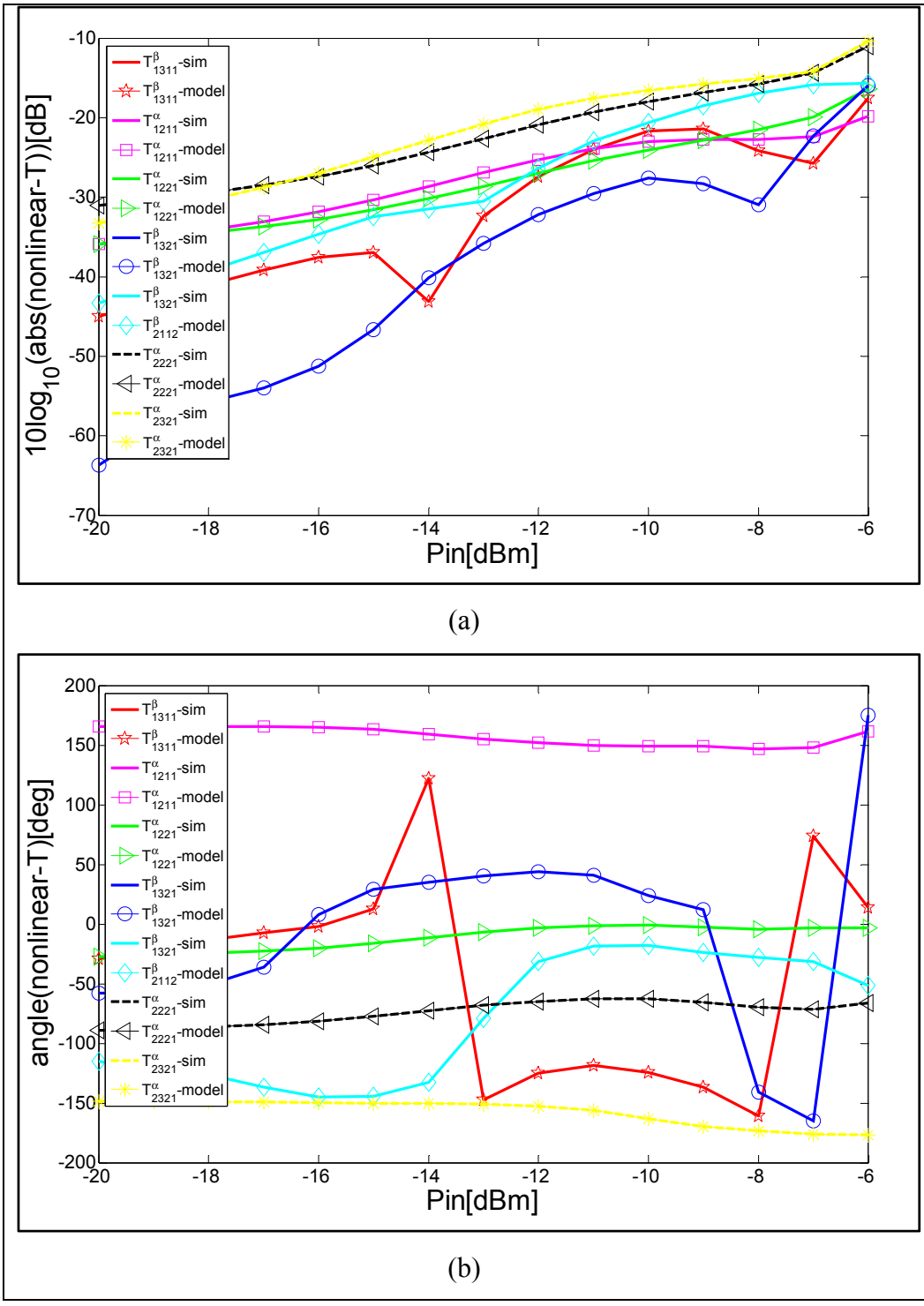


Figure 3.9 Comparison between the logarithmic amplitude (a) and the phase (b) of a random set of nonlinear T-parameters calculated from the X-parameters of a cascaded system and those calculated through the cascaded nonlinear T expressions in (3.71).

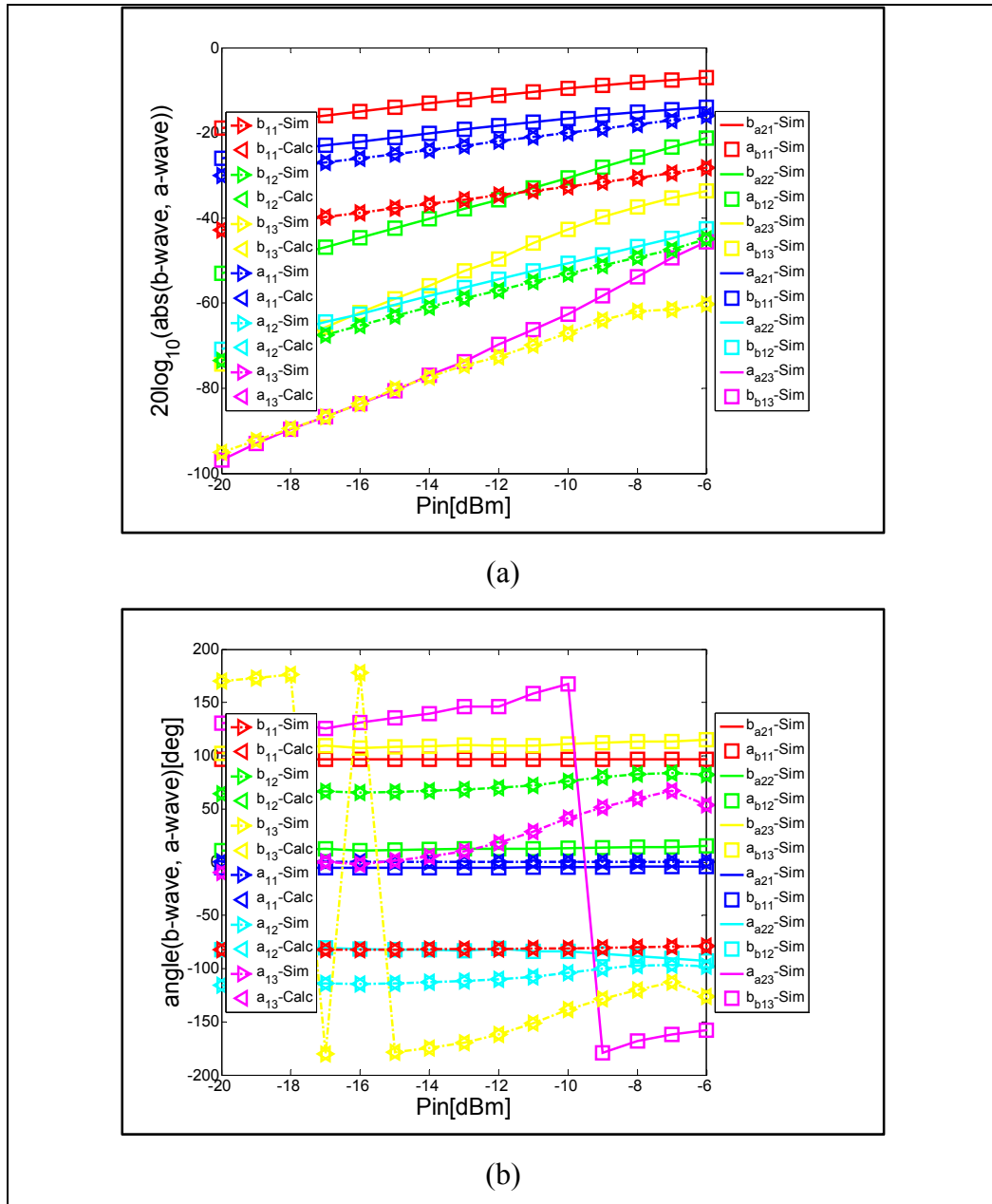


Figure 3.10 Comparison between the logarithmic amplitude (a) and the phase (b) of harmonic A- and B-waves as mentioned in the graph presenting the validation process in Figure 3.6. b_{ij} -sim and a_{ij} -sim are the j th harmonic component of scattered and incident waves, simulated with HB, at the input of cascaded system. a_{ij} -Calc and b_{ij} -Calc are the j th harmonic component of incident and scattered waves at the input of cascaded system calculated through nonlinear T matrix with (3.68). a_{a2j} -sim (a_{b1j} -sim) and b_{a2j} -sim (b_{b1j} -sim) are the j th harmonic component of incident and scattered waves, simulated with HB, at the output (input) of circuit A (circuit B).

3.5.2 Series network configuration

The validity of analytical series nonlinear Z-parameters was evaluated by computing the X-parameters of a nonlinear series system of two mini-circuits PAs, ZFL11AD and ZX602522M. Two types of simulation are used. X-parameters and HB simulations of xnp measurement files in ADS simulator software are sufficient to validate the series model. The process of the validation is summarized in Figure 3.11. X-parameters simulations are used to generate X-parameters data of the whole series system and of each component simulated alone under the same conditions as when it is in the series network. The conditions of input power, source and load terminations are determined through the HB simulation. X-parameters of the whole circuit (circuit A, circuit B, resp.) are then converted to nonlinear Z-parameters $[Z_{nonlinEq}]$ ($[Z_{nonlinA}]$, $[Z_{nonlinB}]$, resp.).

To validate the utility of nonlinear Z-parameters to describe a series nonlinear network, the matrix $[Z_{nonlinEq}]$ is compared to the sum of nonlinear Z matrices calculated from the X-parameters of each component in Figure 3.12. The figure is limited to 7 arbitrary terms: Z_{1213}^α , Z_{1313}^β , Z_{1221}^α , Z_{1322}^α , Z_{2112}^β , Z_{2213}^β , Z_{2323}^α . The figure illustrates a good agreement between the nonlinear Z-parameters calculated from the X-parameters of the series system and the results of the addition of nonlinear Z matrices calculated from the X-parameters of each nonlinear component.

In the analytical development, the assumption that the voltage vector $[V_p] = [V_{pa}] + [V_{pb}]$ where $p=1,2$ and the current vector $[I_p] = [I_{pa}] = [I_{pb}]$ are verified in Figure 3.13. Moreover, in the figure, the harmonic components of voltage at the input and the output of the series circuit calculated through nonlinear Z matrix in (3.46) are compared to those obtained with HB simulation. The agreement between the curves proves more the concept of analytical series nonlinear Z-parameters.

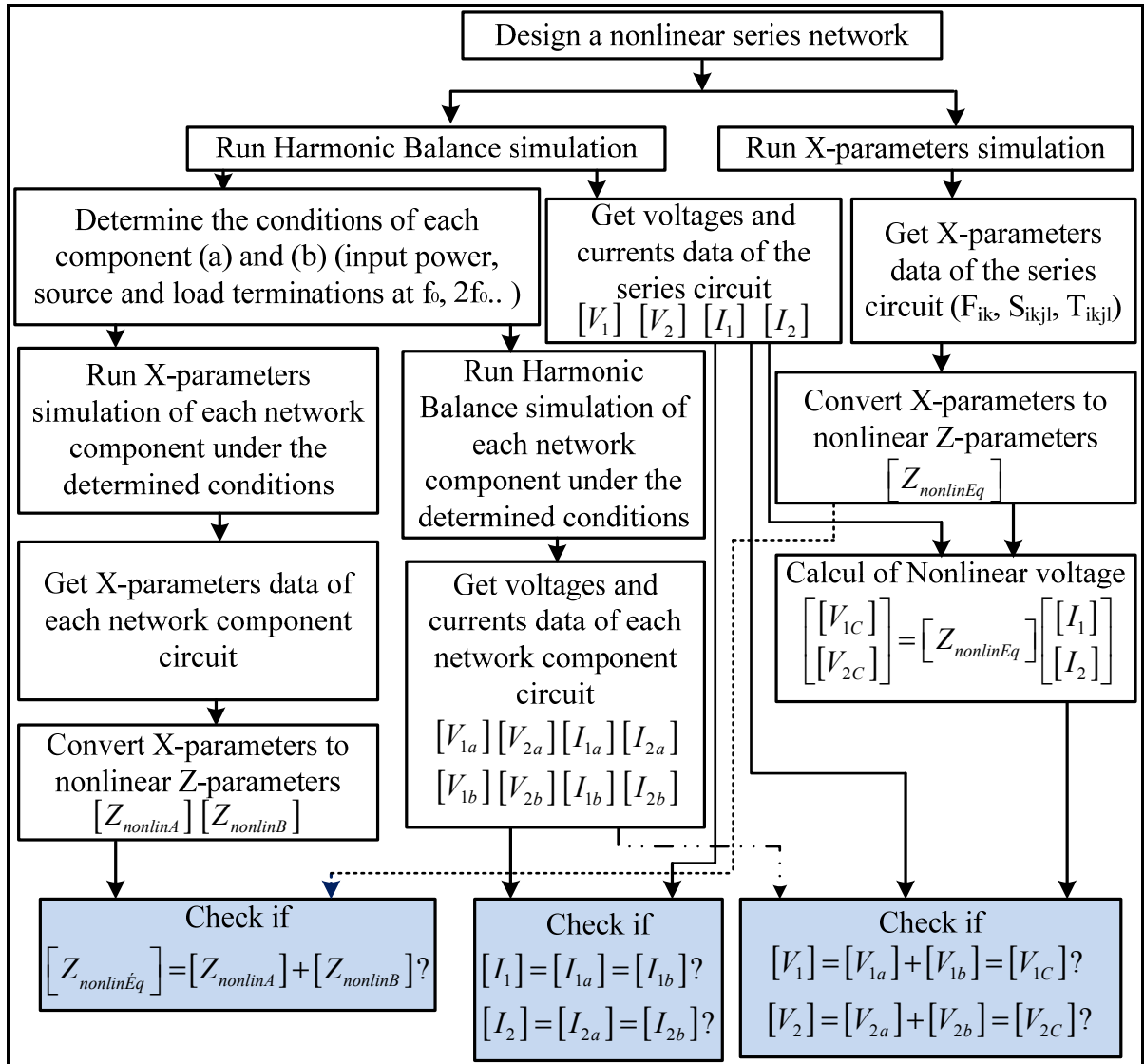


Figure 3.11 Validation process of nonlinear series network configuration.

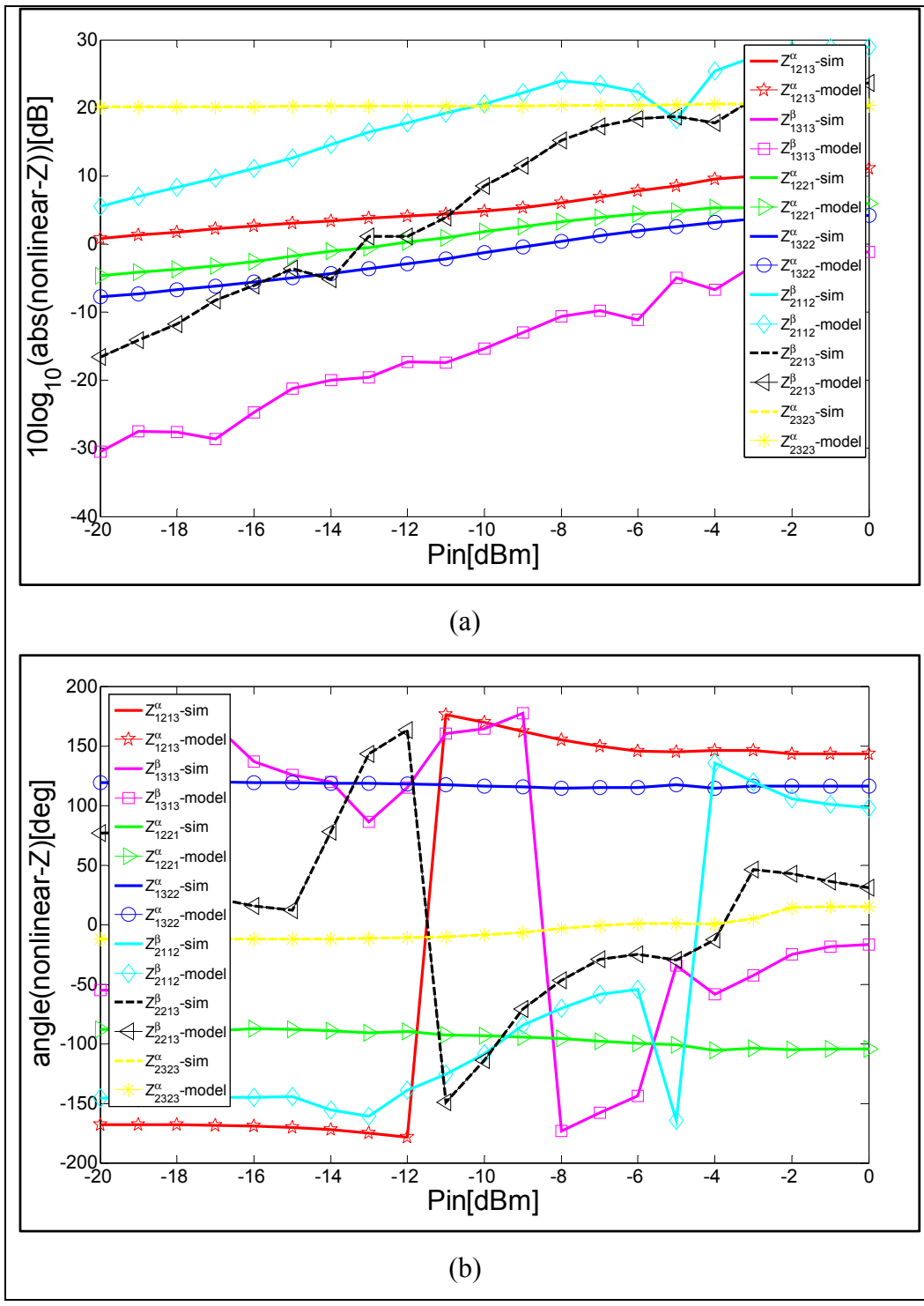


Figure 3.12 Comparison between the logarithmic amplitude (a) and the phase (b) of a random set of nonlinear Z-parameters calculated from the X-parameters of a series system and those calculated through the series nonlinear Z expressions in (3.47).

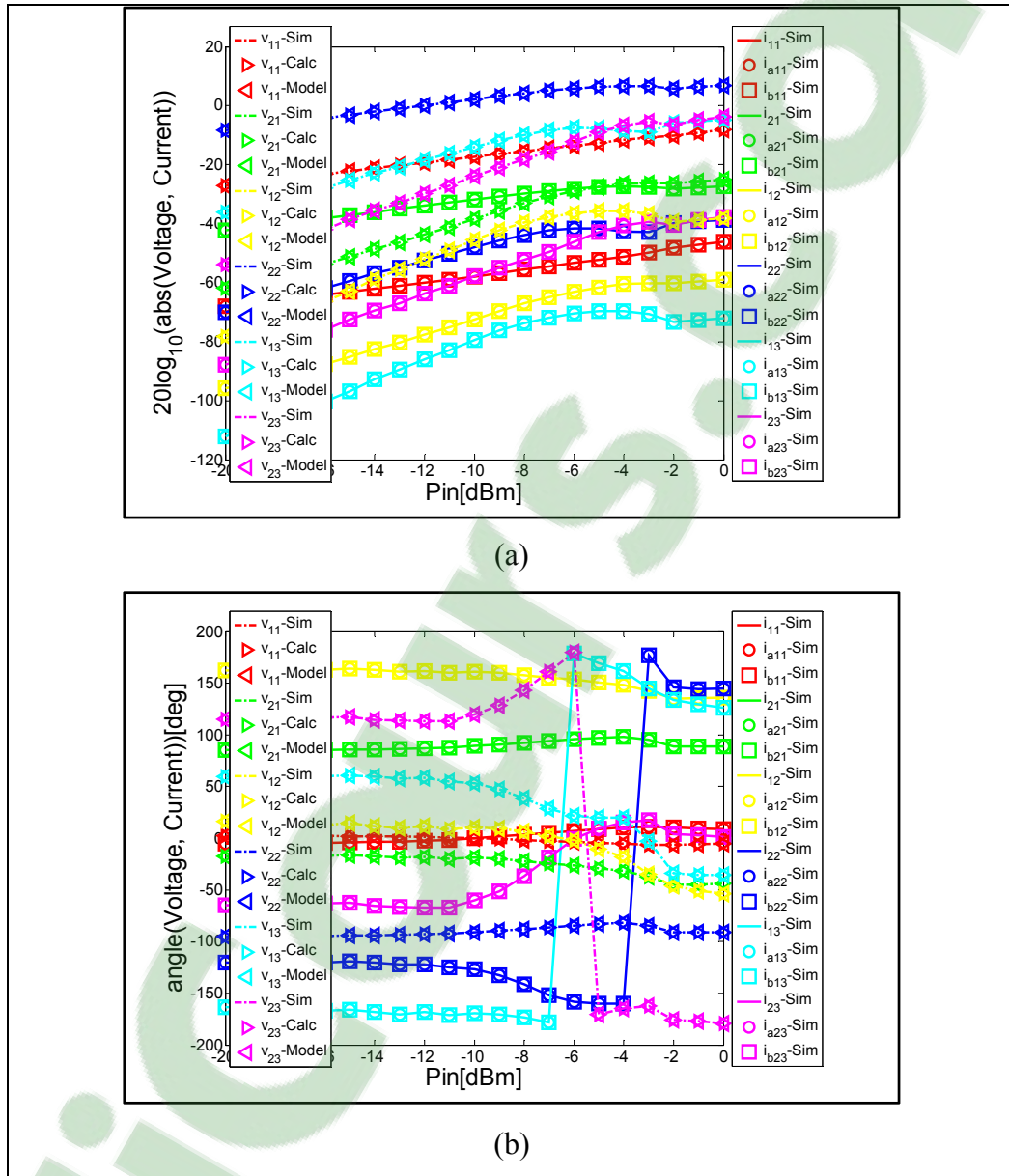


Figure 3.13 Comparison between the logarithmic amplitude (a) and the phase (b) of harmonic voltages and currents as mentioned in the graph presenting the validation process in Figure 3.11. v_{pj} -sim and i_{pj} -sim are the j th harmonic component of voltage and current, simulated with HB, at the input ($p=1$) and output ($p=2$) of the series system. v_{pj} -Calc is the sum of the j th harmonic component of voltages simulated with HB at the port p of circuit A (v_{apj}) and circuit B (v_{bpj}). v_{pj} -Model are calculated through nonlinear Z matrix with (3.53). i_{pj} -sim (i_{apj} -sim, i_{bpj} -sim, resp.) are the j th harmonic component of current, simulated with HB, at the port p of the series circuit (circuit A, circuit B, resp.).

3.5.3 Parallel network configuration

The validity of analytical parallel nonlinear Y-parameters was determined with the X-parameters of a parallel system of ZFL11AD with a cascaded system of ZFL11AD and ZX602522M. The process of the validation is summarized in Figure 3.14. X-parameters simulations are used to generate X-parameters data of the parallel system and of each component simulated alone under the same conditions as when it is in the parallel network.

The conditions of input power, source and load terminations are determined through the HB simulation. X-parameters of the whole circuit (circuit A, circuit B, resp.) are then converted to nonlinear Y-parameters $[Y_{nonlinEq}]$ ($[Y_{nonlinA}], [Y_{nonlinB}]$, resp.). To validate the utility of nonlinear Y-parameters to describe a parallel nonlinear network, the matrix $[Y_{nonlinEq}]$ is compared to the sum of nonlinear admittance matrices ($[Y_{nonlinA}] + [Y_{nonlinB}]$) calculated from the X-parameters of each component in Figure 3.15. The figures are limited to 7 arbitrary terms: Y_{2313}^α , Y_{1123}^α , Y_{1221}^β , Y_{2121}^α , Y_{1321}^β , Y_{2323}^α , Y_{2212}^α . The figure illustrates a good agreement between the nonlinear Y-parameters calculated from the X-parameters of the parallel system and the results of the addition of nonlinear Y matrices calculated from the X-parameters of each nonlinear component.

In the analytical development, the assumption that the current vector $[I_p] = [I_{pa}] + [I_{pb}]$ where $p=1,2$ and the voltage vector $[V_p] = [V_{pa}] = [V_{pb}]$ are verified in Figure 3.16. Moreover, in these figures, the harmonic components of the current at the input and the output of the parallel circuit calculated through nonlinear Y matrix in (3.53) are compared to those obtained with HB simulation. The agreement between the curves proves more the concept of analytical parallel nonlinear admittance parameters.

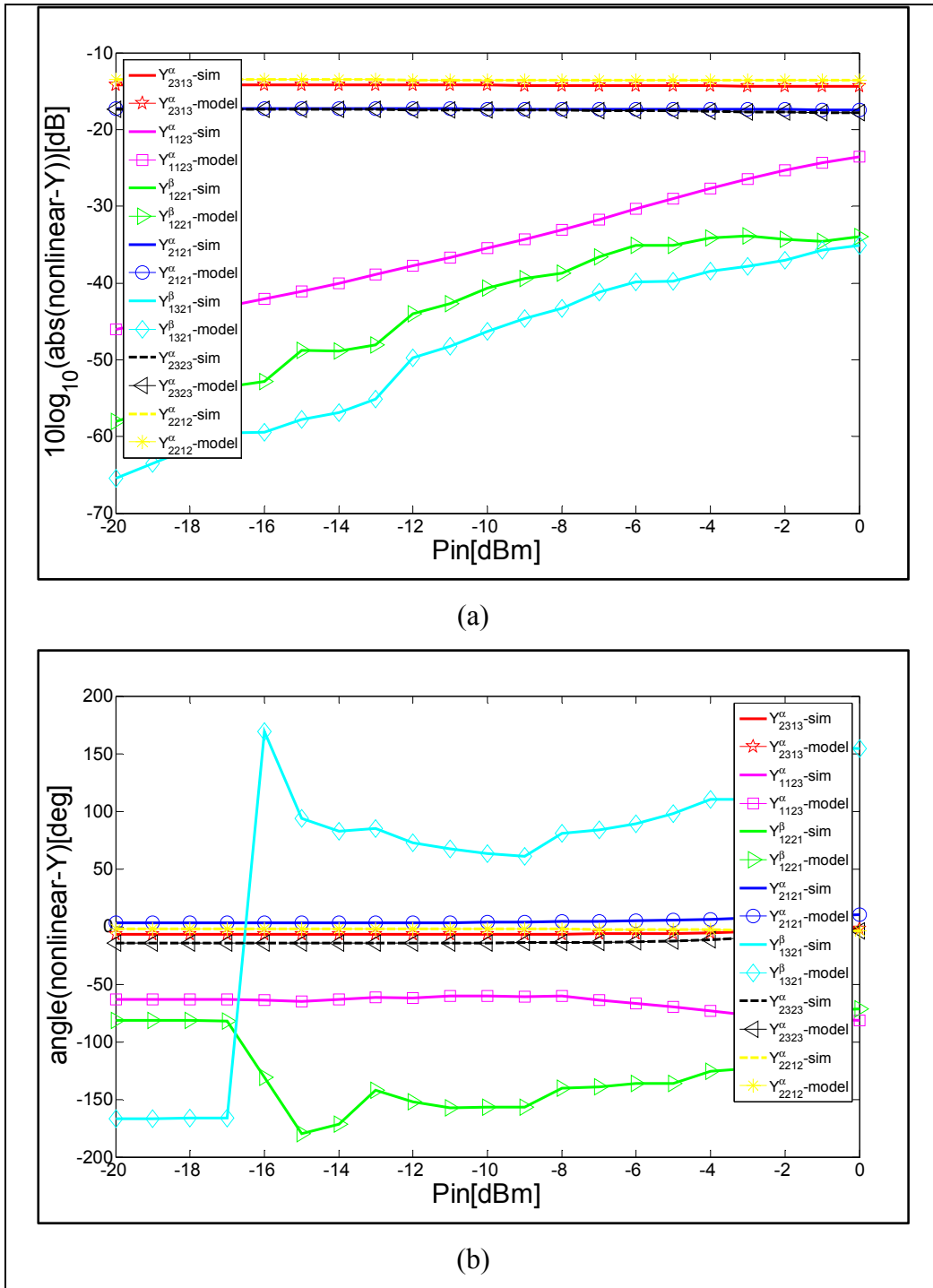


Figure 3.15 Comparison between the logarithmic amplitude (a) and the phase (b) of a random set of nonlinear Y-parameters calculated from the X-parameters of a parallel system and those calculated through the parallel nonlinear Y expressions in (3.54).

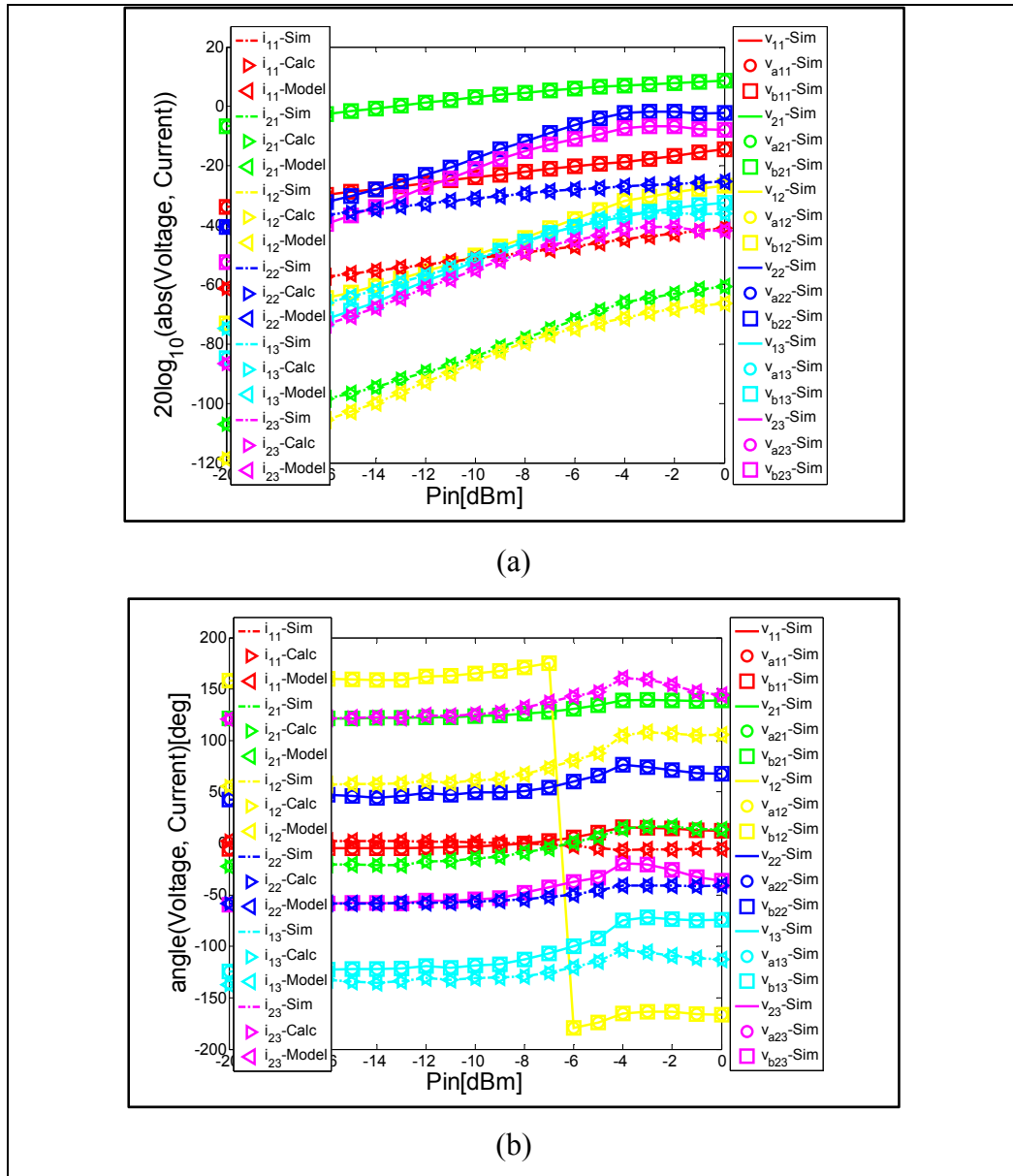


Figure 3.16 Comparison between the logarithmic amplitude (a) and the phase (b) of harmonic voltages and currents as mentioned in the graph presenting the validation process in Figure 3.14. v_{pj} -sim and i_{pj} -sim are the j th harmonic component of voltage and current, simulated with HB, at the input ($p=1$) and output ($p=2$) of the parallel system. i_{pj} -Calc is the sum of the j th harmonic component of currents simulated with HB at the port p of circuit A (v_{apj}) and circuit B (v_{bpj}). i_{pj} -Model are calculated through nonlinear Y matrix with (3.53). v_{pj} -sim (v_{apj} -sim, v_{bpj} -sim, resp.) are the j th harmonic component of voltage, simulated with HB, at the port p of the parallel circuit (circuit A, circuit B, resp.).

3.5.4 Series-to-parallel network configuration

The validity of analytical nonlinear H-parameters was evaluated through the computation of the X-parameters of ZFL11AD with a cascaded system of ZFL11AD and ZX602522M in a series-to-parallel configuration. The process of the validation is summarized in Figure 3.17.

X-parameters simulations are used to generate X-parameters data of the series-to-parallel system and of each component simulated alone under the same conditions as when it is in the whole network. The conditions of input power, source and load terminations are determined through the HB simulation. X-parameters of the whole circuit (circuit A, circuit B, resp.) are then converted to nonlinear H-parameters $[H_{nonlinEq}]$ ($[H_{nonlinA}]$, $[H_{nonlinB}]$, resp.). To validate the utility of nonlinear H-parameters to describe a nonlinear series-to-parallel network, the matrix $[H_{nonlinEq}]$ is compared to the sum of nonlinear admittance matrices ($[H_{nonlinA}] + [H_{nonlinB}]$) calculated from the X-parameters of each component in Figure 3.18. These figure is limited to 7 arbitrary terms: H_{1211}^β , H_{2112}^β , H_{2223}^α , H_{2312}^β , H_{2322}^β , H_{2112}^α and H_{1123}^α . They illustrate a good agreement between the nonlinear H-parameters calculated from the X-parameters of the whole system and the results of the analytic expression of the calculated nonlinear H matrices.

In the analytical development, the assumption that the current vector $[I_2] = [I_{2a}] = [I_{2b}]$ and the voltage vector $[V_1] = [V_{1a}] = [V_{1b}]$ is verified in Figure 3.19. Moreover, in that figure, the harmonic components of the current at the output and of the voltage at the input of the series-to-parallel circuit calculated through nonlinear H matrix in (3.80) are compared to those obtained with HB simulation. The agreement between the curves proves more the concept of analytical nonlinear H-parameters.

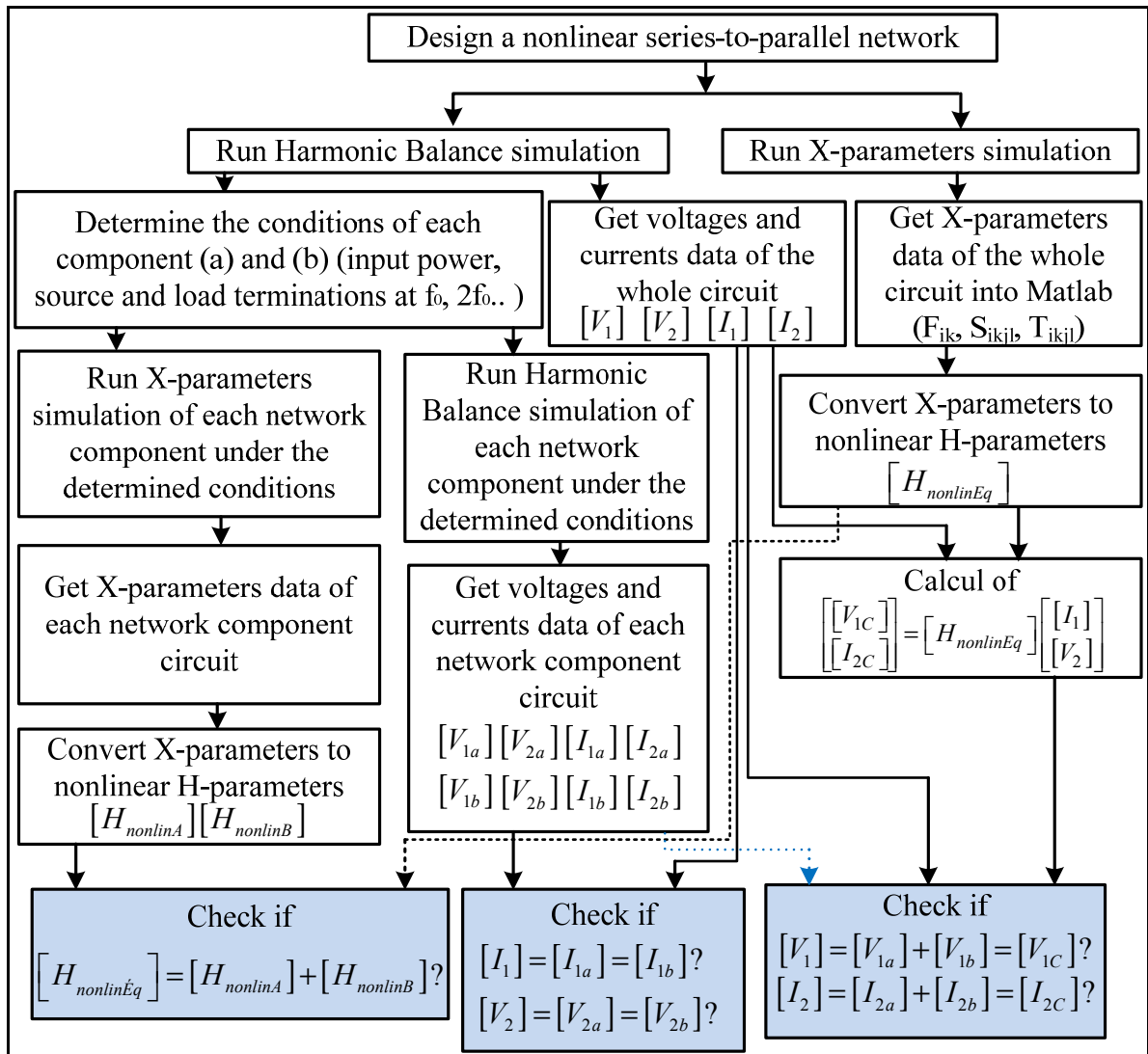


Figure 3.17 Validation process of nonlinear series-to-parallel network configuration.

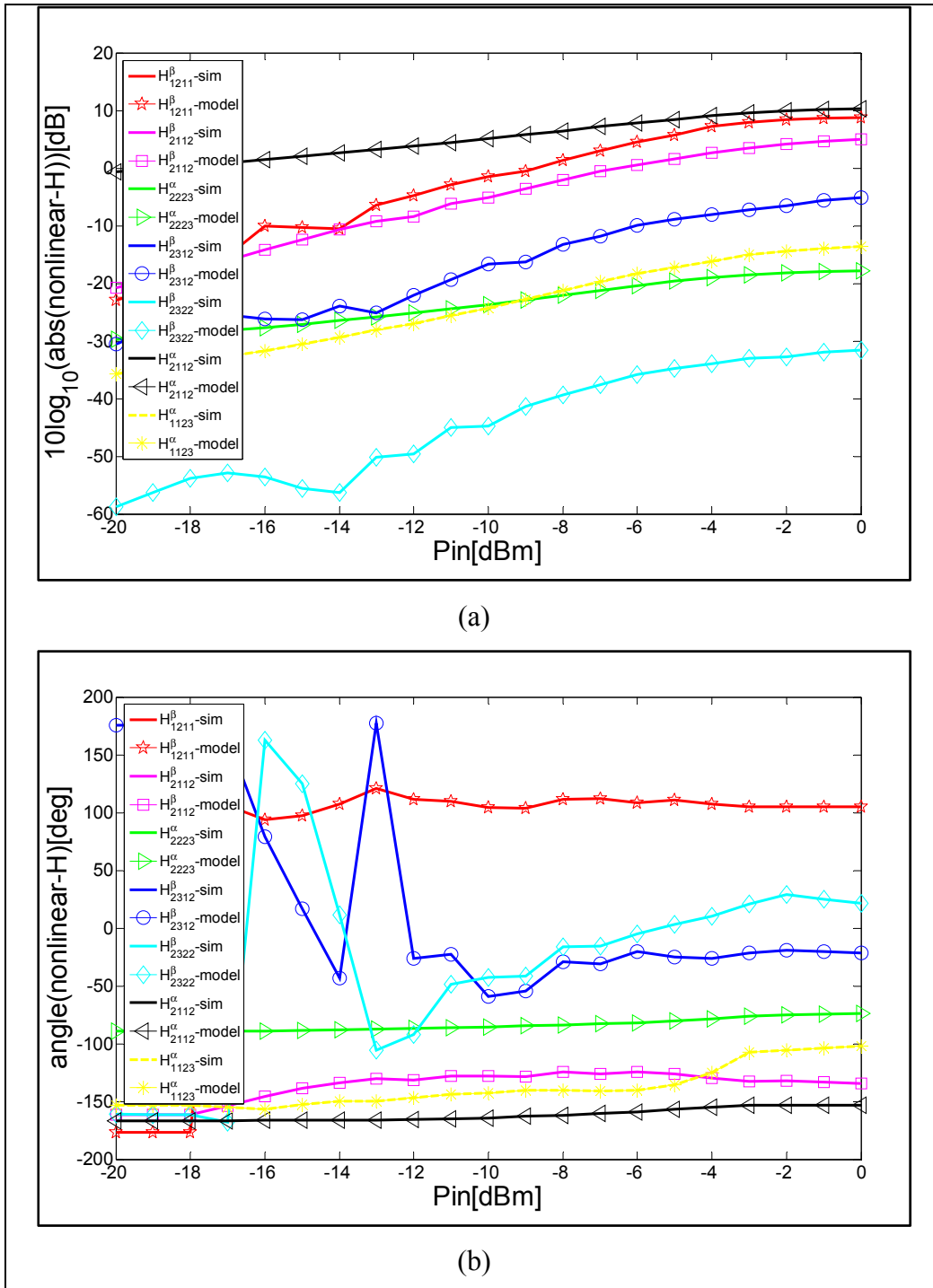


Figure 3.18 Comparison between the logarithmic amplitude (a) and the phase (b) of a random set of nonlinear H-parameters calculated from the X-parameters of a series-to-parallel system and those calculated through the series-to-parallel nonlinear H expressions in (3.81).

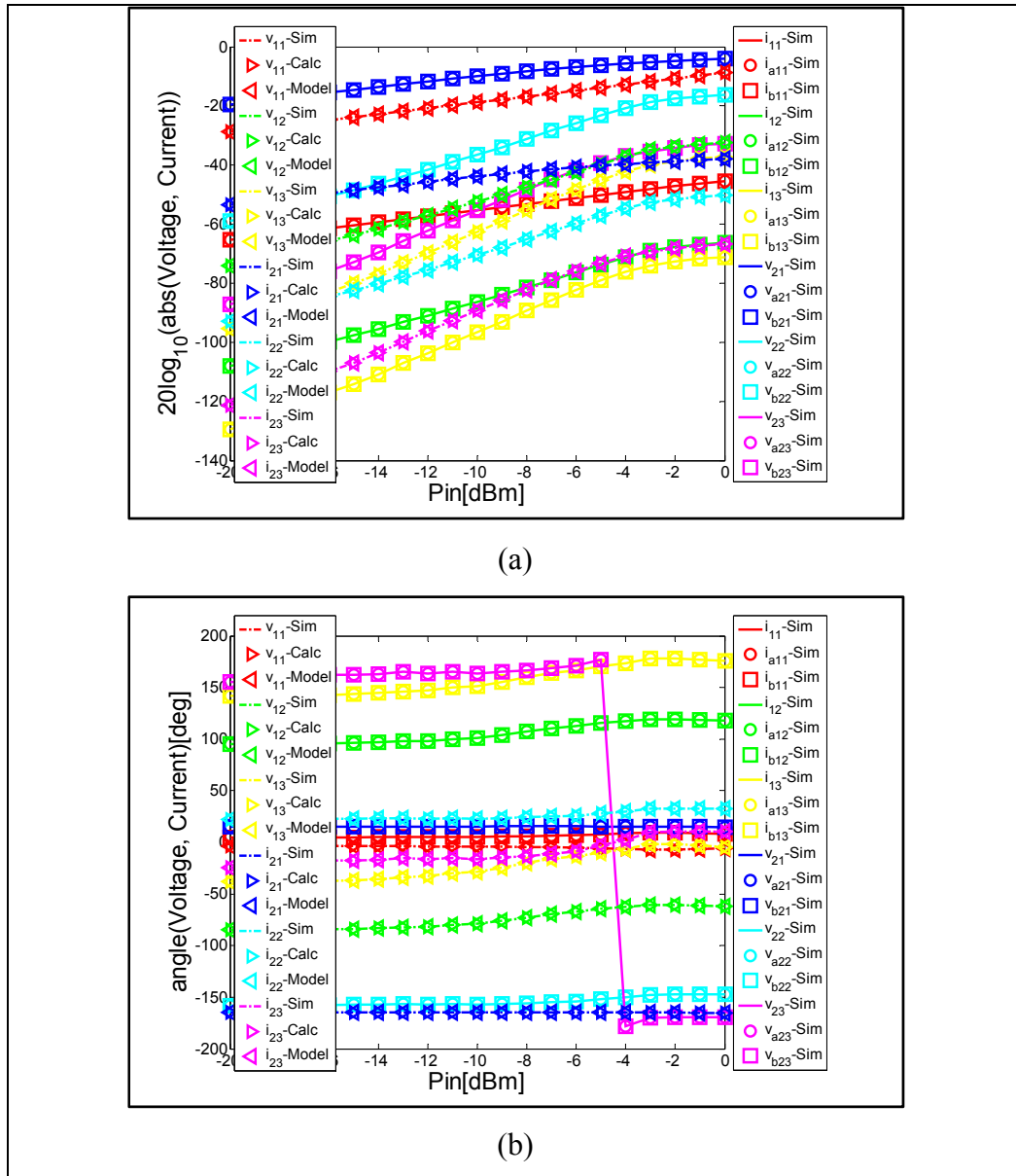


Figure 3.19 Comparison between the logarithmic amplitude (a) and the phase (b) of harmonic voltages and currents as mentioned in the graph presenting the validation process in Figure 3.17 . v_{pj} -sim and i_{pj} -sim are the j th harmonic component of voltage and current, simulated with HB, at the input ($p=1$) and output ($p=2$) of the series-to-parallel system. v_{1j} -Calc (i_{2j} -Calc) are the sum of the j th harmonic component of voltages (currents) simulated with HB at the port 1 (port 2) of circuit A and circuit B. v_{1j} -Model and i_{2j} -Model are calculated through nonlinear H matrix with (3.80). v_{pj} -sim (v_{apj} -sim, v_{bpj} -sim, resp.) and i_{pj} -sim (i_{apj} -sim, i_{bpj} -sim, resp.) are the j th harmonic component of voltage and current, simulated with HB, at the port p of the series-to-parallel circuit (circuit A, circuit B, resp.).

3.5.5 Parallel-to-series network configuration

The validity of analytical nonlinear G-parameters was evaluated by computing the X-parameters of ZFL11AD with a cascaded system of ZFL11AD and ZX602522M in a parallel-to-series configuration.

The process of the validation is summarized in Figure 3.20. X-parameters simulations are used to generate X-parameters data of the parallel-to-series system and of each component simulated alone under the same conditions as when it is in the whole network. The conditions of input power, source and load terminations are determined through the HB simulation. X-parameters of the whole circuit (circuit A, circuit B, resp.) are then converted to nonlinear G-parameters $[G_{nonlinEq}]$ ($[G_{nonlinA}]$, $[G_{nonlinB}]$, resp.).

To validate the utility of nonlinear G-parameters to describe a nonlinear parallel-to-series network, the matrix $[G_{nonlinEq}]$ is compared to the sum of nonlinear admittance matrices ($[G_{nonlinA}] + [G_{nonlinB}]$) calculated from the X-parameters of each component in Figure 3.21. These figures are limited to 7 arbitrary terms: G_{1123}^β , G_{2222}^α , G_{1321}^α , G_{1211}^α , G_{1313}^α , G_{1312}^α , G_{2113}^α and G_{1222}^β . They demonstrate a good agreement between the nonlinear G-parameters calculated from the X-parameters of the whole system and the results of the analytic expressions of nonlinear G matrices calculated with (3.90).

The assumption that the current vector $[I_2] = [I_{2a}] = [I_{2b}]$ and the voltage vector $[V_1] = [V_{1a}] = [V_{1b}]$ is verified in Figure 3.22. Moreover, in these figures, the harmonic components of the current at the input and of the voltage at the output of the parallel-to-series circuit calculated through nonlinear H matrix in (3.91) are compared to those obtained with HB simulation. The agreement between the curves proves more the concept of analytical nonlinear G-parameters.

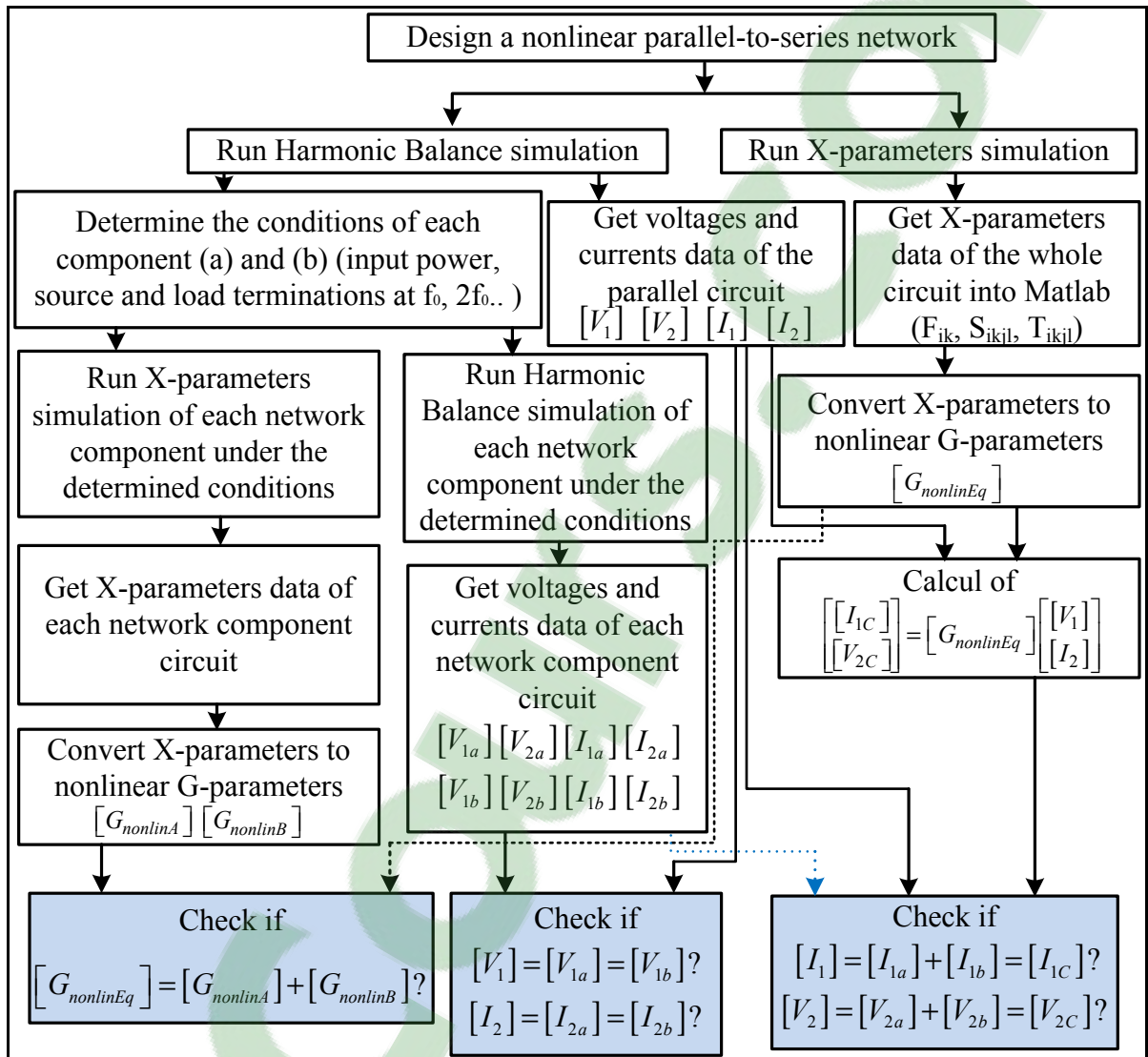


Figure 3.20 Validation process of nonlinear parallel-to-series network configuration.

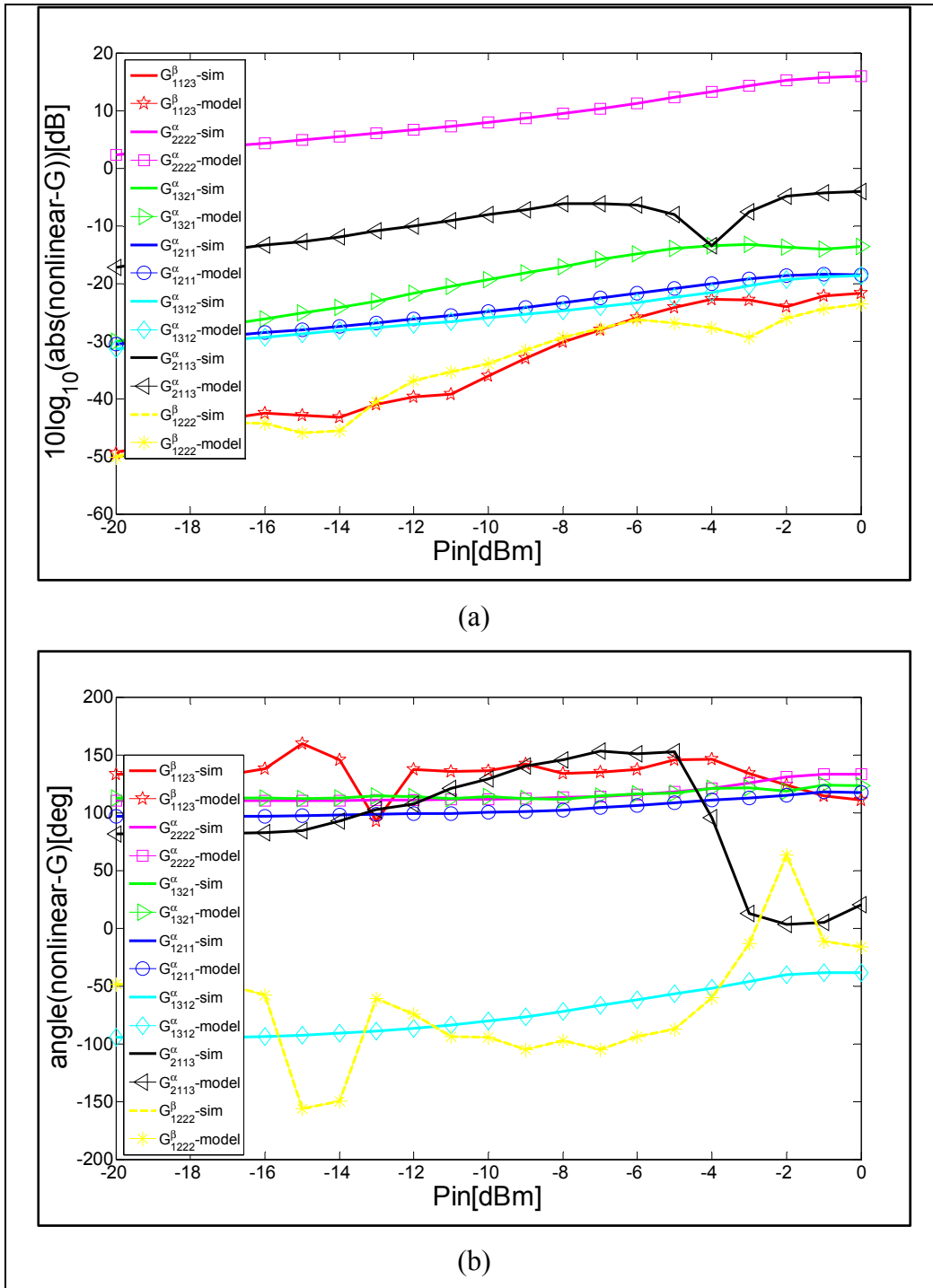


Figure 3.21 Comparison between the logarithmic amplitude (a) and the phase (b) of a random set of nonlinear G-parameters calculated from the X-parameters of a parallel-to-series system and those calculated through the parallel-to-series nonlinear G expressions in (3.90).

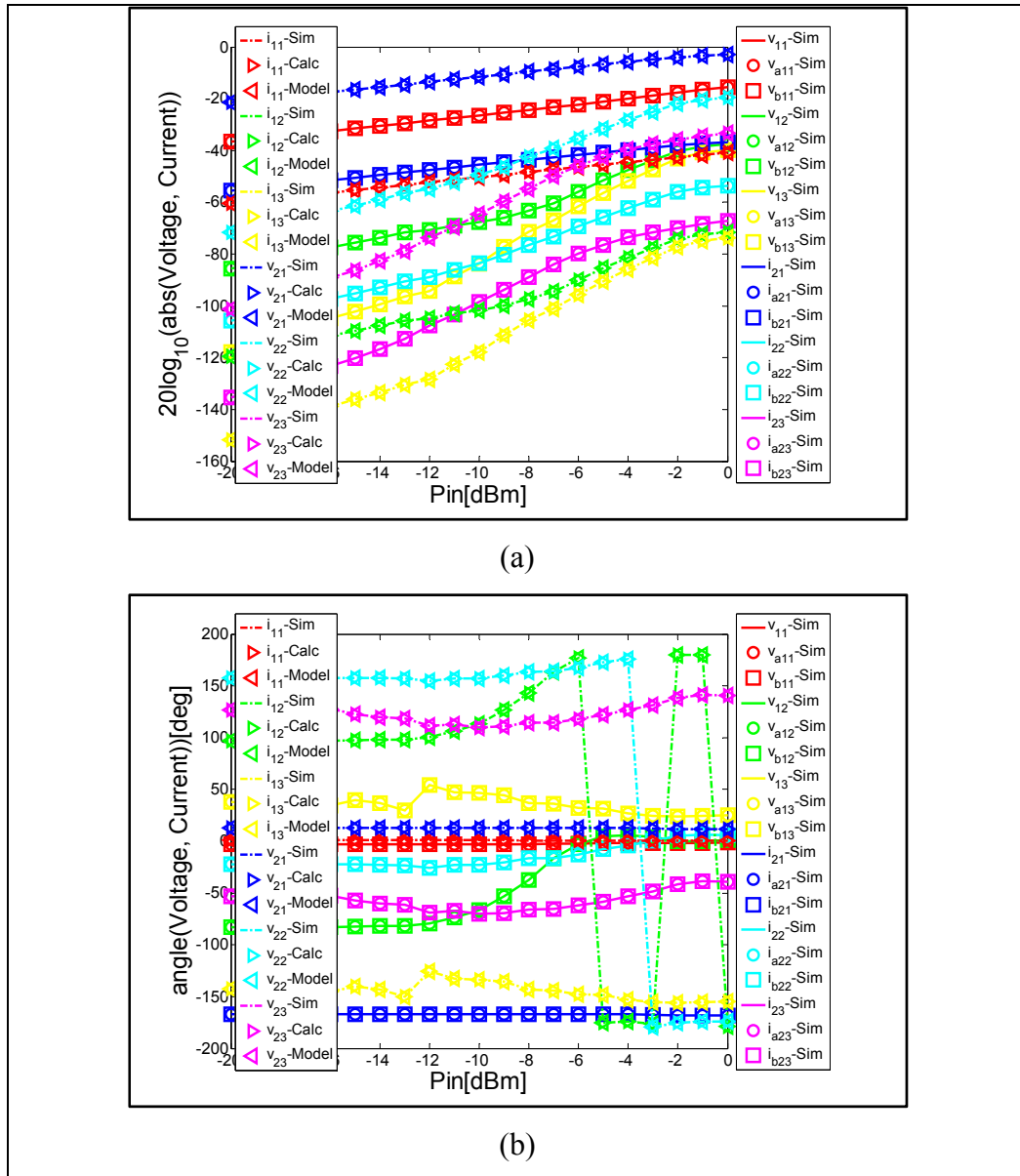


Figure 3.22 Comparison between the logarithmic amplitude (a) and the phase (b) of harmonic voltages and currents as mentioned in the graph presenting the validation process in Figure 3.20. v_{pj} -sim and i_{pj} -sim are the j^{th} harmonic component of voltage and current, simulated with HB, at the input ($p=1$) and output ($p=2$) of the parallel-to-series system. V_{2j} -Calc (i_{1j} -Calc) are the sum of the j^{th} harmonic component of voltages (currents) simulated with HB at the output (input) of whole circuit. V_{2j} -Model and i_{1j} -Model are calculated through nonlinear G matrix with (3.90). v_{pj} -sim (v_{apj} -sim, v_{bpj} -sim, resp.) and i_{pj} -sim (i_{apj} -sim, i_{bpj} -sim, resp.) are the j^{th} harmonic component of voltage and current, simulated with HB, at the port p of the parallel-to-series circuit (circuit A, circuit B, resp.).

3.6 Conclusion

Nonlinear network configurations are important in nonlinear modeling and design. For linear circuits, Z-, Y-, ABCD-, T-, G- and H-parameters that are derived from S-parameters can be successfully used to characterize series, parallel, cascaded, parallel-to-series and series-to-parallel configurations, respectively. Unfortunately, these parameters cannot be used with nonlinear circuits. The new analytical expressions presented in this paper circumvent this limitation. They are more general than those derived from S-parameters.

Based on X-parameters, these parameters can describe topology of all linear, all nonlinear or a mixed of linear and nonlinear components. Nonlinear Z-parameters are used to describe series topology, and the nonlinear Z matrix is simply the sum of the individual nonlinear Z matrices. Nonlinear Y parameters are used to describe parallel topology, and the nonlinear Y matrix is the sum of the individual nonlinear Y matrices. Nonlinear G parameters are used to describe parallel-to-series topology, and the nonlinear G matrix is the sum of the individual nonlinear G matrices. Nonlinear H parameters are used to describe series-to-parallel topology, and the nonlinear H matrix is the sum of the individual nonlinear H matrices. Nonlinear ABCD- or T-parameters are used to describe a cascade topology, and the ABCD or T matrix is the product of the individual nonlinear ABCD or T matrices, respectively.

CHAPTER 4

A NEW GAN HEMT EQUIVALENT CIRCUIT MODELING TECHNIQUE BASED ON X-PARAMETERS

Riadh Essaadali¹, Anwar Jarndal², Ammar Kouki¹ and Fadhel Ghannouchi³

¹Department of Electrical Engineering, École de Technologie Supérieure,
1100 Notre-Dame West, Montreal, Quebec, (H3C 1K3) Canada

²Electrical and Computer Engineering Department of University of Sharjah, Sharjah, UAE

³Intelligent RF Radio Laboratory (iRadio Lab), Department of Electrical and Computer
Engineering, University of Calgary, Calgary, Alberta, (T2N 1N4) Canada

This paper has been submitted for publication in
IEEE Microwave Theory and Techniques Society.

4.1 Abstract

In this paper, a new accurate small- and large-signal equivalent circuit based modeling technique for GaN HEMT transistors grown on silicon substrate is presented. Despite X-parameters are developed as tools for the development of black-box modeling, they are used for equivalent circuit based model extraction. Unlike traditional modeling that uses the small-signal data to build with an indirect manner a nonlinear model, the proposed model is extracted from X-parameters measurements directly. But, similar to the equivalent circuit based models discussed in the literature, the new model is subdivided into extrinsic and intrinsic parts. The extrinsic part consists of linear elements and is related to the physical layout of the transistor. The intrinsic part can be extracted with the proposed analytical de-embedding technique. The nonlinear intrinsic elements are represented by new nonlinear lumped impedances and admittances whose extraction is carried out using a newly proposed technique. This new technique uses nonlinear network parameters, various X-parameter conversion rules and basic analysis techniques of interconnected nonlinear networks. It is accurate and more advantageous than traditional transistor modeling techniques. The modeling procedure was applied to a 10x200 μm GaN HEMT with a gate length of 25 μm . A

very good agreement between model simulation and measurements was obtained, validating the modeling technique approach.

Keywords: X-parameters, equivalent circuit based model, large-signal model, nonlinear lumped element impedance, nonlinear lumped element admittance, parameters extraction, X-parameter de-embedding.

4.2 Introduction

Accurate large-signal models are used to describe the nonlinear behavior of microwave devices and are mandatory for nonlinear circuit design. In conventional approaches, compact models are defined by nonlinear equivalent circuits or by a system of nonlinear ordinary differential equations describing current-voltage and charge-voltage relations for nonlinear lumped elements (Jarndal 2006, Root 2012). Nonlinear models for microwave and millimetre-wave devices are commonly based on DC and S-parameter measurements (Schreurs, Verspecht et al. 1997, Jarndal, Bunz et al. 2006) and their nonlinear elements are described in terms of state functions (Schreurs, Verspecht et al. 2002). The values of the state functions are generally determined via a small-signal detour based on multi-bias S-parameter measurements (Root 2012, Root, Xu et al. 2012). This technique is based on small-signal approximations of the nonlinear state functions at different bias points and requires a large set of S-parameter measurements (Schreurs, Verspecht et al. 1997, Jarndal, Bunz et al. 2006, Root 2012, Root, Xu et al. 2012). Nonlinear RF measurements, such as Pin-Pout, are not part of the model construction and parameter extraction but are used for parameter value optimization and final model validation (Root 2012).

The accuracy limitations of this approach arise from several sources. The main source is that S-parameters are not suitable for the extraction of nonlinear elements. Conventional S-parameters are defined only for linear systems, or systems behaving linearly with respect to a small signal applied around a static operating point from several sources (Verspecht and Root Jun. 2006). Furthermore, DC and S-parameter measurements cannot be made at the same

time. Consequently, devices may not be characterized under the exact same conditions leading to possible errors due to temperature differences and memory effects.

In 2008, Agilent introduced a new Precision Network Analyzer, PNA-X (Technologies), which is a mixer-based Nonlinear Vector Network Analyzer (NVNA) (Horn, Gunyan et al. 2008, Root, Verspecht et al. 2013) capable of measuring the newly developed X-parameters (Root, Verspecht et al. 2013). X-parameters represent new nonlinear scattering parameters, applicable to passive and active circuits under small and large signal excitation (Verspecht 2005, Horn, Gunyan et al. 2008), and are considered as a mathematical superset of small-signal and large signal S-parameters (Horn, Gunyan et al. 2008, Verspecht and Root Jun. 2006). They capture the device behavior at the fundamental and harmonic frequencies in a single measurement for a given bias point. As such, they offer great potential for device modeling that will: (i) do away with DC measurements and (ii) incorporate nonlinear measurement in the model construction and parameter extraction process. Some work has already begun to explore the application of X-parameters to device modeling (Simpson, Horn et al. 2008, Chia-Sung, Kun-Ming et al. 2009, Horn, Root et al. 2010, Root, Xu et al. 2010, Root 2012, Root, Marcu et al. 2012, Root, Xu et al. 2012, Root, Verspecht et al. 2013). In (Root 2012, Root, Xu et al. 2012, Root, Verspecht et al. 2013), the advantages of using NVNA/LSNA measurement systems and X-parameters for transistor characterization and modeling are highlighted. It was shown that parameter extraction, model tuning and validation using NVNA waveform data combined with Artificial Neural Network (ANN) modeling technique is more advantageous than conventional technique. It was also mentioned that X-parameters are becoming useful and increasingly important in the future. X-parameters are explored for transistor modeling applications (Simpson, Horn et al. 2008, Chia-Sung, Kun-Ming et al. 2009, Horn, Root et al. 2010, Root, Xu et al. 2010). However, they are still used as a model only at the external terminals of the device which means that the internal structure of the equivalent circuit topology is not defined.

Equivalent circuit based or compact model is preferred since it is able to indicate which of the material and structural properties of a given transistor affect its electrical performance: ‘it is worth pointing out that it is common to try and place physical meanings and origins on the

circuit elements in the model' (Peter H.Aaen 2007). Equivalent circuit models can be measurement or physically based. The measurement-based equivalent circuit parameter values can be carried out over a range of bias voltages, loads and input power, and the values can be stored in a table. Interpolation can be used to calculate a non-stored case. Mathematical function fittings can also be applied to obtain a nonlinear function that describes the behavior of the extracted element.

In this paper, a new small- and large-signal equivalent circuit modeling technique using X-parameter measurements is proposed. The overall equivalent circuit topology is derived from the commonly used physics-based models and incorporates extrinsic (linear) and intrinsic (nonlinear) elements. The intrinsic elements are represented by new nonlinear lumped impedances and admittances whose extraction is carried out using a newly proposed technique. This new technique uses nonlinear network parameters (Riadh Essaadali, Anwar Jarndal et al. 2011), various X-parameter conversion rules (Riadh Essaadali, Anwar Jarndal et al. 2011) and basic analysis techniques of interconnected nonlinear networks (Riadh Essaadali, Anwar Jarndal et al. 2013).

The remainder of this paper is organized as follows: section II outlines the concept of two-port X-parameters and nonlinear network parameters. The new expressions of nonlinear lumped element impedance and admittance, derived from X-parameters, are also presented in this section. Section III defines the equivalent circuit topology and presents the extrinsic parameter extraction technique. In section IV, a new technique for de-embedding the extracted extrinsic elements from the measured X-parameters is presented. Section V provides the details of the intrinsic parameter extraction from de-embedded X-parameter measurements. The final section presents several validation results.

4.3 X-parameters and nonlinear characteristic parameters

4.3.1 X-parameter formalism

X-parameters are mathematically rigorous supersets of S-parameters and are applicable to linear and nonlinear components under both small-signal and large-signal conditions [7, 10]. For a given device under test (DUT) driven by a large single-tone signal, the function describing the relation between reflected and incident waves is linearized and leads to X-parameter expression as shown in (4.1). In (4.1), the terms b_{ik} (B-waves) and a_{jl} (A-waves) denote the scattered and incident traveling voltage waves, respectively. Indices i and j range from one to the number of signal ports; indices k and l range from one to the highest harmonic index; and, F_{ik} , $S_{ik,jl}$ and $T_{ik,jl}$ are complex functions of input power, DC biasing, source and load terminations, respectively.

$$b_{ik} = F_{ik}(|a_{11}|, V_{gs}, V_{ds}, \Gamma_s, \Gamma_L)P^k + \sum_{(j,l) \neq (1,1)} S_{ik,jl}(|a_{11}|, V_{gs}, V_{ds}, \Gamma_s, \Gamma_L)P^{k-l} a_{jl} + \sum_{(j,l) \neq (1,1)} T_{ik,jl}(|a_{11}|, V_{gs}, V_{ds}, \Gamma_s, \Gamma_L)P^{k+l} a_{jl}^* \quad (4.1)$$

4.3.2 Nonlinear characteristic impedance

Thanks to the conversion rules of X-parameters to other nonlinear parameters, such as nonlinear network impedance, admittance and ABCD parameters (Riadh Essaadali, Anwar Jarndal et al. 2011), and the analysis of cascade, series and parallel configurations of purely nonlinear networks as well as hybrid configurations of linear and nonlinear components (Riadh Essaadali, Anwar Jarndal et al. 2013), it is possible to use X-parameter measurements or data to analyze different nonlinear circuit topologies. These tools (Riadh Essaadali, Anwar Jarndal et al. 2011, Riadh Essaadali, Anwar Jarndal et al. 2013) allow for the modeling of a series topologies, Z-parameters, parallel topologies, Y-parameters and cascaded topologies, ABCD- parameters, and any combination thereof.

Just as X-parameters of a two-port relate harmonic components of B-waves and A-waves at both ports, nonlinear impedance parameters relate harmonic current to harmonic voltage

components at both ports. Furthermore, in the same way that X-parameters include $S_{ik,jl}$ and $T_{ik,jl}$ terms that are associated with a_{jl} and a_{jl}^* (see equation (4.1)), it can be shown (Riadh Essaadali, Anwar Jarndal et al. 2011) that nonlinear Z-parameters include Z_{pmqj}^α and Z_{pmqj}^β term associated with i_{qj} and to its conjugate i_{qj}^* as follows:

$$v_{pm} = \sum_{(q,j)} Z_{pmqj}^\alpha (|a_{11}|) i_{qj} + Z_{pmqj}^\beta (|a_{11}|) i_{qj}^* \quad (4.2)$$

where p and q refer to port numbers, m is the harmonic index at port p and j the harmonic index at port q . Equation (4.2) can be put in matrix form, which, for a two-port network, gives:

$$\begin{bmatrix} [V_1] \\ [V_2] \end{bmatrix} = [Z_{nonlin}] \begin{bmatrix} [I_1] \\ [I_2] \end{bmatrix} = \begin{bmatrix} [Z_{nonlin-11}] & [Z_{nonlin-12}] \\ [Z_{nonlin-21}] & [Z_{nonlin-22}] \end{bmatrix} \begin{bmatrix} [I_1] \\ [I_2] \end{bmatrix} \quad (4.3)$$

where the voltage vector at port p is $[V_p] = [v_{p1} \ v_{p1}^* \ \dots \ v_{pn} \ v_{pn}^*]^T$ and the current vector at the same port $[I_p] = [i_{p1} \ i_{p1}^* \ \dots \ i_{pn} \ i_{pn}^*]^T$. The expressions of $[Z_{nonlin-pq}]$ sub-matrices in terms of Z_{pmqj}^α and Z_{pmqj}^β is:

$$[Z_{nonlin-pq}] = \begin{bmatrix} Z_{p1q1}^\alpha & Z_{p1q1}^\beta & \dots & Z_{p1qn}^\alpha & Z_{p1qn}^\beta \\ Z_{p1q1}^{\beta^*} & Z_{p1q1}^{\alpha^*} & \dots & Z_{p1qn}^{\beta^*} & Z_{p1qn}^{\alpha^*} \\ \vdots & \vdots & \ddots & \vdots & \vdots \\ Z_{pnq1}^\alpha & Z_{pnq1}^\beta & \dots & Z_{pnqn}^\alpha & Z_{pnqn}^\beta \\ Z_{pnq1}^{\beta^*} & Z_{pnq1}^{\alpha^*} & \dots & Z_{pnqn}^{\beta^*} & Z_{pnqn}^{\alpha^*} \end{bmatrix} \quad (4.4)$$

The equivalent nonlinear impedance of a series configuration of N purely nonlinear, purely linear or a mix of linear and nonlinear elements is the sum of the impedances of each component (Riadh Essaadali, Anwar Jarndal et al. 2013):

$$[Z_{nonlin}]_{Eq} = \sum_{i=1}^N [Z_{nonlin}]_i \quad (4.5)$$

Similarly, for nonlinear admittances we use two terms, Y_{pmqj}^{α} and Y_{pmqj}^{β} associated to v_{qj} and to its conjugate v_{qj}^* (Riadh Essaadali, Anwar Jarndal et al. 2011) such that:

$$i_{pm} = \sum_{(q,j)} Y_{pmqj}^{\alpha} (|a_{11}|) v_{qj} + Y_{pmqj}^{\beta} (|a_{11}|) v_{qj}^* \quad (4.6)$$

In matrix form for a two-port network, (4.6) can be written as:

$$\begin{bmatrix} [I_1] \\ [I_2] \end{bmatrix} = [Y_{nonlin}] \begin{bmatrix} [V_1] \\ [V_2] \end{bmatrix} = \begin{bmatrix} [Y_{nonlin-11}] & [Y_{nonlin-12}] \\ [Y_{nonlin-21}] & [Y_{nonlin-22}] \end{bmatrix} \begin{bmatrix} [V_1] \\ [V_2] \end{bmatrix} \quad (4.7)$$

The expressions of $[Y_{nonlin-pq}]$ sub-matrices in terms of Y_{pmqj}^{α} and Y_{pmqj}^{β} is:

$$[Y_{nonlin-pq}] = \begin{bmatrix} Y_{p1q1}^{\alpha} & Y_{p1q1}^{\beta} & \dots & Y_{p1qn}^{\alpha} & Y_{p1qn}^{\beta} \\ Y_{p1q1}^{\beta*} & Y_{p1q1}^{\alpha*} & \dots & Y_{p1qn}^{\beta*} & Y_{p1qn}^{\alpha*} \\ \vdots & \vdots & \ddots & \vdots & \vdots \\ Y_{pnq1}^{\alpha} & Y_{pnq1}^{\beta} & \dots & Y_{pnqn}^{\alpha} & Y_{pnqn}^{\beta} \\ Y_{pnq1}^{\beta*} & Y_{pnq1}^{\alpha*} & \dots & Y_{pnqn}^{\beta*} & Y_{pnqn}^{\alpha*} \end{bmatrix} \quad (4.8)$$

The equivalent nonlinear admittance parameters of a parallel configuration of N pure nonlinear, pure linear or a mix of linear and nonlinear elements is the sum of the admittances of each nonlinear component (Riadh Essaadali, Anwar Jarndal et al. 2013):

$$[Y_{nonlin}]_{Eq} = \sum_{i=1}^N [Y_{nonlin}]. \quad (4.9)$$

Nonlinear ABCD-matrix includes 4 parameter categories: A-, B-, C- and D-terms. A-parameters relate input harmonic voltages to output harmonic voltages. B-parameters relate input harmonic voltages to output harmonic currents (Riadh Essaadali, Anwar Jarndal et al. 2011). C-parameters relate input harmonic currents to output harmonic voltages. D-parameters relate input harmonic currents to output harmonic currents. Each ABCD parameters include two-term categories associated respectively to a harmonic component and its conjugate of voltage and current present at second port. The formulation of the nonlinear model based on nonlinear ABCD-parameters is:

$$v_{1m} = \sum_{(q,j)} A_{1m2j}^{\alpha} (|a_{11}|) v_{2j} + A_{1m2j}^{\beta} (|a_{11}|) v_{2j}^* + \sum_{(q,j)} B_{1m2j}^{\alpha} (|a_{11}|) i_{2j} + B_{1m2j}^{\beta} (|a_{11}|) i_{2j}^*. \quad (4.10)$$

$$i_{1m} = \sum_{(q,j)} C_{1m2j}^{\alpha} (|a_{11}|) v_{2j} + C_{1m2j}^{\beta} (|a_{11}|) v_{2j}^* + \sum_{(q,j)} D_{1m2j}^{\alpha} (|a_{11}|) i_{2j} + D_{1m2j}^{\beta} (|a_{11}|) i_{2j}^*. \quad (4.11)$$

In matrix form, (4.10) and (4.11) can be written as (Riadh Essaadali, Anwar Jarndal et al. 2011):

$$\begin{bmatrix} [V_1] \\ [I_1] \end{bmatrix} = [ABCD_{nonlin}] \begin{bmatrix} [V_2] \\ [I_2] \end{bmatrix} = \begin{bmatrix} [A_{nonlin}] & [B_{nonlin}] \\ [C_{nonlin}] & [D_{nonlin}] \end{bmatrix} \begin{bmatrix} [V_2] \\ [I_2] \end{bmatrix}. \quad (4.12)$$

The expressions of $[ABCD_{nonlin}]$ sub-matrices: $[A_{nonlin}]$, $[B_{nonlin}]$, $[C_{nonlin}]$ and $[D_{nonlin}]$ in terms of A_{pmqj}^{α} , B_{pmqj}^{α} , C_{pmqj}^{α} , D_{pmqj}^{α} , A_{pmqj}^{β} , B_{pmqj}^{β} , C_{pmqj}^{β} and D_{pmqj}^{β} are in (4.13). For simplification purpose, the letter R symbolizes A, B, C and D symbols.

$$[R_{nonlin}] = \begin{bmatrix} R_{1121}^{\alpha} & R_{1121}^{\beta} & \dots & R_{112n}^{\alpha} & R_{112n}^{\beta} \\ R_{1121}^{\beta^*} & R_{1121}^{\alpha^*} & \dots & R_{112n}^{\beta^*} & R_{112n}^{\alpha^*} \\ \vdots & \vdots & \ddots & \vdots & \vdots \\ R_{1n21}^{\alpha} & R_{1n21}^{\beta} & \dots & R_{1n2n}^{\alpha} & R_{1n2n}^{\beta} \\ R_{1n21}^{\beta^*} & R_{1n21}^{\alpha^*} & \dots & R_{1n2n}^{\beta^*} & R_{1n2n}^{\alpha^*} \end{bmatrix}. \quad (4.13)$$

The equivalent nonlinear ABCD parameters of a cascade configuration of N pure nonlinear, pure linear or a mix of linear and nonlinear elements is the product of the ABCD parameters of each nonlinear component (Riadh Essaadali, Anwar Jarndal et al. 2013):

$$[ABCD_{nonlin}]_{Eq} = \prod_{i=1}^N [ABCD_{nonlin_i}]. \quad (4.14)$$

4.3.3 Nonlinear lumped element impedance and admittance

Typically, the intrinsic transistor can be modeled by the equivalent circuit in Figure 4.1 (Jarndal, Bunz et al. 2006). The intrinsic part is composed of nonlinear gate current and charge sources that are obtained by path integration of the intrinsic gate capacitances and conductances (Jarndal, Bunz et al. 2006). The intrinsic nonlinear model can be modeled as a pi network of nonlinear lumped element impedances. These parameters can be extracted directly from X-parameters measurement. Traditionally, a nonlinear circuit can be described by a Taylor series expansion of its nonlinear current/voltage, charge/voltage, or flux/current characteristic (Maas 2003). Power-series and Volterra-series can be used to describe or implement the behavior of a nonlinear component in a CAD software. Unfortunately, none of these models are suitable with X-parameters concept: it is difficult to extract their expression from nonlinear network parameters. In this paper, new expressions of nonlinear lumped element impedance and admittance that are accurate and easy to construct from X-parameters are introduced. The expressions of the new nonlinear lumped element impedance and admittance and their implementation in CAD software are validated in section IV-D.

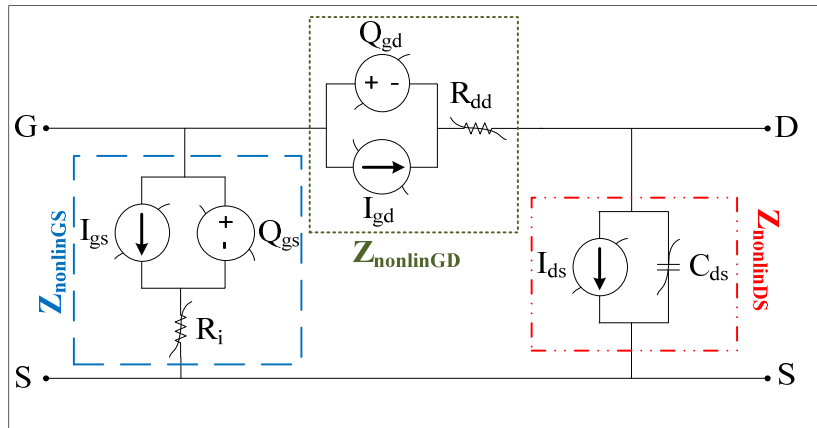


Figure 4.1 GaN HEMT equivalent circuit model

Linear impedance occurs when the current is proportional to the applied voltage (Pozar 1990). In a nonlinear case, the current feeding nonlinear impedance is not proportional to the voltage. The impedance of a nonlinear component can be defined from the availability of X-parameters. The harmonic voltage components of the nonlinear component are expressed in terms of nonlinear impedance and current:

$$[V] = [\bar{\bar{Z}}_{NL}] [I]. \tag{4.15}$$

where the harmonic voltage vector is $[V] = [v_1 \ v_1^* \ \dots \ v_n \ v_n^*]^T$, the harmonic current vector is $[I] = [i_1 \ i_1^* \ \dots \ i_n \ i_n^*]^T$; the terms v_k and i_k represent the voltage and current frequency component, respectively; and, n is the highest harmonic order. To determine the expression of the nonlinear impedance $[\bar{\bar{Z}}_{NL}]$, the expression of the nonlinear ABCD matrix can be used for the two-port network consisting of a series nonlinear impedance between the input and output port illustrated in Figure 4.2 (a). The expression of harmonic voltage and current components at the first port can be expressed as (Riadh Essaadali, Anwar Jarndal et al. 2011):

$$\begin{bmatrix} [V_1] \\ [I_1] \end{bmatrix} = [ABCD_{nonlin}] \begin{bmatrix} [V_2] \\ [I_2] \end{bmatrix} = \begin{bmatrix} [I_d] & [B] \\ [0] & [I_d] \end{bmatrix} \begin{bmatrix} [V_2] \\ [I_2] \end{bmatrix}. \quad (4.16)$$

Where $[B_{nonlin}] = [\bar{\bar{Z}}_{NL}] = \begin{bmatrix} B_{1121}^\alpha & B_{1121}^\beta & \dots & B_{112n}^\alpha & B_{112n}^\beta \\ B_{1121}^{\beta^*} & B_{1121}^{\alpha^*} & \dots & B_{112n}^{\beta^*} & B_{112n}^{\alpha^*} \\ \vdots & \vdots & \ddots & \vdots & \vdots \\ B_{1n21}^\alpha & B_{1n21}^\beta & \dots & B_{1n2n}^\alpha & B_{1n2n}^\beta \\ B_{1n21}^{\beta^*} & B_{1n21}^{\alpha^*} & \dots & B_{1n2n}^{\beta^*} & B_{1n2n}^{\alpha^*} \end{bmatrix}$ and $[I_d]$ is the identity matrix.

Consequently, the expression of each harmonic voltage component v_i can be expressed as a function of nonlinear impedances ($Z_{ij}^\alpha, Z_{ij}^\beta$) and harmonic current components:

$$v_i = \sum_{j=1}^n Z_{ij}^\alpha i_j + \sum_{j=1}^n Z_{ij}^{\beta^*} i_j^*. \quad (4.17)$$

where i is the frequency component index and n is the harmonic order. Equation (4.17) can be rewritten in a matrix form as follows:

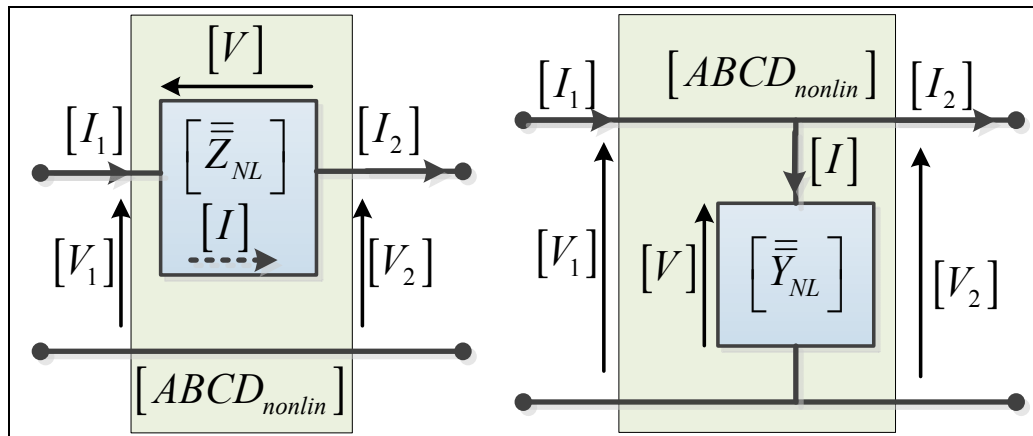


Figure 4.2 A two-port network consisting of a series nonlinear impedance (left) and a parallel nonlinear admittance (right) between the input and output ports

$$\begin{bmatrix} v_1 \\ v_1^* \\ \vdots \\ v_n \\ v_n^* \end{bmatrix} = \begin{bmatrix} Z_{11}^\alpha & Z_{11}^\beta & \dots & Z_{1n}^\alpha & Z_{1n}^\beta \\ Z_{11}^{\beta^*} & Z_{11}^{\alpha^*} & \dots & Z_{1n}^{\beta^*} & Z_{1n}^{\alpha^*} \\ \vdots & \vdots & \ddots & \vdots & \vdots \\ Z_{n1}^\alpha & Z_{n1}^\beta & \dots & Z_{nn}^\alpha & Z_{nn}^\beta \\ Z_{n1}^{\beta^*} & Z_{n1}^{\alpha^*} & \dots & Z_{nn}^{\beta^*} & Z_{nn}^{\alpha^*} \end{bmatrix} \begin{bmatrix} i_1 \\ i_1^* \\ \vdots \\ i_n \\ i_n^* \end{bmatrix}. \quad (4.18)$$

A nonlinear ABCD matrix can be used for the two-port network consisting of a parallel nonlinear admittance between the input and output port as illustrated in Figure 4.2 (b) (Riadh Essaadali, Anwar Jarndal et al. 2011). The expressions of nonlinear sub-matrices $[A_{nonlin}]$, $[B_{nonlin}]$, $[C_{nonlin}]$ and $[D_{nonlin}]$ of nonlinear admittance are $[A_{nonlin}] = [D_{nonlin}] = [I_d]$, $[B_{nonlin}] = [0]$ and

$$[C_{nonlin}] = [\bar{\bar{Y}}_{NL}] = \begin{bmatrix} C_{1121}^\alpha & C_{1121}^\beta & \dots & C_{112n}^\alpha & C_{112n}^\beta \\ C_{1121}^{\beta^*} & C_{1121}^{\alpha^*} & \dots & C_{112n}^{\beta^*} & C_{112n}^{\alpha^*} \\ \vdots & \vdots & \ddots & \vdots & \vdots \\ C_{1n21}^\alpha & C_{1n21}^\beta & \dots & C_{1n2n}^\alpha & C_{1n2n}^\beta \\ C_{1n21}^{\beta^*} & C_{1n21}^{\alpha^*} & \dots & C_{1n2n}^{\beta^*} & C_{1n2n}^{\alpha^*} \end{bmatrix}.$$

The expression of each harmonic current component as a function of nonlinear impedances and harmonic current components is as follows:

$$i_i = \sum_{j=1}^n Y_{ij}^\alpha v_j + \sum_{j=1}^n Y_{ij}^{\beta^*} v_j^*. \quad (4.19)$$

The admittance can easily be deduced from nonlinear impedance:

$$[\bar{\bar{Y}}_{NL}] = [\bar{\bar{Z}}_{NL}]^{-1} = \begin{bmatrix} Y_{11}^\alpha & Y_{11}^\beta & \dots & Y_{1n}^\alpha & Y_{1n}^\beta \\ Y_{11}^{\beta^*} & Y_{11}^{\alpha^*} & \dots & Y_{1n}^{\beta^*} & Y_{1n}^{\alpha^*} \\ \vdots & \vdots & \ddots & \vdots & \vdots \\ Y_{n1}^\alpha & Y_{n1}^\beta & \dots & Y_{nn}^\alpha & Y_{nn}^\beta \\ Y_{n1}^{\beta^*} & Y_{n1}^{\alpha^*} & \dots & Y_{nn}^{\beta^*} & Y_{nn}^{\alpha^*} \end{bmatrix}. \quad (4.20)$$

The electrical nonlinear pi network (Figure 4.3) has three nonlinear impedance branches connected in series to form a closed circuit, with the three junction points forming an output terminal, an input terminal and a common output and input terminal. A nonlinear pi-network model can be extracted directly from nonlinear two-port admittance parameters. The expression of nonlinear harmonic current components as a function of nonlinear harmonic voltage components is:

$$\begin{bmatrix} [I_1] \\ [I_2] \end{bmatrix} = \begin{bmatrix} [\bar{\bar{Y}}_{NL1}] + [\bar{\bar{Y}}_{NL3}] & -[\bar{\bar{Y}}_{NL3}] \\ -[\bar{\bar{Y}}_{NL3}] & [\bar{\bar{Y}}_{NL2}] + [\bar{\bar{Y}}_{NL3}] \end{bmatrix} \begin{bmatrix} [V_1] \\ [V_2] \end{bmatrix}. \quad (4.21)$$

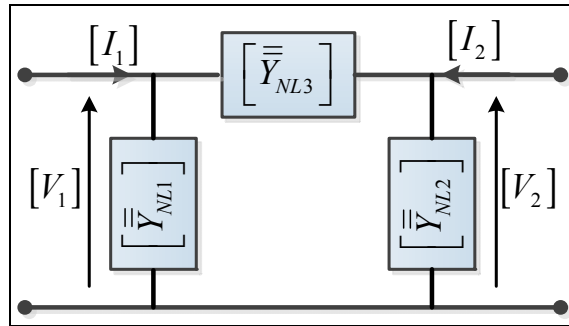


Figure 4.3 A nonlinear pi-network model

4.4 GaN HEMT extrinsic parameters extraction based on X-parameters

Throughout the remainder of this paper, we will consider an on-silicon GaN HEMT device for which the modeling technique is applied.

4.4.1 Model topology definition

The Nitronex GaN HEMT (high-electron mobility transistor) structure to be modeled was grown in a silicon (Si) substrate. A small-signal equivalent circuit for GaN HEMTs on a Si substrate was presented in a paper by (Jarndal 2014). The topology of the developed model is illustrated in

Figure 4.4. In the extrinsic part of this model, C_{gp} and C_{dp} account for parasitic capacitances due to the pad connections, inter-electrode and crossover capacitances (due to air-bridge source connections) between gate, source, and drain (Jarndal 2014). R_g , R_d and R_s represent contact and semiconductor bulk resistances; and, L_g , L_d and L_s model the effect of metallization inductances.

4.4.2 Extrinsic parameter extraction using open structures and cold measurements

In order to model the RF behavior of the DUT accurately, the influence of the parasitic components must be subtracted from the measurements on the test structure. The parasitic elements of the pad contacts can be extracted from open de-embedding structure fabricated on the same wafer of the DUT and cold measurements. Figure 4.5 shows the implemented on-wafer open de-embedding structure and its equivalent circuit model.

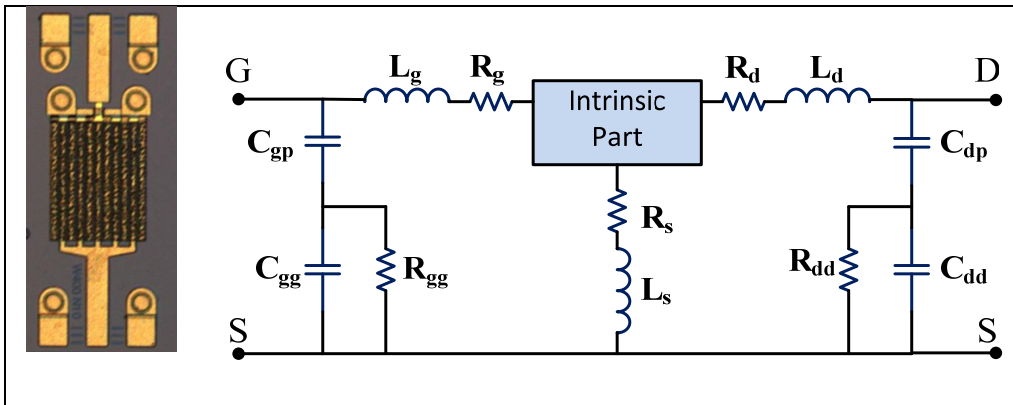


Figure 4.4 A photograph of 200x10µm GaN HEMT on Si Substrate (Left) and its equivalent circuit model (Jarndal, Markos et al. 2011)

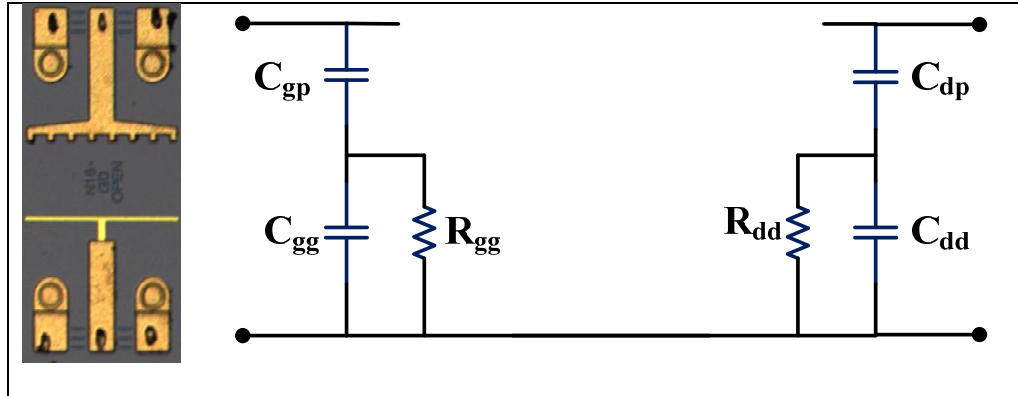


Figure 4.5 On-wafer GaN Open de-embedding structure for a 2mm GaN HEMT (Left) and its equivalent circuit model (Right)

For passive components, X-parameters reduce to S-parameters (Verspecht and Root Jun. 2006), and all nonlinear Z^β terms and all cross frequency Z_{pmqj}^α terms vanish (Riadh Essaadali, Anwar Jarndal et al. 2011). The expressions of the nonlinear Z_{pmqm}^α terms reduce to linear impedance in linear operation mode and are equal to Z_{pq} . The extrinsic elements R_{gg} and R_{dd} can be extracted from the real part of parasitic gate and drain impedances. The Z-parameters of the open structure equivalent circuit can be expressed as follows:

$$Z_{1111}^\alpha = \frac{R_{gg}}{1 + \omega^2 C_{gg}^2 R_{gg}^2} - j \left[\frac{1}{\omega C_{gp}} + \frac{\omega R_{gg}^2 C_{gg}}{1 + \omega^2 C_{gg}^2 R_{gg}^2} \right]. \quad (4.22)$$

$$Z_{2121}^\alpha = \frac{R_{dd}}{1 + \omega^2 C_{dd}^2 R_{dd}^2} - j \left[\frac{1}{\omega C_{dp}} + \frac{\omega R_{dd}^2 C_{dd}}{1 + \omega^2 C_{dd}^2 R_{dd}^2} \right]. \quad (4.23)$$

Extrinsic resistances R_{gg} and R_{dd} can be extracted by extrapolating the curves of the measured real part of Z_{1111}^α and Z_{2121}^α at $\omega = 0$. However, the reliability of extraction depends on the accuracy of extrapolation and measurement uncertainties. Another more accurate method is to extract R_{gg} and R_{dd} from the slope of the curves of

$1/(\omega^2 \text{real}[Z_{1111}^\alpha])$ ($1/(\omega^2 \text{real}[Z_{2121}^\alpha])$) versus $1/\omega^2$. The expressions of these curves are given below:

$$\frac{1}{\omega^2 \text{real}[Z_{1111}^\alpha]} = \frac{1}{R_{gg}} \left(\frac{1}{\omega^2} \right) + R_{gg} C_{gg}^2. \quad (4.24)$$

$$\frac{1}{\omega^2 \text{real}[Z_{2121}^\alpha]} = \frac{1}{R_{dd}} \left(\frac{1}{\omega^2} \right) + R_{dd} C_{dd}^2. \quad (4.25)$$

Parasitic capacities C_{gg} and C_{dd} are derived from the slope of the curves of $1/\text{real}[Z_{1111}^\alpha]$ ($1/\text{real}[Z_{2121}^\alpha]$) versus ω^2 . The expressions of these curves are:

$$\frac{1}{\text{real}[Z_{1111}^\alpha]} = \frac{1}{R_{gg}} + R_{gg} C_{gg}^2 \omega^2. \quad (4.26)$$

$$\frac{1}{\text{real}[Z_{2121}^\alpha]} = \frac{1}{R_{dd}} + R_{dd} C_{dd}^2 \omega^2. \quad (4.27)$$

At higher frequencies, equation $\text{imag}(Z_{1111}^\alpha)\omega$ ($\text{imag}(Z_{2121}^\alpha)\omega$) tends toward $-1/C_{eqg} = -1/C_{gp} - 1/C_{gg}$ ($-1/C_{eqd} = -1/C_{dp} - 1/C_{dd}$).

$$\lim_{\omega \rightarrow \infty} \text{imag}(Z_{1111}^\alpha)\omega = \lim_{\omega \rightarrow \infty} - \left(\frac{1}{C_{gp}} + \frac{C_{gg} R_{gg}^2 \omega^2}{1 + R_{gg}^2 C_{gg}^2 \omega^2} \right) = -\frac{1}{C_{eqg}}. \quad (4.28)$$

$$\lim_{\omega \rightarrow \infty} \text{imag}(Z_{2121}^\alpha)\omega = \lim_{\omega \rightarrow \infty} - \left(\frac{1}{C_{dp}} + \frac{C_{dd} R_{dd}^2 \omega^2}{1 + R_{dd}^2 C_{dd}^2 \omega^2} \right) = -\frac{1}{C_{eqd}}. \quad (4.29)$$

Parasitic capacities $C_{gp}(C_{dp})$ are deduced from $C_{eqp}(C_{eqd})$ as follow:

$$C_{gp} = \frac{C_{eqg} C_{gg}}{C_{gg} - C_{eqg}}. \quad (4.30)$$

$$C_{dp} = \frac{C_{eqd} C_{dd}}{C_{dd} - C_{eqd}}. \quad (4.31)$$

The measured Y-parameters converted from X-parameters of the open structure are then de-embedded from cold Y-parameter measurements at $V_{ds} = 0V$ and $V_{gs} \geq 0V$. Extrinsic inductances L_g , L_d and L_s can then be extracted from the curves of the imaginary part of the stripped Z-parameter measurements by linear regression (Jarndal and Kompa 2005). The extrinsic resistances R_g , R_d and R_s can also be extracted from the curves of the real part of the stripped Z-parameter measurements. The whole extracted values of the extrinsic elements are then optimized to find the best fit for the previously stated cold measurements. The same procedure is used to find the optimal value for each model element (Jarndal and Kompa 2005).

4.5 X-parameter based de-embedding technique

There have been many papers published on the topic of de-embedding techniques for S-parameters (Cho and Burk 1991, Vandamme, Schreurs et al. 2001, Cheolung, Zhaoran et al. 2003) and for large-signal measurements, but very little has been published on X-parameters. A typical or generalized equivalent circuit model of a GaN transistor is shown in Figure 4.6. In order to avoid overloading the demonstrations, admittances G_1 and G_2 are designated to represent the parasitic gate and drain elements, respectively. Impedances Z_1 , Z_2 and Z_3 represent gate, source and drain cascaded configuration of inductance with resistance, respectively. The values of admittances (G_1 and G_2) and impedances (Z_1 , Z_2 and Z_3) are determined by the extrinsic elements' extraction procedure presented in the previous section. X-parameters of the intrinsic part can be easily determined by applying the X-parameters de-embedding procedure explained below. The measurements of X-parameter can

be performed by using a PNA-X network analyzer with an NVNA (nonlinear vector network analyzer) option. X-parameters of the intrinsic part are calculated or deduced by means of transformations between X-parameters, nonlinear Y-parameters and nonlinear Z-parameters (Riadh Essaadali, Anwar Jarndal et al. 2011, Riadh Essaadali, Anwar Jarndal et al. 2013).

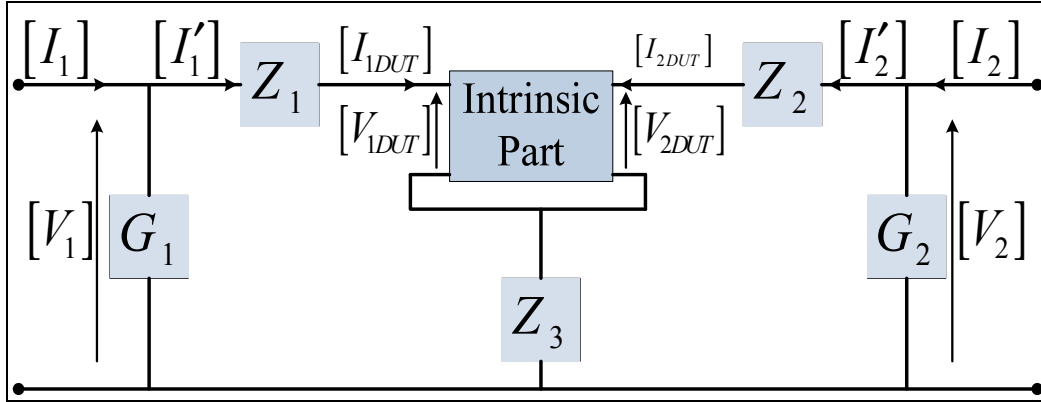


Figure 4.6 GaN HEMT equivalent circuit model

Admittances G_1 and G_2 are in parallel. To subtract their effects, the measured X-parameters $[X]$ of the transistor should be converted to nonlinear parameters $[Y_{nonlin}]$ using the following conversion rule (Riadh Essaadali, Anwar Jarndal et al. 2011):

$$[Y_{nonlin}] = \frac{1}{Z_c} [[Id] + [X]]^{-1} [[Id] - [X]]. \quad (4.32)$$

where $[Id]$ and Z_c are the identity matrix and the characteristic impedance, respectively.

The current vector $[I_i] = [i_{i1} \ i_{i1}^* \ \dots \ i_{in} \ i_{in}^*]^T$ can be expressed as a function of the voltage vector $[V_i] = [v_{i1} \ v_{i1}^* \ \dots \ v_{in} \ v_{in}^*]^T$ through (Riadh Essaadali, Anwar Jarndal et al. 2011):

$$\begin{bmatrix} [I_1] \\ [I_2] \end{bmatrix} = [Y_{nonlin}] \begin{bmatrix} [V_1] \\ [V_2] \end{bmatrix} = \begin{bmatrix} [Y_{nonlin-11}] & [Y_{nonlin-12}] \\ [Y_{nonlin-21}] & [Y_{nonlin-22}] \end{bmatrix} \begin{bmatrix} [V_1] \\ [V_2] \end{bmatrix}. \quad (4.33)$$

The harmonic current components $[I'_1]$ and $[I'_2]$ that flow through impedances $[Z_1]$ and $[Z_2]$ can be calculated as follows:

$$\begin{bmatrix} [I'_1] \\ [I'_2] \end{bmatrix} = \begin{bmatrix} [I_1] \\ [I_2] \end{bmatrix} - \begin{bmatrix} [G_1] & [0] \\ [0] & [G_2] \end{bmatrix} \begin{bmatrix} [V_1] \\ [V_2] \end{bmatrix} = [Y_{nonlin_A}] \begin{bmatrix} [V_1] \\ [V_2] \end{bmatrix}. \quad (4.34)$$

$$\text{where } [G_i]_{i=1,2} = \begin{bmatrix} G_i(\omega) & 0 & \dots & 0 & 0 \\ 0 & G_i^*(\omega) & \dots & 0 & 0 \\ \vdots & \vdots & \ddots & \vdots & \vdots \\ 0 & 0 & \dots & G_i(n\omega) & 0 \\ 0 & 0 & \dots & 0 & G_i^*(n\omega) \end{bmatrix}$$

The resulting nonlinear Y-matrix after de-embedding the admittances G_1 and G_2 is:

$$[Y_{nonlin_A}] = [Y_{nonlin}] - \begin{bmatrix} [G_1] & [0] \\ [0] & [G_2] \end{bmatrix}. \quad (4.35)$$

The harmonic voltage components at the input and the output of the intrinsic part can be expressed as:

$$\begin{bmatrix} [V_{1DUT}] \\ [V_{2DUT}] \end{bmatrix} = \begin{bmatrix} [V_1] \\ [V_2] \end{bmatrix} - \begin{bmatrix} [Z_{11}] & [Z_{12}] \\ [Z_{21}] & [Z_{22}] \end{bmatrix} \begin{bmatrix} [I'_1] \\ [I'_2] \end{bmatrix}. \quad (4.36)$$

where the sub-matrices $[Z_{11}]$, $[Z_{12}]$, $[Z_{21}]$ and $[Z_{22}]$ are:

$$\begin{aligned}
[Z_{11}] &= \begin{bmatrix} Z_1(\omega) + Z_3(\omega) & 0 & \dots & 0 & 0 \\ 0 & Z_1^*(\omega) + Z_3^*(\omega) & \dots & 0 & 0 \\ \vdots & \vdots & \ddots & \vdots & \vdots \\ 0 & 0 & \dots & Z_1(n\omega) + Z_3(n\omega) & 0 \\ 0 & 0 & \dots & 0 & Z_1^*(n\omega) + Z_3^*(n\omega) \end{bmatrix}, \\
[Z_{22}] &= \begin{bmatrix} Z_2(\omega) + Z_3(\omega) & 0 & \dots & 0 & 0 \\ 0 & Z_2^*(\omega) + Z_3^*(\omega) & \dots & 0 & 0 \\ \vdots & \vdots & \ddots & \vdots & \vdots \\ 0 & 0 & \dots & Z_2(n\omega) + Z_3(n\omega) & 0 \\ 0 & 0 & \dots & 0 & Z_2^*(n\omega) + Z_3^*(n\omega) \end{bmatrix}, \\
\text{and } [Z_{12}] = [Z_{21}] &= \begin{bmatrix} Z_3(\omega) & 0 & \dots & 0 & 0 \\ 0 & Z_3^*(\omega) & \dots & 0 & 0 \\ \vdots & \vdots & \ddots & \vdots & \vdots \\ 0 & 0 & \dots & Z_3(n\omega) & 0 \\ 0 & 0 & \dots & 0 & Z_3^*(n\omega) \end{bmatrix}.
\end{aligned}$$

The resulting nonlinear Y-matrix $[Y_{nonlin_A}]$ is transformed into a nonlinear Z-matrix. The effects of series impedances Z_1 , Z_2 and Z_3 are subtracted as follows:

$$[Z_{nonlin_B}] = [Y_{nonlin_A}]^{-1} - \begin{bmatrix} [Z_{11}] & [Z_{12}] \\ [Z_{21}] & [Z_{22}] \end{bmatrix}. \quad (4.37)$$

where $[Z_{nonlin_B}]$ is the nonlinear impedance matrix relating the nonlinear voltage harmonic components at the input and output of the intrinsic part $[V_{1DUT}]$ and $[V_{2DUT}]$, respectively, to nonlinear current harmonic components $[I_{1DUT}]$ and $[I_{2DUT}]$:

$$\begin{bmatrix} [V_{1DUT}] \\ [V_{2DUT}] \end{bmatrix} = [Z_{nonlin_B}] \begin{bmatrix} [I_{1DUT}] \\ [I_{2DUT}] \end{bmatrix}. \quad (4.38)$$

The X-parameters of the intrinsic part are obtained through the conversion rule from nonlinear Z-parameters to X-parameters. The expression of the X-parameters matrix is (Riadh Essaadali, Anwar Jarndal et al. 2011):

$$[X_{DUT}] = \left[[I_d] + \frac{1}{Z_c} [Z_{nonlin_B}] \right]^{-1} \left[\frac{1}{Z_c} [Z_{nonlin_B}] - [I_d] \right]. \quad (4.39)$$

4.6 Intrinsic Parameters extraction

4.6.1 X-parameters based large-signal intrinsic model topology definition and extraction

Once the extraction of the extrinsic elements is complete, the de-embedding of the parasitic parameters enables the X-parameters of the intrinsic part to be determined. Typically, the intrinsic transistor can be modeled by the equivalent circuit in Figure 4.1. The intrinsic part is composed of nonlinear gate and drain current and charge sources that are obtained by path integration of the intrinsic gate and drain conductances and capacitances.

The intrinsic nonlinear model can be modeled as a pi network of nonlinear impedances as shown in Figure 4.7. Nonlinear admittances $[\bar{Y}_{GS}]$, $[\bar{Y}_{GD}]$, $[\bar{Y}_{DG}]$ and $[\bar{Y}_{DS}]$ model the gate-source, gate-drain, drain-gate and drain-source nonlinear junctions, respectively.

The nonlinear impedances can be extracted directly from the de-embedded X-parameters. The intrinsic elements are extracted as a function of the extrinsic gate-source V_{GS} and drain-source V_{DS} voltages. The nonlinear admittance matrix of the intrinsic part of an active device is:

$$\begin{bmatrix} [I_1] \\ [I_2] \end{bmatrix} = \begin{bmatrix} [\bar{Y}_{GS}] + [\bar{Y}_{GD}] & -[\bar{Y}_{GD}] \\ -[\bar{Y}_{DG}] & [\bar{Y}_{DS}] + [\bar{Y}_{DG}] \end{bmatrix} \begin{bmatrix} [V_1] \\ [V_2] \end{bmatrix}. \quad (4.40)$$

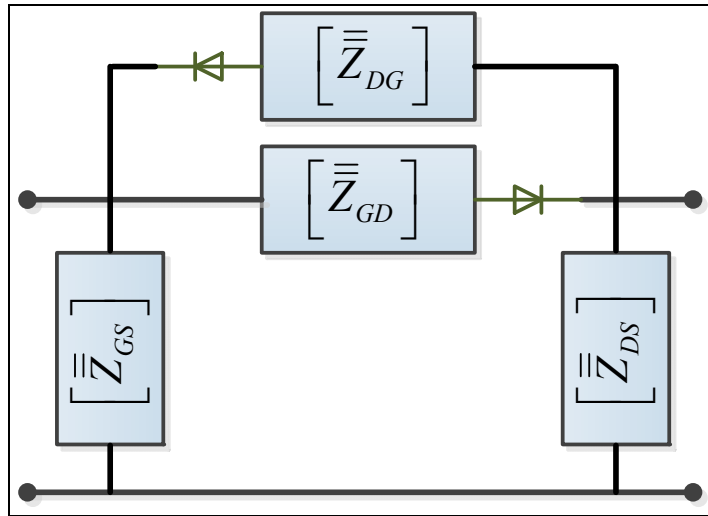


Figure 4.7 Large-signal intrinsic model to be extracted from X-parameters

Nonlinear impedances of intrinsic transistor junctions – gate source $\left[\bar{\bar{Z}}_{GS}\right]$, drain source $\left[\bar{\bar{Z}}_{DS}\right]$, gate drain $\left[\bar{\bar{Z}}_{GD}\right]$ and drain gate $\left[\bar{\bar{Z}}_{DG}\right]$ can be easily determined from (4.40). Their expressions are expressed in (4.41), (4.42), (4.43) and (4.44), respectively.

$$\left[\bar{\bar{Z}}_{GD}(V_{GS}, V_{DS})\right] = -[Y_{12}]^{-1}. \quad (4.41)$$

$$\left[\bar{\bar{Z}}_{DG}(V_{GS}, V_{DS})\right] = -[Y_{21}]^{-1}. \quad (4.42)$$

$$\left[\bar{\bar{Z}}_{GS}(V_{GS}, V_{DS})\right] = [[Y_{11}] + [Y_{12}]]^{-1}. \quad (4.43)$$

$$\left[\bar{\bar{Z}}_{DS}(V_{GS}, V_{DS})\right] = [[Y_{22}] + [Y_{21}]]^{-1}. \quad (4.44)$$

4.6.2 Transistor intrinsic part modeling with frequency-domain defined devices

In ADS, an FDD component enables the current and voltage spectral values to be directly expressed in terms of algebraic relationships of other voltage and current spectral values (Technologies). This component simplifies the development of nonlinear behavioral models that are defined in the frequency domain. An FDD is ideal for modeling the transistor intrinsic part. As illustrated in Figure 4.8, the intrinsic nonlinear part of the transistor is modeled by a cascade of FDD components. The nonlinear impedances shown in Figure 4.8 are intrinsic. However, FDD components can describe input and output voltage components or current components; therefore, the relation between the input or output spectral component voltages and currents is required.

There are two types of configurations in Figure 4.8: series and parallel configurations. The model of a series nonlinear impedance can be described by an FDD component as shown in Figure 4.9(a). The equations of the FDD model that describe the behavior of a nonlinear component in a series configuration are:

$$[I_1] = [\bar{\bar{Z}}_{NL}]^{-1} \{ [V_1] - [V_2] \}. \quad (4.45)$$

$$[I_2] = [\bar{\bar{Z}}_{NL}]^{-1} \{ [V_2] - [V_1] \}. \quad (4.46)$$

The model of parallel nonlinear impedance can be described by the FDD component illustrated in Figure 4.9(b). The equations of the FDD model that describe the behavior of a nonlinear component in a parallel configuration are:

$$[V_1] = [\bar{\bar{Y}}_{NL}]^{-1} \{ [I_1] + [I_2] \}. \quad (4.47)$$

$$[V_2] = [\bar{\bar{Y}}_{NL}]^{-1} \{ [I_1] + [I_2] \}. \tag{4.48}$$

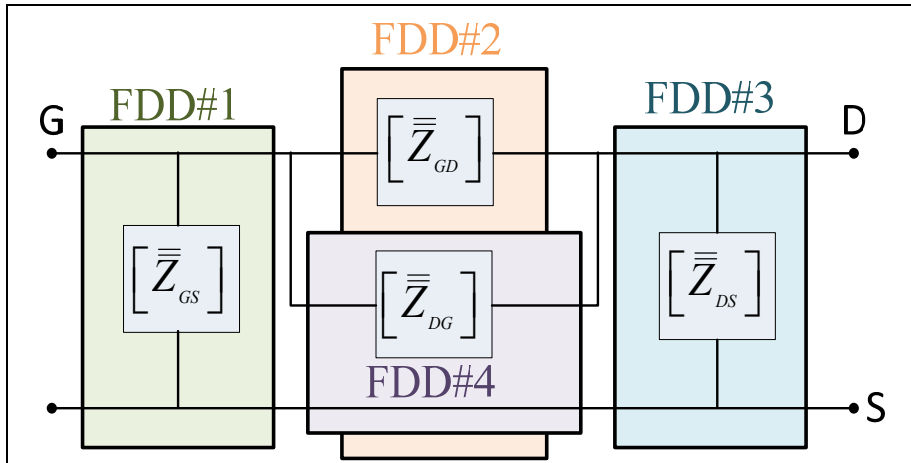


Figure 4.8 Transistor intrinsic part modeling with FDD components

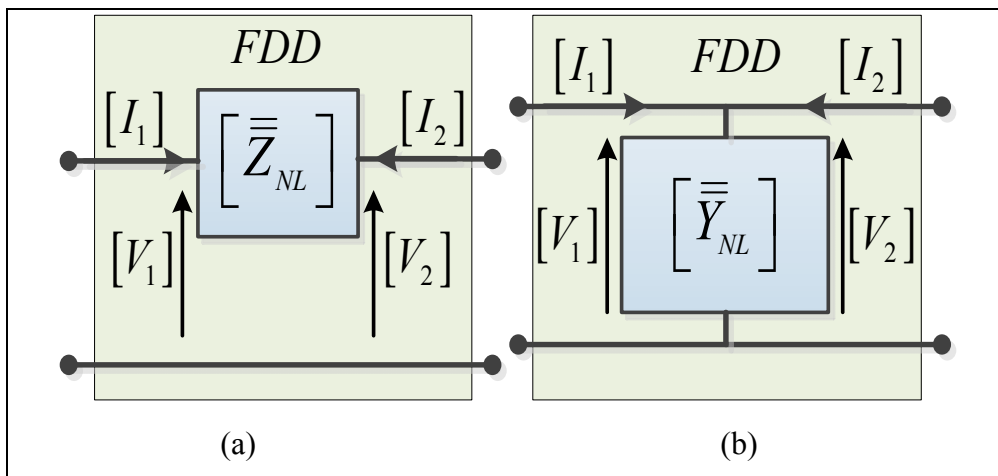


Figure 4.9 Series (a) and parallel (b) nonlinear impedance FDD modeling

4.6.3 Trapping and self-heating effects in model embedding

Trapping effects are related to surface and buffer traps in the active region of the transistor (Jarndal, Bunz et al. 2006). The buffer traps refers to the deep levels located in the interface between the buffer layer and the substrate. Under high electric field condition, due to high

drain-source voltage, electrons moving in the 2DEG (two-dimensional electron gas) channel could get injected into the buffer traps. Due to the longer trapping time constant, the trapped electrons cannot follow the high frequency signal and hence, they are not available for conduction. The trapped electrons produce a negative charge, which depletes the 2DEG, and therefore reduce the channel current. This reduction in the current under RF operation is called current dispersion, or more precisely, buffer traps induced current dispersion. These traps are primarily related to the existing large number of threading dislocation in the GaN layer due to the large lattice mismatch between the GaN and the substrate especially for Si substrate.

In (Jardel, De Groote et al. 2007), it has been shown that modeling the trapping effects improves the large-signal simulation results, particularly when the output loads deviate from the optimum matching conditions. The effects of the traps are taken into account by modifying the command voltage of the current source by adding transients to gate-to-source voltage. These delay times are related to the capture or the emission of charges by traps. The parameters of the lag circuits are extracted from pulsed IV and S-parameters measurements. Dispersion effects can be characterized. In (Raffo, Di Falco et al. Sept. 2010), a nonlinear automated measurement system which is based on low-frequency multi-harmonic signal sources is presented. The system is used for in-depth investigation of low-frequency dispersion. Another concept for the low-frequency dispersion modeling is presented in (van Raay, Quay et al. 2013) by using an integral transform (ITF) approach for the description of the drain current. In (Jarndal and Kompa 2007), an accurate table-based large-signal model for AlGaIn/GaN HEMTs accounting for trapping- and self-heating-induced current dispersion is presented. To include these effects, the RF drain current is modeled as a linear combination of the isothermal dc current and the deviation in the drain current due to the surface-trapping, buffer-trapping and the self-heating effects. The RF drain current is derived from pulsed I-V measurement. The amount of trapping induced current dispersion is controlled by the averaged values of the intrinsic voltages that are extracted by using RC high-pass circuits at gate and drain sides. For the self-heating, the amount of the induced

current dispersion is controlled by a low-pass circuit that determines the value of the normalized channel temperature rise.

In (Raffo, Vadala et al. 2010), a general analytical formulation for the description of low frequency dispersion is presented. The model avoids the simplifying approximations of the description of the complex phenomena related to low frequency dispersion. The RF current depends not only on the instantaneous values of the voltage at the device ports, but also on other variables, such as average values of the voltage.

The trapping and self-heating effects modeling approach presented in this paper is based on X-parameters and consistent with the small-signal Z-parameter model. Z-parameters in the model are function of the input power, dc voltages, fundamental frequency and source and load terminations. The question is how trapping and thermal effects can be embedded in the model.

These two effects result in extremely different values for the drain at low and high RF frequencies. The gate charge could be neglected for frequency less than the intrinsic transient frequency f_T . Thus $\left[\bar{\bar{Z}}_{GS}\right]$ and $\left[\bar{\bar{Z}}_{GD}\right]$ could be kept without any modification.

$$\left[\bar{\bar{Z}}_{GS}\left(|a_{11}|, V_{gs}, V_{ds}, \Gamma_s, \Gamma_L, f_o\right)\right] = \left[\bar{\bar{Z}}_{GS,RF}\left(|a_{11}|, V_{gs}, V_{ds}, \Gamma_s, \Gamma_L, f_o\right)\right]. \quad (4.49)$$

$$\left[\bar{\bar{Z}}_{GD}\left(|a_{11}|, V_{gs}, V_{ds}, \Gamma_s, \Gamma_L, f_o\right)\right] = \left[\bar{\bar{Z}}_{GD,RF}\left(|a_{11}|, V_{gs}, V_{ds}, \Gamma_s, \Gamma_L, f_o\right)\right]. \quad (4.50)$$

Thermal effect influences the electron mobility and saturation velocity of electrons and thus both channel conductance g_{ds} and trans-conductance g_m will be affected under small-signal regime. This will be reflected also on the values of $\left[\bar{\bar{Z}}_{DS}\right]$ and $\left[\bar{\bar{Z}}_{DG}\right]$ under large-signal condition. Thus, these two elements should be a function of channel or junction temperature ΔT in addition to V_{gs} and V_{ds} .

$$\left[\bar{\bar{Z}}_{DS} \left(|a_{11}|, V_{gs}, V_{ds}, \Gamma_s, \Gamma_L, f_o \right) \right] = \left[\bar{\bar{Z}}_{DS,RF} \left(|a_{11}|, V_{gs}, V_{ds}, \Gamma_s, \Gamma_L, f_o \right) \right] + [\alpha_{T1}] \Delta T. \quad (4.51)$$

$$\left[\bar{\bar{Z}}_{DG} \left(|a_{11}|, V_{gs}, V_{ds}, \Gamma_s, \Gamma_L, f_o \right) \right] = \left[\bar{\bar{Z}}_{DG,RF} \left(|a_{11}|, V_{gs}, V_{ds}, \Gamma_s, \Gamma_L, f_o \right) \right] + [\alpha_{T2}] \Delta T. \quad (4.52)$$

Surface and buffer trapping influence the channel electron concentration due to back-gating. The negative charge due to the trapped electrons in the surface and in the buffer modifies the depletion region and thus drains current. However these two effects are observable only under RF and thus the quiescent (V_{gso}, V_{dso}) with fitting matrices $[\alpha_D]$ and $[\alpha_G]$ can be used to simulate this effect as follows:

$$\left[\bar{\bar{Z}}_{DS} \left(|a_{11}|, V_{gs}, V_{ds}, \Gamma_s, \Gamma_L, f_o \right) \right] = \left[\bar{\bar{Z}}_{DS,RF} \left(|a_{11}|, V_{gs}, V_{ds}, \Gamma_s, \Gamma_L, f_o \right) \right] + [\alpha_{T1}] \Delta T + [\alpha_D] V_{dso}. \quad (4.53)$$

$$\left[\bar{\bar{Z}}_{DG} \left(|a_{11}|, V_{gs}, V_{ds}, \Gamma_s, \Gamma_L, f_o \right) \right] = \left[\bar{\bar{Z}}_{DG,RF} \left(|a_{11}|, V_{gs}, V_{ds}, \Gamma_s, \Gamma_L, f_o \right) \right] + [\alpha_{T2}] \Delta T. \quad (4.54)$$

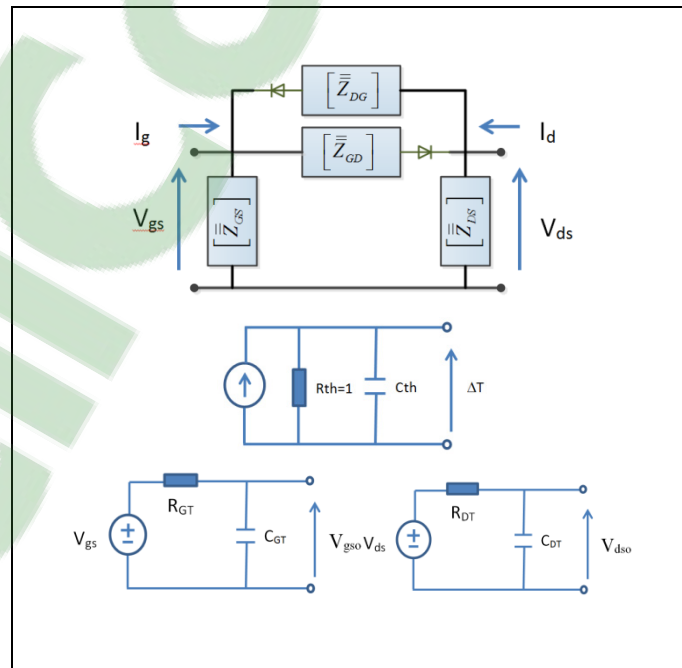


Figure 4.10 Equivalent circuit models for an intrinsic GaN HEMT model coupled with thermal and trapping effects.

The expression of the matrices $[\alpha_{T1}]$, $[\alpha_{T2}]$, $[\alpha_D]$ and $[\alpha_G]$ is in (4.55). For simplification purpose, the letter F represents α_{T1} , α_{T2} , α_D and α_G symbols.

$$[F] = \begin{bmatrix} F_{11}^{\alpha} & F_{11}^{\beta} & \dots & F_{1n}^{\alpha} & F_{1n}^{\beta} \\ F_{11}^{\beta^*} & F_{11}^{\alpha^*} & \dots & F_{1n}^{\beta^*} & F_{1n}^{\alpha^*} \\ \vdots & \vdots & \ddots & \vdots & \vdots \\ F_{n1}^{\alpha} & F_{n1}^{\beta} & \dots & F_{nn}^{\alpha} & F_{nn}^{\beta} \\ F_{n1}^{\beta^*} & F_{n1}^{\alpha^*} & \dots & F_{nn}^{\beta^*} & F_{nn}^{\alpha^*} \end{bmatrix}. \quad (4.55)$$

The equivalent circuit topology of the nonlinear intrinsic model including thermal and trapping effects circuit model is shown in Figure 4.11. The circuit in the top models the intrinsic part of the model based on X-parameters. The circuit in the middle predicts the power dissipation induced temperature. The other two sub-circuits are for simulating the dynamic trapping effects.

At single operating frequency and single input power (with 50 source and load termination, the measured X-parameters and Z-parameters will be a function of just V_{gs} and V_{ds} (the intrinsic voltages including the RF and DC components). Thus $[\bar{\bar{Z}}_{DS}]$ and $[\bar{\bar{Z}}_{DG}]$ can be formulated as:

$$[\bar{\bar{Z}}_{DS}(V_{gs}, V_{ds})] = [\bar{\bar{Z}}_{DS,RF}(V_{gs}, V_{ds})] + [\alpha_{T1}] \Delta T + [\alpha_D] V_{dso}. \quad (4.56)$$

$$[\bar{\bar{Z}}_{DG}(V_{gs}, V_{ds})] = [\bar{\bar{Z}}_{DG,RF}(V_{gs}, V_{ds})] + [\alpha_{T2}] \Delta T + [\alpha_G] V_{gso}. \quad (4.57)$$

The measured Z-parameters (converted from X-parameters) at quiescent voltages (bias voltages) $V_{ds} = 0$ V and $V_{gs} < V_{Pinch-off}$ and RF frequency (> 100 MHz) can be described by

(4.58) and (4.59) . In this condition the static (average) power $V_{ds}I_{ds}$ is negligible and thus $\Delta T=0$.

$$\left[\bar{\bar{Z}}_{DS} (V_{gs}, V_{ds}) \right] = \left[\bar{\bar{Z}}_{DS,RF} (V_{gs}, V_{ds}) \right]. \quad (4.58)$$

$$\left[\bar{\bar{Z}}_{DG} (V_{gs}, V_{ds}) \right] = \left[\bar{\bar{Z}}_{DG,RF} (V_{gs}, V_{ds}) \right] + [\alpha_G] V_{gso}. \quad (4.59)$$

The measured Z-parameters at quiescent voltages (bias voltages) $V_{ds}=0$ V and $V_{gs}=0$ V and RF frequency (> 100 MHz) can be described by (4.60) and (4.61). The dissipated power is also negligible in this case.

$$\left[\bar{\bar{Z}}_{DS} (V_{gs}, V_{ds}) \right] = \left[\bar{\bar{Z}}_{DS,RF} (V_{gs}, V_{ds}) \right]. \quad (4.60)$$

$$\left[\bar{\bar{Z}}_{DG} (V_{gs}, V_{ds}) \right] = \left[\bar{\bar{Z}}_{DG,RF} (V_{gs}, V_{ds}) \right]. \quad (4.61)$$

The measured Z-parameters at quiescent voltages (bias voltages) $V_{ds} = V_{ds,h} > 30$ V and $V_{gs} < V_{Pinch-off}$ and RF frequency (> 100 MHz) can be described by:

$$\left[\bar{\bar{Z}}_{DS} (V_{gs}, V_{ds}) \right] = \left[\bar{\bar{Z}}_{DS,RF} (V_{gs}, V_{ds}) \right] + [\alpha_D] V_{dso}. \quad (4.62)$$

$$\left[\bar{\bar{Z}}_{DG} (V_{gs}, V_{ds}) \right] = \left[\bar{\bar{Z}}_{DG,RF} (V_{gs}, V_{ds}) \right] + [\alpha_G] V_{gso}. \quad (4.63)$$

For static operating condition and at low frequency (< 1 MHz) Z-parameters can be described by:

$$\left[\bar{\bar{Z}}_{DS} (V_{gs}, V_{ds}) \right] = \left[\bar{\bar{Z}}_{DS,RF} (V_{gs}, V_{ds}) \right] + [\alpha_{T1}] \Delta T. \quad (4.64)$$

$$\left[\bar{\bar{Z}}_{DG} (V_{gs}, V_{ds}) \right] = \left[\bar{\bar{Z}}_{DG,RF} (V_{gs}, V_{ds}) \right] + [\alpha_{T2}] \Delta T. \quad (4.65)$$

In this condition, the surface and buffer tapping can be ignored. Using the extracted values of $\left[\bar{\bar{Z}}_{DS,RF} \right]$ and $\left[\bar{\bar{Z}}_{DG,RF} \right]$, the thermal fitting parameters $[\alpha_{T1}]$ and $[\alpha_{T2}]$ can be determined at the considered voltages V_{gs} and V_{ds} . Moreover, by comparing the above equation and applying optimization operation such as the least-square method, the parameters $[\alpha_D]$, $[\alpha_G]$, $\left[\bar{\bar{Z}}_{DS,RF} \right]$ and $\left[\bar{\bar{Z}}_{DG,RF} \right]$ can be determined at each V_{ds} and V_{gs} . However, and unfortunately, the proposed extraction procedure needs pulsed X-parameters measurements which are not available at this moment.

4.7 Measurement results

In this section, the transistor parasitic components extraction results are presented, followed by the validation of the X-parameter de-embedding procedure. With this procedure, X-parameters of the intrinsic part are shown for the first time. As indicated above, X-parameters of the intrinsic part are implemented in ADS by FDD components. In the final section, the results of the nonlinear measurements are presented in order to validate the whole model.

4.7.1 Measurement setup

The measurement setup used to characterize the GaN transistor die and GaN de-embedding structure is illustrated in Figure 4.11. DUTs were mounted on a probe station, and the PNA-X was switched to X-parameter measurements.

The DC power supplies were used to bias the device through bias tees internal to the PNA-X and to supply comb generators. The comb generator, which provides precision phase calibration, ensured superior phase stability and high measurement reliability (Technologies). The setup was controlled by a measurement algorithm to configure the equipment in the setup and to gather data. The transistor used was an on-wafer GaN HEMT on Si substrate.

When performing measurements, systematic errors are often introduced due to the imperfections of the measurement devices (Technologies , Van Moer and Rolain 2006). To minimize these errors, a calibration procedure is required. In addition to standard calibration elements, two additional calibration steps are required: a power and a phase calibration (Technologies , Van Moer and Rolain 2006, Root, Verspecht et al. 2013).

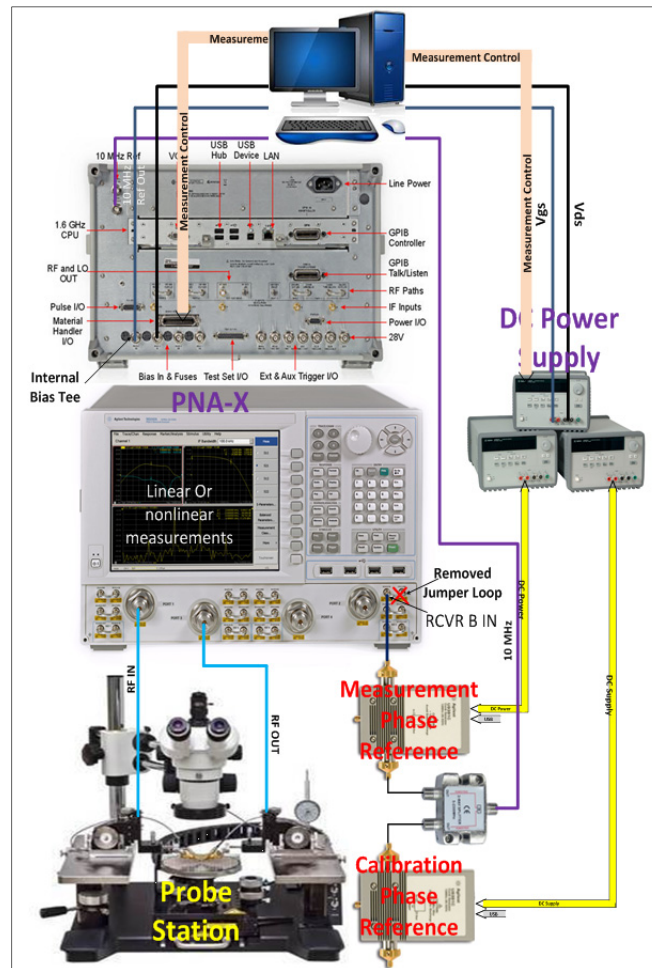


Figure 4.11 X-parameters measurement setup

4.7.2 Extrinsic parameters extraction validation

From the measurements of the open de-embedding structure shown in Figure 4.5, the values of R_{gg} and R_{dd} are extracted from the slope of the curve of $1/(\omega^2 \text{real}[Z_{1111}^\alpha])$ and

$1/(\omega^2 \text{real}[Z_{2121}^\alpha])$ versus $1/\omega^2$. Parasitic capacities C_{gg} and C_{dd} are derived from the slope of the curves of $1/\text{real}[Z_{1111}^\alpha]$ ($1/\text{real}[Z_{2121}^\alpha]$) versus ω^2 . Parasitic capacities C_{gp} (C_{dp}) are deduced from $\text{imag}(Z_{1111}^\alpha)\omega$ ($\text{imag}(Z_{2121}^\alpha)\omega$) at higher frequencies. Using these approaches, the extracted values are indicated in Table 1. The validation of the extracted values of R_{gg} , R_{dd} , C_{gg} , C_{dd} , C_{gp} and C_{dp} consists on comparing the impedances of the open structure model shown in

Figure 4.5 to the measured impedances in Figure 4.12, 4.12 and 4.13. To extract the remaining extrinsic resistances R_g , R_d and R_s and extrinsic inductances L_g , L_d and L_s , the proposed parasitic extraction steps were applied on the measured cold X-parameters of 2 mm GaN on Si HEMT at $V_{gs} = 1.6V$ ($I_{gs} = 87mA$) and $V_{ds} = 0V$ with a frequency range of 0.01 to 40 GHz. Table 4.1 lists the starting and optimized values of the extrinsic elements of the model.

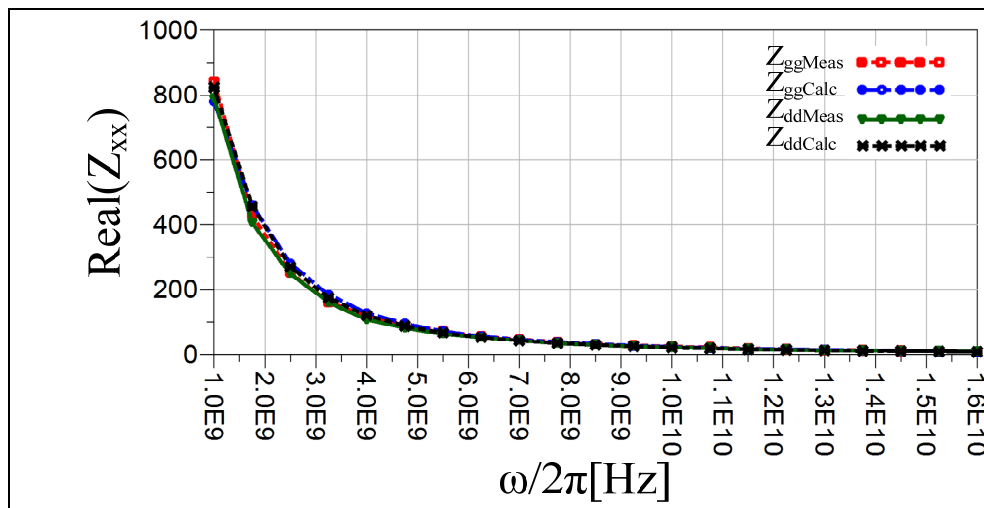


Figure 4.12 Extraction of extrinsic elements R_{gg} and R_{dd} for a 2mm GaN HEMT

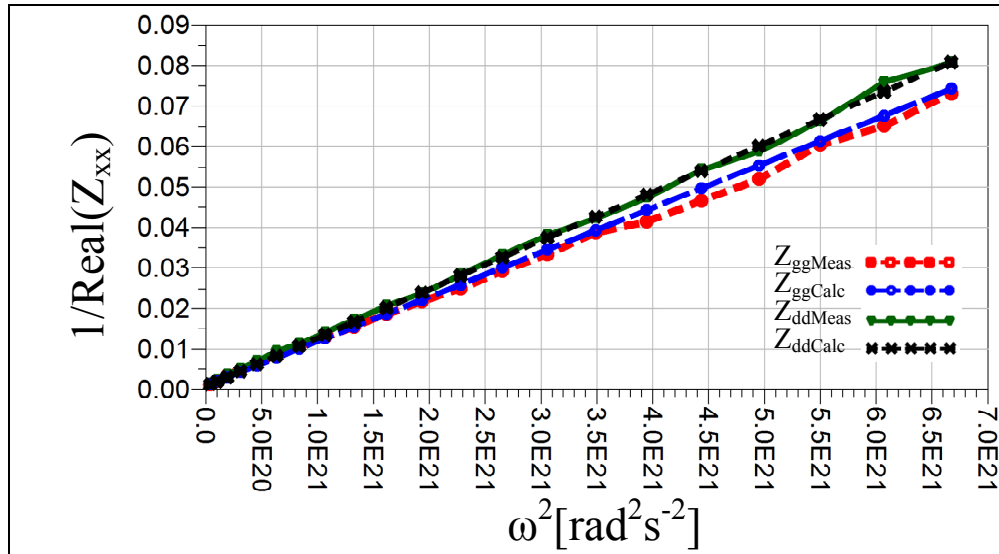


Figure 4.13 Extraction of extrinsic elements C_{gg} and C_{dd} for a 2mm GaN HEMT

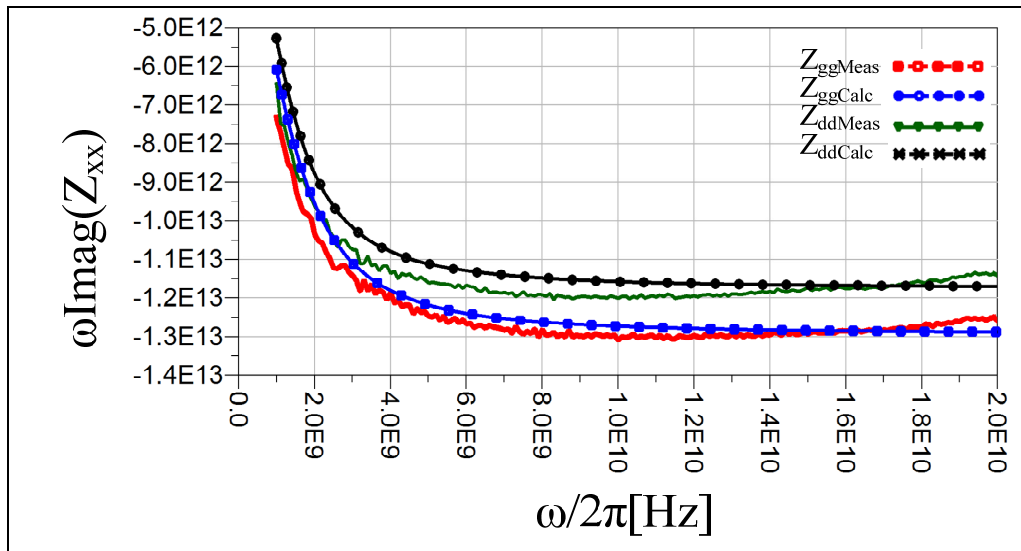


Figure 4.14 Extraction of extrinsic elements C_{pg} and C_{pd} for a 2mm GaN HEMT

Table 4.1 Extracted values of the model extrinsic elements of 2 mm GaN HEMT using X-parameters of open structure and cold device

Model Element	Starting Value	Optimized Value
C_{gp} (pF)	0.92	0.96
C_{dp} (pF)	1.32	1.4
C_{gg} (pF)	0.078	0.08
C_{dd} (pF)	0.08	0.08
R_{gg} (Ω)	1362	1362
R_{dd} (Ω)	3036	3785
L_g (pH)	135	138
L_d (pH)	205	205
L_s (pH)	13	13.3
R_g (Ω)	1.05	1.05
R_d (Ω)	1.01	1.03
R_s (Ω)	0.5	0.5

4.7.3 X-parameter de-embedding technique validation

The de-embedding process was used to remove the effects of parasitic elements. The embedding procedure, which moves the measurement plane from the intrinsic part plane to the device plane, is presented and validated in this section. The conversion from the X-parameters of the intrinsic part to nonlinear Z-parameters using the conversion rule [18] allows the nonlinear harmonic voltage, in terms of the nonlinear harmonic current components, to be expressed as shown in (4.66). This section demonstrates the validation of the large-signal de-embedding technique.

$$\begin{bmatrix} [V_{1DUT}] \\ [V_{2DUT}] \end{bmatrix} = [Z_{nonlin_DUT}] \begin{bmatrix} [I_{1DUT}] \\ [I_{2DUT}] \end{bmatrix}. \quad (4.66)$$

where

$$\left[Z_{nonlin_DUT} \right] = Z_c \left[\left[Id \right] - \left[X_{DUT} \right] \right]^{-1} \left[\left[Id \right] + \left[X_{DUT} \right] \right]. \quad (4.67)$$

Equation (4.66) can be rewritten as:

$$\begin{bmatrix} \left[V_{1DUT} \right] \\ \left[V_{2DUT} \right] \end{bmatrix} = \left[Z_{nonlin_DUT} \right] \begin{bmatrix} \left[I'_1 \right] \\ \left[I'_2 \right] \end{bmatrix}. \quad (4.68)$$

The harmonic voltage components at the input and the output of the die can be expressed as:

$$\begin{bmatrix} \left[V_1 \right] \\ \left[V_2 \right] \end{bmatrix} = \begin{bmatrix} \left[V_{1DUT} \right] \\ \left[V_{2DUT} \right] \end{bmatrix} + \begin{bmatrix} \left[Z_{11} \right] & \left[Z_{12} \right] \\ \left[Z_{21} \right] & \left[Z_{22} \right] \end{bmatrix} \begin{bmatrix} \left[I'_1 \right] \\ \left[I'_2 \right] \end{bmatrix}. \quad (4.69)$$

where $\begin{bmatrix} \left[Z_{11} \right] & \left[Z_{12} \right] \\ \left[Z_{21} \right] & \left[Z_{22} \right] \end{bmatrix}$ is defined in (4.36). Equation (4.69) can be rewritten as:

$$\begin{bmatrix} \left[V_1 \right] \\ \left[V_2 \right] \end{bmatrix} = \begin{bmatrix} \left[Z_{nonlin_DUT} \right] \\ \left[Z_{nonlin_DUT} \right] \end{bmatrix} + \begin{bmatrix} \left[Z_{11} \right] & \left[Z_{12} \right] \\ \left[Z_{21} \right] & \left[Z_{22} \right] \end{bmatrix} \begin{bmatrix} \left[I'_1 \right] \\ \left[I'_2 \right] \end{bmatrix}. \quad (4.70)$$

Note that: $\left[Z_M \right] = \left[Z_{nonlin_DUT} \right] + \begin{bmatrix} \left[Z_{11} \right] & \left[Z_{12} \right] \\ \left[Z_{21} \right] & \left[Z_{22} \right] \end{bmatrix}$. If the voltage vector is expressed as a function of the current vector, the expression of nonlinear impedance of the embedded model becomes:

$$\left[Z_{nonlin_meas} \right] = \left[\left[I_d \right] + \left[Z_M \right] \begin{bmatrix} \left[G_1 \right] & \left[0 \right] \\ \left[0 \right] & \left[G_2 \right] \end{bmatrix} \right]^{-1} \left[Z_M \right]. \quad (4.71)$$

The application of the conversion from nonlinear impedance to X-parameters yields the expression of the embedded X-parameters as follows:

$$[X_{emb}] = \left[[I_d] + \frac{1}{Z_c} \left[[I_d] + [Z_M] \begin{bmatrix} [G_1] & [0] \\ [0] & [G_1] \end{bmatrix} \right]^{-1} [Z_M] \right]^{-1} \left[\frac{1}{Z_c} \left[[I_d] + [Z_M] \begin{bmatrix} [G_1] & [0] \\ [0] & [G_1] \end{bmatrix} \right]^{-1} [Z_M] - [I_d] \right]. \quad (4.72)$$

The validation of the de-embedding procedure depends on the comparison of the measured X-parameters to the X-parameters of the embedded intrinsic part. Measured X-parameters were first de-embedded by using the procedure presented in Section 4.4. The obtained X-parameters of the intrinsic part were then embedded using the embedding procedure presented in the current section. The calculated X-parameters were compared to the measured ones. The X-parameter measurements were determined for a Nitronex GaN HEMT in a Si substrate with a gate width of 200 μm and 10 gate fingers. A photo of the transistor is shown in Figure 4.15.

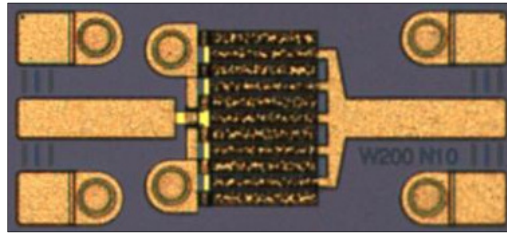


Figure 4.15 A W200N10 GaN HEMT on Si substrate

The X-parameters of the intrinsic part were obtained by de-embedding measured X-parameters. X-parameters of the embedded intrinsic part is calculated from the de-embedded measured X-parameters. The de-embedding and embedding validation results are presented in Figure 4.16 and 4.16. Since a two-port circuit and three harmonic orders have 72 S- and T-terms, the arbitrary terms were limited to seven in order to avoid overloading the figure T_{2323} , T_{1313} , S_{1222} , S_{2122} , S_{2213} , S_{1113} , S_{1212} . Figure 4.16 and 4.17 illustrate an excellent agreement between the measured X-parameters of the die and the embedded X-parameters of the de-embedded intrinsic part.

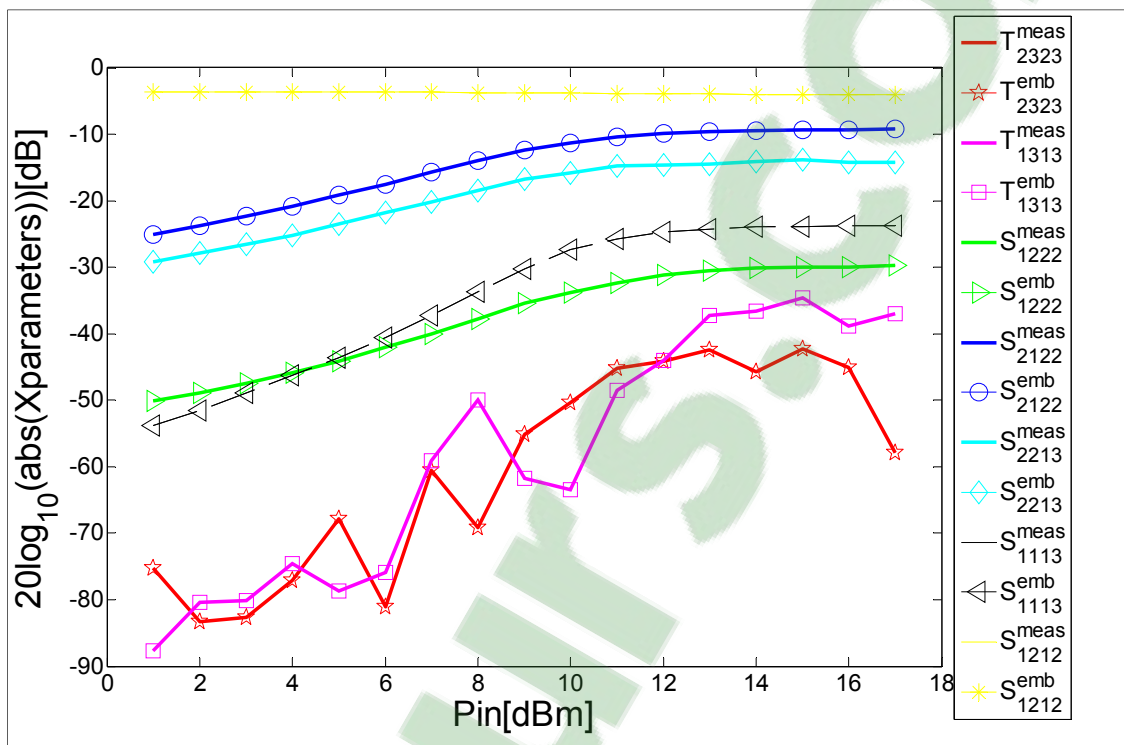


Figure 4.16 Logarithmic amplitude of an arbitrary set of X-parameters. S_{pmqj}^{meas} and T_{pmqj}^{meas} are terms of measured X-parameters, and S_{pmqj}^{emb} and T_{pmqj}^{emb} are terms of embedded intrinsic part X-parameters. The transistor is a 2 mm GaN HEMT on Si substrate biased with $V_{ds}=25V$, $I_d=125mA$, $V_{gs}=-1V$ and $I_g=8mA$ and has an input power between 1 and 17 dBm. The measurement frequency is set to 6 GHz.

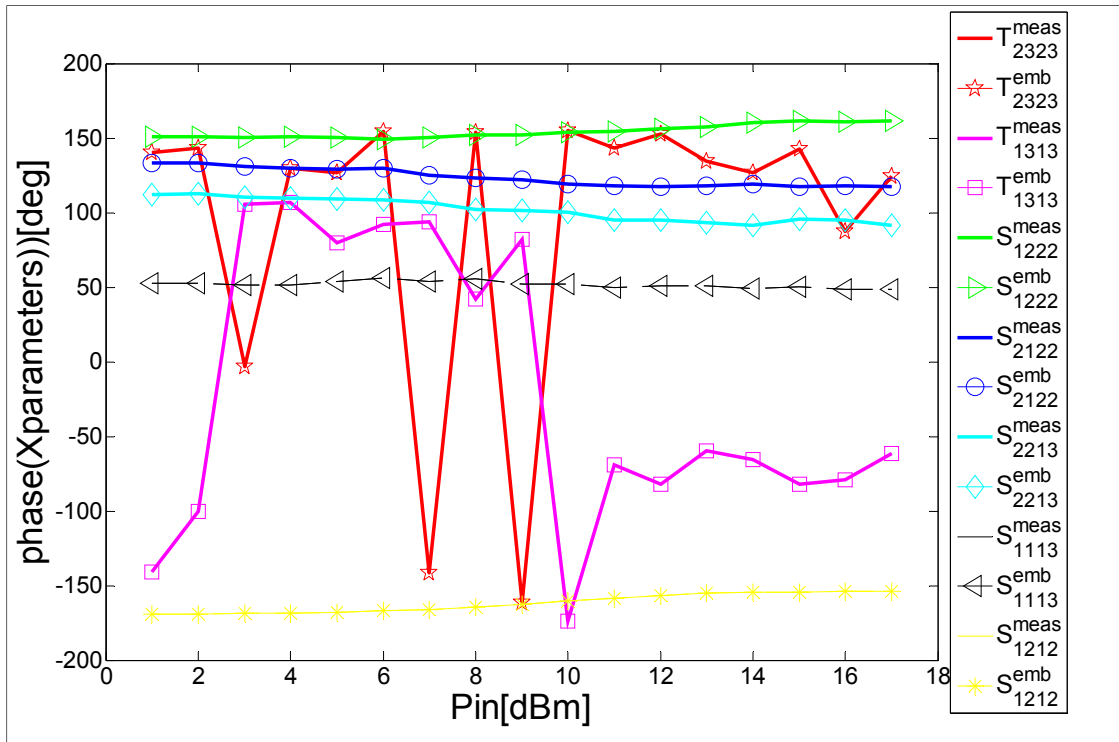


Figure 4.17 Phase of an arbitrary set of X-parameters. S_{pmqj}^{meas} and T_{pmqj}^{meas} are terms of measured X-parameters, and S_{pmqj}^{emb} and T_{pmqj}^{emb} are terms of embedded intrinsic part X-parameters. The transistor is a 2 mm GaN HEMT on Si substrate biased with $V_{ds}=25V$, $I_d=125mA$, $V_{gs}=-1V$ and $I_g=8mA$ and has an input power between 1 and 17 dBm. The measurement frequency is set to 6 GHz.

4.7.4 Nonlinear lumped element impedance and admittance validation

Before validating the GaN HEMT nonlinear intrinsic part extraction technique, validation of nonlinear lumped element impedance and admittance was performed. The implementation of series, parallel and pi networks by FDD components was also validated. The validation of nonlinear lumped element impedance or admittance is demonstrated. In Figure 4.18, the model of parallel nonlinear impedance is described by an FDD component.

The parallel nonlinear capacitor was modeled with an X-parameter simulator in ADS. The conversion of simulated X-parameters to a nonlinear ABCD matrix proves that

$[A_{nonlin}] = [D_{nonlin}] = [I_d]$ and $[B_{nonlin}] = [0]$ and that the nonlinear lumped element admittance matrix was equal to nonlinear $[C_{nonlin}]$ sub-matrix. The nonlinear capacitance model shown in Figure 4.18 can be implemented in ADS by using an FDD component as indicated in Figure 4.9 (b). The implementation was achieved through (4.47) and (4.48). As previously mentioned, the nonlinear lumped element impedance matrix is the inverse of nonlinear lumped element admittance. In Figure 4.19 and 4.20, the extracted nonlinear lumped element impedances of the parallel nonlinear capacitor from the polynomial model are compared to those extracted from the FDD model.

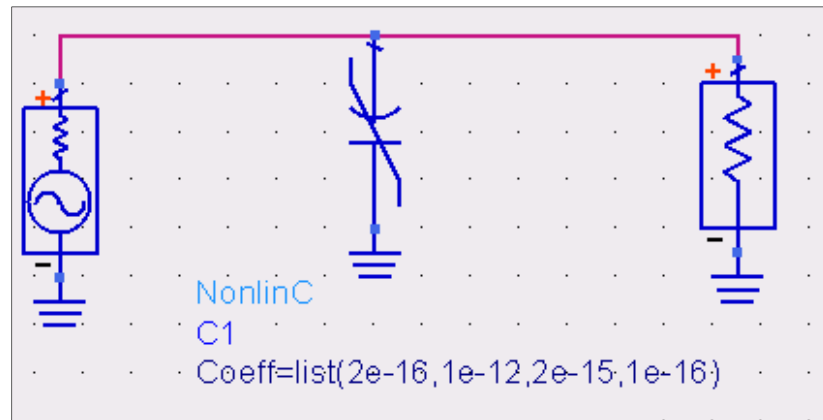


Figure 4.18 Simulation of a parallel nonlinear capacitor

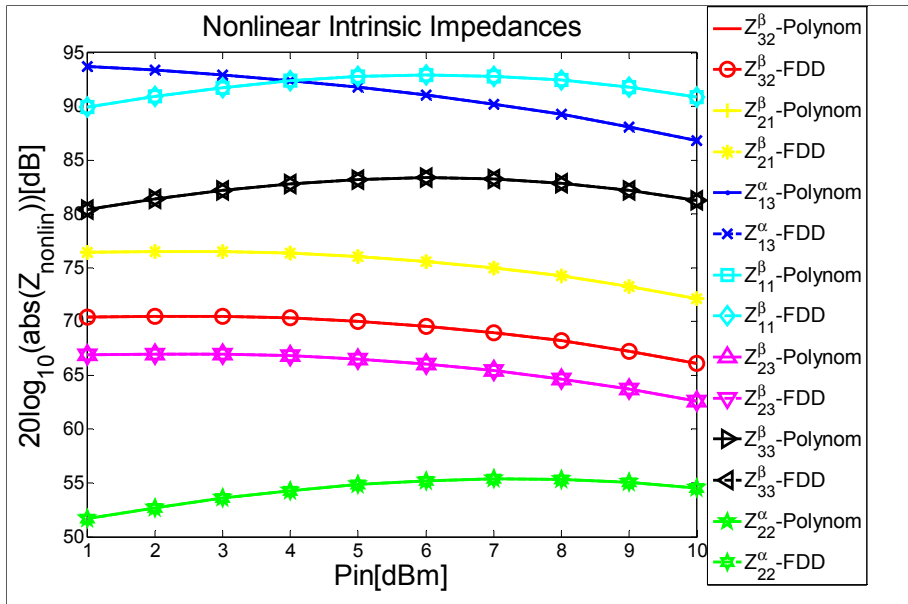


Figure 4.19 Comparison between polynomial and FDD models through the logarithmic amplitude of a random set of nonlinear lumped element impedances of a parallel nonlinear capacitor

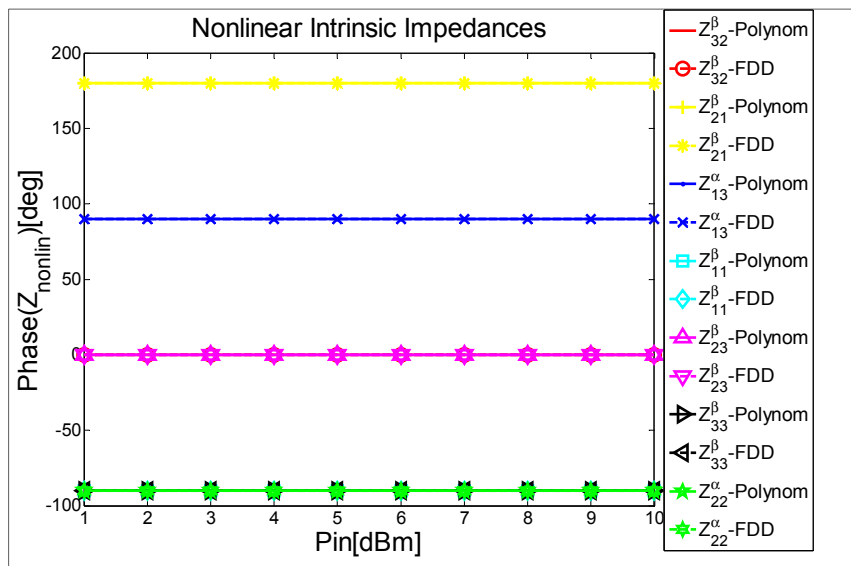


Figure 4.20 Comparison between polynomial and FDD models through the phase of a random set of nonlinear lumped element impedances of a parallel nonlinear capacitor

An example of a series nonlinear component is shown in Figure 4.21. The polynomial model is the standard model used to describe a nonlinear component. The conversion of X-parameters to a nonlinear ABCD matrix proves that $[A]=[D]=[I_d]$ and $[C]=[0]$ and that the nonlinear lumped element impedance matrix was equal to the nonlinear $[B]$ sub-matrix. The nonlinear capacitance model shown in Figure 4.21 can be implemented in ADS by using an FDD component, as indicated in Figure 4.9(a). The implementation was achieved through (4.45) and (4.46).

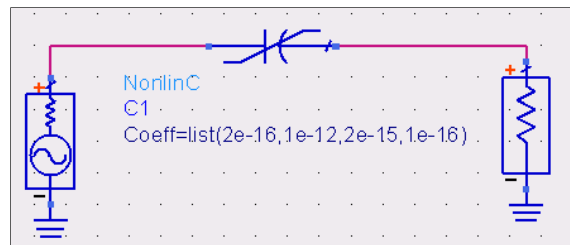


Figure 4.21 Simulation of a series nonlinear capacitor

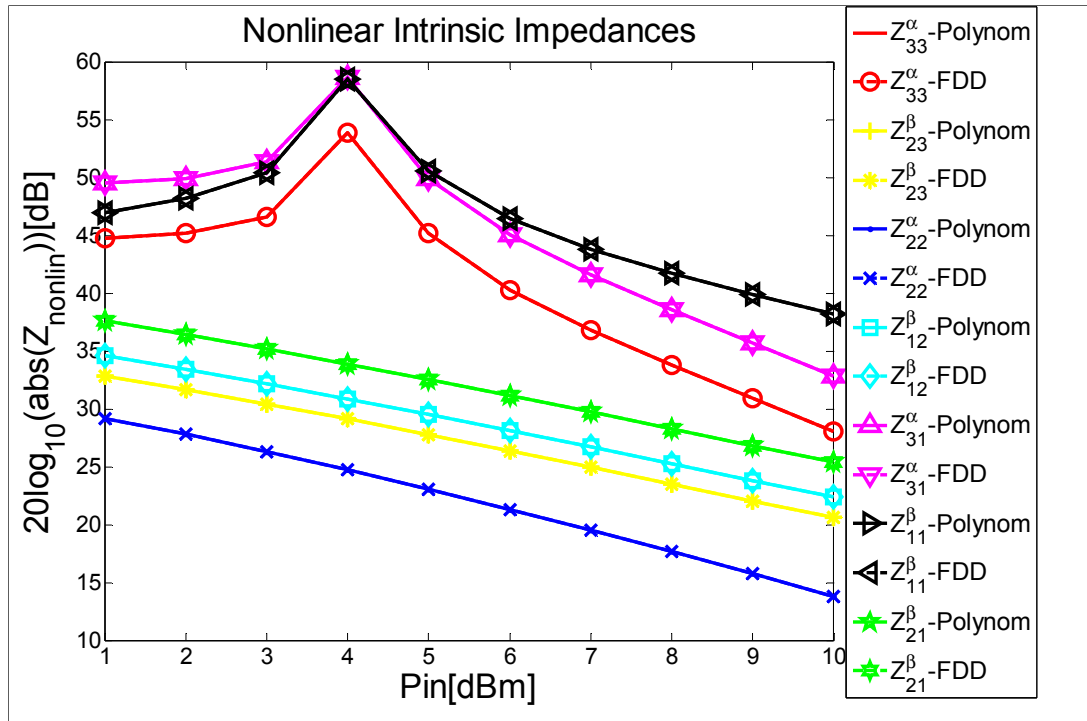


Figure 4.22 Comparison between polynomial and FDD models through the logarithmic amplitude of a random set of nonlinear lumped element impedances of a series nonlinear capacitor

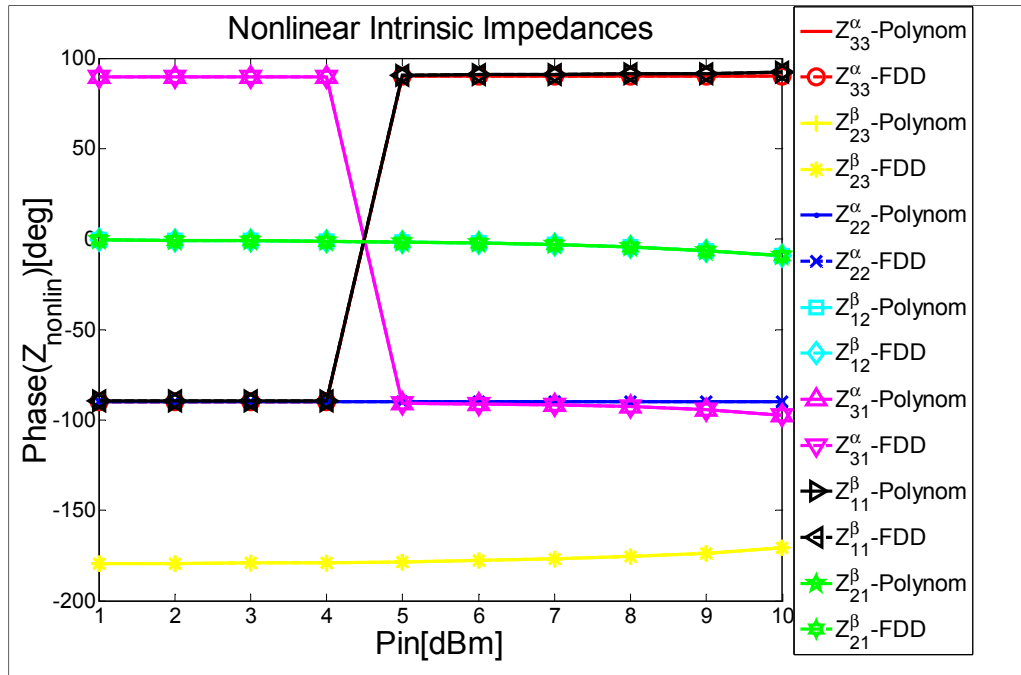


Figure 4.23 Comparison between polynomial and FDD models through the phase of a random set of nonlinear lumped element impedances of a series nonlinear capacitor

In Figure 4.22 and 4.23, the extracted nonlinear lumped element impedances of a series nonlinear capacitor from the polynomial model are compared to those extracted from the FDD model.

In order to validate the pi-network model based on X-parameters, an X-parameter simulation of a nonlinear pi network was conducted, as shown in Figure 4.24. The pi network consists of three nonlinear capacitors. The conversion of the X-parameter of the nonlinear pi network to nonlinear Y matrix proves that $[Y_{12}] = [Y_{21}]$. Nonlinear lumped element admittance matrices $\left[\bar{\bar{Y}}_{NL1} \right]$, $\left[\bar{\bar{Y}}_{NL2} \right]$ and $\left[\bar{\bar{Y}}_{NL3} \right]$ are extracted from the nonlinear Y matrix by using the following equations:

$$\left[\bar{\bar{Y}}_{NL1} \right] = [Y_{11}] + [Y_{12}]. \quad (4.73)$$

$$\left[\bar{\bar{Y}}_{NL2} \right] = [Y_{22}] + [Y_{12}]. \quad (4.74)$$

$$\left[\bar{\bar{Y}}_{NL3} \right] = -[Y_{12}] = -[Y_{21}]. \quad (4.75)$$

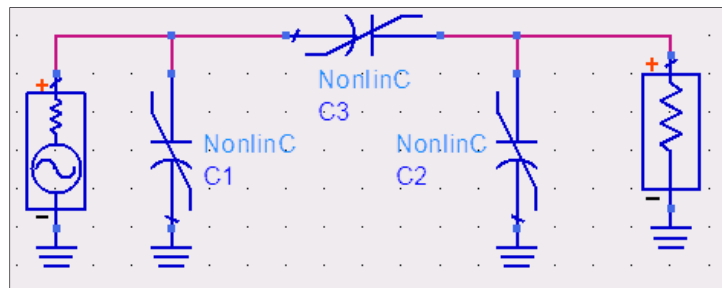


Figure 4.24 Simulation of a nonlinear pi network

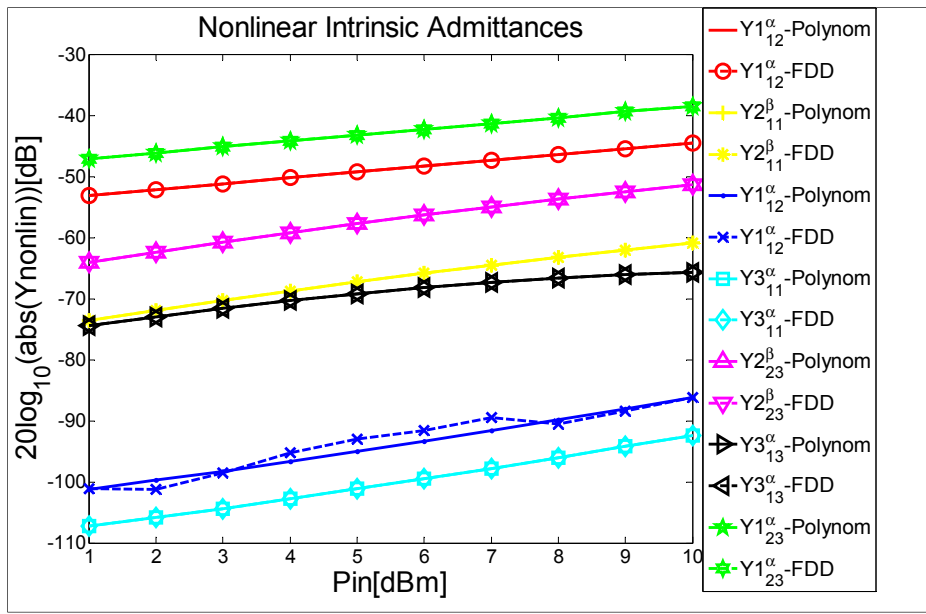


Figure 4.25 Comparison between polynomial and FDD models through the logarithmic amplitude of a random set of nonlinear lumped element admittances of a nonlinear pi network

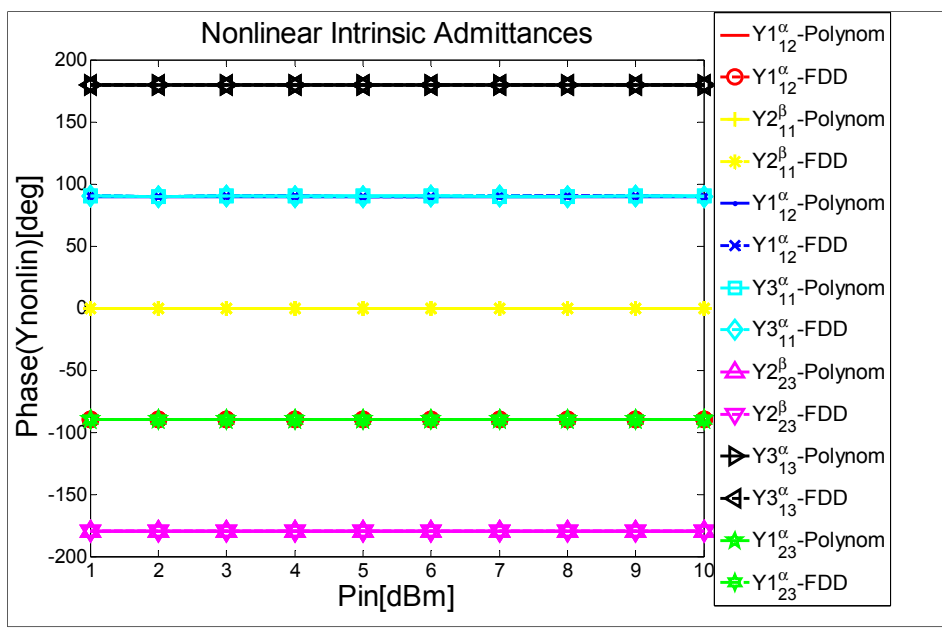


Figure 4.26 Comparison between polynomial and FDD models through the phase of a random set of nonlinear lumped element admittances of a nonlinear pi network

The pi network of nonlinear capacitances can be implemented in ADS by an FDD component using (4.45), (4.46), (4.47) and (4.48). In Figure 4.25 and 4.26, the extracted nonlinear lumped element admittances of the nonlinear pi network, which consist of nonlinear components described with the polynomial model, are compared to the extracted admittances of the same nonlinear pi network, but implemented with the FDD model.

4.7.5 GaN HEMT nonlinear intrinsic part extraction technique validation

As illustrated in Figure 4.7 and 4.8, the nonlinear intrinsic part can be modeled as a pi network of nonlinear impedances: $\left[\bar{\bar{Z}}_{NLGS}\right]$, $\left[\bar{\bar{Z}}_{NLGD}\right]$, $\left[\bar{\bar{Z}}_{NLDG}\right]$ and $\left[\bar{\bar{Z}}_{NLDS}\right]$. Equations (4.34) and (4.35) are used to implement $\left[\bar{\bar{Z}}_{NLGS}\right]$ and $\left[\bar{\bar{Z}}_{NLDS}\right]$ with FDD components, whereas $\left[\bar{\bar{Z}}_{NLGD}\right]$ is implemented with FDD using (4.32) and with $[I_2]$ of the FDD component set to $[0]$. Equations (4.32) and (4.33) are used with $[I_1]$ of the FDD component set to $[0]$ to implement $\left[\bar{\bar{Z}}_{NLDG}\right]$ with FDD. In Figure 4.27 and 4.27, nonlinear lumped element impedances $\left[\bar{\bar{Z}}_{NLGS}\right]$, $\left[\bar{\bar{Z}}_{NLGD}\right]$, $\left[\bar{\bar{Z}}_{NLDG}\right]$ and $\left[\bar{\bar{Z}}_{NLDS}\right]$ of the intrinsic part of the transistor at 2.15 GHz for $V_{ds}=25V$, $I_{ds}=180mA$, $V_{gs}=-1V$ and $I_{gs}=8mA$ are validated. All nonlinear impedances extracted from the de-embedded X-parameters are compared to the impedances extracted from the intrinsic model implemented with FDD components. As shown in the figures, there is agreement between the X-parameters obtained from measurement and the model implemented with FDD components in ADS.

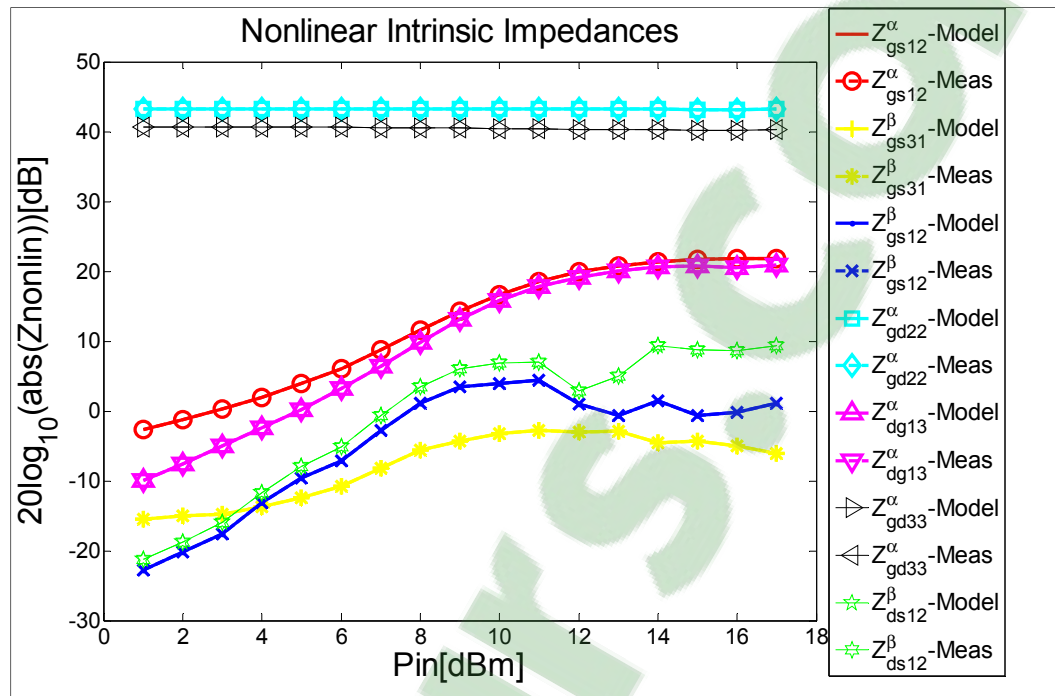


Figure 4.27 Comparison between deembedded X-parameters of a 2 mm GaN HEMT on Si substrate measured at 6 GHz for $V_{\text{ds}}=25\text{V}$, $I_{\text{ds}}=180\text{mA}$, $V_{\text{gs}}=-1\text{V}$ and $I_{\text{gs}}=8\text{mA}$ and FDD models through the logarithmic amplitude of a random set of nonlinear lumped impedances of drain-to-source, gate-to-source, drain-to-gate and gate-to-drain junctions

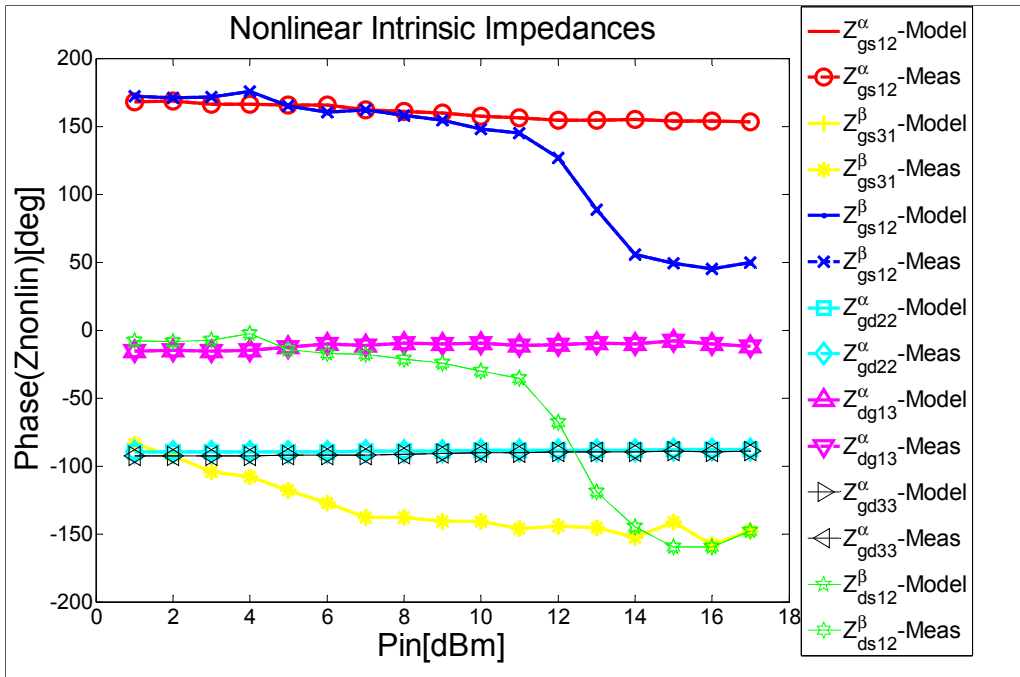


Figure 4.28 Comparison between deembedded X-parameters of a 2 mm GaN HEMT on Si substrate measured at 6 GHz for $V_{ds}=25V$, $I_{ds}=180mA$, $V_{gs}=-1V$ and $I_{gs}=8mA$ and FDD models through the phase of a random set of nonlinear lumped element impedances of drain-to-source, gate-to-source, drain-to-gate and gate-to-drain junctions

4.7.6 GaN HEMT equivalent circuit model validation

The new equivalent circuit model of the GaN HEMT device on a Si substrate is shown in Figure 4.29. The model is subdivided into extrinsic and intrinsic parts. The extrinsic network consists of linear elements that are related to the physical layout of the transistor. The intrinsic part is modeled as a modified Pi-network composed by 4 FDD components to simulate the gate-source, gate-drain, source-drain and drain-source junctions. The nonlinear lumped element impedances are extracted from the intrinsic X-parameters after de-embedding.

Data Access Component (DAC) is used to access to the values of the voltage dependent intrinsic elements. In order to validate the new modeling technique based on X-parameters,

an X-parameter simulation of the equivalent circuit model, shown in Figure 4.29, was conducted and, then, compared to the measurements. As shown in

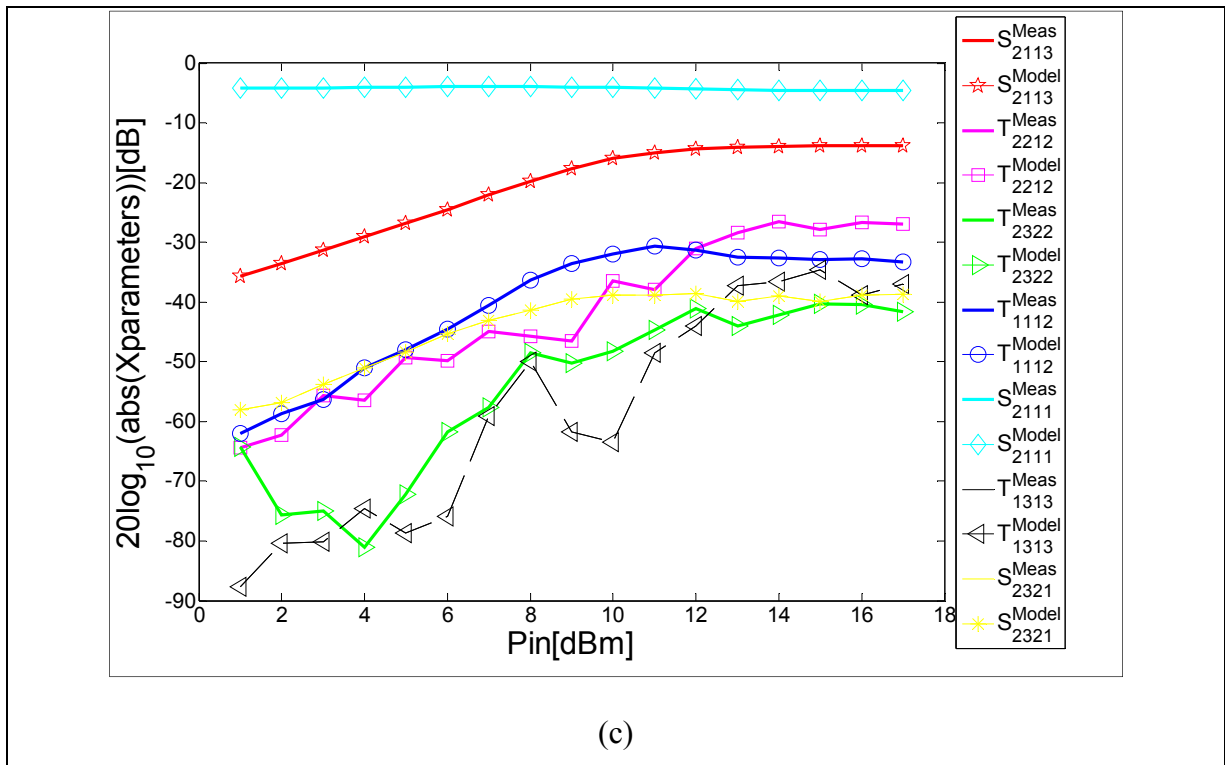


Figure 4.30 and 31, there is a good agreement between the X-parameters obtained from measurements and those obtained from the simulation.

In addition to X-parameters simulation, harmonic balance simulation is also carried out. The time domain measured waveforms of voltage and current at the input and output of the 2 mm GaN HEMT device are compared to those obtained from the harmonic balance simulation of the equivalent circuit model shown in Figure 4.29. As seen in Figure 4.30, the model fit accurately the voltage and current time domain waveforms at the input and the output. Moreover, the time domain simulated waveforms of voltage and current at the input and output of the intrinsic part are compared to de-embedded measurements, in Figure 4.36, which proves the de-embedding techniques.

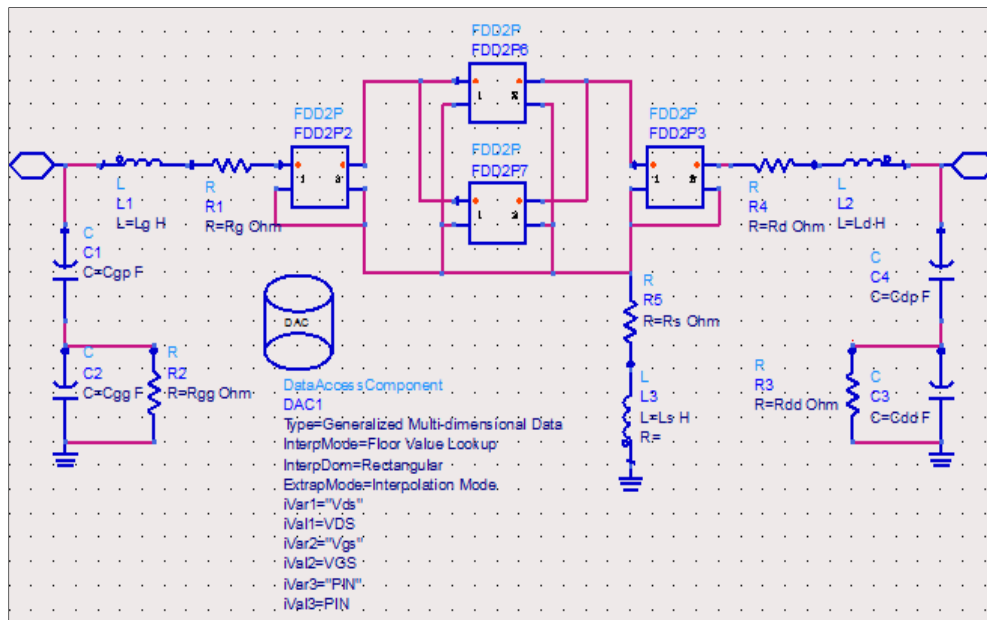
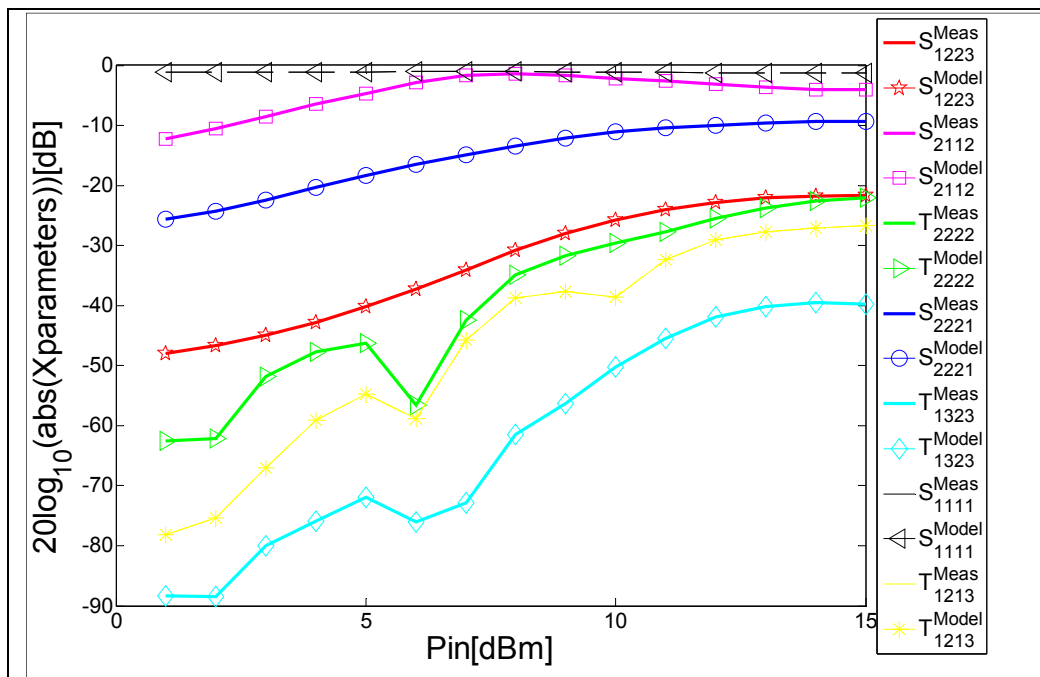
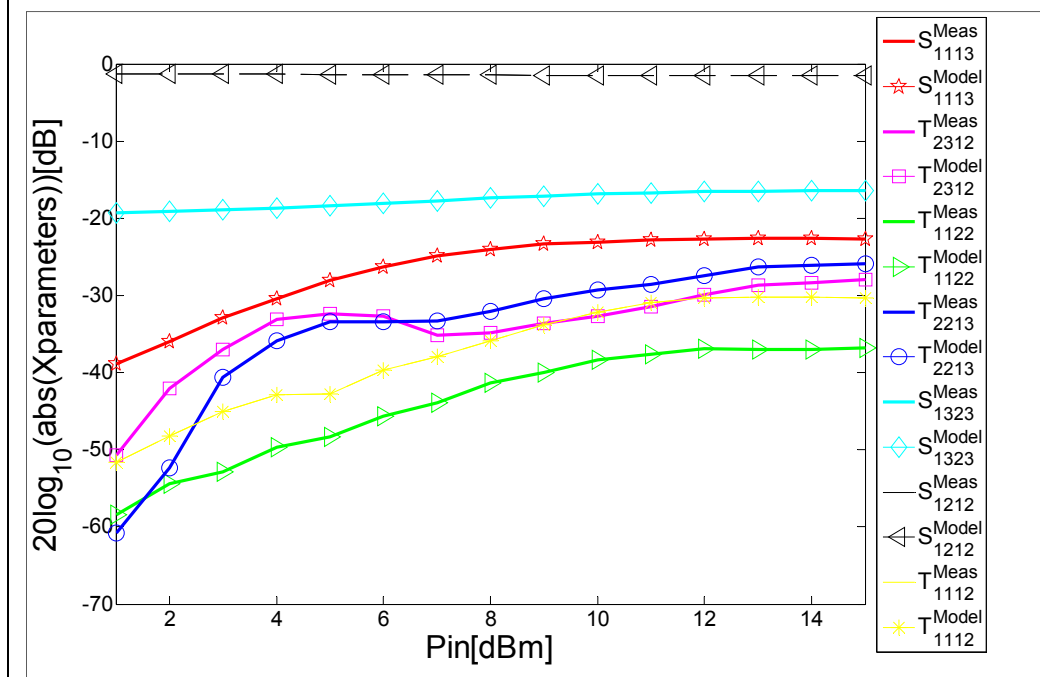


Figure 4.29 Implementation of the equivalent circuit based model on ADS



(a)



(b)

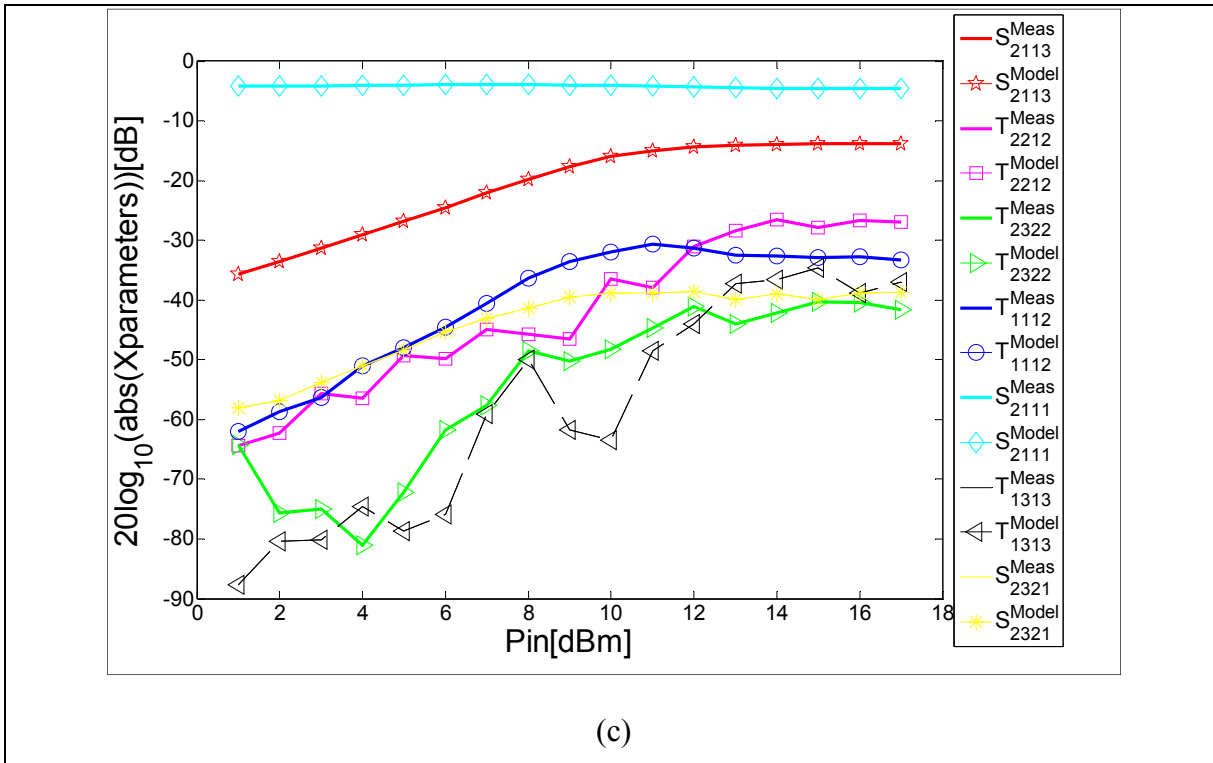
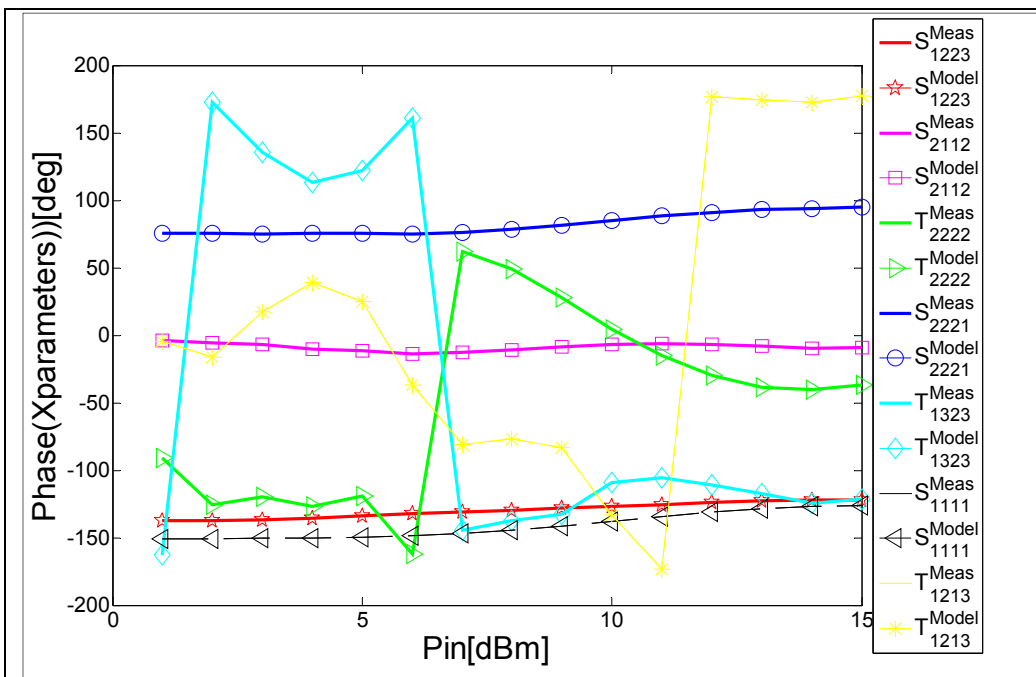


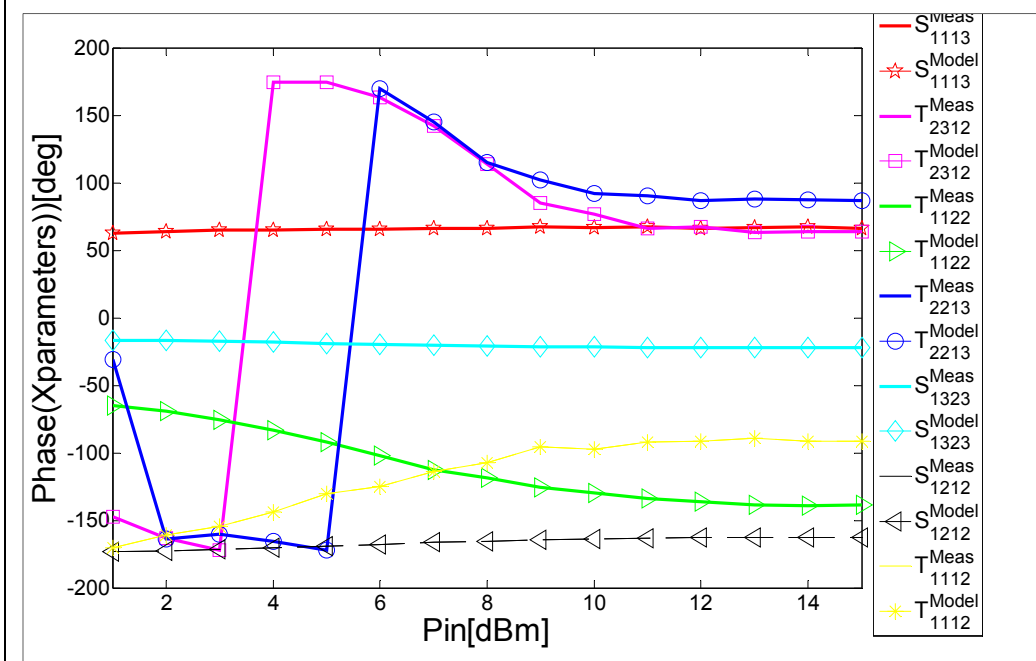
Figure 4.30 Comparison between the logarithmic amplitude of measured and simulated X-parameters of a 2 mm GaN HEMT on Si substrate measured at 750 MHz for $V_{ds}=3V$, $I_d=113mA$, $V_{gs}=-1.28V$ and $I_g=11mA$ (a), at 1500 MHz for $V_{ds}=1V$, $I_d=30mA$, $V_{gs}=-1.48V$ and $I_g=13mA$ (b) and at 6 GHz for $V_{ds}=25V$, $I_d=125mA$, $V_{gs}=-1V$ and $I_g=8mA$ (c). S_{pmqj}^{Meas} and T_{pmqj}^{Meas} are terms of measured X-parameters, and

$$S_{pmqj}^{Model} \text{ and } T_{pmqj}^{Model} \text{ are terms of signal model X-parameters.}$$

The set of X-parameter terms are chosen randomly.



(a)



(b)

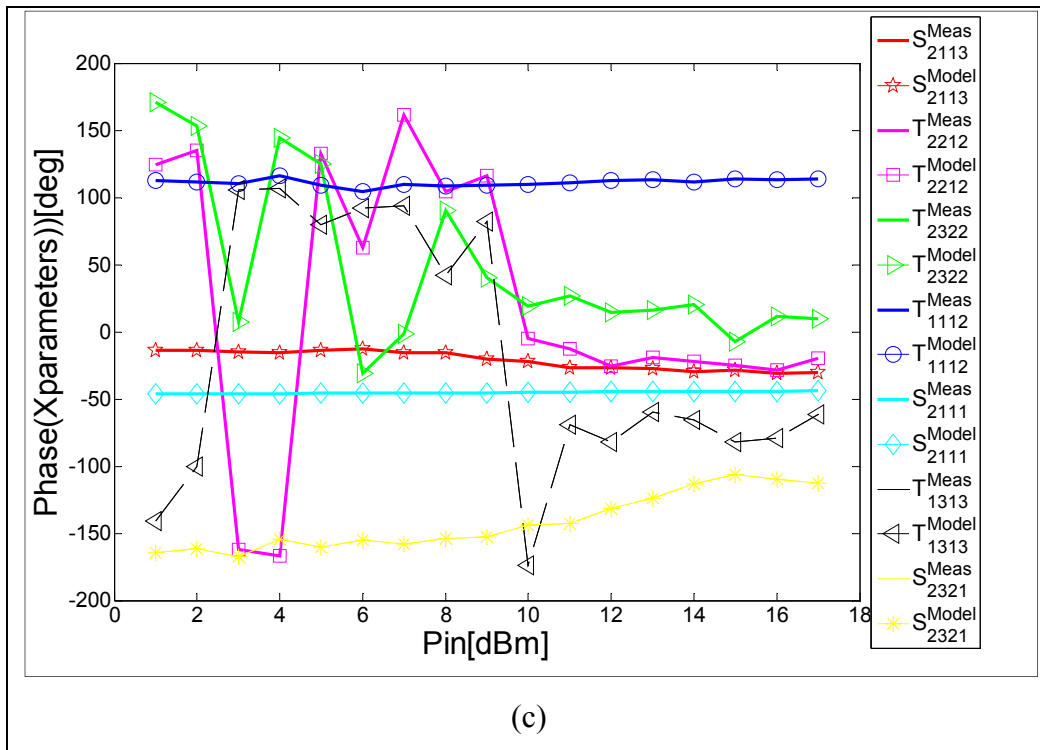
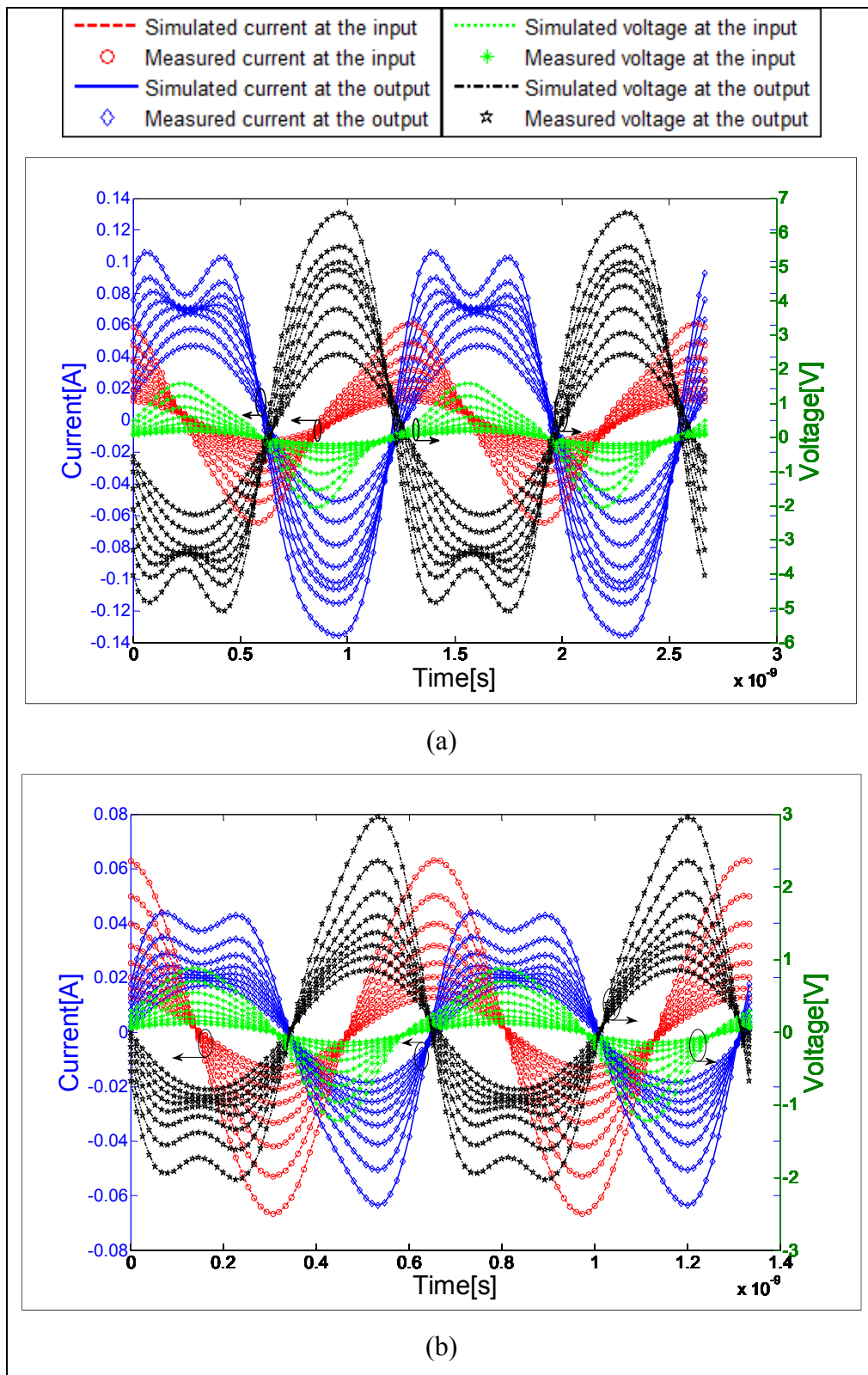


Figure 4.31 Comparison between the phase of measured and simulated X-parameters of a 2 mm GaN HEMT on Si substrate measured at 750 MHz for $V_{ds}=3V$, $I_d=113mA$, $V_{gs}=-1.28V$ and $I_g=11mA$ (a), at 1500 MHz for $V_{ds}=1V$, $I_d=30mA$, $V_{gs}=-1.48V$ and $I_g=13mA$ (b) and at 6 GHz for $V_{ds}=25V$, $I_d=125mA$, $V_{gs}=-1V$ and $I_g=8mA$ (c). S_{pmqj}^{Meas} and T_{pmqj}^{Meas} are terms of measured X-parameters, and S_{pmqj}^{Model} and T_{pmqj}^{Model} are terms of signal model X-parameters. The set of X-parameter terms are chosen randomly.



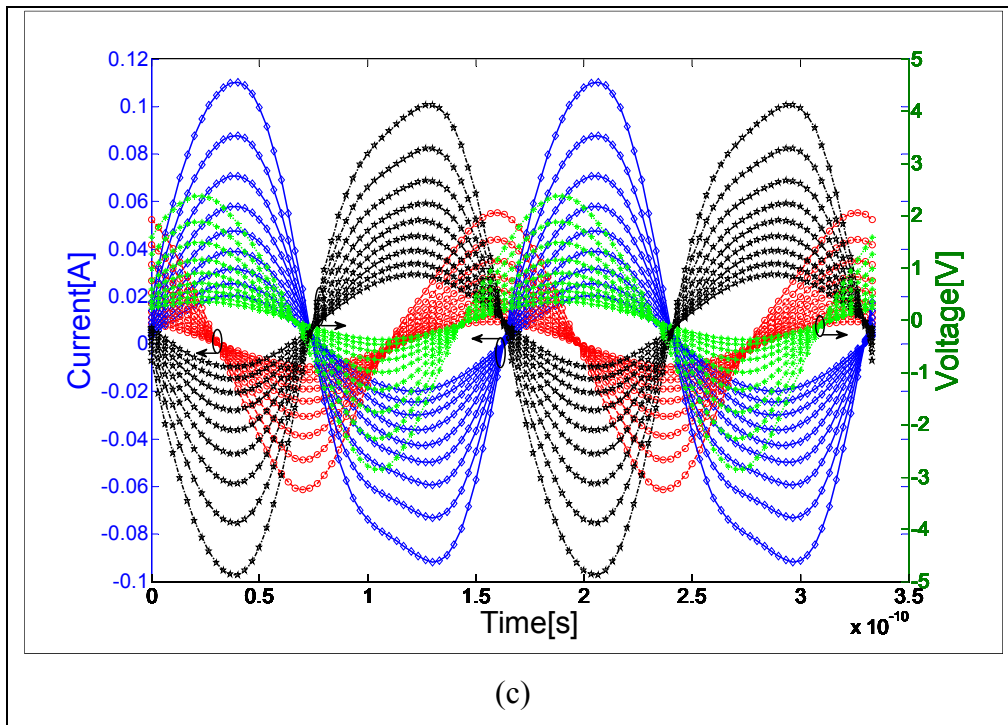
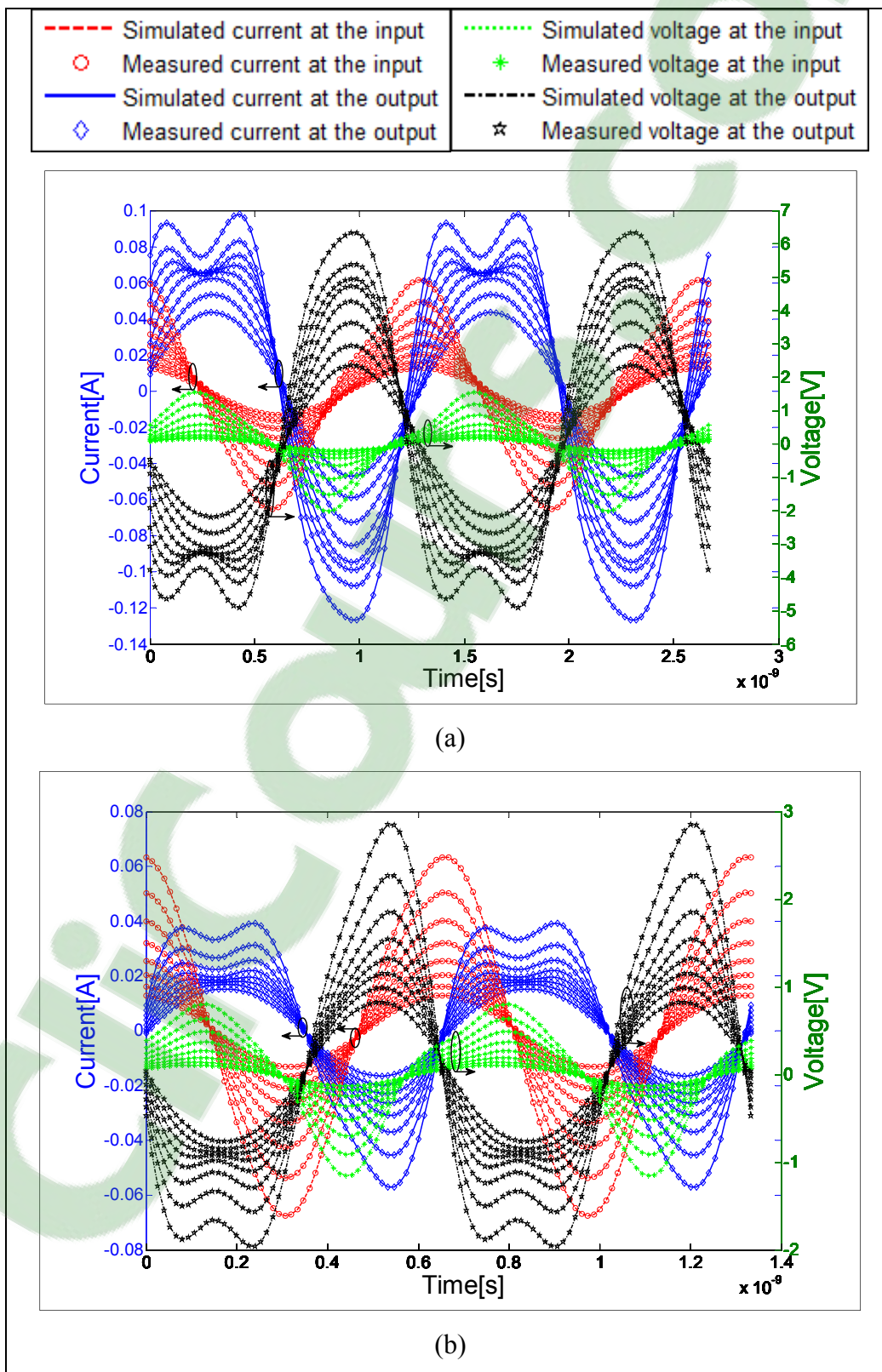


Figure 4.32 Extrinsic input and output voltage and current waveforms simulation (lines) compared to measurements (symbols) of a 2 mm GaN HEMT on Si substrate at 750 MHz for $V_{ds}=3V$, $I_d=113mA$, $V_{gs}=-1.28V$ and $I_g=11mA$ and for an input power sweep between 1 and 15 dBm with a step of 2 dBm (a) and at 1500 MHz for $V_{ds}=1V$, $I_d=30mA$, $V_{gs}=-1V$ and $I_g=13mA$ and for an input power sweep between 1 and 15 dBm with a step of 2 dBm (b) and at 6 GHz for $V_{ds}=25V$, $I_d=125mA$, $V_{gs}=-1V$, $I_g=8mA$ and for an input power sweep between 1 and 17 dBm with a step of 2 dBm (c).



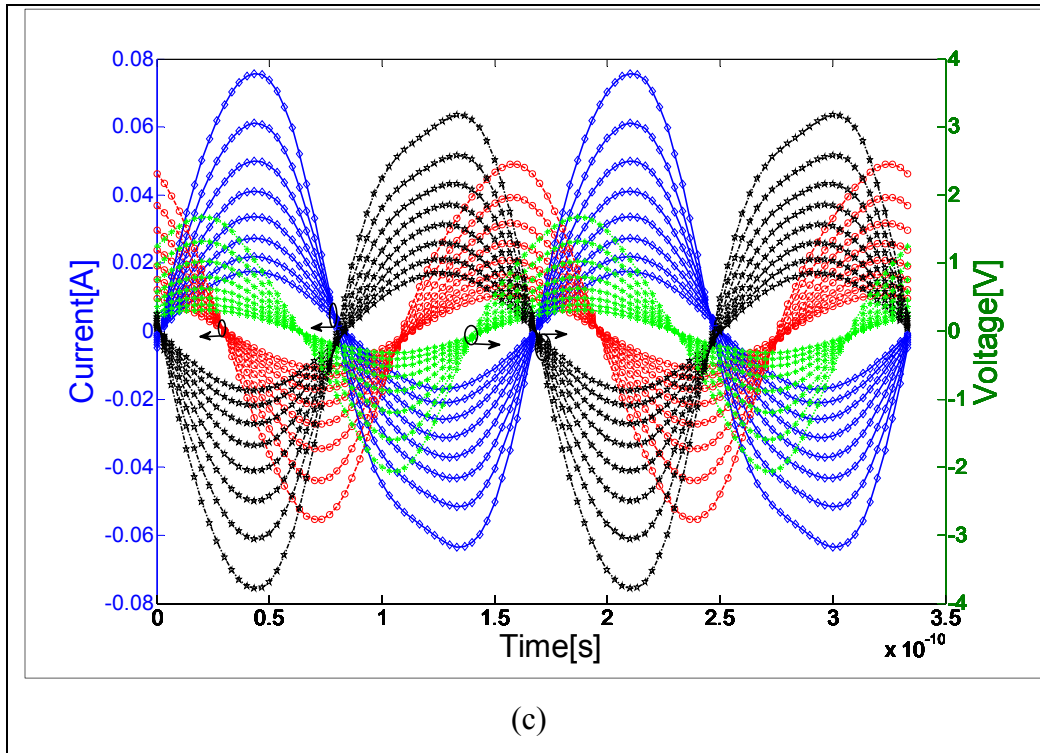


Figure 4.33 Intrinsic (de-embedded) input and output voltage and current waveforms simulation (lines) compared to measurements (symbols) of a 2 mm GaN HEMT on Si substrate at 750 MHz for $V_{ds}=3V$, $I_d=113mA$, $V_{gs}=-1.28V$ and $I_g=11mA$ and for an input power sweep between 1 and 15 dBm with a step of 2 dBm (a) and at 1500 MHz for $V_{ds}=1V$, $I_d=30mA$, $V_{gs}=-1V$ and $I_g=13mA$ and for an input power sweep between 1 and 15 dBm with a step of 2 dBm (b) and at 6 GHz for $V_{ds}=25V$, $I_d=125mA$, $V_{gs}=-1V$, $I_g=8mA$ and for an input power sweep between 1 and 17 dBm with a step of 2 dBm (c).

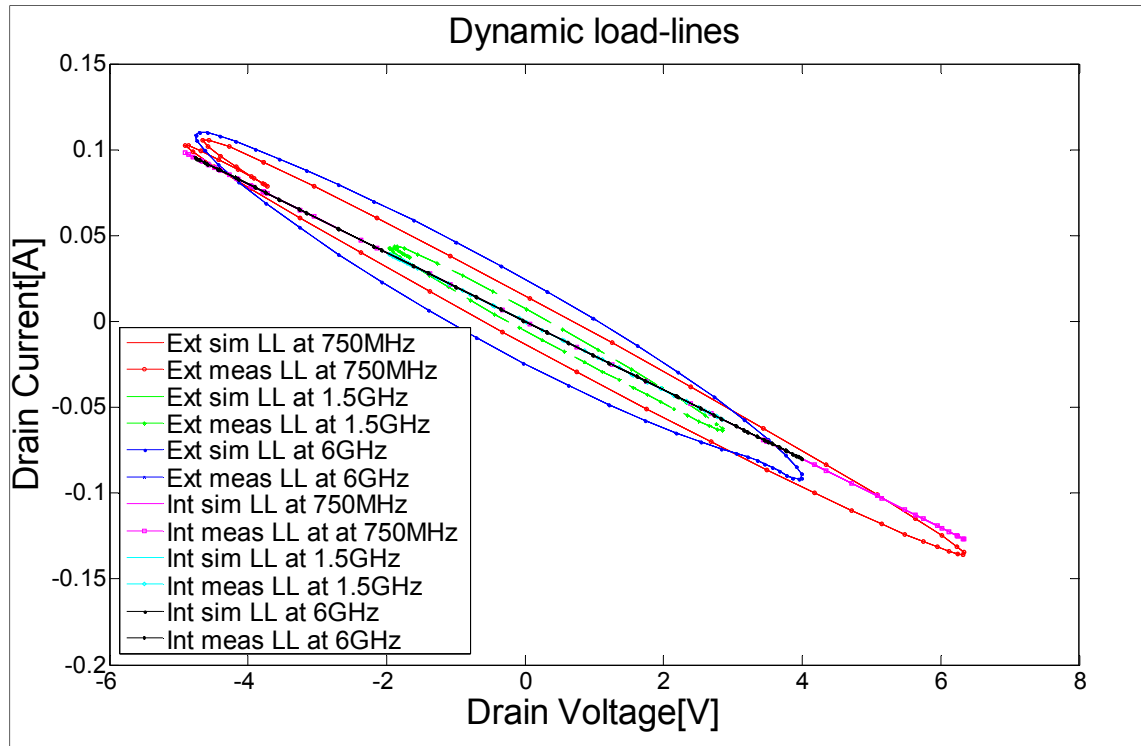
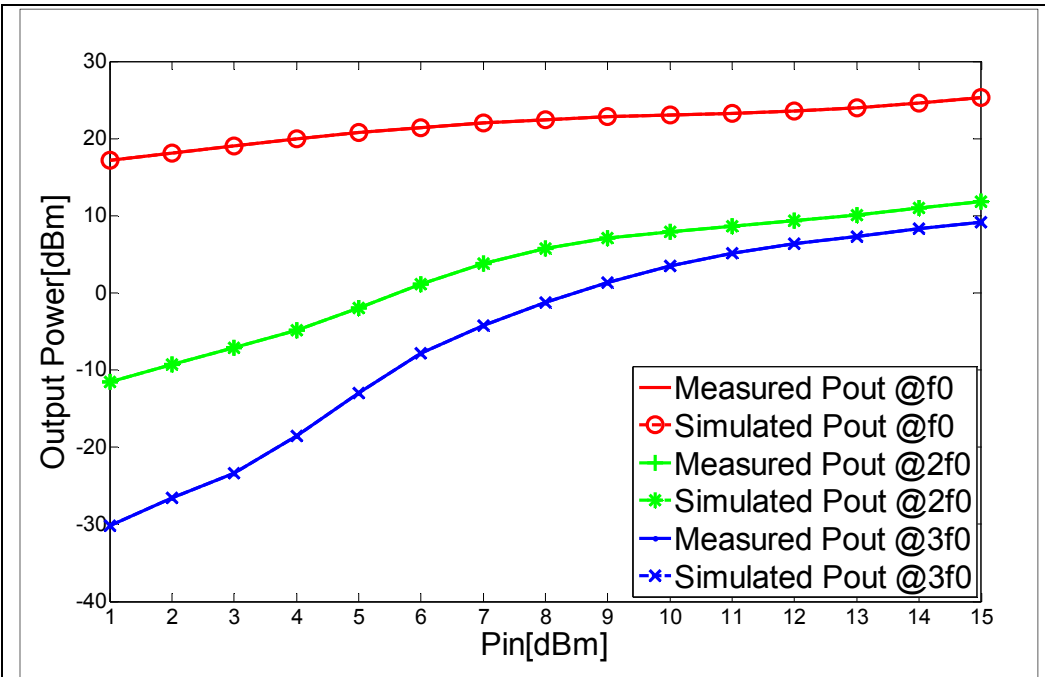


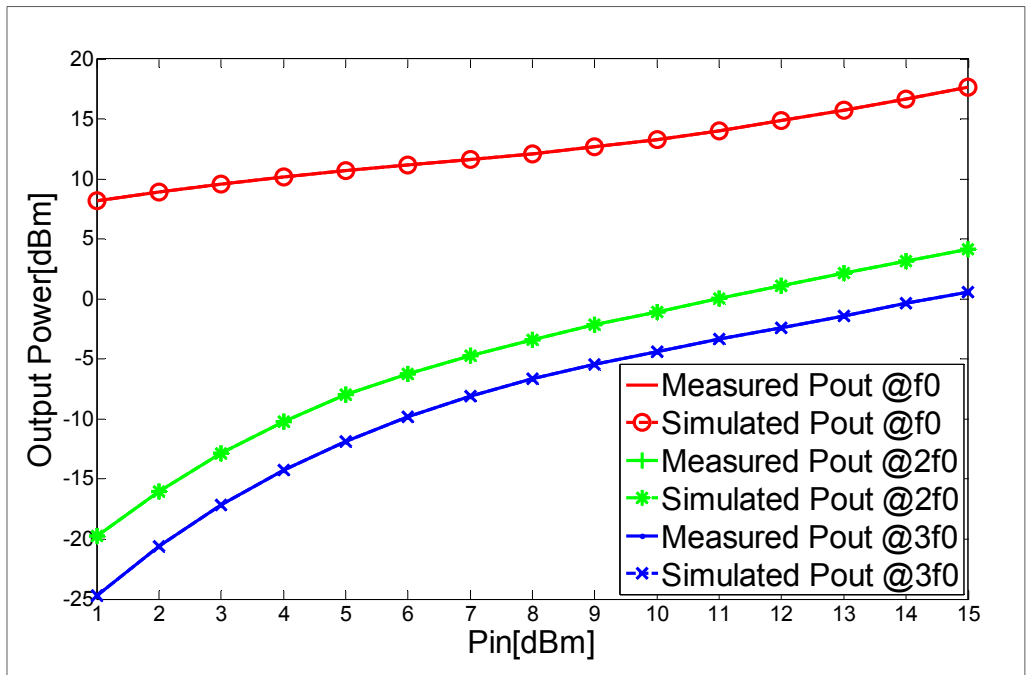
Figure 4.34 Extrinsic and Intrinsic (de-embedded) dynamic loadlines simulation (lines) compared to measurements (symbols) of a 2 mm GaN HEMT on Si substrate at 750 MHz for $V_{ds}=3V$, $V_{gs}=-1.28V$ and for an input power of 15 dBm (a) and at 1500 MHz for $V_{ds}=1V$, $V_{gs}=-1V$ and for an input power of 15 dBm (b) and at 6 GHz for $V_{ds}=25V$, $V_{gs}=-1V$ and for an input power of 17 dBm (c).

Moreover, the model can predict accurately the nonlinear behavior of the device. Figure 4.35 illustrate the measured and simulated output power at the fundamental, second and third harmonics. A good agreement is also seen in Figure 4.36 while comparing AM-AM and AM-PM measurement behaviours to the predicted ones by the model.

In addition to the measurements presented in this section, other measurements were carried and compared to the model simulation. The model is validated within 50 Ohm terminations, for a set of frequencies less than 6 GHz, for V_{ds} between 0V and 25 V, for V_{gs} between -1.8V and -0.5V and for an input power less than 17 dBm. The values of these parameters are chosen randomly.



(a)



(b)

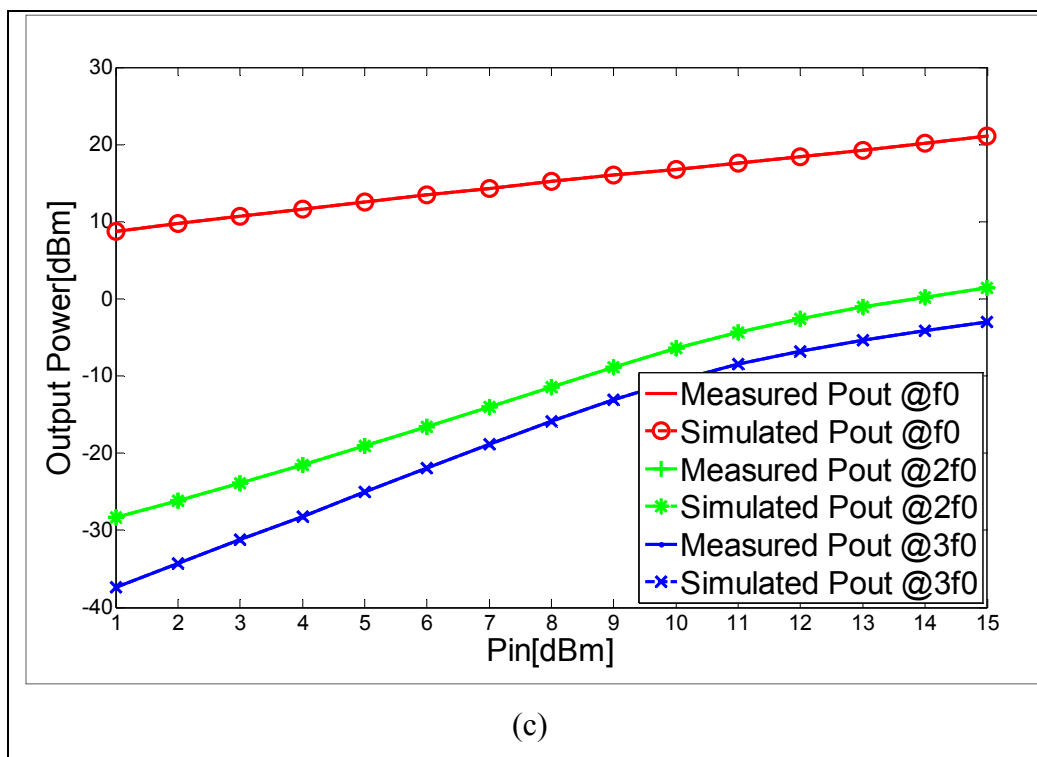
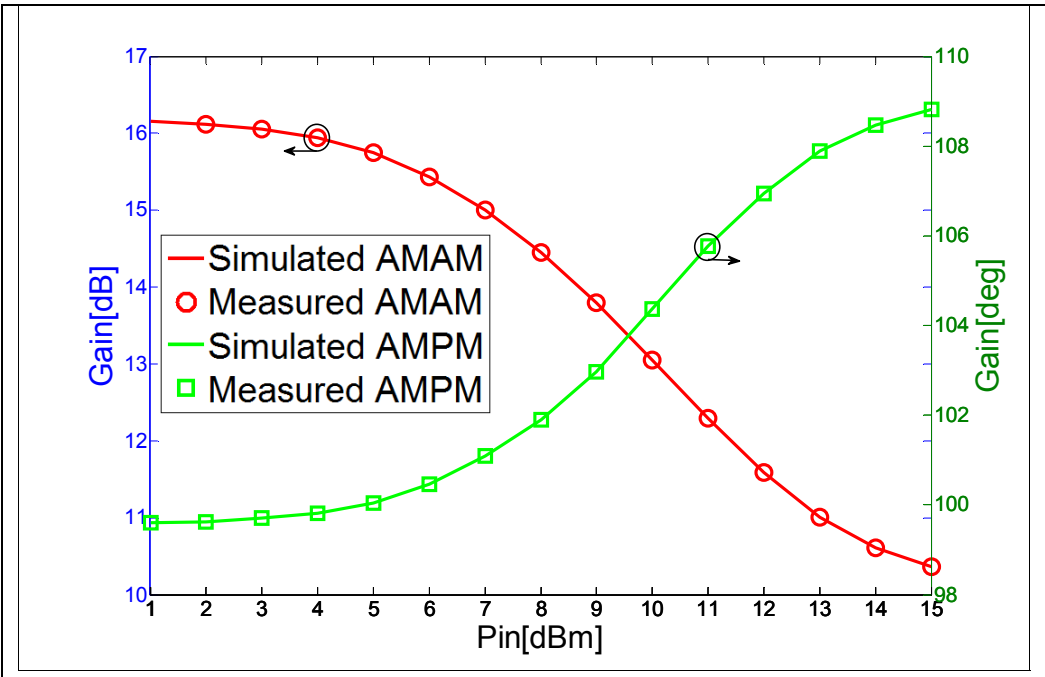
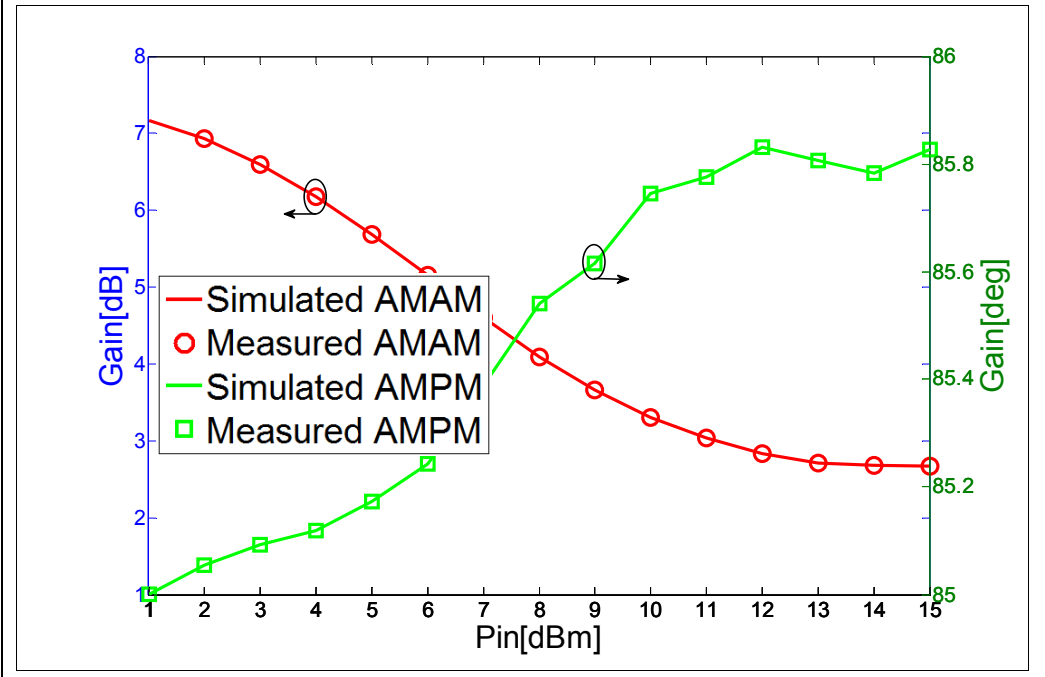


Figure 4.35 Output power simulations (lines) compared with measurements (symbols) of a 2 mm GaN HEMT on Si substrate at 750 MHz for $V_{ds}=3V$, $I_d=113mA$, $V_{gs}=-1.28V$ and $I_g=11mA$ (a), at 1500 MHz for $V_{ds}=1V$, $I_d=30mA$, $V_{gs}=-1.48V$ and $I_g=13mA$ (b) and at 6 GHz for $V_{ds}=25V$, $I_d=125mA$, $V_{gs}=-1V$ and $I_g=8mA$ (c).



(a)



(b)

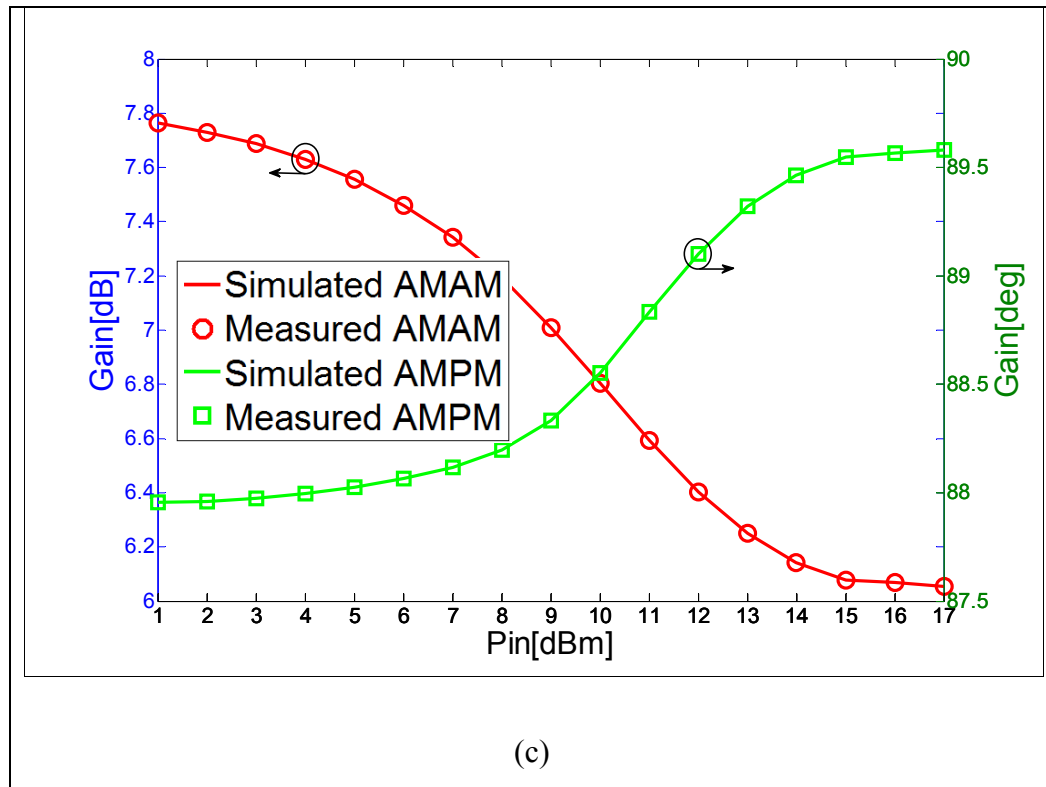


Figure 4.36 AM-AM and AM-PM simulations (lines) compared with measurements (symbols) of a 2 mm GaN HEMT on Si substrate at 750 MHz for $V_{ds}=3V$, $I_d=113mA$, $V_{gs}=-1.28V$ and $I_g=11mA$ (a), at 1500 MHz for $V_{ds}=1V$, $I_d=30mA$, $V_{gs}=-1.48V$ and $I_g=13mA$ (b) and at 6 GHz for $V_{ds}=25V$, $I_d=125mA$, $V_{gs}=-1V$ and $I_g=8mA$ (c).

4.7.7 Small- and large-signal S-parameters simulation

Unlike small-signal S-parameters, which are based on a small-signal simulation of a linearized circuit, large-signal S-parameters are based on a harmonic balance simulation of the full nonlinear circuit (Technologies 2009). Large-signal S-parameters are also called power-dependent S-parameters. This means that the large-signal S-parameters can change as power levels are varied. Indeed, in linear operation mode, X-parameters reduce to S-parameters when the device is operated in linear mode. For small $|a_{11}|$ (linear operation), all F_{ik} terms for $k>1$ vanish as well as all cross frequency S_{ikjl} terms and all T_{ikjl} terms. S-parameters are compared to the following terms:

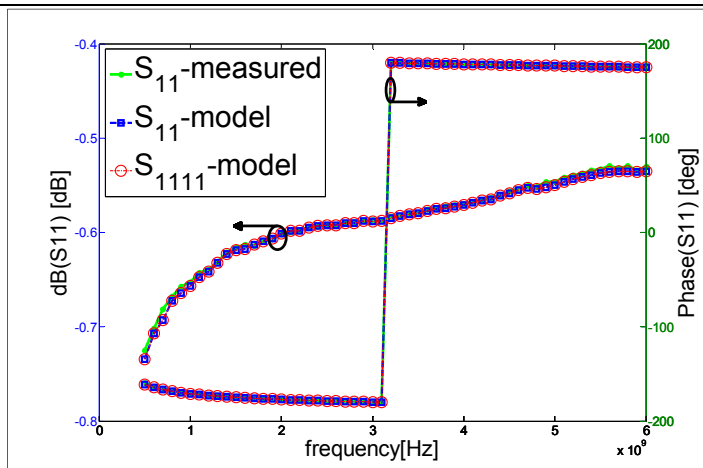
$$S_{11} = \frac{X_{11}^F}{a_{11}} = S_{1111}. \quad (4.76)$$

$$S_{21} = \frac{X_{21}^F}{a_{11}} = S_{2111}. \quad (4.77)$$

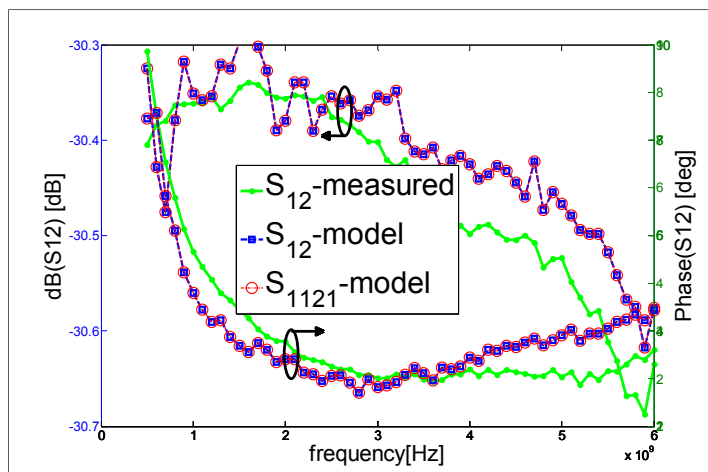
$$S_{12} = S_{1121}. \quad (4.78)$$

$$S_{22} = S_{2121}. \quad (4.79)$$

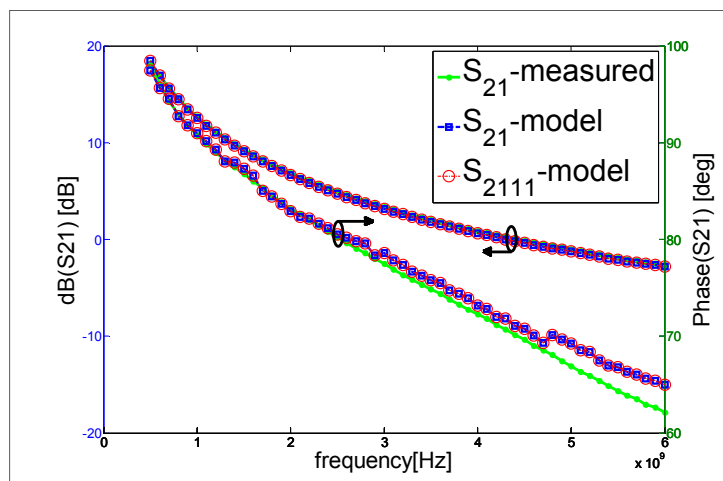
The model is simulated under small- and large-signal S-parameters and compared to S-parameters measurements. Small-signal S-parameters simulation runs but it gives an unexpected result. This is due to the fact that the FDD is not fully compatible with all the different circuit analysis modes of Advanced Design System (Technologies 2008). However, large-signal S-parameters (LSSP) simulation gives the expected results. LSSP simulation of the xnp file that includes X-parameters measurements are compared to the simulation of the equivalent-circuit model. Then, they are compared to S-parameters measured by the NVNA: The NVNA is able to run S-parameters measurement which allows keeping the same setup and the same calibration, and therefore the same conditions. The model is validated within 50 Ohm terminations, for a set of frequencies between 500 MHz and 6 GHz, for $V_{ds}=10V$, $I_{ds}=189mA$, $V_{gs}=-1V$ and $I_{gs}=14mA$ and for an input power equal to -20 dBm where the device operates linearly. A good agreement between measured S-parameters and to the predicted ones is seen in Figure 4.37. S-parameters measurements are also compared to the X-parameters mentioned in (4.76), (4.77), (4.78) and (4.79).



(a)



(b)



(c)

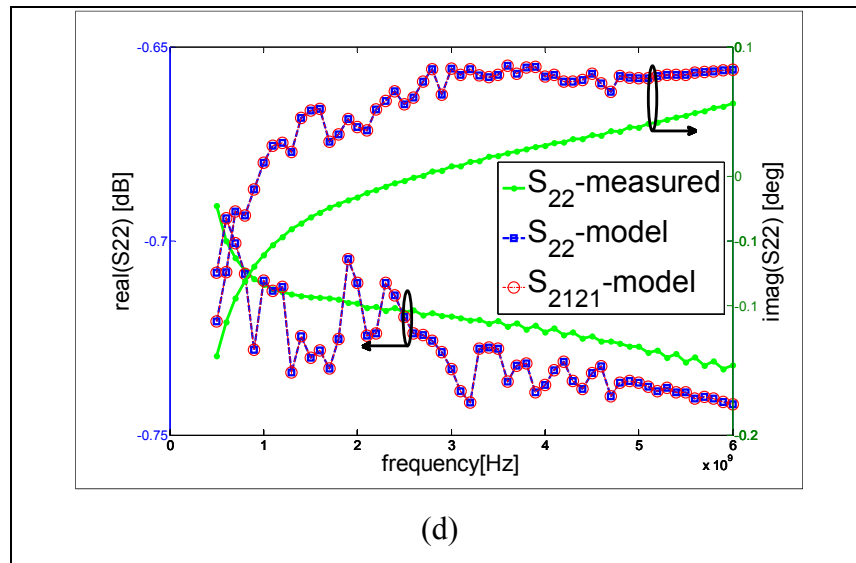


Figure 4.37 Measured S-parameters (S_{11} (a), S_{12} (b), S_{21} (c) and S_{22} (d)) compared to the simulated ones of the equivalent-circuit based model with ADS LSSP and to the simulated Xparameters (S_{1111} , S_{1121} , S_{2111} and S_{2121}) of the model with ADS X-parameters. The transistor is a 2 mm GaN HEMT on Si substrate biased with $V_{ds}=10V$, $I_{ds}=189mA$, $V_{gs}=-1V$ and $I_{gs}=14mA$ and has an input power of -20 dBm. The frequency range is between 500 MHz and 6 GHz.

4.8 DISCUSSION

The advantage of using this new modeling technique is that it reduces significantly the number of required measurements by extracting the nonlinear impedances of the intrinsic part of the transistor directly from X-parameter measurements. For an amplifier working in a 50-ohm environment and for a given bias voltage, input power and load, there is no need to run a high set of measurements comparing to the conventional modeling technique.

Another advantage is that the model is easy, fast to construct and mimic the physical operation of the transistor. It is consistent with the physical structure of the transistor and is more suitable for design improvement. For this purpose, after de-embedding the extrinsic elements, the intrinsic part, which is related to the core of the transistor, is obtained by a

direct extraction of the intrinsic elements from X-parameter measurements. In order to keep connection to the basic device physics, the intrinsic part is represented by four nonlinear impedances describing the gate-source, drain-gate, gate-drain and drain-source impedances. Thus it has a good link to the physical operation which is advantageous for circuit level simulation: It allows a seamless transition from transistor level to circuit level.

In addition to these benefits, the model is accurate in either small- and large-signal operation mode which is due to the use of X-parameters to characterize the device and its capability to capture the nonlinear behavior accurately, better than dc and S-parameters. Thus, the developed model is able to operate under large signal stimulus and predicts accurately the harmonics and mismatch affects. Its accuracy and generality guarantee its exploitation with confidence in active RF circuit design for modern communication systems. Thanks to this modeling technique, the development of die model is quick as well as package model just by adding the bonding and package models.

As any equivalent-circuit model, this model takes into account electro-thermal and trapping effects. It is easier to embed such a complex phenomenon in an equivalent circuit based model. Then, it is possible to identify the sources of memory effects and their extent which can be advantageous for memory effects removing or reducing trials.

The different types of simulations performed in ADS with the proposed model such as harmonic balance, LSSP, X-parameters are fast and no convergence issues were observed. The proposed approach is better than the conventional procedure that uses the small-signal data to build with an indirect manner a nonlinear model. The models obtained by conventional method may provide accurate results under DC and small-signal operating conditions (Bandler, Qi-Jun et al. 1989, Werthorf, van Raay et al. May. 1993). However, they may not be accurate enough for high-frequency and large-signal operation since they are determined under small-signal conditions and then used to predict the behavior for large-signal operations (Bandler, Qi-Jun et al. 1989, Kopp and Heston May. 1988). Moreover, they have additional drawbacks: (i) discrepancy between dc and small-signal characteristics due to

time-dependent trapping effects (ii) error in load-pull measurements and (iii) nonphysical model due to numerical optimization techniques (Ce-Jun, Lan et al. 1995). On the other side, the new approach uses directly the nonlinear measured response (X-parameters) of the device under realistic stimulus: In the model extraction process, the DUT is in a similar state as the usual operating conditions. Thus, this new approach can provide more accurate and more reliable large-signal model. Moreover, it benefits from X-parameters that measure accurately the different harmonics. That's why no optimization algorithms are used to extract the nonlinear intrinsic parameters in this procedure.

4.9 Conclusion

The GaN HEMT is applied in diverse high efficient RF power amplifier because of its good performances. To design a high efficient RF power amplifier, a large signal model is necessary. A transistor can be physics model, black box model or a lumped element based model. Equivalent circuit based or compact models are preferred because they have good performances in terms of convergence, operating range, extrapolation accuracy, physical transistor insight, modeling process easiness and usability for circuit design. Conventional large-signal compact transistor models are extracted from small-signal data (multi-bias S-parameters) indirectly. This method limits its accuracy to predict nonlinear distortion. To overcome this limitation, the development and the extraction of compact models based on X-parameters instead of multi-bias S-parameters is proposed in this paper. However, in its form, X-parameters are not suitable to develop an equivalent circuit based model. Thus, new modeling tools are needed. That's why a set of new nonlinear two-port network parameters that are extracted from X-parameters, conversion rules and equations for different nonlinear circuit topologies were developed. These modeling tools are helpful for the development of the new equivalent circuit based modeling technique, especially for the de-embedding and intrinsic part extraction.

Similar to the equivalent circuit based models discussed in the literature, the new model is subdivided into extrinsic and intrinsic parts. The extrinsic part consists of linear elements and

is related to the physical layout of the transistor. After determining the values of extrinsic elements, the X-parameters of the intrinsic part can be determined with the proposed analytical de-embedding technique. The embedding technique is also developed in this paper which allows translating the inner reference plane at the device intrinsic boundary to the measurement reference plane at the external and accessible ports of the device.

The intrinsic part is modeled as a modified pi network of nonlinear lumped element impedances of drain-to-source, gate-to-source, drain-to-gate and gate-to-drain junctions. The concept of nonlinear lumped element impedances or admittances derived from X-parameters is presented. It is shown that nonlinear lumped element impedances or admittances can be easily extracted from X-parameters in series, parallel or pi network configurations.

The topology of the transistor intrinsic part is modified to describe the non-unilaterality. The extraction procedure and the implementation of the model in CAD software are presented and are successfully validated.

In the future, the model will be extended to include thermal and memory effect extraction results. Mathematical function fitting techniques will be applied to the intrinsic part element parameters. Artificial Neural Networks (ANN) would be potentially used because they can fit data in any dimension and they have infinitely many non-vanishing partial derivatives (Root, Xu et al. 2012). Combining ANN based model with the table based model can be effective. ANN allows overcoming the limitations of tables and interpolation schemes used in the proposed model. ANN is a powerful mathematical function approximation technique that can be used to fit any nonlinear function of any number of independent variables (Root 2012).

The equivalent-circuit based model is extracted for a 10x200 μm GaN HEMT with a gate length of 25 μm . This model can be scaled to the remaining devices. Scaling study that will be carried in the future will allow simulating the other devices with different geometrical dimensions manufactured with the same foundry process. Moreover, the model has already a

lower number of parameters but re-gridding will certainly reduce the set of dependent parameters of the nonlinear intrinsic elements.

CONCLUSION

High power amplifiers have been receiving increasing attention as key components responsible for a sizable portion of base station cost in terms of power loss and cooling equipments in wireless communication systems (Jarndal, Aflaki et al. 2010). They are also responsible in large part for battery life and size of the mobile terminals. Thus, high power and high efficiency amplifiers with low power loss are critically needed (Oualid, Slim et al. 2006). To meet these requirements, higher attention should be given to the employed active devices and the circuit design. Today, GaN HEMT devices are the best choice in this regard since they can produce higher output power with lower self-heating and leakage currents, which accordingly results in good power efficiency (Nuttinck, Gebara et al. 2002, Oxley and Uren 2005, Bae, Negra et al. 2007, Milligan, Sheppard et al. 2007, Bensmida, Hammi et al. 2008, Aflaki, Negra et al. 2009, Tanaka, Ueda et al. 2010, Jarndal, Markos et al. 2011). The design of high efficient power amplifier based on AlGaIn/GaN HEMT requires an accurate large-signal model for this device (Jarndal, Markos et al. 2011).

Large- and small- signal modeling of GaN HEMTs, which is the aim of our work, is an important step for high power amplifier designer. In general, most of the published models are accurate only in linear mode since they are relied on DC and multi-bias S-parameters measurements for model parameters extraction. The availability of X-parameters measurements and their benefits compared to S-parameters are an opportunity for incorporating non-linear data directly in the modeling process.

Nonlinear network Z-, Y-, ABCD-, T-, G- and H-parameters are essential to extract and validate large-signal model based on X-parameters. The expression of the new nonlinear network parameters are derived from X-parameters. Like X-parameters, each of these new nonlinear network parameters includes components associated with the independent current/voltage variables as wells their complex conjugate. The conversion rules between these new parameters and the measureable X-parameters have been developed and presented. The validation process showed that, just as X-parameters represent a superset of the linear S-

parameters; these new nonlinear parameters are also supersets of their corresponding linear versions. Moreover, the nonlinear network parameters can describe any topology of pure linear or nonlinear or a mixed of linear and nonlinear components. The most successful method for the characterization of such devices is to use a lumped circuit model that includes a mix of linear and nonlinear components. The new nonlinear network parameters can be used to characterize and analyze different nonlinear circuits with arbitrary topologies. Nonlinear Z -parameters are used to describe series topology, and the nonlinear Z matrix is simply the sum of the individual nonlinear Z matrices. Nonlinear Y parameters are used to describe parallel topology, and the nonlinear Y matrix is the sum of the individual nonlinear Y matrices. Nonlinear G parameters are used to describe parallel-to-series topology, and the nonlinear G matrix is the sum of the individual nonlinear G matrices. Nonlinear H parameters are used to describe series-to-parallel topology, and the nonlinear H matrix is the sum of the individual nonlinear H matrices. Nonlinear ABCD- or T-parameters are used to describe a cascade topology, and the ABCD or T matrix is the product of the individual nonlinear ABCD or T matrices, respectively.

A new equivalent circuit modeling technique based on X -parameter measurements is proposed. Similar to the equivalent circuit based models discussed in the literature, the new model is subdivided into extrinsic and intrinsic parts. The extrinsic part consists of linear elements and is related to the physical layout of the transistor. After determining the values of extrinsic elements, the X -parameters of the intrinsic part can be determined with the proposed de-embedding technique. The new nonlinear network parameters were very helpful to translate the measurement reference plane at the external and accessible ports of the device to the inner reference plane at the device intrinsic boundary. The intrinsic part is modeled as a modified pi network of nonlinear lumped element impedances of drain-to-source, gate-to-source, drain-to-gate and gate-to-drain junctions. The topology of the transistor intrinsic part is modified to describe the non-unilaterality. The extraction procedure and the implementation of the model in CAD software are presented and are successfully validated. The advantage of using this new modeling technique is that it reduces significantly the number of required measurements by extracting the nonlinear impedances of the intrinsic

part of the transistor directly from X-parameter measurements. Another advantage is that the model is easy, fast to construct and mimic the physical operation of the transistor. For this purpose, after de-embedding the extrinsic elements, the intrinsic part, which is related to the physical operation of the transistor, is obtained by a direct extraction of the intrinsic elements from X-parameter measurements. In order to keep connection to the basic device physics, the intrinsic part is represented by four nonlinear impedances describing the gate-source, gate-drain, source-drain and drain-source junctions. In addition to these benefits, the model is accurate in either small- and large-signal operation mode which is due to the use of X-parameters to characterize the device and its capability to capture the nonlinear behavior accurately, better than dc and S-parameters.

In the future, the model extracted in this thesis can be scaled to the remaining devices. Scaling will allow simulating the other devices with different geometrical dimensions manufactured in the same wafer. Moreover, re-gridding of nonlinear impedances of the intrinsic part will certainly reduce the set of dependent parameters of the nonlinear intrinsic elements. The regridded model will be extended to include thermal and memory effect extraction results. Then, mathematical function fitting techniques, such as Artificial Neural Networks (ANN), will be applied to the intrinsic part element parameters, which will overcome the limitations of tables and interpolation schemes used in the proposed model.

BIBLIOGRAPHY

Aflaki, P., et al. (2009). "Dedicated Large-Signal GaN HEMT Model for Switching-Mode Circuit Analysis and Design." IEEE Microw. and Wireless Comp. Letters 19(11): 740-742.

Ambacher, O. (1998). "Growth and applications of Group III-nitrides." Journal of Applied Physics 31(20).

Ambacher, O., et al. (2000). "Two dimensional electron gases induced by spontaneous and piezoelectric polarization in undoped and doped AlGa_N/Ga_N heterostructures." J. Appl. Phys. 87(1): 334-344.

Ammar B. Kouki, G. P. (2008). Method and apparatus for amplifying a signal modulated in amplitude. U. Patent. USA. US 11/450,410.

Angelov, I., et al. (2005). On the large-signal modelling of AlGa_N/Ga_N HEMTs and SiC MESFETs. Proc. IEEE EGAAS.

Bae, H. G., et al. (2007). High-efficiency GaN class-E power amplifier with compact harmonic-suppression network. Proc. Europ. Microw. Conf.

Bandler, J. W., et al. (1989). "Efficient large-signal FET parameter extraction using harmonics." IEEE MTT-S Int. Microw. Symp. Dig 37(12): 2099-2108.

Batyrev, I. G., et al. (2011). "Dislocations and stacking faults in hexagonal GaN." Phys. Stat. Solid. Appl. and Mat. Scienc. 208(7): 1566-1568.

Belevitch, V. (1962). Summary of the History of Circuit Theory. Proc. IRE.

Benedikt, J. and P. J. Tasker (2002). High-power time-domain measurement bench for power amplifier development. Proc. ARFTG.

Bensmida, S., et al. (2008). High efficiency digitally linearized GaN based power amplifier for 3G applications. Proc. IEEE Radio and Wireless Symp.

Birafane, A., et al. (2010). "Analyzing LINC Systems." IEEE Microw. Mag 11(5): 59-71.

Ce-Jun, W., et al. (1995). "Waveform-based modeling and characterization of microwave power heterojunction bipolar transistors." IEEE Trans. Microw. Theory Techn. 43(12): 2899-2903.

Cheolung, C., et al. (2003). Test-structure free modeling method for de-embedding the effects of pads on device modeling. Proc. Electron. Comp. Technol. Conf.

- Chia-Sung, C., et al. (2009). Characterization of annular-structure RF LDMOS transistors using polyharmonic distortion model. Proc. IEEE MTT-S Int. Microw. Symp. Dig.
- Chireix, H. (1935). High Power Outphasing Modulation. Proc. IRE.
- Cho, H. and D. E. Burk (1991). "A three-step method for the de-embedding of high-frequency S-parameter measurements." IEEE Trans. Electron Devices 38(6): 1371-1375.
- Corporation, M. M. (2003) Large-Signal Network Analyzer Technology: Preliminary Product Overview
- Corporation, N. (2008). Substrates for GaN RF Devices. GaN Essentials.
- Dambrine, G., et al. (1988). "A new method for determining the FET small-signal equivalent circuit." IEEE Trans. Microw. Theory Techn. 36(7): 1151-1159.
- Degachi, L. and F. M. Ghannouchi (2006). "Systematic and rigorous extraction method of HBT small-signal model parameters." IEEE Trans. Microw. Theory Techn. 54(2): 682-688.
- Doherty, W. H. (1936). A New High Efficiency Power Amplifier for Modulated Waves. Proc. IRE.
- Dominique schreurs, M. O. d., Anthony A. Goacher, and Michael Gadringer RF Power Amplifier Behavioral Modeling, Cambridge University Press.
- El-Asmar, M., et al. (2012). "Analytical Design Methodology of Outphasing Amplification Systems Using a New Simplified Chireix Combiner Model." IEEE Trans. Microw. Theory Techn. 60(6): 1886-1895.
- Environment, N. I. A. D. "Nonlinear Behavioral Model Compatible with Agilent's X-parameters® (from file): XPARAM." from <https://awrcorp.com/download/faq/english/docs/Elements/XPARAM.htm>.
- Essaadali, R., et al. (2015). Modeling of extrinsic parasitic elements of Si based GaN HEMTs using two step de-embedding structures. Proc. WAMICON.
- Fadhel M Ghannouchi, M. S. H. Load-Pull Techniques with Applications to Power Amplifier Design Springer
- Fadhel M Ghannouchi, R. D. (2012). Extended bandwidth digital doherty transmitter. Canada.
- Fadhel M. Ghannouchi, F. B., Ammar B. Kouki, Marco Bouchard (2001). Adaptive linearization of a feedforward amplifier by complex gain stabilization of the error amplifier. 6275105.

Fernandez-Barciela, M., et al. (2014). "Stretching the Design: Extending Analytical Circuit Design from the Linear to the Nonlinear Domain." IEEE Microw. Mag 15(6): 106-120.

Gonzalez, G. (1997). Microwave transistor amplifiers : analysis and design. Upper Saddle River, N.J., Prentice Hall.

Guoquan, S. (2008). The basic study of nonlinear scattering functions. Proc. ICMMT.

Hamdane, W., et al. (2007). An Adaptive MILC Amplification System for Adaptive MQAM Transmitters. Proc. IEEE ICSPC.

Hammi, O., et al. (2013). Generalized twin-nonlinear two-box digital predistorter for GaN based LTE Doherty power amplifiers with strong memory effects. Proc. IEEE IWS.

Helaoui, M., et al. (2007). "A New Mode-Multiplexing LINC Architecture to Boost the Efficiency of WiMAX Up-Link Transmitters." IEEE Trans. Microw. Theory Techn. 55(2): 248-253.

Horn, J., et al. (2008). Measurement-based large-signal simulation of active components from automated nonlinear vector network analyzer data via X-parameters. Proc. COMCAS.

Horn, J., et al. (2010). GaN Device Modeling with X-Parameters. Proc. IEEE CSICS.

Hui, Z., et al. (2012). An improved large-signal model of GaN HEMT. Proc. ICCP.

Islam, S. S. and A. F. M. Anwar (2004). "Self-heating and trapping effects on the RF performance of GaN MESFETs." IEEE Trans. Microw. Theory Techn. 52(4): 1229-1236.

Jan Verspecht, D. B., Jean-Pierre Teyssier and Jean-Michel Nébus. (2005). "Hot S-Parameter Techniques: $6 = 4 + 2$." Proc. ARFTG.

Jardel, O., et al. (2007). "An Electrothermal Model for AlGaIn/GaN Power HEMTs Including Trapping Effects to Improve Large-Signal Simulation Results on High VSWR." IEEE Trans. Microw. Theory Techn. 55(12): 2660-2669.

Jarndal, A. (2014). "AlGaIn/GaN HEMTs on SiC and Si substrates: A review from the small-signal-modeling's perspective." Int. J. of RF and Microw. Computer-Aided Eng. 24(3): 389-400.

Jarndal, A. (2014). "AlGaIn/GaN HEMTs on SiC and Si substrates: A review from the small-signal-modeling's perspective." Int. J. RF Microw. Computer-Aid. Eng. 24(3): 389-400.

Jarndal, A., et al. (2010). "Large-signal model for AlGaIn/GaN HEMTs suitable for RF switching-mode power amplifiers design." Solid-State Electronics 54(7): 696-700.

- Jarndal, A., et al. (2006). Accurate Large-Signal Modeling of AlGaIn-GaN HEMT Including Trapping and Self-Heating Induced Dispersion. Proc. IEEE ISPSD, Napoli, Italy.
- Jarndal, A., et al. (2016). "A Reliable Model Parameter Extraction Method Applied to AlGaIn/GaN HEMTs." IEEE Trans. Comput.-Aided Design Integr. Circuits Syst. 35(2): 211-219.
- Jarndal, A. and G. Kompa (2005). "A new small-signal modeling approach applied to GaN devices." IEEE Trans. Microw. Theory Techn. 53(11): 3440-3448.
- Jarndal, A. and G. Kompa (2007). Large-Signal Model for AlGaIn/GaN HEMT for Designing High Power Amplifiers of Next Generation Wireless Communication Systems. Proc. IEEE ICSPC.
- Jarndal, A. and G. Kompa (2007). "Large-Signal Model for AlGaIn/GaN HEMTs Accurately Predicts Trapping- and Self-Heating-Induced Dispersion and Intermodulation Distortion." IEEE Trans. Electron Devices 54(11): 2830-2836.
- Jarndal, A., et al. (2011). "Improved Modeling of GaN HEMTs on Si Substrate for Design of RF Power Amplifiers." IEEE Trans. Microw. Theory Techn. 59(3): 644-651.
- Jarndal, A. H. (2006). Large-Signal Modeling of GaN Device for High Power Amplifier Design. Dept. Elect. Eng. Germany, kassel univ. Ph.D. dissertation.
- Khan, M. A., et al. (2005). New Developments in Gallium Nitride and the Impact on Power Electronics. Proc. IEEE PESC.
- Killat, N., et al. (2012). "Thermal Properties of AlGaIn/GaN HFETs on Bulk GaN Substrates." IEEE Electr. Dev. Letters 33(3): 366-368.
- Komninou, P., et al. (2005). "Partial dislocations in wurtzite GaN." Appl. and Mater. Sc. 202(15): 2888-2899.
- Kompa, G. (1995). "Modeling of dispersive microwave FET devices using a quasi-static approach." Int. J. of Microw. and Millimeter-W. Computer-Aid. Eng. 5(3): 173-194.
- Kopp, B. and D. D. Heston (May. 1988). High-efficiency 5-watt power amplifier with harmonic tuning. IEEE MTT-S Int. Microw. Symp. Dig.
- Laredj, M., et al. (2011). Extrinsic extraction procedure for a small-signal GaN-HEMT model. Proc. ICM.
- Lazar, S., et al. (2004). "Nanopipes in GaN: photo-etching and TEM study." Euro. Phy. Journal-Appl. Physics 27(1-3): 275-278.

Lecklider, T. (2009). Boldy Going Beyond S-Parameters. Evaluation Engineering. Chicago: 18-31.

Liu, D., et al. (2012). GaN HEMT large-signal model research. proc. MMWCST.

Liu, Z. H., et al. (2011). "Temperature-dependent forward gate current transport in atomic-layer-deposited metal-insulator-semiconductor high electron mobility transistor." Appl. Phys. Lett. 98(16): 163501-163501-163503.

Lott, U. (1989). "Measurement of magnitude and phase of harmonics generated in nonlinear microwave two-ports." IEEE Trans. Microw. Theory Techn. 37(10): 1506-1511.

Maas, S. A. (2003). Nonlinear Microwave and RF Circuits, Artech House Publishers.

Marchetti, M., et al. (2008). "Active Harmonic LoadPull With Realistic Wideband Communications Signals." IEEE Trans. Microw. Theory Techn. 56(12): 2979-2988.

microwave, F. (1996). "Product Note 33: ALPS-308, Active Load Pull System for PCN Applications." from <http://focus-microwaves.com/sites/default/files/PN-33.pdf>.

Milligan, J. W., et al. (2007). SiC and GaN Wide Bandgap Device Technology Overview. Proc. IEEE Radar Conf.

Mishra, U. K., et al. (2002). "AlGaIn/GaN HEMTs-an overview of device operation and applications." Proc. of the IEEE 90(6): 1022-1031.

Negra, R., et al. (2007). "Switch-based GaN HEMT model suitable for highly-efficient RF power amplifier design." Proc. IEEE MTT-S Int. Microw. Symp. Dig.: 794-7972215.

Nitronex (2009). "GaN Essentials." from <http://www.nitronex.com/ganessentials.html>.

Nuttinck, S., et al. (2002). "Development of GaN wide bandgap technology for microwave power applications." IEEE Microw. Mag. 3(1): 80-87.

Oualid, H., et al. (2006). RF Power Amplifiers for Emerging Wireless Communications: Single Branch Vs. Multi-Branch Architectures. Proc. IEEE CCECE.

Oxley, C. H. and M. J. Uren (2005). "Measurements of unity gain cutoff frequency and saturation velocity of a GaN HEMT transistor." IEEE Trans. Microw. Theory Techn. 52(2): 165-169.

Packard, H. (1995). "S-Parameter Techniques for Faster, More Accurate Network Design."

Pelaez-Perez, A. M., et al. (2011). Experimental verification of analytical design equations based on X-parameters for predicting role of series feedback. Proc. EuMIC.

Peter H.Aaen, J. A. P., John Wood (2007). Modeling and Characterization of RF and Microwave Power FETs. Cambridge Cambridge University Press.

Peter Javorka, A. B., Slowakei (2004). Fabrication and Characterization of AlGaN/GaN High Electron Mobility Transistors. Dept. Elec. and Comp. Eng., Rheinisch-Westfälischen Technischen Hochschule Aachen univ.

Pozar, D. M. (1990). Microwave engineering. Don Mills, Ont., Addison-Wesley.

Predeep, P. P. (2011). Optoelectronics - Materials and Techniques, InTech.

Raffo, A., et al. (Sept. 2010). "Characterization of GaN HEMT Low-Frequency Dispersion Through a Multiharmonic Measurement System." IEEE Trans. Microw. Theory Techn. 58(9): 2490-2496.

Raffo, A., et al. (2010). "Nonlinear Dispersive Modeling of Electron Devices Oriented to GaN Power Amplifier Design." IEEE Trans. Microw. Theory Techn. 58(4): 710-718.

Riadh Essaadali, et al. (2014). Technical Report: New GaN HEMT Equivalent Circuit Model Based on X-parameter Measurements, École de technologie Supérieure

Riadh Essaadali, et al. (2011). Technical Report: New Nonlinear Network Parameters and their conversion rules. Montréal, École de technologie supérieure.

Riadh Essaadali, et al. (2013). Technical Report: Series, Parallel, cascaded, series-to-parallel and parallel-to-series nonlinear network configuration. Montréal, École de technologie supérieure.

Root, D. E. (2012). "Future Device Modeling Trends." IEEE Microw. Mag 13(7): 45-59.

Root, D. E. and S. Fan (1992). Experimental evaluation of large-signal modeling assumptions based on vector analysis of bias-dependent S-parameter data from MESFETs and HEMTs. Proc. IEEE MTT-S.

Root, D. E., et al. (2012). Scaling of X-parameters for device modeling. IEEE MTT-S Int. Microw. Symp. Dig.

Root, D. E., et al. (2013). X-parameters : characterization, modeling, and design of nonlinear RF and microwave components. Cambridge, Cambridge University Press.

Root, D. E., et al. (2010). Device modeling with NVNAs and X-parameters. Proc. IEEE INMMIC.

Root, D. E., et al. (2012). Compact and behavioral modeling of transistors from NVNA measurements: New flows and future trends. Proc. IEEE CICC.

Rudolph, M., et al. (2012). Nonlinear transistor model parameter extraction techniques. The Cambridge RF and microwave engineering series. Cambridge, UK ; New York, Cambridge University Press,.

Schreurs, D., et al. (1997). Direct Extraction of the Non-Linear Model for Two-Port Devices from Vectorial Non-Linear Network Analyzer Measurements. Proc. 27th Eur. Microwave Conf, Jerusalem, Palestine.

Schreurs, D. M. M., et al. (2002). "Straightforward and accurate nonlinear device model parameter-estimation method based on vectorial large-signal measurements." IEEE Trans. Microw. Theory Techn. 50(10): 2315-2319.

Simpson, G., et al. (2008). Load-pull + NVNA = enhanced X-parameters for PA designs with high mismatch and technology-independent large-signal device models. Proc. ARFTG.

Siti, M. M. H., et al. (2009). Characterization of on-wafer RF passive components for RFIC devices using three-steps de-embedding method. Proc. IEEE MICC.

Tanaka, T., et al. (2010). Highly efficient GaN power transistors and integrated circuits with high breakdown voltages. Proc. IEEE ICSICT.

Technologies, A. "ADS2009 Help."

Technologies, A. "Agilent U9391C/F/G Comb Generator Operating and Service Manual."

technologies, A. (2008). "X-Parameter Measurements." from http://na.tm.agilent.com/pna/nvna/NVNAWebHelp/XParameter_Measurements.htm.

technologies, A. (2009). "Advanced Design System 2009 Update 1." from <http://edocs.soco.agilent.com/display/ads2009U1/X-Parameter+Generator+Basics>.

technologies, K. "Advanced Design System (ADS)." from <http://www.keysight.com/en/pc-1297113/advanced-design-system-ads?cc=US&lc=eng>.

Technologies, K. "N5247A PNA-X Microwave Network Analyzer, 67 GHz." from <http://www.keysight.com/en/pd-1898852-pn-N5247A/pna-x-microwave-network-analyzer?cc=US&lc=eng>.

Technologies, K. (2008). "Advanced Design System 2008 Documentation: Custom Modeling with Frequency-Domain Defined Devices." from

http://cp.literature.agilent.com/litweb/pdf/ads2008/modbuild/ads2008/Custom_Modeling_with_Frequency-Domain_Defined_Devices.html.

Technologies, K. (2009). "Large-Signal S-Parameter Simulation." from <http://cp.literature.agilent.com/litweb/pdf/rfde2003c/rfdecktsimlssp/cklssp014.html>.

Tektronix Overcoming Nonlinear Measurement Challenges: Application Note.

Van Moer, W. and Y. Rolain (2006). "A large-signal network analyzer: Why is it needed?" IEEE Microw. Mag 7(6): 46-62.

van Raay, F., et al. (2013). "New Low-Frequency Dispersion Model for AlGaIn/GaN HEMTs Using Integral Transform and State Description." IEEE Trans. Microw. Theory Techn. 61(1): 154-167.

Van Valkenburg, M. E. (1974). Circuit theory: foundations and classical contributions. Stroudsburg, Pa., Dowden Hutchinson & Ross.

Vandamme, E. P., et al. (2001). "Improved three-step de-embedding method to accurately account for the influence of pad parasitics in silicon on-wafer RF test-structures." IEEE Trans. Electron Devices 48(4): 737-742.

Vassil Palankovski, R. Q. (2004). Analysis and Simulation of Heterostructure Devices. Austria, SpringerWienNewYork.

Verspecht, J. (2005). "Large-signal network analysis." IEEE Microw. Mag. 6(4): 82-92.

Verspecht, J. (2008). "About Jan Verspecht." from <http://www.janverspecht.com/>.

Verspecht, J. and D. E. Root (Jun. 2006). "Polyharmonic distortion modeling." IEEE Microw. Mag 7(3): 44-57.

Verspecht, J., et al. (2005). "Linearization of large-signal scattering functions." IEEE Trans. Microw. Theory Techn. 53(4): 1369-1376.

Von, V. (2007). Large Signal Modeling of GaN HEMTs for UMTS Base Station Power Amplifier Design Taking into Account Memory Effects. Dept. Elect. and electron. Eng. Germany, Rheinisch-Westfälischen Technischen Hochschule Aachen univ.

Werthorf, A., et al. (May. 1993). "Direct nonlinear FET parameter extraction using large-signal waveform measurements." IEEE Microw. Guided Wave Lett 3(5): 130-132.

Wongtanarak, C. and S. Chalermwisutkul (2011). Design and implementation of a 1 GHz GaN HEMT class-F power amplifier for transistor model evaluation. Proc. ECTI-CON.

Wood, C. and D. Jena (2008). Polarization Effects in Semiconductors : From Ab Initio Theory to Device Applications. Boston, MA, Springer-Verlag US.

Yong-Sub, L. and J. Yoon-Ha (2007). Applications of GaN HEMTs and SiC MESFETs in High Efficiency Class-E Power Amplifier Design for WCDMA Applications. Proc. IEEE MTT-S.

Young S. Park, Y. H. K. H. I., Woong Jung Hyungsang Kim, Minseon Kim, W. C. Yang Junho Lee, Hong Goo Choi, Cheong Hyun Roh and Cheol-Koo Hahn (2010). "Dislocation Defects in GaN Epilayers Grown on Si (100) Substrates by Metal-organic Chemical-vapor Deposition." J. of the Kor. Physic. Soc. 56(4): 1172-1175.